



REFERENCE ONLY

UNIVERSITY OF LONDON THESIS

Degree PhD Year 2007 Name of Author FOULKES, Thomas

COPYRIGHT

This is a thesis accepted for a Higher Degree of the University of London. It is an unpublished typescript and the copyright is held by the author. All persons consulting this thesis must read and abide by the Copyright Declaration below.

COPYRIGHT DECLARATION

I recognise that the copyright of the above-described thesis rests with the author and that no quotation from it or information derived from it may be published without the prior written consent of the author.

LOANS

Theses may not be lent to individuals, but the Senate House Library may lend a copy to approved libraries within the United Kingdom, for consultation solely on the premises of those libraries. Application should be made to: Inter-Library Loans, Senate House Library, Senate House, Malet Street, London WC1E 7HU.

REPRODUCTION

University of London theses may not be reproduced without explicit written permission from the Senate House Library. Enquiries should be addressed to the Theses Section of the Library. Regulations concerning reproduction vary according to the date of acceptance of the thesis and are listed below as guidelines.

- A. Before 1962. Permission granted only upon the prior written consent of the author. (The Senate House Library will provide addresses where possible).
B. 1962-1974. In many cases the author has agreed to permit copying upon completion of a Copyright Declaration.
C. 1975-1988. Most theses may be copied upon completion of a Copyright Declaration.
D. 1989 onwards. Most theses may be copied.

This thesis comes within category D.

Empty square box

This copy has been deposited in the Library of UCL

Empty square box

This copy has been deposited in the Senate House Library, Senate House, Malet Street, London WC1E 7HU.



# **The Role of p11 (S100A10) in Nociception**

**Thomas Foulkes**

A thesis submitted for the degree of Doctor of Philosophy to the University  
of London

Department of Biology  
University College London

2007

UMI Number: U592809

All rights reserved

INFORMATION TO ALL USERS

The quality of this reproduction is dependent upon the quality of the copy submitted.

In the unlikely event that the author did not send a complete manuscript and there are missing pages, these will be noted. Also, if material had to be removed, a note will indicate the deletion.



UMI U592809

Published by ProQuest LLC 2013. Copyright in the Dissertation held by the Author.  
Microform Edition © ProQuest LLC.

All rights reserved. This work is protected against  
unauthorized copying under Title 17, United States Code.



ProQuest LLC  
789 East Eisenhower Parkway  
P.O. Box 1346  
Ann Arbor, MI 48106-1346

## DECLARATION

I, Thomas Foulkes, confirm that the work presented in this thesis is my own. Where information has been derived from other sources, I confirm that this has been indicated in the thesis.

30/07/2007 .

## ABSTRACT

---

The S100-family protein p11 (S100A10) is involved in a variety of physiological processes, including channel trafficking and angiogenesis. In this thesis, we used genetic approaches to investigate the functional roles of p11. p11 modulates the plasma membrane trafficking of the sensory neuron-specific voltage-gated Na<sup>+</sup> channel Nav1.8 and numerous other proteins. Since Nav1.8 performs a specialised function in the detection of noxious stimuli (nociception), we investigated the role of p11 in peripheral pain pathways. We used the *Cre-loxP* system to delete p11 exclusively from nociceptive neurons, allowing the examination of this aspect of p11 function without confounding effects from roles of p11 in other tissues. p11-null neurons showed deficits in the functional expression of Nav1.8. Noxious coding in wide-dynamic range neurons in the dorsal horn was compromised in p11-null animals. Acute mechanical pain behaviour was attenuated, but no deficits in inflammatory pain were observed. Reduced neuropathic pain behaviour was apparent in nociceptor-specific p11-null mice. While certain effects of p11 deletion can be explained by reduced Nav1.8 trafficking, Nav1.8 is not required for neuropathic pain. p11 therefore acts through both Nav1.8-dependent and alternative mechanisms to control nociceptive thresholds. This suggests it is a potential therapeutic target.

Given the importance of p11-dependent modulation of Nav1.8, we investigated the p11-binding site on the Nav1.8 N-terminus. *In vitro* fluorescence resonance energy transfer (FRET) assays were used to examine this interaction. In contrast to previous studies, we found the interaction to be complex, involving two distinct binding sites and an autoinhibitory domain. The p11-Nav1.8 interaction is therefore not well-suited to small molecule-based inhibition.

p11 has been reported to play an important role in processes required for angiogenesis. In assays of angiogenesis-dependent tumour growth, global p11 deletion resulted in increased tumour volume and altered vascular morphology. This may have implications for novel anti-cancer therapies targeting p11.

## FUNDING

I thank the BBSRC, Vernalis Pharmaceuticals and Ionix Pharmaceuticals for funding this project.



## PUBLICATIONS

### Papers

**Foulkes T**, Nassar MA, Lane T, Matthews EA, Baker MD, Gerke V, Okuse K, Dickenson AH, Wood JN (2006) Deletion of annexin 2 light chain p11 in nociceptors causes deficits in somatosensory coding and pain behavior. *J Neurosci* 26:10499-10507.

**Foulkes T**, Szestak T, Wood JN, Dekker LV (2007) A model for the interaction between the TTX-resistant sodium channel Na<sub>v</sub>1.8 and p11 (S100A10) based on a FRET interaction assay. *Manuscript submitted*.

**Foulkes T**, Wood JN (2007) Cold Pain (Review). *Channels* 1(3).

### Abstracts/Oral Presentations

**Foulkes T**, Nassar MA, Wood JN (2005). Poster: Conditional deletion of p11 (S100A10) in the mouse. *The Annexins 2005, Switzerland*.

**Foulkes T** (2006) Oral Presentation: The role of p11 in peripheral pain pathways. *Spring Pain Research Conference 2006, Grand Cayman*.

# CONTENTS

<b>Title.....</b>	<b>1</b>
<b>Declaration.....</b>	<b>2</b>
<b>Abstract.....</b>	<b>3</b>
<b>Funding.....</b>	<b>4</b>
<b>Publications.....</b>	<b>4</b>
<b>Contents.....</b>	<b>5</b>
<b>List of Figures.....</b>	<b>10</b>
<b>List of Tables.....</b>	<b>12</b>
<b>Acknowledgements.....</b>	<b>13</b>
<b>1 Introduction.....</b>	<b>14</b>
<b>1.1 The S100 Proteins.....</b>	<b>14</b>
1.1.1 S100-target interactions.....	15
<b>1.2 p11 (S100A10).....</b>	<b>16</b>
1.2.1 p11-protein interactions and physiological roles.....	17
1.2.1.1 Annexin 2.....	18
1.2.1.2 Nav1.8.....	19
1.2.1.3 5-HT <sub>1B</sub> .....	20
1.2.1.4 ASIC1a.....	21
1.2.1.5 TASK-1.....	22
1.2.1.6 TRPV5/6.....	23
1.2.1.7 Tissue plasminogen activator.....	24
1.2.1.8 BAD.....	26
1.2.1.9 AHNAK.....	26
1.2.1.10 Phospholipase A2.....	27
1.2.1.11 Cathepsin B.....	28
1.2.1.12 PCTAIRE-1.....	28
1.2.2 Importance of p11 in cellular function.....	29
<b>1.3 Pain and Nociception.....</b>	<b>30</b>
<b>1.4 Nociception and DRG primary afferent neurons.....</b>	<b>31</b>
1.4.1 Anatomical and functional classification of DRG neurons.....	33
1.4.2 Differential gene expression in distinct populations of nociceptors.....	34
1.4.3 Transduction of noxious stimuli.....	35
1.4.3.1 Transduction of noxious mechanical stimuli.....	35
1.4.3.2 Transduction of noxious thermal stimuli.....	38
1.4.3.3 Transduction of noxious chemical stimuli.....	44
1.4.4 Transmission of noxious stimuli.....	46
1.4.5 Inflammatory pain.....	47
1.4.6 Neuropathic pain.....	51
1.4.7 Central processing.....	53
<b>1.5 Voltage-gated sodium channels.....</b>	<b>56</b>
1.5.1 Pharmacology.....	58
1.5.2 VGSC properties and expression in sensory neurons.....	59

1.5.3	$\beta$ -subunits.....	61
1.5.4	Nav1.8.....	62
1.5.4.1	Modulators of Nav1.8 expression and properties.....	63
1.5.4.2	Nav1.8 in pain.....	65
1.5.5	VGSCs and nociception.....	66
<b>1.6</b>	<b>Project Outline.....</b>	<b>68</b>
<b>2</b>	<b>Materials and Methods.....</b>	<b>69</b>
<b>2.1</b>	<b>Molecular Biology.....</b>	<b>69</b>
2.1.1	Agarose Gel Electrophoresis.....	69
2.1.2	Recovery of DNA from agarose gels.....	69
2.1.3	The Polymerase Chain Reaction.....	69
2.1.4	Addition of 3' A Overhangs for TOPO-TA Cloning.....	70
2.1.5	TOPO-TA Cloning ®: Insertion of DNA Fragments into pCRII.....	70
2.1.6	Transformation of Chemically Competent Bacterial Cells.....	70
2.1.7	Screening Bacterial Clones by Colony PCR.....	71
2.1.8	Isolation of Plasmid DNA by Mini- and Midiprep.....	71
2.1.9	Restriction Digests.....	71
2.1.10	Ligation of Fragments into pET14b.....	71
2.1.11	DNA Sequencing.....	71
2.1.12	Isolation of Genomic DNA from Tissue Samples.....	72
2.1.13	Southern Blot.....	72
2.1.13.1	DNA Separation and Blotting.....	72
2.1.13.2	Pre-Hybridization.....	73
2.1.13.3	Probe Labelling and Hybridisation.....	73
2.1.13.4	Membrane Washing and Imaging.....	73
2.1.14	RNA Extraction.....	73
2.1.15	Reverse Transcription Reaction.....	74
2.1.16	Quantitative (Real-Time) PCR.....	74
<b>2.2</b>	<b>Protein Biology.....</b>	<b>75</b>
2.2.1	Recombinant Protein Expression.....	75
2.2.2	Purification of Recombinant Proteins.....	75
2.2.2.1	Purification of Nav1.8 1-120 (Wild-type & Mutant).....	76
2.2.2.2	Buffer exchange.....	76
2.2.2.3	Cy3 Labelling of Nav1.8 1-120.....	76
2.2.2.4	Isolation of Pure p11.....	77
2.2.2.5	Cy5 Labelling of p11.....	77
2.2.3	Measurement of Protein Concentration.....	77
2.2.3.1	Bradford Assay.....	78
2.2.3.2	Micro Lowry Assay (Peterson's Modification).....	78
2.2.3.3	Measurement of Protein Concentration by Absorbance at 280nm....	78
2.2.3.4	BCA Method.....	79
2.2.4	Measurement of p11- Nav1.8 1-120 Interaction by Fluorescence Resonance Energy Transfer (FRET).....	79
2.2.5	Analysis of FRET Protein Interaction Studies.....	79
2.2.6	SDS-PAGE.....	80
2.2.7	Coomassie Blue Staining.....	80
2.2.8	Western Blotting.....	80
2.2.9	Immunocytochemistry.....	81
2.2.10	Immunohistochemistry.....	81
<b>2.3</b>	<b>Electrophysiology.....</b>	<b>83</b>

2.3.1	Whole-cell patch-clamp recordings .....	83
2.3.2	<i>In vivo</i> recordings from dorsal horn neurons .....	83
<b>2.4</b>	<b>Animal Breeding &amp; Behavioural Analysis.....</b>	<b>85</b>
2.4.1	Motor Function .....	85
2.4.2	Mechanical Withdrawal Thresholds .....	85
2.4.2.1	Randall-Selitto .....	85
2.4.2.2	von Frey .....	85
2.4.3	Thermal Thresholds .....	86
2.4.3.1	Hargreaves' Apparatus.....	86
2.4.3.2	Hot Plate.....	86
2.4.4	Inflammatory Pain Models.....	86
2.4.4.1	Intraplantar Nerve Growth Factor.....	86
2.4.4.2	Intraplantar Carrageenan.....	86
2.4.4.3	Intraplantar Formalin .....	87
2.4.5	Neuropathic Pain Model .....	87
<b>2.5</b>	<b>Angiogenesis assays.....</b>	<b>88</b>
2.5.1	Tumour cell growth.....	88
2.5.2	Melanoma cell injection.....	88
<b>3</b>	<b>Mapping the Nav1.8-p11 interaction.....</b>	<b>89</b>
<b>3.1</b>	<b>Introduction.....</b>	<b>89</b>
3.1.1	Nav1.8-p11 Interaction .....	89
3.1.2	Identification of binding domains for p11- protein interactions .....	90
3.1.3	FRET .....	92
3.1.4	Protein-protein interaction models.....	93
<b>3.2</b>	<b>Methods.....</b>	<b>95</b>
<b>3.3</b>	<b>Results .....</b>	<b>98</b>
3.3.1	Nav1.8 N-terminus and p11 can be expressed at high levels and purified to >95% purity .....	98
3.3.1.1	Nav1.8 N-terminus.....	98
3.3.1.2	p11.....	98
3.3.2	FRET-based assays effectively measure the site-specific interaction between Nav1.8 and p11 .....	99
3.3.3	Annexin 2 and Nav1.8 bind to distinct sites on p11 .....	100
3.3.4	Amino acids 74-103 of Nav1.8 are sufficient to bind p11 .....	101
3.3.5	Amino acids 2-40 of Nav1.8 do not interact with p11 .....	102
3.3.6	Amino acids 41-80 of Nav1.8 interact with p11 .....	102
3.3.7	Amino acids 81-120 of Nav1.8 inhibit Nav1.8 1-120 binding to p11 ..	103
3.3.8	Summary .....	104
3.3.9	3-amino acid deletions in the region 74-103 of Nav1.8 have subtle effects on affinity for p11, but do not prevent binding .....	104
3.3.10	Nav1.8 74-81 is sufficient to bind p11 .....	107
3.3.11	Summary of Results .....	108
<b>3.4</b>	<b>Discussion.....</b>	<b>109</b>
3.4.1	FRET-based assays are suitable for the quantitative investigation of protein-protein interactions .....	109
3.4.2	The Nav1.8-p11 interaction is best described by a single-site binding model .....	110
3.4.3	Amino acids 77-85 of Nav1.8 are the critical residues in the 74-103 binding domain .....	110
3.4.4	An additional binding site at residues 41-74.....	112

3.4.5	Residues 86-100 of Nav1.8 contain an inhibitory domain for the Nav1.8-p11 interaction.....	113
3.4.6	A 2-site model for the Nav1.8-p11 interaction .....	115
3.4.7	Comparison with other p11 interactions .....	116
3.4.8	Annexin 2 binds p11 at a site distinct from that of Nav1.8.....	116
3.4.9	Importance of the Nav1.8-p11 interaction to analgesic drug discovery 117	
3.4.10	FRET interaction studies are suitable for use with other proteins .....	119
<b>4</b>	<b>p11 in pain pathways .....</b>	<b>120</b>
<b>4.1</b>	<b>Introduction.....</b>	<b>120</b>
4.1.1	Genetic technology for the investigation of protein function .....	120
4.1.2	Gene targeting and homologous recombination .....	122
4.1.3	Production of a mutant mouse .....	124
4.1.4	Site-specific recombination.....	124
4.1.4.1	The Cre/ <i>loxP</i> recombination system .....	126
4.1.4.2	The Flp/ <i>FRT</i> recombination system.....	127
4.1.4.3	The Nav1.8Cre mouse.....	128
4.1.5	Behavioural assessment of nociceptive thresholds .....	128
4.1.5.1	Measurement of noxious mechanical thresholds .....	130
4.1.5.1.1	Randall-Selitto .....	130
4.1.5.1.2	von Frey .....	130
4.1.5.2	Thermal nociception .....	131
4.1.5.2.1	Hargreaves' test.....	131
4.1.5.2.2	Hot plate .....	131
4.1.5.3	Inflammatory pain models .....	131
4.1.5.3.1	Formalin .....	131
4.1.5.3.2	Nerve Growth Factor .....	132
4.1.5.3.3	Carrageenan .....	132
4.1.5.4	Neuropathic pain models .....	132
4.1.6	Electrophysiology .....	134
4.1.6.1	Whole-cell patch-clamp of DRG neurons.....	134
4.1.6.2	Electrophysiological recording from wide dynamic range neurons of the spinal cord .....	135
4.1.7	Angiogenesis.....	136
4.1.8	Aims .....	137
<b>4.2</b>	<b>Methods.....</b>	<b>138</b>
4.2.1	Gene targeting: generation of <i>loxP</i> -flanked <i>S100A10</i> mice.....	138
4.2.2	Breeding strategy .....	139
4.2.3	Confirmation of correct gene targeting .....	140
4.2.4	Proving selective/global deletion .....	140
4.2.5	Effect on cell survival .....	141
4.2.6	Analysis of p11 conditional-null phenotype .....	141
4.2.7	Urine Analysis.....	141
4.2.8	Tumour growth/angiogenesis testing .....	142
<b>4.3</b>	<b>Results .....</b>	<b>143</b>
4.3.1	A successful recombination event was detected in 129 embryonic stem cells .....	143
4.3.2	Embryonic stem cell transplantation produced viable p11 floxed mice .... .....	144

4.3.3	Conditional deletion: p11 is deleted from Nav1.8-expressing neurons, but not from other tissues.....	145
4.3.4	Conditional p11 deletion does not affect the survival of DRG neurons ....	148
4.3.5	Global deletion: p11 is deleted from all tissues.....	150
4.3.6	Plasma membrane trafficking of Nav1.8 in DRG neurons is reduced by p11 deletion.....	151
4.3.7	No changes in plasma membrane trafficking of annexin 2, ASIC1 or 5-HT <sub>1B</sub> in DRG neurons were seen following deletion of p11 .....	153
4.3.8	p11 deletion does not affect Ca <sup>2+</sup> excretion.....	154
4.3.9	TTX-R Na <sup>+</sup> current density is reduced in p11 conditional-null mutants ...	155
4.3.10	Wide dynamic range neurons in the spinal cord show deficits in noxious somatosensory coding following p11 deletion.....	158
4.3.11	p11 conditional-null mice show no gross abnormalities.....	160
4.3.12	p11 conditional-null mice show behavioural deficits in noxious mechanosensation .....	160
4.3.13	p11 conditional-null mice do not show behavioural deficits in noxious thermosensation .....	161
4.3.14	p11 conditional-null mice show no deficits in response to noxious cold ..	162
4.3.15	p11 conditional-null mice show no deficits in models of inflammatory pain .....	163
4.3.16	p11 conditional-null mice display reduced neuropathic pain behaviour ...	165
4.3.17	p11 plays a complex role in neoangiogenesis and tumour growth .....	167
<b>4.4</b>	<b>Discussion.....</b>	<b>168</b>
4.4.1	Effects of p11 deletion on protein trafficking and nociceptor properties ..	169
4.4.2	Effects of p11 deletion on pain behaviour .....	174
4.4.3	Sources of compensation for p11 deletion.....	180
4.4.4	p11 deletion enhances tumour growth and neoangiogenesis.....	181
<b>5</b>	<b>Summary.....</b>	<b>184</b>
<b>6</b>	<b>References.....</b>	<b>186</b>

## LIST OF FIGURES

<b>Figure 1.1</b>	The complex of p11 and the annexin 2 N-terminal peptide	<b>18</b>
<b>Figure 1.2</b>	Diagram illustrating nociceptor subtypes	<b>32</b>
<b>Figure 1.3</b>	Processes contributing to inflammatory hyperalgesia in primary afferent neurons	<b>50</b>
<b>Figure 1.4</b>	Voltage-gated sodium channel structure	<b>57</b>
<b>Figure 3.1</b>	Fluorescence resonance energy transfer used to detect protein-protein interactions	<b>92</b>
<b>Figure 3.2</b>	Overview of cloning and generation of mutants for Nav1.8 1-120	<b>95</b>
<b>Figure 3.3</b>	Confirmation of protein identity and purity	<b>98</b>
<b>Figure 3.4</b>	Titration of Cy3-Nav1.8 against 250ng Cy5-p11	<b>99</b>
<b>Figure 3.5</b>	Competition of the Cy3-Nav1.8 - Cy5-p11 interaction by unlabelled Nav1.8 1-120	<b>100</b>
<b>Figure 3.6</b>	FRET competition assays illustrating distinct binding sites	<b>101</b>
<b>Figure 3.7</b>	Competition of the Cy3-Nav1.8 - Cy5-p11 interaction by unlabelled Nav1.8 74-103	<b>102</b>
<b>Figure 3.8</b>	Competition by $\Delta$ 2-40	<b>102</b>
<b>Figure 3.9</b>	Binding at residues 41-80	<b>103</b>
<b>Figure 3.10</b>	Inhibition of interaction by residues 81-120	<b>103</b>
<b>Figure 3.11</b>	Examples of 3-amino acid deletion assays	<b>105</b>
<b>Figure 3.12</b>	Effects of 3-amino acid deletions	<b>106</b>
<b>Figure 3.13</b>	Localisation of binding site to residues 74-81	<b>107</b>
<b>Figure 3.14</b>	Summary of results	<b>108</b>
<b>Figure 3.15</b>	Human Nav1.8 74-103: comparison with other VGSCs	<b>111</b>
<b>Figure 3.16</b>	Alignment of protein sequence for human VGSCs	<b>113</b>
<b>Figure 3.17</b>	Nav1.8 N-terminus domains	<b>115</b>
<b>Figure 3.18</b>	Predicted structure of Nav1.8 N-terminus	<b>116</b>

<b>Figure 4.1</b>	Gene targeting construct design	<b>123</b>
<b>Figure 4.2</b>	The Cre- <i>loxP</i> recombination system	<b>127</b>
<b>Figure 4.3</b>	Models of neuropathic pain	<b>134</b>
<b>Figure 4.4</b>	The whole-cell patch-clamp circuit	<b>135</b>
<b>Figure 4.5</b>	Plasmin formation and downstream effects	<b>137</b>
<b>Figure 4.6</b>	Exon structure of <i>Sl00A10</i> gene	<b>138</b>
<b>Figure 4.7</b>	Gene targeting process	<b>143</b>
<b>Figure 4.8</b>	Southern blotting to detect p11-floxed cells	<b>144</b>
<b>Figure 4.9</b>	Southern blotting to detect p11-floxed cells	<b>145</b>
<b>Figure 4.10</b>	Confirmation of conditional p11 deletion	<b>146</b>
<b>Figure 4.11</b>	Conditional deletion of p11	<b>147</b>
<b>Figure 4.12</b>	Distribution of p11-null neurons in the conditional-null animal	<b>148</b>
<b>Figure 4.13</b>	Conditional deletion of p11 does not affect neuronal survival	<b>149</b>
<b>Figure 4.14</b>	Effect of p11 deletion on neuron size	<b>150</b>
<b>Figure 4.15</b>	p11 is deleted from all tissues in the global-null mouse line	<b>150</b>
<b>Figure 4.16</b>	Global deletion of p11	<b>151</b>
<b>Figure 4.17</b>	Plasma membrane trafficking of Nav1.8. assessed by western blot	<b>152</b>
<b>Figure 4.18</b>	Anti-Nav1.8 immunocytochemistry	<b>152</b>
<b>Figure 4.19</b>	Plasma membrane trafficking of annexin 2	<b>153</b>
<b>Figure 4.20</b>	Plasma membrane trafficking assessed by western blot	<b>154</b>
<b>Figure 4.21</b>	Excretion of Ca <sup>2+</sup> and Na <sup>+</sup> in the p11-null mouse	<b>155</b>
<b>Figure 4.22</b>	Electrophysiology of p11-null DRG neurons	<b>156</b>
<b>Figure 4.23</b>	Current densities in small-diameter DRG neurons	<b>156</b>
<b>Figure 4.24</b>	Current-voltage relationship for TTX-R currents in small-diameter DRG neurons	<b>157</b>
<b>Figure 4.25</b>	Resting potentials of cultured DRG neurons	<b>158</b>
<b>Figure 4.26</b>	Electrophysiological recordings from WDR neurons in the dorsal horn	<b>159</b>
<b>Figure 4.27</b>	Acute mechanical pain behaviour in p11 conditional-null mice	<b>161</b>
<b>Figure 4.28</b>	Acute thermal pain behaviour in p11 conditional-null mice	<b>162</b>
<b>Figure 4.29</b>	Acute cold pain behaviour in p11 conditional-null mice	<b>163</b>

<b>Figure 4.30</b>	Inflammatory pain behaviour in p11 conditional-null mice	<b>164</b>
<b>Figure 4.31</b>	Formalin-induced inflammatory pain behaviour in p11 conditional-null mice	<b>165</b>
<b>Figure 4.32</b>	Neuropathic pain behaviour in p11 conditional-null mice	<b>166</b>
<b>Figure 4.33</b>	Effect of p11 deletion on tumour growth	<b>167</b>
<b>Figure 4.34</b>	Deleted regions of p11	<b>168</b>
<b>Figure 4.35</b>	Anti-angiogenic effects of p11	<b>183</b>

## LIST OF TABLES

<b>Table 1.1</b>	Na <sup>+</sup> channel $\alpha$ -subunits	<b>61</b>
<b>Table 3.1</b>	Mutant proteins produced using the His-Tag bacterial expression/purification system	<b>96</b>
<b>Table 3.2</b>	Peptides produced by chemical synthesis	<b>97</b>
<b>Table 3.3</b>	Summary of effects of 3-amino acid deletions	<b>106</b>

## ACKNOWLEDGEMENTS

Thank you to my supervisor, John Wood. It has been a pleasure to work in his lab, and his enthusiasm for scientific discovery has inspired me throughout the course of my PhD. I am grateful for his expert guidance and instruction, and for sharing his extensive knowledge, which has been invaluable.

I thank Lodewijk Dekker, my second supervisor, for welcoming me into his lab in the early stages of my PhD, and for his expert supervision during this period. His excellent teaching and inquiring attitude made this project both enjoyable and productive, and enabled me to learn skills which were of great use throughout my PhD.

Mohammed Nassar and Bjarke Abrahamsen provided outstanding advice and scientific instruction, and a great deal of experimental assistance. I am extremely grateful for their generosity. I am indebted to Mark Baker for his instruction in electrophysiological theory and practice. His expert knowledge and patience are remarkable. Kenji Okuse was kind enough to engage in many productive discussions about this project, for which I thank him. Thank you to Ramin Raouf for sharing his extensive knowledge of science and for helpful criticism of this thesis. Thanks also to Elizabeth Matthews and Anthony Dickenson, who performed spinal cord recordings and provided valuable instruction, and to Volker Gerke, who provided useful reagents and advice.

Thank you to all the members of the Wood and Dekker labs for being fantastic colleagues, and for continuing guidance and assistance.

My gratitude goes to Rebecca Slater for her excellent proof reading and advice. I thank her for her compassion and generosity during the course of this thesis.

I wish to thank my friends, especially Frankie and John, Nick and James, Sally, Sarah, Hugo and Tom, for making my life enjoyable and providing a useful sense of perspective.

Finally, I thank my family for their kindness, support and excellent advice.

# 1 INTRODUCTION

This thesis examines the role of the S100 protein p11 in pain pathways, in particular through its interaction with the voltage-gated sodium channel  $\text{Na}_v1.8$ . The introduction will give an overview of p11 and the S100 proteins, followed by a discussion of the clinical aspects of pain and the physiological process of nociception. This will be followed by an introduction to voltage-gated sodium channels, focusing on  $\text{Na}_v1.8$  and others expressed in damage-sensing neurons.

## 1.1 THE S100 PROTEINS

The S100 proteins are small (10-12kDa), acidic proteins, found exclusively in vertebrates (Schafer and Heizmann, 1996a), and are members of the EF-hand superfamily. EF-hand proteins are defined by the presence of between 2 and 12 helix-turn-helix structural motifs, each consisting of two  $\alpha$ -helices separated by a short loop region of around 12 amino acids. The EF-hand motif is usually capable of binding a  $\text{Ca}^{2+}$  ion, via aspartate and glutamate side chains (Marsden et al., 1990), which causes a conformational change. This allows functional regulation of S100 proteins by changes in intracellular  $\text{Ca}^{2+}$  concentration.

The S100 family contains over 25 distinct isoforms with 25-65% amino acid identity, the genes for which are clustered at chromosome locus 1q21 in humans (chromosome 3 in the mouse) (Schafer and Heizmann, 1996b). They are characterised by two consecutive EF-hands (N-terminal unconventional with low  $\text{Ca}^{2+}$  affinity, C-terminal canonical, with high affinity for  $\text{Ca}^{2+}$  (Donato, 1986a)) connected by a flexible linker region (the "hinge"), and flanked by conserved hydrophobic residues with N- and C-terminal extensions. The sequences of the linker and the C-terminal extension are the most variable regions, and are often involved in target binding (Donato, 2001;Kligman and Hilt, 1988). Structurally, the S100 proteins are similar to calmodulin, although they do not share its ubiquitous expression. Instead, they are expressed in certain cell types at varying levels, often changing in response to environmental factors. Members of the S100 family are under complex transcriptional control (Chen and Barraclough, 1996;e.g. Cohn et al., 2001).

With the exception of calbindin (which functions as a  $\text{Ca}^{2+}$  buffer), S100 proteins exist as non-covalent homo- and hetero-dimers, related by a 2-fold axis of rotation. This dimerisation is important for functional activity (Donato, 2003), and may be dynamic (Santamaria-Kisiel et al., 2006). The binding of  $\text{Ca}^{2+}$  to S100 proteins causes a conformational change in structure, resulting in a 40% alteration in the position of the 3<sup>rd</sup>  $\alpha$ -helix, which exposes a broad

hydrophobic surface (e.g. Dempsey et al., 2003). This is proposed to allow the interaction of S100 proteins with their target proteins under conditions of high  $\text{Ca}^{2+}$  concentration. One member of the family, S100A10 (p11), has a mutation in each EF loop, rendering it  $\text{Ca}^{2+}$ -independent and resulting in a permanently-active conformation (Gerke and Weber, 1985b; Rety et al., 1999).

The S100 proteins generally act via effector molecules, such as ion channels, enzymes, or components of the cytoskeleton. For the  $\text{Ca}^{2+}$ -dependent S100 proteins, this provides a mechanism for the regulation of cellular function by changes in  $\text{Ca}^{2+}$  levels. Yeast two-hybrid screens have played a large part in the identification of target proteins to which S100 members bind, although this method has limited biological relevance and interactions must therefore be confirmed by other methods. For example, the low  $\text{Ca}^{2+}$  levels in yeast (~200nM) (Halachmi and Eilam, 1993) would prevent the detection of many  $\text{Ca}^{2+}$ -dependent interactions. Additionally, proteins forced to co-localise in the nucleus (by the addition of nuclear localisation signals) may not come into contact in a physiological setting. *In vivo* colocalisation studies have been of use in recent years, supplemented by immunoprecipitation assays to demonstrate a physical interaction.

### 1.1.1 S100-target interactions

The dissociation constant ( $K_d$ ) for the  $\text{Ca}^{2+}$  dependence of most S100 proteins is around 10-50nM (Donato, 1986b), meaning that the majority will assume the active conformation during an intracellular  $\text{Ca}^{2+}$  spike (~1 $\mu\text{M}$ ). This provides a mechanism for the control of interactions by intracellular  $\text{Ca}^{2+}$  levels. Some interactions, however, are  $\text{Ca}^{2+}$ -independent, and presumably regulated by alternative mechanisms. Over 90 proteins to which S100 proteins may bind have been identified (including tubulin, glial fibrillary acidic protein and F-actin), although *in vivo* confirmation of binding has only been performed for a subset of these.

Whilst all S100 proteins act by binding to other proteins, the effects of S100 binding on these proteins are diverse. Effects on oligomerisation, steric inhibition of kinase-mediated phosphorylation (e.g. Yu and Fraser, 2001), retention of proteins in the ER (e.g. Renigunta et al., 2006), masking of ER retention signals to allow subsequent trafficking (e.g. Girard et al., 2002), interactions with the cytoskeleton (e.g. Yamasaki et al., 2001), regulation of ion channel activity, regulation of enzyme activity (e.g. Duda et al., 1996) and acting as co-receptors for enzyme-substrate interactions (e.g. Kwon et al., 2005a) have all been described. Additionally, secreted S100 proteins have been shown to act in a cytokine-like manner through the receptor for advanced glycosylation end products (RAGE).

## 1.2 p11 (S100A10)

p11 (S100A10, calpactin light-chain, annexin 2 light-chain) is an 11kDa member of the S100 protein family, consisting of 96 amino acids (*Mus musculus*, *Homo sapiens*). The *S100A10* gene, highly conserved among vertebrates, is located in the S100 cluster of genes, on chromosome 1q21 in the human, and chromosome 3 in the mouse. p11 is unique among the S100 proteins in being insensitive to  $\text{Ca}^{2+}$ , due to mutations in both EF hands resulting in a permanently active ("Ca<sup>2+</sup> on") conformation (Gerke and Weber, 1985a; Rety et al., 1999).

p11 was first identified through its association with annexin 2 (described in detail later), when its similarity to other S100 proteins was described (Gerke and Weber, 1985c). p11 exists as a heterotetramer with annexin 2, in which state the majority of its functions are performed (for review, see Gerke and Moss, 2002). The nucleotide and amino acid sequences of p11 are well-conserved between species (determined using *GenBank* sequences), showing a degree of homology with other S100 proteins (Saris et al., 1987b). It is expressed widely, in organs including kidney, intestine and lung (high levels), thymus, brain and spleen (intermediate levels) and liver, heart and testis (low levels) (Saris et al., 1987a). Additionally, more recent reports have shown p11 mRNA to be present at high levels in dorsal root ganglion (DRG) neurons, including small-diameter putative nociceptors (>98% of Na<sub>v</sub>1.8-positive cells also expressed p11 transcript) (Okuse et al., 2002).

p11 is constitutively expressed in many cell types, and has a promoter sequence which does not contain a TATA box and is GC-rich, similar to other "housekeeping" genes (Bird, 1986; Harder et al., 1992). Despite this, more recent studies have revealed that p11 expression is inducible (Huang et al., 2003a), and is modulated by a variety of factors. Importantly, Okuse et al. (2002) described a large increase in p11 mRNA levels in rat DRG neurons following treatment with nerve growth factor (NGF), which is known to reduce pain thresholds in animal models. p11 mRNA and protein production were found to be induced by dexamethasone (Yao et al., 1999b), a glucocorticoid with anti-inflammatory properties, in contrast with the putative pro-inflammatory role of p11 via NGF. Transforming growth factor- $\alpha$  also increased p11 protein levels (Akiba et al., 2000b), as did epidermal growth factor, possibly via receptor tyrosine kinase stimulation of p38 MAP kinase leading to transcriptional activation (Huang et al., 2002). Pawliczak et al. (2001) reported an increase in p11 expression in human bronchial epithelial cells in response to nitric oxide donors, which was found to be mediated by cGMP and protein kinase G, acting on an AP-1 site in the p11 promoter. Finally, interferon- $\gamma$ , the antiviral, anti-tumour and immunoregulatory cytokine, was shown to induce p11 gene and protein expression via the STAT1 protein, which binds to the p11 promoter (Huang et al., 2003b). Interestingly, this paper also reported that reduced p11 expression resulted in enhanced interferon- $\gamma$  release,

suggesting a counter-regulatory (negative feedback) role for interferon- $\gamma$ -stimulated p11 expression. The tricyclic antidepressant imipramine has recently been reported to increase transcript p11 levels; this effect was specific to the forebrain and did not occur in other brain areas (Svenningsson et al., 2006). Progesterone also appears to upregulate p11 expression (Zhang and Wu, 2007). The regulation of p11 expression by intercellular signalling molecules is thus complex.

In addition to transcriptional control of p11 expression, post-translation mechanisms for regulation have also been described. Expression of the binding partner of p11, annexin 2, upregulates cellular levels of p11. In this case, there is no increase in p11 transcript levels, but the half-life of p11 protein is increased more than 6-fold in the presence of annexin 2 (Puisieux et al., 1996). The presence of a stable p11 protein therefore appears to require annexin 2, suggesting that p11 may always act in the form of the annexin 2 heterotetramer. It has also been reported that retinoic acid reduces p11 protein levels by a post-translational mechanism (Gladwin et al., 2000), although more precise details of this effect are lacking. Finally, covalent modification of p11 by transglutaminases has been reported, at both the N- and C-terminal regions of the protein (Ruse et al., 2001). This may be a general mechanism for the regulation of p11 function.

The complex regulation of p11 by growth factors, and by inflammatory mediators such as nitric oxide and IFN- $\gamma$ , suggests that p11 performs a variety of roles in different tissues. Changes in p11 levels have been reported in a variety of disease states, although the aetiological involvement of p11 is not always clear. Alterations in p11 levels have been observed in several forms of cancer, including increased levels in renal cell carcinoma (Domoto et al., 2006a) and anaplastic large cell lymphoma (Rust et al., 2005a). In contrast, a substantial reduction in p11 protein appears to be an essential early stage in the development of prostate cancer, probably caused by a gene methylation-mediated decrease in annexin 2 expression (Chetcuti et al., 2001b). p11 increases have also been reported in irritable bowel syndrome (Camilleri et al., 2007), alcoholic hepatitis (Seth et al., 2003), nerve injury (De et al., 1991) and animal models of multiple sclerosis (Craner et al., 2003a). A decrease in p11 levels was recently described in the anterior cingulate cortex of patients suffering from unipolar major depression disorder, with a causal link proposed via the 5-HT<sub>1B</sub> receptor (Svenningsson et al., 2006).

### **1.2.1 p11-protein interactions and physiological roles**

p11 interacts with many proteins and is involved in a wide variety of physiological processes, including membrane protein trafficking and angiogenesis. A selection of protein interactions

and roles of p11 are discussed here. For a recent review, see Svenningsson and Greengard (2007).

### 1.2.1.1 Annexin 2

p11 exists as a heterotetramer with annexin 2. Although monomeric annexin 2 has been reported, it is not clear whether p11 exists in the cell independently of annexin 2; molar ratios and the rapid degradation of p11 in the absence of annexin 2 would suggest that the majority of p11 protein exists in the heterotetrameric form. Annexin 2 is a  $\text{Ca}^{2+}$ - and phospholipid-binding protein with several N-terminal splice variants (Upton and Moss, 1994), which is translocated to the plasma membrane upon binding to p11, the control of which is effected by a phosphorylation switch on annexin 2 (Deora et al., 2004). The crystal structure of the annexin-2-p11 heterotetramer and p11 alone was described by Rety et al. (1999), with a predicted structure based on this proposed in a subsequent paper (Sopkova-de Oliveira et al., 2000). This is illustrated in Figure 1.1. The interaction is non-covalent, with each annexin 2 peptide forming hydrophobic interactions with both p11 monomers. Helices III and IV of p11 bind to the N-terminus of annexin 2 with high-affinity (Kube et al., 1992). N-terminal acetylation of annexin 2 is essential for its high-affinity interaction with p11.

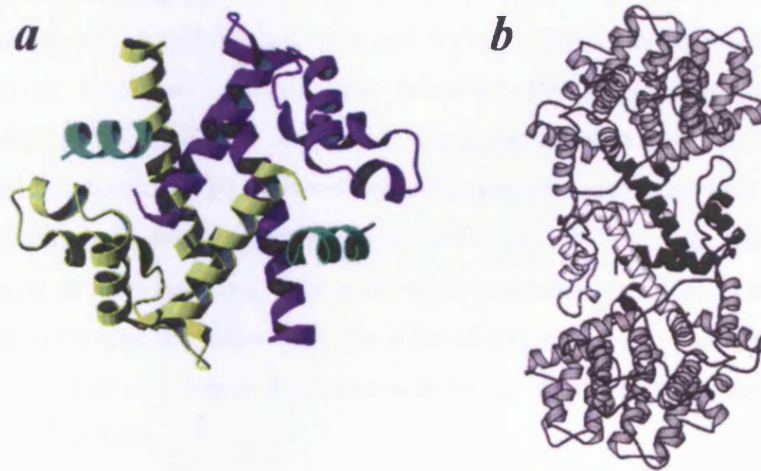


**Figure 1.1** The complex of p11 and the annexin 2 N-terminal peptide. **a:** Crystal structure. p11 is shown in blue and yellow, the annexin 2 N-terminal peptide in green. Taken from Rety et al. (1999). **b:** Predicted p11-annexin 2 heterotetramer model. p11 dimer is shown in black and white, annexin 2 N-terminal peptides in dark grey. Taken from Sopkova-de Oliveira et al. (2000).

Many functions of annexin 2 require its presence at the cell surface. The trafficking of annexin 2 to the cell surface was shown to be p11-dependent, under the control of a phosphorylation switch on annexin 2 (Deora et al., 2004).

The p11-annexin 2 heterotetramer is involved in several processes, one of the most fundamental of which is the organisation of membrane microdomains. These microdomains are regions of membrane with a particular composition, often rich in cholesterol and related lipids, and sometimes referred to as "lipid rafts". Membrane microdomains are thought to be important for the organisation of signalling pathways and molecular trafficking, through colocalisation of membrane proteins. Menke et al. (2005) described the lateral organisation of the annexin 2-p11 heterotetramer in artificial membranes and its influence on the lateral organisation of membrane lipids. The annexin 2-p11 heterotetramer was found to be capable of inducing lipid segregation and therefore likely to affect the presence of membrane microdomains. In a similar vein, Gokhale et al. (2005) reported the induction of membrane microdomain formation by the annexin 2-p11 heterotetramer, via an effect on the regulation of PtdIns(4, 5)P<sub>2</sub> (a phospholipid component of the plasma membrane) clustering. Annexin 2 was recently shown to interact directly with both polymerised and monomeric actin, which was found to have an essential role in maintaining the plasticity of the dynamic-membrane associated actin cytoskeleton (Hayes et al., 2006a). The annexin 2-p11 heterotetramer is also capable of F-actin bundling (Ikebuchi and Waisman, 1990), membrane-cytoskeleton linkage, perhaps via an interaction with actin (Gerke and Weber, 1984), collagen (Wirtl and Schwartz-Albiez, 1990) or tenascin-C (Chung and Erickson, 1994), membrane trafficking and endocytosis (Zobiack et al., 2003). Annexin 2 is required for actin polymerisation-dependent vesicle locomotion, demonstrated by the effects of dominant-negative annexin 2 constructs on the process of macropinocytic rocketing (Merrifield et al., 2001) and thought to be through annexin 2 control of actin polymerisation at the actin-pinosome interface. In addition to these functions, it is likely that the majority of the roles of p11 are in fact performed by the p11-annexin 2 heterotetramer. These functions will be discussed in the subsequent sections according to target protein.

### **1.2.1.2 Nav1.8**

The voltage-gated sodium channel Nav1.8 is expressed exclusively in a subset of sensory neurons, over 85% of which are involved in the detection of noxious stimuli (nociception) (Akopian et al., 1996; Djouhri et al., 2003a), and plays a specialised role in pain pathways (Akopian et al., 1999). Current densities of Nav1.8 expressed in heterologous systems are substantially below endogenous levels in DRG (England, 1998), with channels displaying

properties different from those in DRG neurons (FitzGerald et al., 1999). Microinjection of  $\text{Na}_V1.8$  cDNA into the nuclei of superior cervical ganglion (SCG) or  $\text{Na}_V1.8$ -null mutant DRG neurons, however, produces sodium currents with similar properties and magnitude to wild-type DRG neurons (England, 1998), implying that these cells contain additional factors required for endogenous levels of  $\text{Na}_V1.8$  functional expression. With this in mind, Okuse *et al.* (2002) used the yeast two-hybrid system to search for proteins interacting with the intracellular domains of  $\text{Na}_V1.8$ . p11 was among the proteins identified (Malik-Hall et al., 2003), and was found to increase functional plasma membrane expression of  $\text{Na}_V1.8$ , measured by both electrophysiological and immunological methods (Dekker et al., 2005; Okuse et al., 2002). This effect was shown to be mediated by an interaction between the N-terminus of  $\text{Na}_V1.8$  (proposed to be residues 74-103) and residues 33-78 of p11, corresponding to helix III. The region 74-103 of  $\text{Na}_V1.8$  has a characteristic cluster of acidic and basic amino acids divided by a putative  $\beta$ -strand, which is well-conserved in other species, including mouse (Poon et al., 2004). Two domains with low homology to other sodium channels have been identified (residues 87-90 and 98-102), which may play a role in binding to p11. Other than these regions, however, a fairly high degree of homology with other VGSCs is seen.

The involvement of annexin 2 in the  $\text{Na}_V1.8$ -p11 interaction has not been investigated. 2 models for the annexin 2-p11 complex, a heterotetramer and a heterooctamer, have been proposed (Lewit-Bentley et al., 2000). In both cases, the putative binding domains for  $\text{Na}_V1.8$  are the most peripheral and exposed (Poon et al., 2004). Since annexin 2 is present in higher quantities in the cell than p11 (SE Moss, personal communication), it is likely that annexin 2 forms part of the p11- $\text{Na}_V1.8$  complex.

The p11- $\text{Na}_V1.8$  interaction is discussed further in Chapter 3.

### 1.2.1.3 5-HT<sub>1B</sub>

p11 was recently shown to bind to the serotonin receptor 5-HT<sub>1B</sub>, again through a yeast two-hybrid screen (Svenningsson et al., 2006). 5-HT<sub>1B</sub> is a G-protein-coupled receptor, coupled to the inhibitory subunit G<sub>i</sub> (which inhibits adenylate cyclase, reducing levels of cyclic AMP), p70 S6 kinase and the mitogen-activated protein kinase ERK-2 (Pullarkat et al., 1998), and plays a central role in the regulation of serotonin (5-HT) neurotransmission. Roles have been suggested for the 5-HT<sub>1B</sub> receptor in the pathophysiology of obsessive compulsive disorder, drug addiction, depression, anxiety, aggression and sleep disorders (Gingrich and Hen, 2001; Moret and Briley, 2000b; Saudou et al., 1994). They act as autoreceptors on 5-HT-containing neurons originating from the raphe nuclei, and as heteroreceptors on other neurons

that do not contain 5-HT (Maroteaux et al., 1992; Moret and Briley, 2000a). p11 and 5-HT<sub>1B</sub> (but not related receptors) were found to coimmunoprecipitate and colocalise at the cell surface in the brain, and trafficking of 5-HT<sub>1B</sub> in COS-7 cells was enhanced by p11. p11-null mice showed reduced 5-HT<sub>1B</sub> functional expression and a depression-like phenotype, while mice overexpressing p11 acted as though they had been treated with antidepressants. Cortical slices from p11-null mice displayed characteristics distinct to those of wild-type controls: application of 5-HT depressed the amplitude of field excitatory post-synaptic potentials in wild-type mice only. Consistent with a negative regulation of 5-HT metabolism by 5-HT<sub>1B</sub> receptors, p11-null mice displayed increased levels of 5-HT metabolism. Interestingly, this study described an upregulation of p11 mRNA in the cortices of mice treated with the antidepressants imipramine and tranylcypromine, and with electroconvulsive therapy. p11 mRNA and protein were downregulated in the anterior cingulate cortex in patients suffering from unipolar major depressive disorder. Taken together, these observations support a mechanistic role for p11 in the pathophysiology and treatment of depression. This study concluded that 5-HT<sub>1B</sub> receptor function is modulated by p11, and that this process may be important in neuronal networks that are dysregulated in depression-like states (Svenningsson et al., 2006).

#### **1.2.1.4 ASIC1a**

p11 interacts with the acid-sensing ion channel ASIC1a (Donier et al., 2005). ASIC1a is a voltage-independent, proton-gated ion channel permeable to Na<sup>+</sup> and Ca<sup>2+</sup>, primarily expressed in the brain and dorsal root ganglia (particularly small-diameter nociceptors). In dorsal root ganglion neurons, ASIC1a detects acidification of the extracellular fluid, which can be caused by inflammation, ischaemia and other painful conditions (Voilley, 2004b), and is involved in mechanosensation in neurons innervating the viscera (Page et al., 2004b). In the brain, ASIC1a carries the main proton-gated current, and has been shown to be important in synaptic plasticity and fear conditioning (Wemmie et al., 2002; Wemmie et al., 2003; Wemmie et al., 2004). Ca<sup>2+</sup> overload via ASIC1a activation also appears to be responsible for the majority of ischaemic damage during stroke, following channel activation by ischaemia-induced acidification (Immke and McCleskey, 2001). Interestingly, pharmacological block of ASIC1a has been shown to be effective in limiting ischaemic damage to the brain (Xiong et al., 2004).

Using a yeast two-hybrid assay, Donier et al. (2005) found that p11 binds to the N-terminal domain of ASIC1a, but not to other ASICs. Both membrane-associated immunoreactivity and ASIC1a peak currents were increased by around 2-fold when p11 was co-expressed with ASIC1a in CHO cells, compared to expression of ASIC1a alone. No kinetic or pH-dependence changes in ASIC1a-mediated currents were observed, implying that p11 acts by increasing cell

surface levels of ASIC1a, probably by a trafficking action. The precise residues required for the ASIC1a-p11 interaction have yet to be determined; the N-terminus of ASIC1a, however, does not share sequences with the binding domains identified on other proteins that interact with p11, suggesting a distinct mode of interaction.

### 1.2.1.5 TASK-1

TASK-1 (TWIK-related acid-sensitive K<sup>+</sup> channel-1) is a two-pore-domain K<sup>+</sup> channel, considered to be the prototype of background K<sup>+</sup> channels that set the resting potential and regulate action potential duration, slope and frequency in excitable cells (Duprat et al., 1997). TASK-1 channels are highly regulated by pH, losing most of their activity below pH 6.9, and are inhibited by a variety of hormones and neurotransmitters via phospholipase C activity (Czirjak et al., 2000; Millar et al., 2000a; Talley et al., 2000b). This can result in substantial changes in resting potential and thus cellular excitability (Millar et al., 2000c). TASK-1 is expressed in a wide range of tissues, including brain and other nervous tissue (Lesage and Lazdunski, 2000). It has been shown to play important roles in the regulation of sleep (Meuth et al., 2003), chemoreception in respiratory neurons (Bayliss et al., 2001), initiation of neuronal apoptosis (Lauritzen et al., 2003), excitatory post-synaptic potentials (Millar et al., 2000b; Talley et al., 2000a) and ion transport in the kidney (Hebert et al., 2005).

Two groups have reported the interaction of TASK-1 and p11, describing different binding sites and modes of action. Girard et al. (2002) found that p11 binds to a consensus sequence, Ser-Ser-Val (SSV), at the extreme C-terminus of TASK-1, and that binding is abolished upon deletion of these residues. The association of p11 and TASK-1 masks an endoplasmic reticulum retention signal, Lys-Arg-Arg (KRR), on TASK-1. This sequence normally prevents trafficking to the plasma membrane, but upon p11 binding this restriction is removed, allowing functional TASK-1 expression at the cell surface. Electrophysiological and immunological measurement of TASK-1 indicated an increase in membrane levels in the presence of p11, which was inhibited by a competing C-terminal peptide. More recently, however, Renigunta et al. (2006) published conflicting data, reporting that p11 reduces functional expression of TASK-1 by providing an endoplasmic retention signal. In this study, the C-terminal SSV sequence was not required for interaction with p11, and a helical 40 amino acid domain 120-80 residues proximal to the C-terminus was found to be responsible for the interaction. Binding of p11 to TASK-1 was reported to retard surface expression due to the presence of a di-lysine endoplasmic retention signal at the p11 C-terminus, with supporting electrophysiological and immunological data. Disruption of the interaction increased surface expression of TASK-1, as did removal of the di-lysine motif of p11, consistent with this hypothesis.

The contradictions between these studies have yet to be resolved. Renigunta et al. (2006) suggest that the observation that C-terminal truncation of TASK-1 reduces whole-cell currents (Girard et al., 2002) may be explained by the disruption of another interaction, between TASK-1 and a 14-3-3 family protein, which is known to recognise the RRSSV motif (Rajan et al., 2002b). No explanations were offered, or apparent, for other contradictions. It may be that differences in expression systems are responsible, or that p11 does in fact act in 2 alternate ways upon TASK-1.

Renigunta et al. (2006) observe that TASK-1 binds to the same or overlapping regions of p11 as annexin 2. It therefore appears that TASK-1 trafficking/retention is not mediated by the annexin 2-p11 heterotetramer, but by p11 alone. It is possible that a p11-TASK-1 heterotetramer is formed, but this hypothesis has yet to be tested. Although p11 has been reported to be very unstable in the absence of annexin 2 (Puisieux et al., 1996), it is possible that interaction with TASK-1 is capable of preventing p11 degradation.

#### **1.2.1.6 TRPV5/6**

TRPV5 and TRPV6 are epithelial  $Ca^{2+}$  channels, belonging to the transient receptor potential (TRP) superfamily. They mediate the rate-limiting influx step in active  $Ca^{2+}$  reabsorption in the kidney, proximal intestine and placenta (Hoenderop et al., 2001c; Hoenderop et al., 2002). Their activity is regulated by a  $Ca^{2+}$ -dependent feedback mechanism (Nilius et al., 2002), and by reinsertion of channels from an intracellular pool (Nilius et al., 2001). They contain conserved motifs for regulatory activities including protein kinase C phosphorylation, ankyrin repeats and PDZ domains (Hoenderop et al., 2001d).

Both TRPV5 and TRPV6 were shown to interact with p11, via the C-terminal tail sequence VATTV between amino acids 598 and 603 on TRPV5 and corresponding residues on TRPV6 (van de Graaf et al., 2003). This is similar to the SSV sequence proposed to be the TASK-1 p11 interaction site (Girard et al., 2002). TRPV5 interacts with the p11-annexin 2 heterotetramer, since annexin 2 was able to be co-immunoprecipitated with TRPV5 in the presence (but not absence) of p11. p11 binding to TRPV5 and TRPV6 was shown to be critical for channel activity, assessed by whole-cell patch-clamp analysis in HEK293 cells. This was ascribed to the requirement of p11 for TRPV5/6 trafficking, visualised immunocytochemically (van de Graaf et al., 2003). No reports of TRPV5 and TRPV6 expression in dorsal root ganglia exist, meaning that a role in the peripheral nervous system is unlikely.

### 1.2.1.7 Tissue plasminogen activator

Plasmin is a serine protease, the key function of which is the degradation of fibrin, (a major component of blood thrombi and clots). Other significant functions include collagenase activation and the degradation of other circulating proteins. Extracellular matrix proteolysis by plasmin (and other proteases) is required for the invasiveness of cancer cells and for angiogenesis, which in turn is necessary for tumour growth. Plasmin is synthesised as a precursor, plasminogen, and released in this form into the circulation. Plasminogen is expressed by a variety of cells types, with the majority of production coming from the liver. The conversion of plasminogen to plasmin is performed by another serine protease, tissue plasminogen activator (tPA), at the surface of endothelial cells.

p11 is expressed as a heterotetramer with annexin 2 on the surface of endothelial (Kassam et al., 1998b) and tumour (Yeatman et al., 1993b) cells. It was shown to stimulate the activation of plasminogen via a tPA-dependent process, increasing the catalytic activity 20-90 fold (Kassam et al., 1998e;Kassam et al., 1998a). The C-terminal penultimate and ultimate lysine residues of p11 (helix IV) were shown to participate in this stimulation, since their cleavage by basic carboxypeptidases resulted in a loss of tPA-stimulatory ability (Fogg et al., 2002). Although early studies focused on annexin 2 as the plasminogen/tPA receptor, Macleod et al. (2003) used surface plasmon resonance on an immobilised lipid bilayer to demonstrate that p11, but not annexin 2, binds directly to plasminogen and tPA via the C-terminal lysine residues. This interaction results in the colocalisation of plasminogen and tPA, providing a mechanism for the increased catalytic activity observed in the presence of p11. The binding of tPA and plasmin to p11 also protects against inhibition by physiological inhibitors, PAI-1 and alpha2-antiplasmin, respectively (Kwon et al., 2005a). Deletion of annexin 2, however, was found to result in impaired fibrinolysis and reduced neoangiogenesis *in vivo* (Ling et al., 2004), appearing to contradict this localisation of the tPA binding site. This can be explained, however, by the observation that annexin 2 is required for post-translational stability of p11, with rapid degradation occurring in its absence (Puisieux et al., 1996). p11 levels are thus likely to be very low in the annexin 2-null mouse.

A degree of regulation occurs in the stimulation of plasminogen activation by p11. Thrombin, a protease involved in fibrin production, induces endothelial cell-surface expression of the annexin 2-p11 heterotetramer, with the ultimate effect of increasing fibrinolysis (Peterson et al., 2003). In a curious twist, Kwon et al. (2002) reported that the annexin 2-p11 heterotetramer acts as a plasmin reductase via the cysteine residues 61 and 82 on p11. This results in plasmin autoproteolysis and the release of A(61), an anti-angiogenic protein, opposing the plasmin-

generating, pro-angiogenic role of p11. The annexin 2-p11 heterotetramer also inhibits plasmin-dependent fibrinolysis, providing a further layer of regulation (Choi et al., 1998a).

The role of p11 in plasmin generation and thus extracellular matrix degradation and angiogenesis has led to its investigation in several cancers. In many cases, changes in p11 expression have been linked to tumourigenesis. For example, p11 expression in renal cell carcinoma was reported to be upregulated (Domoto et al., 2006b) with a similar result in anaplastic large cell lymphoma (Rust et al., 2005b). In contrast, a substantial reduction in p11 protein appears to be an essential early stage in the development of prostate cancer, probably caused by a gene methylation-mediated decrease in annexin 2 expression (Chetcuti et al., 2001a). RNA interference-mediated silencing of p11 was shown to attenuate the invasiveness of colorectal cancer cells, via a reduction in plasmin generation and thus extracellular matrix degradation (Zhang et al., 2004). Finally, regulation of fibrosarcoma cell invasiveness by p11, via extracellular plasmin production, was reported (Choi et al., 2003).

The involvement of the annexin 2-p11 heterotetramer in angiogenic processes, following the identification of annexin 2 as a tPA activator (Hajjar et al., 1994), led to the investigation of the effects of annexin 2 deletion on angiogenesis in the mouse. Ling et al. (2004) described increased fibrin deposition, reduced clearance of arterial thrombi and deficiencies in endothelial cell surface plasmin generation. Endothelial cell migration and invasion through *in vitro* fibrin/collagen lattices and in *in vivo* Matrigel assays was markedly reduced, as was neovascularisation of oxygen-primed neonatal retina. The paper concluded that annexin 2-bound endothelial cell surface plasmin acts both intra- and extravascularly to promote neoangiogenesis. The relevance of these findings to tumour growth was shown in a recent report describing contributions of annexin 2 to tumour invasion and progression in breast cancer (Sharma et al., 2006a). An antibody against annexin 2 was found to inhibit lung carcinoma growth via reduced plasminogen activation, suggesting that annexin 2 may be a target for angiostatin, and demonstrating the therapeutic potential of work on this system (Sharma et al., 2006b).

tPA is also capable of converting pro-BDNF (brain-derived neurotrophic factor) to its active form, BDNF (Pang et al., 2004c). This activity appears to be essential for long-term hippocampal plasticity and long-term potentiation, required for long-term memory (Pang et al., 2004b). It is not clear if p11 is involved in this tPA-dependent activation, but it appears likely.

### 1.2.1.8 BAD

BAD (Bcl-xL/Bcl-2-Associated Death Promoter) is a member of the Bcl-2 family of apoptosis-regulating proteins. It promotes apoptosis via pathways leading to changes in mitochondrial membrane permeability, and is believed to act in a manner different to other Bcl-2 family members, due to the lack of an otherwise conserved C-terminal transmembrane domain (Hsu et al., 1997b). p11 was reported to bind preferentially to the underphosphorylated form of BAD, in contrast to the 14-3-3 proteins, which bind upon phosphorylation (Hsu et al., 1997e). In the same study, the expression of p11 in CHO cells was found to suppress BAD expression-induced apoptosis, without affecting BAD levels. Expression of p11 is therefore anti-apoptotic, in agreement with the interesting observation that p11 expression is increased following transformation induced by viral oncogenes (Ozaki and Sakiyama, 1993). Nerve growth factor (NGF) is required for the survival of a subset of sensory neurons. p11, which is upregulated by NGF, can substitute for NGF in this function. The mechanism of action of NGF on cell survival is thus thought to be via p11-mediated inhibition of apoptosis (Masiakowski and Shooter, 1990).

### 1.2.1.9 AHNAK

AHNAK (non-acronymic) was first identified as a gene undergoing transcriptional repression in cell lines derived from human neuroblastoma and certain other tumours (Shtivelman et al., 1992). It is also downregulated by transforming (oncogenic) forms of the small G-protein RAS in fibroblasts (Zuber et al., 2000). AHNAK is an exceptionally large protein of around 700kDa, encoded by an intronless gene (Kudoh et al., 1995; Shtivelman and Bishop, 1993b). Its exact biological function is unknown, although its abundance increases dramatically upon cell differentiation (Shtivelman and Bishop, 1993a), and several interacting proteins have been identified. AHNAK associates with cardiac L-type  $\text{Ca}^{2+}$  channels at the plasma membrane, transmitting information from  $\beta$ -adrenoreceptors via protein kinase A (Haase et al., 1999), and has been proposed to play a role in the maintenance and functional organisation of the subsarcolemmal cytoarchitecture by providing a link between L-type channels and the actin cytoskeleton (Hohaus et al., 2002). AHNAK is also localised to the plasma membrane in a variety of other cell types, the process of which appears to be regulated by  $\text{Ca}^{2+}$  signalling (Borgonovo et al., 2002). Benaud et al. (2004) demonstrated that AHNAK interacts with actin and the annexin 2-p11 heterotetramer at the plasma membrane, which is required for AHNAK plasma membrane localisation. p11 was found to mediate the interaction between annexin 2 and the C-terminal regulatory domain of AHNAK. They reported that downregulation of AHNAK affects the cell membrane cytoarchitecture of cells, preventing actin cytoskeleton reorganisation and providing a molecular mechanism for the observed membrane organisation

effect of annexin 2 (Babiyshuk et al., 2002;Gerke and Moss, 2002). Although p11 contains the residues that bind to AHNAK, neither p11 nor annexin 2 are capable of AHNAK interaction alone: annexin 2 interaction with p11 is required for high-affinity binding of p11 to AHNAK (De et al., 2006a). The C-terminal domain of AHNAK involved in p11 binding was defined as a 20 amino-acid sequence, which did not show homology to any other proteins outside the AHNAK family. This paper also reported that the localisation of the annexin 2-p11 heterotetramer at the plasma membrane was controlled by cellular signalling, in agreement with previous observations.

The functional significance of the interaction between AHNAK and the annexin 2-p11 heterotetramer appears to be through organisation of the cell membrane cytoarchitecture, through interactions with actin and perhaps other entities. The role of annexin 2 in membrane organisation has been well documented, and is likely to be important in a range of physiological processes, including channel clustering and endo/exocytosis.

#### **1.2.1.10 Phospholipase A<sub>2</sub>**

Phospholipase A<sub>2</sub> (PLA<sub>2</sub>) represents a group of enzymes that catalyse the hydrolysis of an ester bond in phospholipids, generating lipid products which can serve as intracellular 2<sup>nd</sup> messengers or can be metabolised to inflammatory mediators. In particular, the release of arachidonic acid (AA) from cellular membranes, which can then be converted to pro-inflammatory leukotrienes, prostaglandins and other eicosanoids, is a central process in inflammation. Cytosolic PLA<sub>2</sub> (cPLA<sub>2</sub>) is a large 85kDa protein and is regulated at both transcriptional and post-translational levels by cytokines and other pro-inflammatory factors (see references within Wu et al., 1997d). Wu et al. (1997c) used a yeast two-hybrid screen to identify p11 as a protein interacting with the C-terminal domain of cPLA<sub>2</sub>, confirming the interaction by co-immunoprecipitation from a human epithelial cell line. *In vitro*, p11 was shown to inhibit cPLA<sub>2</sub> activity, while p11 antisense increased PLA<sub>2</sub> activity in the epithelial cell line. The inhibition of cPLA<sub>2</sub> by p11 was found to be independent of annexin 2, although annexin 2 does produce a small additive inhibition of cPLA<sub>2</sub> (Wu et al., 1997b).

The inhibitory effect of p11 on cPLA<sub>2</sub> provides a mechanism for the control of pro-inflammatory molecule levels. Akiba et al. (2000a) found that transforming growth factor- $\alpha$  was able to stimulate prostaglandin generation under the control of p11, while another group reported that the anti-inflammatory compound dexamethasone reduced arachidonate release by inducing p11 expression, thus inhibiting cPLA<sub>2</sub> activity (Yao et al., 1999a). Epidermal growth factor induced p11 expression and thus downregulated AA release in human epithelial cells

(Huang et al., 2002). The opposite effect was observed upon application of retinoic acid, which reduced p11 protein levels by a post-translational mechanism and thus increased cPLA2 activity (Gladwin et al., 2000).

In addition to the anti-inflammatory role of p11 suggested by these findings, the interaction between p11 and cPLA2 was reported to control AA release as a function of epithelial cell confluence (Bailleux et al., 2004b). This study found that intercellular contacts between kidney cells directly control cPLA2 activity through alterations in the stoichiometry of the p11-cPLA2 interaction. The regulation of cPLA2 activity by p11 thus plays a role in multiple processes, and contributes to the control of inflammatory mediator release induced by intercellular signalling molecules.

#### **1.2.1.11 Cathepsin B**

For tumour cell invasion and metastasis, limited degradation of the extracellular matrix is required to facilitate invasion, angiogenesis and other processes. The lysosomal cysteine protease cathepsin B is one of the proteases involved in this degradation. Cathepsin B is capable of degrading extracellular matrix proteins laminin, fibrin and collagen IV at the neutral or acidic pH often found in sites of tumour growth (Buck et al., 1992; Lah et al., 1989). It has been observed that its activity, secretion and membrane association are increased in malignant tumours, in particular at their invasive edges, and that this correlates with a poor prognosis (Campo et al., 1994; Emmert-Buck et al., 1994; Frosch et al., 1999; Rempel et al., 1994). Cathepsin B can also activate other proteolytic enzymes, including urokinase-type plasminogen activator, allowing actions on cellular signalling pathways (Kobayashi et al., 1991).

Mai et al. (2000) found that p11 interacts with cathepsin B both *in vitro* and *in vivo*. A complex consisting of the annexin 2-p11 heterotetramer and cathepsin B was reported, the formation of which appeared to result in the activation of procathepsin B. p11 and cathepsin B were found to colocalise on the cell surface, suggesting a role for p11 in cathepsin B trafficking. Upregulation of annexin 2 on the surface of tumour cells (Yeaman et al., 1993a) implies that this may result in increased cathepsin B activity, leading to matrix degradation and increased tumour invasiveness.

#### **1.2.1.12 PCTAIRE-1**

PCTAIRE-1 (name deriving from residues in a conserved region) is a protein kinase with similarities to the cyclin-dependent kinase family. It is ubiquitously expressed and present at

high levels in neuronal cells, including the brain. The function of PCTAIRE-1 has yet to be defined, although roles have been proposed in  $\text{Ca}^{2+}$ -dependent exocytosis (Liu et al., 2006) and neurite outgrowth (Graeser et al., 2002). Yeast two-hybrid screen discovered an interaction between PCTAIRE-1 and p11, confirmed using pure recombinant proteins (Sladeczek et al., 1997). This interaction was later shown to occur *in vivo*, in rodent brain, and was found to require the presence of both the N- and C-terminal domains (but not the catalytic core domain) of PCTAIRE-1 (Le et al., 1998). The functional significance of this interaction is currently unclear.

### **1.2.2 Importance of p11 in cellular function**

The interactions of p11 with target proteins are remarkable in both diversity and physiological relevance. Proteins from many different families, with a variety of distinct functions are bound by p11, often resulting in a change in physiological activity. Many are trafficked to the plasma membrane, while others are inhibited or activated. The distinct binding sites of each of these proteins (where defined) suggest the possibility of multiple simultaneous interactions between p11 and other proteins. Combined with the ability of p11 to organise membrane microdomains, this advocates a model where p11 regulates cellular function by the formation of defined areas of plasma membrane, populated by controlled groups of membrane proteins. p11 thus appears to be an important regulatory molecule for the control of cellular function, perhaps with a more general role in the control of membrane trafficking and organisation.

### 1.3 PAIN AND NOCICEPTION

This thesis examines the role of p11 in pain pathways in the peripheral nervous system. The following section provides an introduction to the process of pain sensation, from detection of noxious stimuli to the processing and interpretation of these signals in the brain.

Pain is defined as “an unpleasant sensory and emotional experience associated with actual or potential tissue damage or described in terms of such damage” (International Association for the Study of Pain: [www.iasp-pain.org](http://www.iasp-pain.org)). This is distinct from nociception, the detection of noxious (tissue-damaging) stimuli, in that it involves cognitive and emotional (affective) components requiring higher-level cortical processing. As such, pain can occur in disease states in the absence of nociception, while nociception does not necessarily result in pain. In the majority of circumstances, however, pain results from nociception, arising from the application of a noxious stimulus.

Nociception has an intrinsic physiological value in promoting withdrawal from tissue-damaging stimuli, through spinal reflex pathways in response to afferent input. Higher-level processing, however, allows the association of negative affective responses with the circumstances surrounding the noxious stimulus, resulting in aversion and subsequent behavioural modification to avoid these circumstances and thus further injury. Under conditions of inflammation, pain thresholds are lowered by both peripheral and central neuronal plasticity, resulting in hyperalgesia (increased pain in response to a noxious stimulus) or allodynia (pain caused by a normally innocuous stimulus). This increased sensitivity has survival value in promoting the protection of injured tissues, allowing healing to occur. Under conditions of chronic inflammation, however, the reduction in pain thresholds may outlive its usefulness. Additionally, pain can result from nerve damage, for example from mechanical trauma, HIV infection, diabetic neuropathy or certain drugs. This pain, described as neuropathic in origin, is generally spontaneous or allodynic in nature, in the absence of nociception, and as such confers no survival value. Instead, chronic inflammatory and neuropathic pain often cause significant emotional distress and result in reduced quality of life.

Pain is an important clinical problem, and is one of the most common reasons for seeking medical attention. A large-scale study by the World Health Organisation found that 22% of adult primary care patients reported persistent pain, resulting in increased likelihood of psychological disorders (including depression), poor health perception, and interference with work (Gureje et al., 1998). Whilst acute pain can be treated effectively with a range of pharmacological agents, including volatile anaesthetics, opioids and ketamine, chronic

inflammatory and neuropathic pain states are frequently refractory to analgesics. Inflammatory pain is often treated with anti-inflammatory compounds in an attempt to reduce the cause of hyperalgesia. In particular, non-steroidal anti-inflammatory drugs (NSAIDs), which inhibit the enzyme cyclo-oxygenase, are often efficacious in the treatment of inflammatory pain. Neuropathic pain, however, is more complex. Different patients may respond to differing pharmacological agents, often leading to an iterative (trial and error) approach to treatment. In many cases, effective treatment is achieved using drugs with primary indications for other conditions, such as gabapentin (an anticonvulsant) and tricyclic antidepressants (e.g. amitriptyline), although the mechanisms by which these suppress neuropathic pain are still under investigation. Cancer-related pain, present in 30-45% of cancer patients on diagnosis and rising to 65-90% with advanced disease, is thought to be a combination of inflammatory and neuropathic pain. Damage to invaded tissues causes the release of inflammatory mediators, while direct mechanical pressure on sensory nerves can occur upon tumour growth. Certain cytotoxic drugs used to treat cancer can also cause nerve damage and thus neuropathic pain. Treatment is with a combination of pharmacological agents, non-pharmacological interventions (e.g. surgery) and psychological therapy. A significant proportion of patients suffering from chronic or neuropathic pain, however, do not obtain complete relief (Sindrup and Jensen, 1999). For example, 10-20% of cancer patients do not experience adequate pain control free from side effects (Meuser et al., 2001). In all areas of pain, treatment is often accompanied by adverse side effects, including gastrointestinal irritation by NSAIDs and central effects, such as drowsiness and dependence, from opioids. There is therefore a need for novel therapeutic approaches to the treatment of pain. Of particular interest are agents acting on the peripheral nervous system, allowing the elimination of centrally-mediated side effects. This possibility has been used to promote the study of nociception with a view to identifying novel therapeutic targets.

#### **1.4 NOCICEPTION AND DRG PRIMARY AFFERENT NEURONS**

The interaction between p11 and Nav1.8, which is one of the main topics of this thesis, occurs in a subset of primary afferent neurons involved in the detection of noxious stimuli. This section discusses the physiology and histology of these cells, and the mechanisms by which they transduce and transmit information from noxious stimuli.

The primary afferent neurons of the somatosensory nervous system convey sensory information from their peripheral termini to the spinal cord. The cell bodies of sensory neurons innervating the limbs and trunk are contained within the dorsal root ganglia (DRG), while for orofacial structures the trigeminal ganglia perform this role.

Multiple subtypes of sensory neuron are contained within the DRG. These neurons are often classified according to anatomical features, most notably diameter, termination site and degree of myelination, and functional characteristics, including conduction velocity and the modality of stimuli to which they respond. Additionally, grouping based on neurotrophin dependence or gene expression (including membrane proteins, neurotransmitters and transcription factors) has proven useful in defining subgroups of sensory neurons. While it is often assumed that neurons within a functional group display identical anatomical and physiological characteristics and gene expression profiles, new levels of complexity continue to be described. Only the broadest categories, therefore, are fully characterised at present. These are discussed below; also see Wood (2000) and Julius & Basbaum (2001a). Figure 1.2 illustrates the distinct types of nociceptor currently identified.

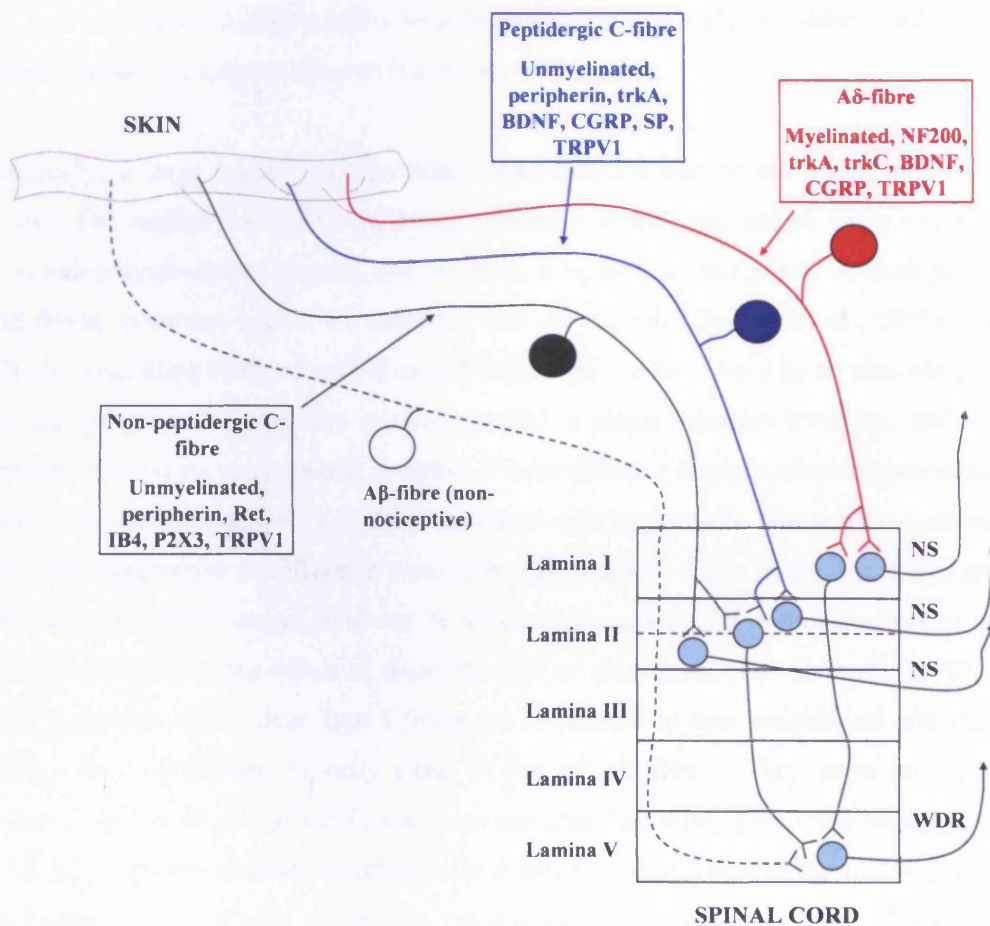


**Figure 1.2 Diagram illustrating nociceptor subtypes.** Subsets of primary afferent neurons express different genes and terminate in different laminae of the spinal cord dorsal horn. Nociceptor-specific (NS) and wide dynamic range (WDR) neurons project from the spinal cord to higher structures. BDNF: brain derived neurotrophic factor; CGRP: calcitonin gene-related peptide; SP: substance P. Note that this diagram is extremely simplified, and for clarity omits dendritic connections from projection neurons.

### 1.4.1 Anatomical and functional classification of DRG neurons

One of the primary criteria used to categorise primary afferent neurons is conduction velocity (Perl, 1992). A $\alpha$ -fibres conduct at  $>30\text{m}\cdot\text{sec}^{-1}$ , A $\beta$  at  $10\text{-}30\text{m}\cdot\text{sec}^{-1}$ , A $\delta$  at  $1.2\text{-}10\text{m}\cdot\text{sec}^{-1}$ , and C-fibres at  $<1.2\text{m}\cdot\text{sec}^{-1}$  (approximate for mouse/rat). These differences in conduction velocities are due to a combination of axon diameter and the degree of myelination present, with larger diameter and more heavily myelinated axons conducting faster than smaller, unmyelinated axons. A $\alpha$  and A $\beta$ -fibres are thus heavily myelinated, large diameter neurons. A $\delta$ -fibres are thinly myelinated and of intermediate diameter, while C-fibres are small diameter and unmyelinated. A and C-fibres can be distinguished histologically by staining with Nissl substance: cell bodies of A-fibres appear as large, light cells, whereas those of C-fibres appear small and dark (Lawson, 1979). Immunochemical discrimination is also possible using antibodies to the 200kDa neurofilament subunit N200, present in A-fibres (Lawson et al., 1984), and peripherin, an intermediate neurofilament expressed only in C-fibres and often used to identify small, nociceptive neurons (Goldstein et al., 1991).

Interestingly, a large number of functional characteristics can be correlated to conduction velocity. The majority of A $\beta$ -fibres detect innocuous stimuli, particularly light touch. They also include proprioceptive neurons, and innervate skin, muscles and joints. A small proportion of A $\beta$ -fibres, however, appear to transduce noxious stimuli (Djouhri et al., 1998a; Lawson, 2002), demonstrating that anatomical classification can not be viewed as an absolute guide to functional properties. A $\beta$ -fibres generally detect a single stimulus modality, and display adaptation in response to a repeated stimulus. Fibres detecting noxious stimuli (nociceptors), in contrast, are often polymodal, and show sensitisation in response to repeated noxious stimuli, an essential requirement for effective protection against further tissue injury. A $\delta$ -fibres respond to noxious mechanical stimuli, and can be subdivided according to responsiveness to intense thermal stimulation or the effect of tissue damage on thresholds (Treede et al., 1998). Two distinct categories are evident: type I fibres are responsive to heat, mechanical and chemical stimuli, with a conduction velocity close to that of A $\beta$ -fibres. They show an increasing response to intense heat, and sensitise to burn and chemical injury (Wall and Melzack, 1999). Type II A $\delta$ -fibres are generally mechanically insensitive, responding to thermal and chemical stimuli only, with a reduced conduction velocity compared to type I fibres. They show an adapting response to intense heat, and are not sensitised to heat injury (Wall and Melzack, 1999). C-fibres are generally polymodal nociceptors, responding to both noxious thermal and mechanical stimuli, and to chemical stimuli associated with tissue damage, such as acid and ATP. Around 10% of C-fibres, however, convey only innocuous thermal information (Hunt and Mantyh, 2001a). Itch is also thought to be C-fibre-mediated, although the subgroups responsible have yet to be identified. The presence of "silent" nociceptors, which do not

appear to possess a natural stimulus but become active only when sensitised by tissue injury, has also been revealed (Michaelis et al., 1996). Both A and C-fibre silent nociceptors have been identified following peripheral inflammation (Xu et al., 2000).

Action potential characteristics vary between classes of DRG neuron. Two classes of action potential are evident: narrow (when displayed as voltage over time), tetrodotoxin (TTX)-sensitive, and broad/inflected potentials containing a TTX-resistant component. These differences can be ascribed to the differential expression of TTX-resistant voltage-gated sodium channels (VGSCs), and to the involvement of high-threshold voltage-gated calcium channels (Blair and Bean, 2002). A robust correlation between action potential shape and fibre type exists, with all C-fibres displaying broad action potentials. The shape of A-fibre action potentials appears to be dependent on receptive properties: low threshold mechanosensitive neurons have narrow action potentials, while those with high thresholds have an inflected action potential (Ritter and Mendell, 1992). It is interesting to note that all nociceptive fibres have long-duration afterhyperpolarisations (AHPs), in contrast to the short AHPs of non-nociceptive A and C-fibres (Djouhri et al., 1998b).

#### **1.4.2 Differential gene expression in distinct populations of nociceptors**

Several distinct populations of nociceptors can be defined based on gene expression profile. A number of genes are used to classify nociceptors in this way, most commonly growth factor receptors, neurotransmitters, ion channels and transcription factors.

In early stages of development, cells destined to become nociceptive neurons express the high-affinity nerve growth factor tyrosine kinase receptor TrkA, and require nerve growth factor (NGF) for survival. NGF null-mutant mice are born lacking almost all small-diameter sensory neurons, and are accordingly profoundly hypoalgesic (Crowley et al., 1994). Postnatally, however, a proportion of C-fibres lose dependence on NGF, with a concurrent downregulation of TrkA expression (Molliver and Snider, 1997). These cells express the tyrosine kinase receptor RET, and become dependent on glial cell line-derived neurotrophic factor (GDNF, the endogenous ligand of RET) (Molliver et al., 1997). GDNF-sensitive C-fibres express cell surface glycoconjugates that bind the lectin IB4, the enzyme fluoride-resistant acid phosphatase (FRAP) and are non-peptidergic; that is, they do not synthesise neuropeptides such as calcitonin gene-related peptide (CGRP). Additionally, the ATP-gated receptor P2X<sub>3</sub> is expressed almost exclusively in IB4-positive neurons in rats (Burgard et al., 1999). The subset of C-fibres retaining NGF sensitivity, accounting for around 40% of total DRG cells, constitutively synthesise the neuropeptides CGRP and substance P, but do not bind IB4.

Although quantitative functional differences have been shown between these groups (Stucky and Lewin, 1999) with respect to heat sensitivity, TTX-resistant currents and action potential duration, distinct functional roles have yet to be determined. IB4-negative neurons were also found to express a transient proton-gated current (taken to be indicative of acid-sensing ion channel (ASIC) expression), absent in IB4-positive cells, with a quantitative difference in capsaicin sensitivity (Dirajlal et al., 2003). It is not yet clear if these groups perform distinct roles in chronic inflammatory or neuropathic pain states.

### **1.4.3 Transduction of noxious stimuli**

To convey information regarding a noxious stimulus to the brain, primary afferent neurons must convert the original stimulus modality into an electrical signal, a process known as transduction. This signal, the generator potential, produces a local depolarisation of the plasma membrane, which with sufficient magnitude will initiate an action potential. Nociceptors are capable of detecting thermal, mechanical or chemical stimulus modalities, with many being polymodal. Each stimulus modality is transduced by a distinct mechanism, although not all are well understood. In general, transduction is performed by ion channels gated by the stimulus modality in question. This is rapid, usually in the millisecond timescale, to allow an appropriate behavioural response to be made before major tissue damage occurs.

#### **1.4.3.1 Transduction of noxious mechanical stimuli**

Many painful clinical conditions involve mechanically-induced pain, often occurring as a result of a normally innocuous stimulus (allodynia). Neuronal mechanosensory channels mediate the sensations of hearing, light touch and noxious mechanical stimulation. Mechanotransduction in hair cells of the inner ear, required for hearing, has been studied extensively, and may inform the search for the noxious mechanosensor. Corey et al. (2004a) found that siRNA to the transient receptor potential (TRP) channel TRPA1 diminished hair cell transduction currents, making this channel a promising candidate for the hair cell mechanotransducer. This hypothesis, however, was questioned by the findings of two independent studies, both of which reported that TRPA1 knockout mice displayed no deficits in a number of measures of auditory detection (Bautista et al., 2006c; Kwan et al., 2006d). These mice, however, expressed a truncated transcript of TRPA1 due to the deletion strategy used, although one study inserted an endoplasmic reticulum (ER) retention signal to prevent cell surface expression in the event of the expression of a truncated protein (Kwan et al., 2006e). A more likely explanation for the discrepancy, however, is an off-target effect of the siRNA used by Corey et al. (2004b). The identity of the hair cell mechanotransducer has therefore yet to be determined.

Both polymodal C-fibre nociceptors and a subset of A $\delta$ -fibres respond to noxious (but not innocuous) mechanical stimuli. Neurons from the superior cervical ganglion, however, are not mechanosensitive, providing a useful control when searching for the noxious mechanosensor: a key requirement is its differential expression between these cell types. Since mechanonociceptors terminate in free nerve endings, and neuromas and cultured DRG neurons are mechanosensitive, specialised organs appear unnecessary for noxious mechanotransduction. Channels from several families have been proposed as the mechanotransducer for noxious stimuli, including the ASIC and TRP families. While mechanically-gated channels are abundant, this may not always be of physiological relevance, since channels gated by mechanical stimuli at the single-channel level often exist in mechanically insensitive cells (Morris and Horn, 1991), or have an established physiological function (e.g. NMDA receptors (Paoletti and Ascher, 1994)). In these cases, it is possible that non-physiological membrane deformation favours an open channel conformation, generating a mechanosensitive artefact. Likewise, proteins clearly identified to play a role in mechanosensation may not function as mechanically-gated ion channels (e.g. Wetzel et al., 2007b), suggesting that mechanotransduction may require a multi-protein complex.

The proteins required for noxious mechanosensation in mammals have yet to be identified, despite the provision of many leads from the study of *C.elegans* and *Drosophila*. Mammalian ASICs belong to the same family as the ENaC ion channel subunits MEC-4, MEC-6 and MEC-10, which are required for light touch sensation in *C.elegans* (Ernstrom and Chalfie, 2002). ASIC2 (Garcia-Anoveros et al., 2001; Price et al., 2000a) and ASIC3 (Price et al., 2001b) are detectable by immunological methods in mechanosensory structures, consistent with a role in mechanosensation. Null-mutant mice for ASIC2, assessed using the skin-nerve preparation, were found to have normal responses to supra-threshold mechanical stimulation of A $\delta$  and C-fibres, but a decreased firing rate of A $\beta$ -fibres (Price et al., 2000b), suggesting a role for ASIC2 in light touch sensation, but not noxious mechanosensation. In ASIC3-null mice, however, A $\delta$  mechano-nociceptors displayed a reduction in firing to supra-threshold stimuli, along with a small increase in mechanical threshold (Price et al., 2001c), although no change in C-fibre mechanical response was observed. Behaviourally, ASIC3 knockout mice have been assessed in 2 independent studies (Chen et al., 2002d; Price et al., 2001a). While neither group found an effect on acute mechanical withdrawal thresholds, measured using von Frey hairs, Chen et al. (2002c) observed reduced responses to high-intensity noxious stimuli, regardless of modality. This suggests that rather than a direct role in mechanotransduction, ASIC3 is involved in the modulation of moderate- to high-intensity pain sensation. Using mechanical stimulation of the neuronal cell body as a model of sensory terminal mechanosensation, Drew et al. (2004) demonstrated that mechanotransduction in DRG neurons from ASIC2 and ASIC3 null-mutants

comparable to wild-type. It therefore seems likely that ASIC2 and ASIC3 are not noxious mechanotransducers. A recently-identified blocker of mechanically activated currents in DRG neurons was found to have no effect on ASIC-mediated currents (Drew and Wood, 2007b).

It has been proposed that the noxious mechanosensor may be a member of the TRP family of ion channels, since currents mediated by these channels share properties with mechanically-activated currents in DRG neurons. Both are inhibited by micromolar concentrations of gadolinium and ruthenium red, are attenuated by extracellular  $\text{Ca}^{2+}$ , and have non-selective cation permeability (Drew et al., 2002; Watanabe et al., 2002a). TRPV4 shows a degree of homology to a mechanically-gated channel expressed in *C.elegans* (Liedtke and Friedman, 2003), and is gated by hypotonicity (Liedtke et al., 2000a), suggesting that it may play a part in mechanosensation. Subsequent work, however, found that TRPV4 is an unlikely candidate for the noxious mechanosensor, due to the lack of effect of pressure on channel gating (Strotmann et al., 2000b), and the slow time course of hypotonicity-induced activation (Liedtke et al., 2000b; Strotmann et al., 2000a). Xu et al. (Xu et al., 2003) later performed work strongly implying that gating of TRPV4 by hypotonicity is via an indirect mechanism, involving the tyrosine phosphorylation of the channel by an Src kinase. TRPV4 null-mutants displayed impaired but not absent pressure sensation, assessed by Randall-Selitto assay, but no change in von Frey withdrawal thresholds (Suzuki et al., 2003). This study also reported the expression of TRPV4 in only 11% of DRG neurons. It remains unclear whether TRPV4 can be activated directly by mechanical stimuli, but at present it does not appear to be a strong candidate for the noxious mechanosensor.

TRPA1 is another candidate for the noxious mechanosensor in DRG neurons. It is expressed at free nerve endings by small neurons of the DRG, as well as those of the trigeminal root ganglia, and displays behaviours expected of nociceptive transducers, including block by ruthenium red and calcium sensitivity. Inactivation does not appear to occur in depolarised cells, consistent with the non-desensitising nature of mechanical pain (Nagata et al., 2005). TRPA1 null-mutant mice were found to have an increased von Frey withdrawal threshold, and a reduced response to supra-threshold stimulation compared to control animals (Kwan et al., 2006b). A gene dosage effect was also suggested by the intermediate phenotype of heterozygotes. TRPA1, however, is expressed in C but not A $\delta$ -fibres (Kobayashi et al., 2005), despite the pricking pain induced on A $\delta$ -fibre stimulation. It therefore appears that, while TRPA1 may contribute to or even be responsible for noxious mechanotransduction in C-fibres, another high-threshold mechanotransducer fulfils this function in A $\delta$ -fibres.

While direct mechanotransduction by a mechanically-gated ion channel remains the most likely mechanism for the detection of noxious mechanical stimuli, various accessory proteins required for this process have been identified. Wetzel et al. (2007a) found that stomatin-like protein 3 (SLP3), a mammalian *mec-2* (a gene involved in mechanosensation in *C.elegans*) homologue expressed in sensory neurons, appears to be an essential subunit of a mammalian mechanotransducer. Using the skin-nerve preparation, they found a substantial reduction in the number of A $\beta$  and A $\delta$ -fibres responding to mechanical stimuli, but no change in C-fibre mechanoreceptive properties.

Drew et al. (2007a) recently identified FM1-43, a fluorescent dye used to label cell membranes, as a permeant blocker of mechanically-activated currents in DRG neurons. Intraplantar FM1-43 was shown to increase noxious mechanical withdrawal thresholds, assessed by both von Frey filaments and Randall-Selitto test. As mentioned previously, this dye does not affect currents mediated by ASICs. FM1-43 may prove to be a useful tool for the identification of the noxious mechanotransducer.

It is possible that the transduction of noxious mechanical stimuli is mediated indirectly, by a chemical process. Mechanical pressure would cause the release of a diffusible chemical messenger, which then acts (intra-or extracellular) on chemically-gated ion channels. In the bladder, stretch promotes the release of ATP from epithelial cells, activating P2X3 receptors on primary sensory neurons. P2X3 null mice show reduced urination as a result of this (Cockayne et al., 2000b). In particular, recent work suggests a role for keratinocytes in noxious mechanotransduction (Lumpkin and Caterina, 2007). Due to the time delay inherent in indirect signalling, however, it is likely that normal noxious mechanotransduction occurs via a direct mechanism.

#### **1.4.3.2 Transduction of noxious thermal stimuli**

Both noxious heat and noxious cold are detected by primary afferent nociceptors. In culture, around 45% of small to medium diameter neurons display heat-evoked currents with a threshold of 43°C, while 5-10% respond to heat with a threshold of 52°C (Nagy and Rang, 1999); (Caterina et al., 2000b). Noxious cold (4°C) activates only 10-15% of C-fibres, but a greater proportion of nociceptors appear to be activated by temperatures  $\leq 0^\circ\text{C}$  (Simone and Kajander, 1997a).

Noxious thermal stimuli are transduced by members of the TRP channel family, labelled the “thermoTRPs”. TRPV1 (VR1) is expressed at free nerve endings of nociceptive neurons

(Tominaga et al., 1998b), and is activated by the vanilloid capsaicin and by extracellular acidification (Caterina et al., 1997a). It confers sensitivity to heat when expressed in heterologous systems, and is expressed almost exclusively in small-diameter sensory neurons (Caterina et al., 1997b), mostly C-fibres. The thermal activation threshold for this channel is around 43°C, similar to that observed in a subset of nociceptors, and single channel currents can be evoked by heat, demonstrating direct thermal gating (Tominaga et al., 1998a). Interestingly, heat-activated currents are inhibited by the TRPV1 antagonists ruthenium red and capsazepine, and nearly all heat-sensitive neurons are capsaicin-sensitive (Nagy and Rang, 1999). These factors strongly suggest that TRPV1 is a transducer of noxious heat in DRG neurons. Simultaneous publications from two groups reported the phenotype of TRPV1-null mice, both showing deficits in thermosensation (Caterina et al., 2000a; Davis et al., 2000b). Caterina et al. (2000f) reported that TRPV1-null mice had reduced responses to acute thermal stimuli above 50°C, but not at lower temperatures. In contrast, Davis et al. (2000a) found no significant differences acute thermal nociception, although a trend to reduced sensitivity was observed ( $p=0.053$ ), and comment was made by the authors that the mixed strain background may have masked a difference. Both groups found that TRPV1 DRG neurons did not show currents activated by heat of 43-50°C, and Caterina et al. (2000c) described changes in heat sensitivity in C-fibres, using the skin nerve preparation, and in spinal neurons, recording at the dorsal horn, at 41-43°C. This corresponds to the threshold at which TRPV1 is activated, implying a direct link between the lack of TRPV1 and these deficits. The confinement of behavioural deficits to temperatures above 50°C, however, require a more complex explanation, which may involve a limited and specific role for TRPV1-positive neurons in behavioural responses to noxious heat. Differences between behavioural studies and those using isolated neurons may be due to a lack of expression of other heat-sensitive channels in dissociated cells, or could suggest the involvement of non-neuronal cells in the detection of noxious heat.

A key observation from these studies is the continued ability to detect noxious heat in TRPV1-null animals, implying that other mechanisms for the transduction of noxious thermal stimuli exist. Caterina et al. (1999b) used an *in silico* screen to identify sequences related to TRPV1. The majority of sequences detected corresponded to TRPV2, named vanilloid receptor-like protein 1 (VRL-1) at the time of the study. TRPV2 was studied in HEK293 cells and *Xenopus* oocytes, and was found to be insensitive to capsaicin and protons. Thermal stimuli sufficient to cause pain (43°C) did not activate the channel, but the channel was found to be gated by high temperatures, with a threshold of around 52°C, and inhibited by ruthenium red. TRPV2 is not expressed in IB4-positive or substance P-positive neurons (i.e. C-fibres), but is confined to myelinated medium to large diameter DRG neurons, a proportion of which express CGRP

(Caterina et al., 1999a) and correspond to a subpopulation of A $\delta$  neurons (McCarthy and Lawson, 1997). This subpopulation displays properties consistent with the high thermal threshold Type I A $\delta$  neurons (Wall and Melzack, 1999). In culture, a subset of medium diameter, capsaicin-sensitive DRG neurons were found to express a high threshold, heat-activated current, correlated with TRPV2 and a lack of TRPV1 expression (Ahluwalia et al., 2002). Caterina et al. (2000e) also reported similar currents in DRG cultures from TRPV1-null mutant mice. These data strongly suggest that TRPV2 is responsible for the thermal sensitivity of high threshold, Type I A $\delta$  neurons. The generation and analysis of TRPV2-null mice will provide a definitive test of this hypothesis.

Woodbury et al. (2004) reported that nociceptors lacking TRPV1 and TRPV2 in the mouse have normal heat responses, indicating that other channels are important in the transduction of noxious heat. The detection of noxious heat is thus performed by more than one transducer. TRPV3 and TRPV4 are also thermally gated (Smith et al., 2002b; Watanabe et al., 2002b; Xu et al., 2002), but do not appear to mediate heat-activated currents in the DRG. TRPV channels, however, can form heteromultimers: for example, TRPV1 and TRPV3 heteromultimerise in heterologous systems and colocalise in small DRG neurons (Smith et al., 2002a). This means that the transduction of thermal stimuli of different intensities may be mediated by a variety of TRPV channel combinations. The differential expression patterns of various TRPs in subpopulations of DRG neurons suggests a mechanism for intensity coding of noxious thermal stimuli.

Noxious cold is also capable of producing the sensation of pain. Spontaneous pain with the sensation of coldness is a common feature of certain types of neuropathic pain syndromes, and subpopulations of both C and A $\delta$ -fibres respond to noxious cold (Simone and Kajander, 1997b). The cyclic terpene alcohol menthol, which occurs naturally in mint oils, produces a cooling sensation when applied to the skin. Like capsaicin, the topical application of small doses produces a mild analgesic effect. Higher doses cause burning, irritation and pain (Green, 1992; Wasner et al., 2004). Since cold-sensitive fibres are directly activated or sensitised by menthol (Henzel and Zotterman, 1951), it has proven to be a useful tool in the search for transducers of noxious cold. Several theoretical mechanisms have been proposed for the transduction of cold stimuli, including direct action at a cold-gated channel, modulation of channel properties, or inhibition of protein function.

Reid and Flonta (2001c) first described an ionic current activated by cooling in DRG neurons. Using Ca<sup>2+</sup> imaging to identify cold-responsive neurons (around 7% of DRG neurons), they compared electrophysiological properties to those of cold-insensitive cells. All cold-sensitive

neurons expressed a cold-activated mixed cationic current, potentiated by menthol, insensitive to amiloride, and sensitive to changes in  $Ca^{2+}$  concentration. Menthol was shown to increase intracellular  $Ca^{2+}$  concentration via stimulation of  $Ca^{2+}$  entry, providing a mechanism for neuron activation. In a later paper, Reid et al. (2002) described properties of cold-sensitive DRG neurons distinct from cold-insensitive nociceptors. Cold-sensitive nociceptors had shorter action potentials, smaller AHPs and more rapidly decaying  $Na^+$  currents. The majority of the cold/menthol-activated current was carried by  $Na^+$  ions, and was blocked by high concentrations of the TRPV1 antagonist capsazepine, although this is known to act at other channels at high concentration.

The molecular identity of a channel conferring cold sensitivity in DRG was identified by expression cloning, using Fura-2  $Ca^{2+}$  imaging to identify cells responding to menthol (McKemy et al., 2002a). A trigeminal ganglia (TG) cDNA library, chosen due to the high proportion of cold-sensitive neurons compared to DRG, was expressed in HEK293 cells for screening. A single cDNA clone conferring cold sensitivity was identified, and termed CMR1. When expressed in *Xenopus* oocytes, electrophysiological analysis revealed currents elicited by menthol and icilin (a super-cooling agent), but not by analogous compounds or capsaicin. In transfected HEK293 cells, menthol- and cold-evoked currents displayed properties similar to those observed in trigeminal neurons. CMR1 was found to have significant homology to certain members of the TRP channel family, most notably those of the TRPM class, and was found to be the rat orthologue of the human channel TRPM8. Transcripts for this protein were found in a subset of small-diameter sensory neurons in DRG and TG, similar to that expressing TRPV1, and representing C and possibly  $A\delta$ -fibres. Transcripts were not found in larger diameter neurons, but were more prevalent in TG than DRG, consistent with the greater proportion of cold-sensitive cells in this structure.

Peier et al. (2002) identified TRPM8 as a cold sensor at the same time as the work by McKemy et al. (2002b), using an alternative approach. A bioinformatic search based on TRP channel homology identified TRPM8, which was found to be expressed in a subset of small diameter sensory neurons, and not co-expressed with CGRP and TRPV1. A cold- and menthol-activated current was produced upon expression in CHO cells, with similar properties to the cold-activated current in DRG. This approach was used by the same group to identify ANKTM1, a TRP-like channel expressed in nociceptors and activated by cold temperatures (Story et al., 2003). ANKTM1 was shown to be expressed in a peptidergic population of nociceptors expressing TRPV1 (a distinct population from those expressing TRPM8). Expression in CHO cells identified a sensitivity to low temperatures ( $\leq 17^\circ C$ ), resulting in  $Ca^{2+}$  influx, sensitive to icilin but not menthol. A subpopulation of DRG neurons was found to possess properties

consistent with ANKTM1 expression. This channel was later shown to be responsible for currents evoked by pain-causing mustard oil (Jordt et al., 2004). ANKTM1 was later termed TRPA1, and found to be upregulated by nerve damage and inflammation, contributing to the cold hypersensitivity observed under neuropathic and inflammatory conditions (Obata et al., 2005). Interestingly, this paper reported TRPA1 (but not TRPM8) upregulation by administration of NGF, via the p38 MAPK pathway.

Two independent studies analysed the effect of TRPA1 deletion from mice. Kwan et al. (2006c) found deficits in behavioural responses to noxious cold, assessed using cold plate (0°C) and acetone tests. This effect was found to be gender-dependent: a trend towards diminished sensitivity in TRPA1-null males was greater in female mice, adding an additional layer of complexity to the role of TRPA1 in the detection of noxious cold. Bautista et al. (2006b), however, found no difference from control in either cold plate or acetone tests, and further found no differences in electrophysiological assays of cold sensitivity in DRG neurons. These differences may arise from subtle differences in assay methodology; for example, Kwan et al. (2006a) recorded the number of responses in a fixed period, whereas Bautista et al. (2006a) measured time to first response. Additionally, different constructs for TRPA1 deletion were used in each study. In both cases, a truncated fragment was expressed, but Kwan et al. (2006f) included an ER retention signal to retard fragment trafficking, as described previously in the discussion of mechanotransduction. Since TRP channels are known to form heteromultimers, it is possible that truncated TRPA1 fragments could exert dominant-negative effects on a variety of other channels, confounding phenotypic analysis. Alternatively, difficulties in assessing cold-induced pain behaviour (for example, some mice shown no response to very cold temperatures (Story and Gereau, 2006)) may explain these discrepancies.

A recent paper from Zurborg et al. (2007) provides an explanation for the differences between cellular and whole-animal studies on the role of TRPA1 in cold sensing. They used a heterologous expression system to show that intracellular  $Ca^{2+}$  activates TRPA1 via an EF-hand domain, and that it is increased intracellular  $Ca^{2+}$  concentration during cooling that activates the channel, rather than gating by cold. This study used a logical series of experiments to demonstrate that this indirect, non-physiological mechanism is responsible for previous observations of TRPA1 gating by cold. Responses to cold were seen in TRPA1-expressing cells but also in TRPA1-negative neurons, with almost identical thresholds.  $Ca^{2+}$ -insensitive TRPA1 mutants showed cold sensitivity comparable to controls animals.  $Ca^{2+}$ -buffered whole cell patch-clamp experiments also found no activation of TRPA1 channels by cold. The role of TRPA1 as a noxious cold sensor is thus unclear.

Several studies report populations of cold-sensitive DRG neurons expressing neither TRPM8 nor TRPA1. Munns et al. (2006) found that a third of cold-responsive DRG neurons did not respond to any TRP channel agonist, including menthol (TRPM8) and mustard oil (TRPA1). Another group reported a novel cold-sensitive DRG neuron subpopulation, sensitive to cold but with rapid adaptation, expressing neither TRPA1 nor TRPM8, and possibly corresponding to the rapidly-adapting cold sensors described *in vivo* (Babes et al., 2006). Bautista et al. (2006d) also observed two distinct populations of cold-sensitive neurons in DRG culture, one responding to menthol but neither to mustard oil, suggesting the presence of an additional transduction mechanism for noxious cold in DRG neurons. Inhibition of  $K^+$  channels (Viana et al., 2002b) and of the  $Na^+/K^+$  ATPase (Spray, 1986) have both been suggested as mechanisms for depolarisation in response to cold. Inhibition of the  $Na^+/K^+$  ATPase by ouabain elicited a depolarisation of only 10-15% of that induced by cooling, and did not produce action potentials in DRG neurons (Reid and Flonta, 2001a), implying a secondary role in cold transduction. Cooling did, however, inhibit a background  $K^+$  current by 49-72% (32-20°C) that was found to be resistant to tetraethylammonium (TEA) and 4-aminopyridine (4-AP). This current was suggested to be carried by the two-pore domain channel TREK-1, although this was speculative (Reid and Flonta, 2001b). Subsequently, Viana et al. (2002a) found that cold-sensitive TG neurons differed from cold-insensitive by  $K^+$  current expression profile. In cold-sensitive neurons, cooling inhibited  $K^+$  leak channels, causing depolarisation and firing limited by the slower reduction of  $I_h$ , a cationic inward current. In cold-insensitive neurons this inhibition also occurred, but did not cause depolarisation due to the presence of another  $K^+$  current,  $IK_D$ . This current acts as an “excitability brake” in cold-insensitive neurons. 4-AP block of  $IK_D$  induced cold-sensitivity in previously unresponsive neurons, leading to the suggestion that cold allodynia could be caused by changes in  $K^+$  channel distribution in sensory nerve termini. For this mechanism of cold transduction to be physiologically relevant, the relative distributions of the  $K^+$  channels observed here (in the soma) must be similar to that at the nerve termini, the site of cold transduction.

The transduction of noxious cold stimuli thus appears to involve several ion channels, the relative contributions of which have yet to be assessed. A more detailed characterisation of cold-sensing DRG neurons and the roles of various channels, similar to that performed for the detection of noxious heat, is likely to provide a more specific model for this process.

### 1.4.3.3 Transduction of noxious chemical stimuli

Tissue damage and inflammation cause the release of a variety of chemical mediators, the detection of which induces protection of the affected body part from further trauma. Nociceptive nerve termini in the vicinity of tissue damage are exposed to these mediators, and are able to transduce this exposure into electrical activity. Certain chemicals are able to activate nociceptors directly, while others cause sensitisation to other stimulus modalities. Hypoxia-induced alterations in extracellular fluid (ECF) composition, often occurring during exercise or compromised cardiac function, are also capable of causing nociceptor excitation.

Upon tissue damage, inflammation and hypoxia, the extracellular environment surrounding the nociceptor terminal is acidified. Extracellular pH may fall from 7.4 to around 6 under these conditions, due to release of protons from lysed cells, degranulation of stimulated mast cells, and lactic acid formation where metabolism exceeds oxygen supply. These conditions, along with exposure to exogenous acid or iontophoresis of protons, evoke pain (Jones et al., 2004; Voilley, 2004a). Upon application of acid to a receptive field, around 40% of nociceptors, primarily mechanoheat polymodal C-fibres, display a sustained, non-desensitising action potential discharge (Steen et al., 1992; Steen et al., 1995).

Several cation channels expressed in DRG neurons are gated by protons, notably TRPV1 and the ASIC family. Most ASIC subtypes are expressed in DRG, with ASIC1b and ASIC3 showing exclusive or preferential expression. Heterologous expression of most ASIC subtypes results in a rapidly-desensitising current in the physiological pH range, inconsistent with the sustained activity observed in nociceptors, or a biphasic, Na<sup>+</sup>-selective sustained current activated by non-physiological pH drops (reviewed in Julius and Basbaum, 2001b). ASICs are known to form heteromultimers *in vivo*, with properties distinct from that of their component subunits (Benson et al., 2002; Xie et al., 2002). Co-expression of ASIC2b and ASIC3, a combination specific to sensory neurons, produces currents resembling native acid-evoked currents in DRG, with a sustained, non-selective cation permeable component (Lingueglia et al., 1997a). Additionally, while most ASIC-mediated currents are activated only on rapid changes of pH, currents mediated by ASIC3-containing channels can be activated by the gradual acidification more likely to occur in physiological conditions (Lingueglia et al., 1997b). Amiloride, the non-specific ASIC blocker, was found to reduce pain resulting from transdermal iontophoresis of protons in humans (Jones et al., 2004), and from abdominal acetic acid and intraplantar formalin in animal models (Ferreira et al., 1999). Although amiloride also affects other ion channels, the specific ASIC antagonist A-317567 displayed clear analgesic effects in an animal model of post-operative pain (Dube et al., 2005), in which the central role of decreasing pH in pain induction has been established (Woo et al., 2004). Studies on ASIC3-

null mice produced conflicting results, showing electrophysiological (at pH 5 but not pH 4) but not behavioural deficits to acidic stimuli (Chen et al., 2002b; Price et al., 2001d). Mice expressing a dominant-negative form of ASIC3, intended to investigate the role of ASIC3 heteromultimers, displayed a substantial reduction in ASIC-mediated proton-induced currents in DRG neurons, but increased behavioural sensitivity to mechanical and chemical (including acidic) stimuli (Mogil et al., 2005). It has been found that several ASICs are upregulated during inflammation (Voilley et al., 2001), although no proton-induced action potential generation was observed under these conditions. Overall, these data suggest an important but not exclusive role for ASICs in the detection of protons by nociceptors.

TRPV1, the heat-sensitive capsaicin receptor expressed in DRG neurons, is also gated by protons. TRPV1-mediated responses to capsaicin and heat are potentiated by protons in the physiological range (pH 6-8), while activation occurs at room temperature (and therefore by body temperature) at pH < 6 (Tominaga et al., 1998c). It has been shown that protons produce this effect by direct interaction with TRPV1, via several negatively-charged residues in putative extracellular loops (Jordt et al., 2000). The responses of TRPV1 to low pH are similar to currents observed in dissociated DRG neurons (Bevan and Yeats, 1991), suggesting that TRPV1 could be the transducer of low pH in DRG neurons. Additionally, acid sensitivity and TRPV1 expression (measured by capsaicin sensitivity) show a strong correlation (Bevan and Geppetti, 1994). DRG from TRPV1-deficient mice show a marked reduction in sustained proton-evoked currents, supporting the role of TRPV1 in acid-evoked nociception. Proton sensitivity is not abolished, however, implying a role for other pH-sensitive channels (Caterina et al., 2000d), perhaps including the ASICs.

Tissue damage often results in the release of ATP from necrotic cells, which is normally absent from the extracellular fluid. ATP is thus a specific indicator of cell damage, and can be detected by nociceptors. Receptors for ATP and related substances, known as "purinergic" receptors, are present on DRG neurons, in addition to many other cell types. Purinergic receptors fall into 2 groups, ligand-gated ion channels (ionotropic, P2X family) and G-protein-coupled (metabotropic) receptors (P2Y family). Expression of P2X<sub>3</sub>, an ionotropic ATP receptor, is limited to putative nociceptors (Chen et al., 1995; Cook et al., 1997), suggesting a role in nociception. The P2X<sub>3</sub>-mediated current, however, is rapidly desensitising, inconsistent with nociceptor properties (Virginio et al., 1998). Coexpression of P2X<sub>3</sub> with P2X<sub>2</sub> results in a slowly-adapting ATP-gated current similar to that observed in nociceptors, suggesting that the P2X<sub>2</sub>/P2X<sub>3</sub> heteromultimer underlies this current (Lewis et al., 1995). DRG neurons from P2X<sub>2</sub>/P2X<sub>3</sub> double knockout mice were found to be insensitive to exogenous ATP application and behavioural responses to intraplantar formalin (which causes tissue damage) were reduced (Cockayne et al., 2005), consistent with this hypothesis. Certain data, resulting from analysis

of a P2X<sub>3</sub>-null mouse, suggest that homomultimeric P2X<sub>3</sub> receptors are sufficient to account for ATP-induced nociception (Cockayne et al., 2000a), but this remains unclear. Likewise, the role of other P2X or P2Y receptors in ATP-induced pain has yet to be investigated.

Bradykinin (BK), a peptide inflammatory mediator involved in the induction of hyperalgesia, is capable of exciting nociceptors directly (Inoue and Ueda, 2000b). It acts primarily on the free nerve endings of C-fibres (Ueda et al., 2000) to cause depolarisation and subsequent pain-related behaviour in naïve animals (Inoue and Ueda, 2000a). BK acts through the receptor subtypes B<sub>1</sub> and B<sub>2</sub>, both G-protein coupled receptors linked to phospholipase C (PLC). Activation of these receptors generates IP<sub>3</sub> and DAG. DAG causes depolarisation of the nerve membrane by stimulation of protein kinase C (PKC) (Burgess et al., 1989b), which phosphorylates a non-specific cation channel, causing increased opening and thus depolarisation (Wall and Melzack, 1999). BK activation of sensory neurons increases intracellular Ca<sup>2+</sup> via IP<sub>3</sub> production and voltage-gated Ca<sup>2+</sup> channel activation, with multiple effects on the neuron (Burgess et al., 1989a). In naïve animals, these actions are likely to be mediated by the B<sub>2</sub> receptor, which is expressed constitutively by nociceptors, rather than B<sub>1</sub>, the expression of which is induced upon tissue damage.

The plant-derived compounds capsaicin, menthol and mustard oil are all capable of exciting nociceptors and causing pain. The molecules involved in transducing these stimuli have been discussed previously in this section. Other ligands acting on nociceptors include 5-HT (serotonin), histamine and noradrenaline.

#### **1.4.4 Transmission of noxious stimuli**

Following the transduction of a noxious stimulus into a localised depolarisation at the distal nerve terminal, this signal must be transmitted to the spinal cord synapse. This is achieved by the generation of an action potential, a self-propagating depolarisation along the length of the axon. The majority of the depolarising (inward cationic) current required for this action potential is carried by voltage-gated sodium channels (VGSCs), of which there are many subtypes with varying biophysical properties, expression profiles, and cellular localisation. The subtypes Na<sub>v</sub>1.1, 1.2, 1.6, 1.7, 1.8 and 1.9 are expressed in the mature DRG, while Na<sub>v</sub>1.3 is expressed in the embryonic sensory nervous system. The expression of Na<sub>v</sub>1.8 and 1.9 is limited to a subset of neurons in the sensory nervous system, over 85% of which are putative nociceptors (Akopian et al., 1996; Djouhri et al., 2003a). VGSCs are discussed in more detail subsequently.

Potassium channels are important regulators of neuronal excitability. Several  $K^+$  currents have been described in DRG, including delayed rectifiers ( $I_K$ ), which open in response to depolarisation, and  $I_A$  currents, which activate rapidly in response to depolarisation, then inactivate (Gold et al., 1996). Depending on their opening characteristics, they can control the rate of repolarisation following an action potential, the membrane excitability, or the rate of firing. Activation of  $K^+$  channels in DRG neurons is controlled either by intracellular  $Ca^{2+}$  concentration (which rises following an action potential) or by membrane hyperpolarisation.

Voltage-activated calcium channels, activated by membrane depolarisation, also contribute to the action potential, in particular to the characteristic “hump” on the falling phase of the C-fibre action potential.  $Ca^{2+}$  entry regulates excitability via the control of  $Ca^{2+}$ -gated ion channels, but also causes a variety of responses through intracellular signalling cascades. In particular,  $Ca^{2+}$  entry is critical for presynaptic neurotransmitter release. At least 5 types of voltage-activated  $Ca^{2+}$  channel are expressed in sensory neurons (L, N, P/Q, T and R), each having distinct effects on neuronal excitability (Wall and Melzack, 1999).

#### **1.4.5 Inflammatory pain**

Following inflammation, nociceptive thresholds are decreased. This sensitisation is mediated by changes to both peripheral and central components of pain sensation. Central sensitisation involves processes including long-term potentiation, which strengthens synapses, increases in descending facilitation and decreases in descending inhibition in the spinal cord, discussed briefly in subsequent sections. Peripheral sensitisation is a result of plastic changes in nociceptors, resulting in reduced thresholds either to all stimuli (i.e. an effect on transmission), or to a specific stimulus modality (an effect on transduction).

Tissue damage results in the release of inflammatory mediators from recruited immune cells, particularly mast cells, and from proteolytic plasma cascades. Moreover, repeated nociceptor excitation results in the release of pro-inflammatory compounds from their distal termini, a process known as neurogenic inflammation and resulting in local vasodilatation, plasma extravasation and mast cell degranulation. Inflammatory mediators released by these routes include NGF, cytokines (TNF- $\alpha$ , interleukin-1/6), histamine, prostaglandins (particularly PGE<sub>2</sub> and bradykinin), 5-HT, protons, CGRP and substance P (released mainly from nociceptors), although this is not a comprehensive list. These mediators induce plastic changes in nociceptors, resulting in enhanced sensitivity to noxious (or previously innocuous) stimuli. Interestingly, a normally-unresponsive (“silent”) class of nociceptors become active under

conditions of inflammation (Lewin and Mendell, 1994; Meyer et al., 1991), resulting in a greater spinal input for a given stimulus intensity.

A variety of post-translational mechanisms contribute to peripheral sensitisation. In particular, ligand binding to G-protein-coupled receptors such as  $H_1$  (histamine), coupled to  $G_s$ , results in the formation of cyclic AMP, activating protein kinase A (PKA). This effect can be opposed by opiates and cannabinoids, the receptors for which couple to  $G_i$  and therefore inhibit adenylate cyclase. Bradykinin binds to  $BK_2$   $G_q$ -coupled receptors which stimulate phospholipase C, activating PKC. Other ligands, such as NGF, bind to tyrosine kinase receptors which activate protein kinase C (PKC). PKA and PKC phosphorylate a variety of target proteins to induce sensitisation. Phosphorylation of  $Na_v1.8$  by PKA or PKC causes a shift in the current-voltage relationship and possibly the voltage-dependence of activation (FitzGerald et al., 1999; Gold et al., 1998; Vijayaragavan et al., 2004a), making the neurons more excitable to all stimulus modalities. Bradykinin induces PKC- $\epsilon$ -mediated phosphorylation of TRPV1 and TRPV2, resulting in thermal but not mechanical hyperalgesia (Cesare et al., 1999; Cesare and McNaughton, 1996). Some inflammatory mediators act directly on ion channels, without the need for 2<sup>nd</sup> messenger pathways. For example, protons bind to the extracellular loops of TRPV1, causing an increased channel sensitivity to heat or capsaicin (Tominaga et al., 1998e; Welch et al., 2000). In the presence of pH 6 or lower, even ambient body temperature can activate TRPV1 (Tominaga et al., 1998d).

Changes in gene expression levels also contribute to peripheral sensitisation following inflammation. For example, NGF acts through the tyrosine kinase receptor TrkA to activate p38 MAPK pathways (Ganju et al., 1998), resulting in an increase in expression of TRPV1 and therefore thermal hyperalgesia (Ji et al., 2002). Actions of NGF through TrkA also result in increased expression of  $Na_v1.8$ , while GDNF causes upregulation of both  $Na_v1.8$  and  $Na_v1.9$  (Fjell et al., 1999b; Fjell et al., 1999a). Many other transcriptional changes are induced by inflammatory mediators to effect peripheral sensitisation.

Voltage-gated sodium channels (VGSCs) are thought to play a significant role in the development of inflammatory hyperalgesia.  $Na_v1.8$  was thought to be important in this process, due to its phosphorylation and transcriptional upregulation by inflammatory mediators, but deletion of  $Na_v1.8$  from the mouse had only a small effect (although this was proposed to be due to compensatory upregulation of other VGSCs) (Akopian et al., 1999). Nociceptor-specific deletion of  $Na_v1.7$ , however, resulted in a substantial reduction in inflammatory pain, suggesting a major role for this channel in peripheral sensitisation (Nassar et al., 2004). Several human genetic conditions that result in spontaneous inflammatory-type pain

(erythromelalgia) have been mapped to the  $Na_v1.7$  gene, with gain-of-function mutations causing increased channel activity (Choi et al., 2006b; Cummins et al., 2004b; Dib-Hajj et al., 2005a; Han et al., 2006b; Han et al., 2007; Harty et al., 2006a; Lampert et al., 2006b; Sheets et al., 2007a). A gain-of-function mutation in  $Na_v1.7$ , resulting in a reduction in fast inactivation and therefore a persistent  $Na^+$  current, was recently shown to be the cause of paroxysmal extreme pain disorder, a genetic disorder resulting in spontaneous pain with some inflammatory character (Fertleman et al., 2006b). Surprisingly, loss-of-function mutations in this gene appear to result in complete insensitivity to pain, with no other neurological changes (Cox et al., 2006a).

For a review of the mechanisms of inflammatory pain, see Julius and Basbaum (2001d) or Kidd and Urban (2001). A diagram illustrating a selection of peripheral mechanisms of inflammatory hyperalgesia is shown in Figure 1.3.

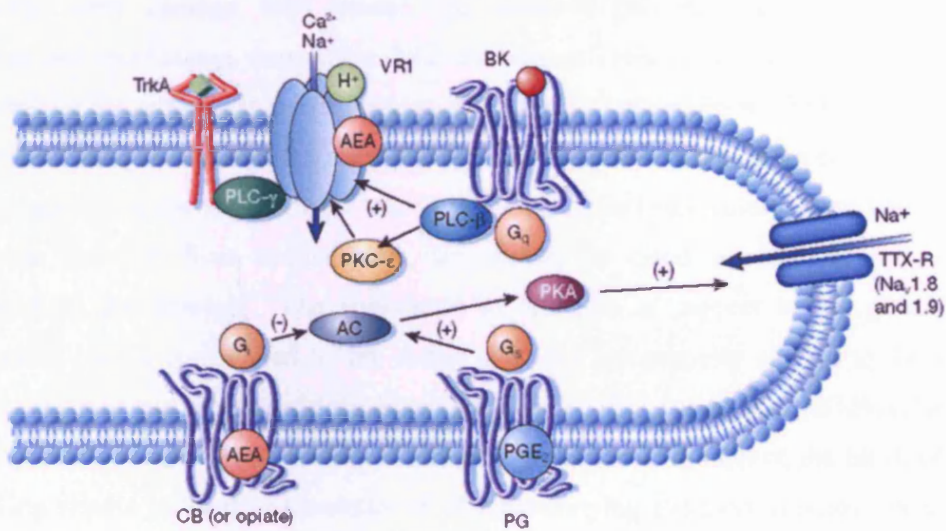
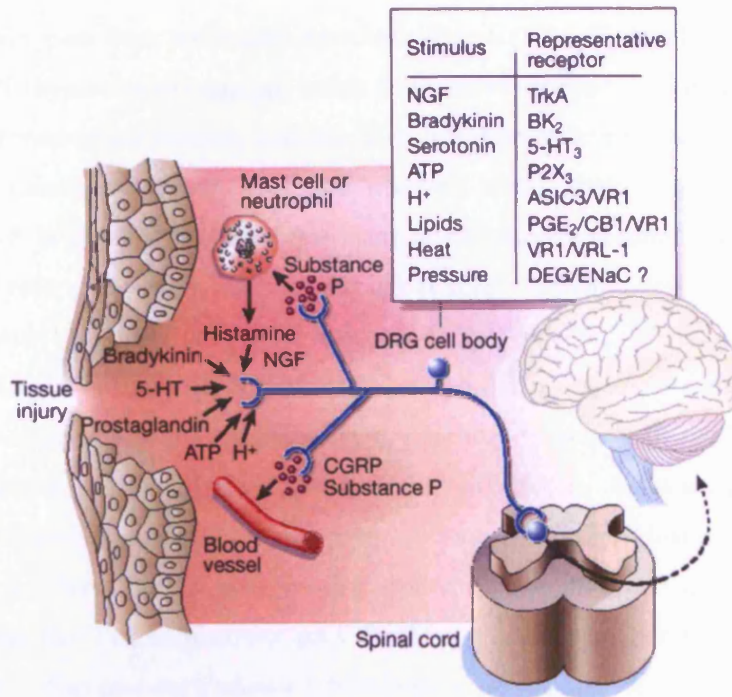


**Figure 1.3** Processes contributing to inflammatory hyperalgesia in primary afferent neurons. Taken from Julius and Basbaum (2001c).

While a proportion of the processes involved in peripheral sensitisation by inflammation have been identified, it is likely that others remain to be discovered. It should be noted that many processes important to the development of inflammatory hyperalgesia occur at the level of the spinal cord or higher structures. Central nervous system changes important in hyperalgesia are currently the focus of investigation by many groups, and may provide novel therapeutic targets.

### 1.4.6 Neuropathic pain

Spontaneous pain, pain from previously innocuous stimuli (allodynia) and increased pain from noxious stimuli (hyperalgesia) can all result from nerve damage. This damage can be a consequence of mechanical trauma, diabetes, HIV infection, cancer or many other conditions, and generally causes neuropathy (necrotic neuronal death, often described as Wallerian degeneration). It is generally believed that many of the changes required for the maintenance of neuropathic pain occur at the level of the spinal cord. A particularly interesting example described recently involves microglial-induced BDNF release, which causes decreased expression of the Cl<sup>-</sup> channel KCC2. The resulting shift in Cl<sup>-</sup> gradient switches light touch-related GABA-ergic interneuron function from inhibitory to neutral or facilitatory, allowing light touch to cause pain (Coull et al., 2003c; Coull et al., 2005a). Since the primary neuronal damage that triggers a neuropathic pain state occurs peripherally, however, changes in the properties of peripheral nerves must be responsible for the induction of neuropathic pain. Additionally, the fact that neuropathic pain develops gradually implies that changes in gene expression, rather than post-translational modifications, are responsible.

Following nerve damage, both injured and uninjured primary afferent neurons display abnormal and spontaneous activity (the "afferent barrage") (Han et al., 2000). This is likely to be the trigger for subsequent plastic changes in the spinal cord and brain. The first stage in the phenotypic changes causing abnormal activity in damaged primary afferents is the loss of trophic support, in the form of NGF and GDNF (and related molecules), since growth factor retrograde transport from source (cells surrounding the distal terminal) to cell soma is prevented by the damage. The importance of this loss of support in the generation of neuropathic pain is emphasised by the ability of GDNF exogenously applied to the soma to reverse this pain and the associated phenotypic changes (Bennett et al., 2000; Boucher et al., 2000; Boucher and McMahon, 2001c). Aside from loss of trophic support, the block of axonal trafficking results in local accumulation of channel-carrying transport vesicles; for example, VGSCs have been shown to accumulate in painful neuroma endings and in patches of demyelination in both animal models and human patients (Kretschmer et al., 2002b). The degeneration of injured nerves results in the release of cell contents, many of which act externally as inflammatory mediators, onto nearby uninjured neurons, either in the same or an adjacent nerve.

Axotomy, through loss of trophic support but also other mechanisms, causes changes in DRG neuron gene expression profiles, upregulating or downregulating both transcript and protein. A recent report used microarray analysis to show that expression levels of hundreds of genes were altered after peripheral nerve injury (Costigan et al., 2002), illustrating the highly complex

nature of neuropathic pain. For example, substance P and CGRP are both downregulated following axotomy. Due to interest as potential drug targets, however, the majority of research has focused on changes in expression of ion channels, particularly voltage-gated sodium channels (VGSCs). Increased functional expression of VGSCs would theoretically result in increased membrane excitability, possibly including spontaneous activity.  $\text{Na}_v1.8$  and  $\text{Na}_v1.9$  were reported to be downregulated at the level of both transcript and protein (Decosterd et al., 2002; Dib-Hajj et al., 1996), while levels of the embryonic  $\text{Na}_v1.3$  increase (Black et al., 1999). A persistent  $\text{Na}^+$  conductance, carried by the channel  $\text{Na}_x$ , is also upregulated. In adjacent uninjured fibres, however, an increase in  $\text{Na}_v1.8$  functional expression, but not total protein, was observed, representing a redistribution of protein along the axon (Gold et al., 2003). A complete description of VGSC changes following axotomy is given in a recent review by Devor (2006). Although observations of changes in gene expression can inform the search for proteins contributing to neuropathic pain, the use of gene deletion technology in mouse lines provides a more definitive test of relevance.  $\text{Na}_v1.3$  (Nassar et al., 2006),  $\text{Na}_v1.7$  (Nassar et al., 2005),  $\text{Na}_v1.8$  (Akopian et al., 1999) and  $\text{Na}_v1.7/\text{Na}_v1.8$  (Nassar et al., 2005) conditional-null mutant mice showed no deficits in animal models of neuropathic pain. Interestingly, the ectopic discharges from damaged sensory neurons that are characteristic of neuropathic pain generation were found to be present in  $\text{Na}_v1.3$  conditional-null mice, demonstrating that another mechanism is responsible for this element of the primary afferent barrage (Nassar et al., 2006).

Aside from VGSCs, several other groups of ion channels have been proposed to play a role in the primary afferent component of neuropathic pain, through a combination of theoretical mechanistic proposals and experimental observation. Voltage-gated  $\text{Ca}^{2+}$  channels, particularly the accessory subunit  $\alpha_2\delta-1$ , are thought to play a role in neuropathic pain processes in the periphery. Interestingly,  $\alpha_2\delta-1$  is thought to be the target for gabapentin, often effective in treating neuropathic pain, and is upregulated following nerve injury (Luo et al., 2002). The  $I_h$  pacemaker  $\text{K}^+$  current, carried by CNH, may also play a role in neuropathic pain (Chaplan et al., 2003b). This current is activated by hyperpolarisation, and regulates the rate at which repetitive firing can occur. An increase in channel activity is observed following nerve damage, resulting in pacemaker-driven spontaneous action potentials in the injured nerve (Chaplan et al., 2003a).  $\text{K}^+$ -carrying KCNQ channels are reported to play a key role in the control of nociceptor excitability, meaning that alterations in expression may induce neuropathic pain (Passmore et al., 2003).

Given the prevalence of potential mechanisms for neuropathic pain, a unified theory for its origin remains elusive. While many changes reproducibly occur, dissecting those that are

essential for neuropathic pain from those which do not play a significant role has proven to be a challenge. The use of transgenic technologies, alongside the growing pharmacological repertoire isolated from previously undiscovered sources will prove valuable in defining the processes essential for neuropathic pain.

### **1.4.7 Central processing**

Information about noxious stimuli from primary afferent nociceptors is transmitted to the brain via the dorsal horn of the spinal cord. The dorsal horn is divided anatomically into laminae, designated I-VI from outermost inwards. Peptidergic (NGF-dependent) C-fibres terminate in lamina I and the outer segment of lamina II, while non-peptidergic (GDNF-dependent) C-fibres synapse in the inner segment of lamina II. A $\delta$ -fibres synapse primarily in lamina I (Wall and Melzack, 1999). In contrast, A $\beta$ -fibres innervate lamina V. In the dorsal horn, nociceptive neurons synapse with either nociceptor-specific (NS) or wide-dynamic-range (WDR) projection neurons, which carry information to higher structures. NS neurons respond only to high-intensity stimuli, while WDR neurons respond to both high- and low-intensity stimulation with a graded output. In lamina I and II, the majority of projection neurons are nociceptor-specific, while lamina V contains primarily WDR neurons. In lamina V, WDR neurons synapse with A $\beta$ -fibres, but also receive input from C- and A $\delta$ -fibre neurons via spinal interneurons.

Sensory neurons communicate with spinal neurons via a variety of neurotransmitters. The main excitatory neurotransmitter released is glutamate, which activates post-synaptic ionotropic NMDA, AMPA and kainate receptors, as well as metabotropic (G-protein-coupled) glutamate receptors. A $\delta$ -fibres and NGF-responsive C-fibres also release brain-derived neurotrophic factor (BDNF), which activates TrkB receptors. Substance P and calcitonin gene-related peptide (CGRP) are also released by this class of C-fibre, acting on post-synaptic NK1 and CGRP receptors respectively. Protons and ATP are also likely to play a role in synaptic transmission in the dorsal horn of the spinal cord. While glutamate is released by relatively moderate activity, Substance P required more intense nociceptor activation, and BDNF is released following repetitive bursts of C-fibre activity.

Higher centres can modulate dorsal horn activity through descending inhibition and descending facilitation. Here, neurons descending from the brainstem and other higher structures release neurotransmitters, particularly 5-HT and noradrenaline, which act both pre- and post-synaptically to enhance or inhibit transmission. These processes are thought to be important in chronic pain states: for example, evidence exists showing enhanced serotonergic descending

input following formalin-induced inflammation and peripheral nerve injury. 5-HT released acts on primary afferent 5-HT<sub>3</sub> excitatory ionotropic receptors, increasing neurotransmitter release from these neurons (Green et al., 2000; Suzuki et al., 2004). In contrast,  $\alpha_{2A}$  adrenoreceptors mediate a large component of anti-nociceptive descending control. Pre-synaptic mechanisms of descending control allow selective regulation of nociceptive and non-nociceptive inputs, while post-synaptic actions do not discriminate between sources.

Excitatory and inhibitory interneurons in the dorsal horn allow a complex interplay between stimuli. Some pathways of descending control act through interneurons, and primary afferent input to interneurons in one lamina of the dorsal horn can influence the synaptic activity of connections in other laminae. The interconnectivity provided by dorsal horn interneurons allows fine control of somatosensory coding to ascending pathways, but makes the investigation of nociceptive pathways complex. In addition to neuronal influences, non-neuronal cells such as glia and microglia can modulate dorsal horn activity through the release of brain-derived neurotrophic factor (BDNF) and other substances.

Persistent activity in nociceptors can induce plastic changes in the dorsal horn. This central sensitisation plays an important role in inflammatory hyperalgesia and neuropathic pain, and is characterised by increased synaptic efficiency, lowered thresholds of activation and wider dorsal horn neuron receptive fields. In response to persistent low-frequency nociceptor activity, the phenomenon of wind-up can be observed. This consists of a summing dorsal horn response, with a constant afferent input generating increasing activity in dorsal horn neurons. Wind-up occurs rapidly (seconds) and does not persist beyond the duration of the stimulus. The primary mechanism behind this phenomenon is the removal of Mg<sup>2+</sup> block from the pore of NMDA receptors, allowing increased Ca<sup>2+</sup> currents. This removal occurs due to repeated depolarisation displacing the Mg<sup>2+</sup> ion from the pore. A related phenomenon, long-term potentiation (LTP), describes a lasting synaptic facilitation in response to repeated high-frequency nociceptor activity. This process involves the activation of metabotropic glutamate and NK1 receptors, activating 2<sup>nd</sup> messenger signalling pathways and resulting in the phosphorylation of NMDA and AMPA receptors. Increased Ca<sup>2+</sup> influx through NMDA receptors results in the activation of the transcription factor CREB (cAMP-response-element binding protein), which induces the transcription of *c-fos* and other immediate-early genes that contribute to synaptic strengthening. Many other transcriptional changes occur following inflammation or nerve damage, contributing to the generation and maintenance of abnormal pain states. In addition to changes in neuronal properties, activation of microglia and other non-neuronal cells can influence synaptic strength and contribute to hyperalgesic and allodynic states.

Information is conveyed to the brain from the spinal cord by many pathways, the most well-described of which are the spinothalamic, spinoparabrachial and spinoreticular. On a very simple level, the spinothalamic tract originates in deeper layers of the dorsal horn, projecting through the thalamus to the primary somatosensory cortex (which generates the conscious perception of pain) through the thalamocortical tract. The spinoparabrachial pathway projects from the most superficial layer of the dorsal horn to the periaqueductal grey, the hypothalamus (emotion and vascular response) then amygdala (memory and emotion). The spinoreticular pathway ascends to the thalamus, then to a variety of brain areas including the anterior cingulate gyrus (emotion), the amygdala and the hypothalamus. These pathways can be associated with distinct components of pain. Pain is often described as having sensory (discriminative, e.g. thermal vs. mechanical) and affective (emotional, unpleasantness) dimensions, with secondary effects of chronic pain such as anxiety and depression (Price, 2000). There is evidence to suggest that different ascending pathways mediate these distinct components of pain sensation. The spinothalamic pathway is thought to be responsible for the sensory discriminative aspects of pain sensation. The spinoparabrachial and spinoreticular pathways, in contrast, project onto brain areas, including the hypothalamus and amygdala, that mediate the affective components of pain and control autonomic activity (e.g. Lumb and Lovick, 1993), as well as detecting pain intensity (Bernard et al., 1996). The spinoparabrachial pathway originating from lamina I appears to play a role in signalling pain intensity, with emotional/aversive and autonomic components, but not in discriminative activity (Bester et al., 2000; Doyle and Hunt, 1999).

For a detailed review of higher pain pathways, see Mantyh and Hunt (2001b).

## 1.5 VOLTAGE-GATED SODIUM CHANNELS

The interaction between the voltage-gated sodium channel  $\text{Na}_v1.8$  and p11 is examined in this thesis. The following section introduces the voltage-gated sodium channel family, and provides further information on  $\text{Na}_v1.8$ .

The voltage-gated sodium channels (VGSCs) are responsible for the depolarising component of the action potential, and are thus of substantial interest in the study of nociceptive mechanisms in primary afferent neurons. VGSCs consist of a pore-forming  $\alpha$ -subunit, responsible for carrying  $\text{Na}^+$  ions across the plasma membrane, and accessory  $\beta$ -subunits ( $\beta1-4$ ), which modulate channel properties. The  $\alpha$ -subunits (260kDa) are a family of 10 structurally-related transmembrane proteins, arising from evolutionary gene duplication events and 75% identical over transmembrane and extracellular domains (Catterall, 2000). Each  $\alpha$ -subunit consists of 4 internally homologous domains, each containing 6 transmembrane  $\alpha$ -helices. The  $\text{Na}^+$ -selective pore is formed by residues in the loop between segments S5 and S6, known as the P-loop. Exchange of residues DEKA in the inner pore to EEEE, their counterparts in calcium channels, resulted in a change from  $\text{Na}^+$  to  $\text{Ca}^{2+}$  selectivity (Heinemann et al., 1992). Other mutations to these residues likewise produce alterations in ion selectivity (Schlieff et al., 1996; Sun et al., 1997). The general structure of the VGSCs is shown in Figure 1.4.

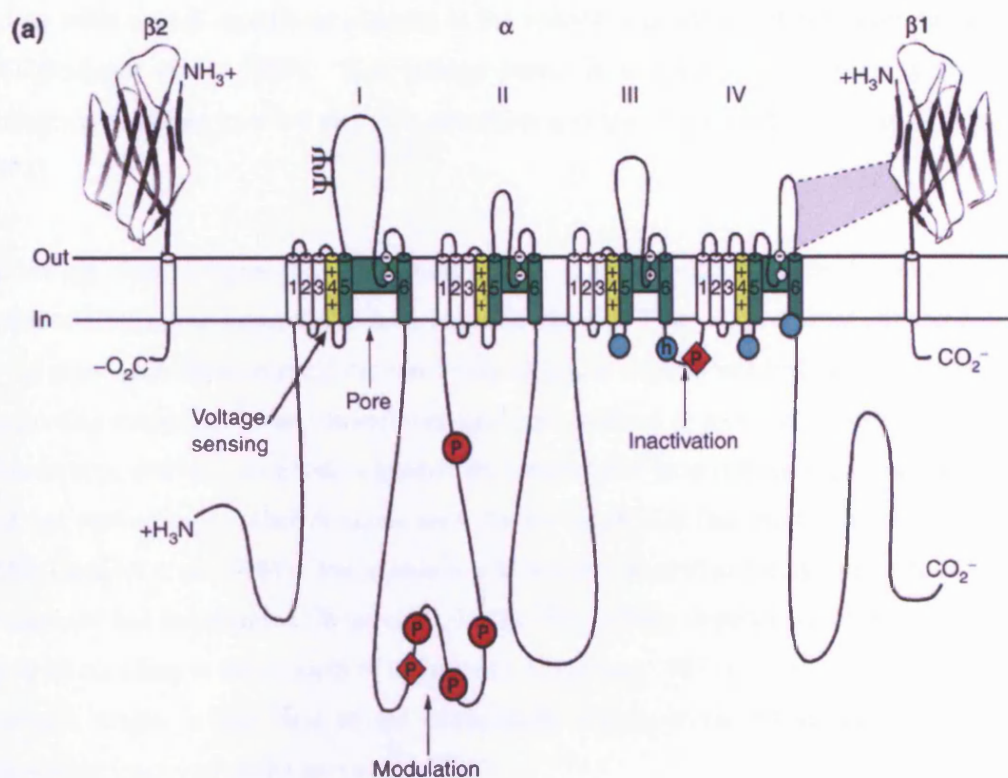


**Figure 1.4 Voltage-gated sodium channel structure.** The  $\alpha$  subunit of the  $\text{Na}_v1.2$  channel is illustrated together with the  $\beta 1$  and  $\beta 2$  subunits; the extracellular domains of the  $\beta$ -subunits are shown as immunoglobulin-like folds, which interact with the loops in the  $\alpha$ -subunits as shown. Roman numerals indicate the domains of the  $\alpha$ -subunit; segments 5 and 6 (shown in green) are the pore-lining segments and the S4 helices (yellow) make up the voltage sensors. Blue circles in the intracellular loops of domains III and IV indicate the inactivation gate IFM motif and its receptor (h, inactivation gate); P, phosphorylation sites (in red circles, sites for protein kinase A; in red diamonds, sites for protein kinase C);  $\psi$ , probable *N*-linked glycosylation site. The circles in the re-entrant loops in each domain represent the amino acids that form the ion selectivity filter (the outer rings have the sequence EEDD and inner rings DEKA). Figure taken from Yu and Catterall (2003).

Voltage gating is mediated by the  $\alpha$ -helical S4 transmembrane segments. Positively-charged lysine or arginine residues occur at 3 amino acid intervals, producing a linear array of positive charges as a result of the helical structure. Upon membrane depolarisation, this segment moves across the membrane electrical field, causing the channel to open. This movement has been detected directly using a combination of mutagenesis and covalent modification. Substitution of cysteines for the positively-charged residues, followed by exposure to charged sulfhydryl compounds, provides a system for the measurement of movement in response to membrane potential. Experiments using this system demonstrated that 3 positively-charged residues from this region became accessible to the extracellular region during channel gating (Yang et al., 1996; Yang and Horn, 1995). Further evidence in support of the central role of these residues in voltage gating is given by experiments showing that mutagenesis of these residues to neutral

amino acids causes significant changes in the voltage dependence of activation (Kontis et al., 1997; Stuhmer et al., 1989). The voltage sensor is trapped by  $\beta$ -scorpion toxins, shifting voltage-dependence to more negative potentials and thus enhancing activation (Cestele et al., 1998).

Following channel opening, inactivation occurs on a millisecond timescale, mediated by the residues IFM in the intracellular loop between domains III and IV. Initial experiments in the squid giant axon demonstrated the sensitivity of inactivation to intracellular protease perfusion, suggesting mediation by an intracellular gate and resulting in an internal ball and chain model (Armstrong, 1981b). Antibodies against the intracellular loop connecting domains III and IV, but not antibodies to other domains were shown to prevent fast inactivation (Vassilev et al., 1989; Vassilev et al., 1988). Mutagenesis of this region identified the hydrophobic IFM triad as critical for fast inactivation (West et al., 1992). The voltage dependence of inactivation comes from its coupling to the process of activation (Armstrong, 1981a). This link is uncoupled by  $\alpha$ -scorpion toxins, which bind to the extracellular region of the S4 segment in domain IV, preventing inactivation (Rogers et al., 1996).

The 10 VGSC  $\alpha$ -subunits,  $\text{Nav}1.1$ - $1.9$  and  $\text{Na}_x$ , show diversity of biophysical and pharmacological characteristics. Subtypes show differential expression and developmental regulation, and in some cases specialised functional roles. Nociceptive sensory neurons express a wide range of  $\alpha$ -subunits. Several explanations have been proposed for this, all providing for control of neuronal properties under changing physiological conditions. The relative expression levels, topological relationships, differential phosphorylation and varied effects of phosphorylation, and differential trafficking of subtypes all allow the control of activation (and therefore pain) thresholds by external factors (Wood et al., 2004a).

### 1.5.1 Pharmacology

Although pharmacological tools for the investigation of VGSCs are rare, channels can be categorised according to their sensitivity to tetrodotoxin (TTX), a guanidinium compound isolated from the puffer fish *Fugu*. TTX is produced by several bacterial species, which colonise puffer fish in a mutualistic (symbiotic) manner, rendering them an undesirable target for predators. Several other species also use TTX for protection, while for the blue-ringed octopus it is a potent venom. The majority of VGSCs are blocked by nanomolar concentrations of TTX and are defined as TTX-sensitive (TTX-S). Others are resistant to micromolar TTX and are therefore described as TTX-resistant (TTX-R). TTX binds to a hydrophobic/aromatic residue in the first P-loop of the ion selectivity pore of VGSCs, which is

mutated to serine (hydrophilic) in TTX-R channels (Noda et al., 1989; Satin et al., 1992). Channel sensitivities are summarised in Table 1.1:  $\text{Na}_v1.8$  and  $1.9$  are resistant to TTX,  $\text{Na}_v1.5$  is resistant to a lesser extent, and the other VGSCs are sensitive to nanomolar concentrations of TTX. Saxitoxin, produced by marine dinoflagellates, acts in a manner comparable to TTX. VGSCs are also blocked non-specifically by local anaesthetics such as lignocaine, some of which travel through the outer pore to bind to the inner pore, showing use-dependence as a result. Others cross the plasma membrane to act, and are therefore sensitive to small changes in extracellular pH. Unlike  $\text{Ca}^{2+}$  or  $\text{K}^+$  channels, for which a range of specific blockers are available, few pharmacological tools exist that are specific to a particular VGSC subtype, meaning that VGSC research has been centred around molecular biological techniques rather than traditional pharmacology. Recently, however, a group identified two closely-related conotoxins (peptide toxins from marine cone shells),  $\mu\text{O}$ -conotoxin MrVIA and MrVIB, which selectively inhibit the TTX-R current carried by  $\text{Na}_v1.8$  (Ekberg et al., 2006). These should prove a useful experimental tool, in addition to having therapeutic potential (discussed later).

## 1.5.2 VGSC properties and expression in sensory neurons

The properties and expression profiles of the VGSCs are summarised in Table 1.1. The TTX-S channels  $\text{Na}_v1.1$ ,  $1.2$ ,  $1.3$  and  $1.6$  are remarkably similar in sequence and biophysical properties ( $\text{Na}_v1.4$  and  $1.5$  are not expressed in neurons). Typically, the TTX-S channels are rapidly-activating and inactivating, with a threshold of activation of  $-25$  to  $-40\text{mV}$ , whereas the TTX-R channels display slower kinetics (Wall and Melzack, 1999).  $\text{Na}_v1.8$  activates and inactivates slowly, with a relatively high (depolarised) threshold of activation (Akopian et al., 1996). The inactivation potential is similarly depolarised (half inactivation potential  $-30$  to  $-40\text{mV}$ ), meaning that channels are fully available at normal resting potentials. A faster rate of recovery from inactivation compared to TTX-S channels has also been observed (Wall and Melzack, 1999). The higher threshold and reduced inactivation time of this channel mean that it is suited to generating continuous action potential bursts in response to high-intensity stimuli.  $\text{Na}_v1.9$  generates a persistent current, with kinetics that are too slow to contribute to the action potential. Its threshold of activation, however, is such that it is likely to have a depolarising effect on the resting membrane potential (Dib-Hajj et al., 1998b; Ekberg and Adams, 2006).  $\text{Na}_v1.9$  is inactivated at resting/holding potentials of  $>-60$ , allowing electrophysiological separation from currents mediated by  $\text{Na}_v1.8$  (Dib-Hajj et al., 1998a).

Of the VGSC  $\alpha$ -subunits, six are expressed at high levels in sensory neurons.  $\text{Na}_v1.1$ ,  $1.2$ ,  $1.3$  and  $1.6$  are highly expressed in brain and spinal cord in addition to sensory neurons (although  $\text{Na}_v1.3$  is expressed in the embryonic but not adult DRG under normal conditions), while

Nav1.7 is expressed in sensory neurons, sympathetic neurons and Schwann cells. The TTX-R channels Nav1.8 and Nav 1.9, however, are unique in that their expression is restricted only to sensory neurons, and are not detectable in other cell types under normal conditions. Nav1.8 expression is restricted to a precise subset of small- to medium-diameter sensory neurons, over 85% of which are likely to be nociceptors (Akopian et al., 1996; Djouhri et al., 2003a). Nav1.8 expression has also been observed in cerebellar Purkinje cells under conditions of experimental autoimmune encephalomyelitis or multiple sclerosis, with associated changes in neuronal firing characteristics (Black et al., 2000b), although the physiological relevance of this has yet to be described fully.

The subcellular localisation of VGSCs has also been examined to a limited extent. Toledo-Aral et al. (1997) found that Nav1.7 is targeted to the nerve terminals of cultured DRG neurons, rather than being concentrated along the axon or in the cell body. Likewise, Brock et al. (1998b) described the localisation of TTX-R currents, probably attributable to Nav1.8, to the distal terminal of probable nociceptors in the cornea. In contrast, Nav1.6 is localised at nodes of Ranvier in myelinated neurons (Caldwell et al., 2000), while Nav1.1, 1.2 and 1.3 are likely to be mainly axonal. These observations suggest that different channels have distinct roles in the generation and propagation of action potentials, with channels clustered at nerve termini controlling the sensitivity (or gain) of transduction mechanisms. Nav1.7 and Nav1.8 are thus well-placed to regulate nociceptor sensitivity in conditions such as inflammation.

Primary Name	Alternative Names	Gene	Distribution	TTX Sensitivity (IC <sub>50</sub> )
Nav1.1	Rat I	<i>SCN1A</i>	CNS, sensory neurons	TTX-S (6nM)
Nav1.2	Rat II	<i>SCN2A</i>	CNS, sensory neurons	TTX-S (12nM)
Nav1.3	Rat III	<i>SCN3A</i>	CNS, embryonic sensory neurons	TTX-S (4nM)
Nav1.4	μ1	<i>SCN4A</i>	Skeletal muscle	TTX-S (5nM)
Nav1.5	H1	<i>SCN5A</i>	Cardiac muscle, immature & denervated skeletal muscle	TTX-R (1-2μM)
Nav1.6	NaCh6	<i>SCN8A</i>	CNS, sensory neurons, nodes of Ranvier in CNS/PNS	TTX-S (1nM)
Nav1.7	PN1	<i>SCN9A</i>	Sensory neurons, sympathetic neurons, Schwann cells	TTX-S (4nM)
Nav1.8	SNS/PN3	<i>SCN10A</i>	Sensory neurons	TTX-R (60μM)
Nav1.9	SNS2/NaN	<i>SCN11A</i>	Sensory neurons	TTX-R (40μM)
Na <sub>x</sub>	NaG	<i>SCN7A</i>	Lung, nerve	TTX-S

**Table 1.1 Na<sup>+</sup> channel α-subunits.** Adapted from Ekberg et al. (2006) and Wood et al. (2004b).

### 1.5.3 β-subunits

VGSC auxiliary β-subunits are not required for channel activity, but modulate channel properties and interact with cytoskeletal and extracellular matrix proteins, stabilising channels in the plasma membrane. They consist of a single 22-36kDa transmembrane domain with an extracellular immunoglobulin-like region (Isom and Catterall, 1996). Four subtypes exist, denoted β<sub>1-4</sub>. β<sub>1</sub> and β<sub>2</sub> were first identified due to their association with α-subunits, followed by functional investigation in heterologous expression systems (Isom et al., 1992). In contrast, β<sub>3</sub> and β<sub>4</sub> were identified by molecular cloning (Morgan et al., 2000; Yu et al., 2003). A splice variant of β<sub>1</sub> (β<sub>1A</sub>) has also been described, expressed only during embryonic development and apparently resulting from an intron retention event (Kazen-Gillespie et al., 2000). All currently-known β-subunits are expressed in the peripheral nervous system, although expression in putative nociceptors may be somewhat more restricted. β<sub>1</sub>, β<sub>2</sub> and β<sub>3</sub> are all expressed in small- and medium-diameter DRG neurons, while β<sub>4</sub> is expressed in large- but not small- or medium diameter primary afferents (Chahine et al., 2005). Investigation of the functional roles of β-subunits has been hindered by sensitivity to the particular heterologous expression system used (Isom, 2001), although considerable progress has been made despite this.

Of particular interest is the role of VGSC  $\beta$ -subunits in neuropathic pain, where changes in functional expression and biophysical properties of VGSCs are observed. In rat models of neuropathic pain, changes in expression levels of  $\beta$ -subunits have been reported in both DRG neurons and in the spinal cord. Following nerve damage,  $\beta_1$  mRNA levels in the dorsal horn (laminae I-II) of the spinal cord were increased, while  $\beta_2$  expression was reduced in laminae I-IV (Blackburn-Munro and Fleetwood-Walker, 1999). The downregulation of  $\beta_2$  was proposed to disrupt interaction with tenascins, promoting axonal growth and projection of neurons into superficial laminae, with the possibility of new synaptic contact formation. A more recent study also reported an increase in  $\beta_3$  expression in the trigeminal ganglia in an orofacial neuropathic pain model (Eriksson et al., 2005), confirming previous reports of  $\beta_3$  but not  $\beta_1$  or  $\beta_2$  upregulation in the DRG following nerve injury (Shah et al., 2000; Takahashi et al., 2003). It has been proposed that increased levels of  $\beta_3$  may contribute to the generation of ectopic activity in axotomised DRG neurons (Takahashi et al., 2003). Deletion of  $\beta$ -subunits leads to a complex phenotype including seizures and epileptogenic activity (Chen et al., 2002a; Chen et al., 2004), precluding investigation of pain sensation. The development of subtype- and tissue-specific null mutant mice may help to shed light on the contributions of  $\beta$ -subunits to pain pathways.

For a comprehensive review of VGSC  $\beta$ -subunits, see Isom (2001).

#### **1.5.4 $\text{Na}_v1.8$**

The trafficking of the VGSC  $\text{Na}_v1.8$  by p11 is one of the main topics of this thesis. This section provides additional background on this channel.

The TTX-R  $\text{Na}^+$  channel  $\text{Na}_v1.8$  was first cloned in 1996 using a difference cloning method to identify genes expressed selectively in DRG neurons (Akopian et al., 1996; Sangameswaran et al., 1996). It was shown to mediate the TTX-R current first described by Matsuda et al. (1978), with an aromatic to hydrophilic amino acid alteration in the channel atrium conferring TTX-resistance (Akopian et al., 1996). The murine  $\text{Na}_v1.8$  gene, *SCN10A*, was characterised soon after and shown to have 95.3% amino acid sequence homology with the rat gene. The gene is located on chromosome 9 and comprised of 27 exons, spanning approximately 90kb (Souslova et al., 1997).  $\text{Na}_v1.8$  carries a slowly-activating, slowly-inactivating current, with an activation threshold of -40 to -30mV, relatively depolarised compared to TTX-S channels. Importantly,  $\text{Na}_v1.8$  is inactivated only at relatively depolarised potentials ( $\sim$ -30mV), and reprimed rapidly from fast inactivation (Cummins and Waxman, 1997b; Elliott and Elliott, 1993), allowing

neuronal excitability under conditions of sustained depolarisation. This allows nociceptor activity to continue in the event of prolonged stimuli, with associated survival value.

The expression profile of  $\text{Na}_v1.8$  has been examined in detail by several groups, including correlation with electrophysiological properties of neurons. Under naïve conditions,  $\text{Na}_v1.8$  expression was found to be restricted to a subset of primary afferent neurons. It is expressed in at least 50% of unmyelinated (C-fibre) DRG neurons, in both NGF- and GDNF-responsive populations, and in a proportion of medium-diameter  $\text{A}\delta$ -fibres. Expression has also been observed in a small proportion of large-diameter  $\text{A}\beta$  neurons, and in the trigeminal and nodose ganglia. Of the 10% of A-fibres expressing  $\text{Na}_v1.8$ , all are TrkA-positive, and many express the vanilloid-like receptor TRPV2 (Amaya et al., 2000b). Djouhri et al. (2003a) recently examined the relationship between  $\text{Na}_v1.8$  expression and neuronal properties.  $\text{Na}_v1.8$  immunoreactivity was found to be present in 83% of C-fibres, 93% of  $\text{A}\delta$ -fibres, and 25% of  $\text{A}\alpha/\beta$ -fibres, a significantly higher proportion than previously observed. In addition, 88% of C-unresponsive neurons, representing a “silent” population of nociceptors activated under conditions of inflammation, displayed  $\text{Na}_v1.8$  immunoreactivity. Over 80% of nociceptive neurons, assessed by sensory receptive properties, were  $\text{Na}_v1.8$ -positive. It can be deduced from this study and that of Akopian et al. (1996) that over 85% of  $\text{Na}_v1.8$ -expressing cells are nociceptors (Stirling et al., 2005).  $\text{Na}_v1.8$  expression levels are significantly higher in nociceptive than non-nociceptive neurons (Djouhri et al., 2003a). In addition to the cellular distribution of  $\text{Na}_v1.8$ , subcellular localisation has also been examined. Brock et al. (1998d) reported TTX-R currents located in the distal termini of nociceptors, suggesting that  $\text{Na}_v1.8$  channels play an important role in action potential generation immediately following stimulus transduction.

The expression and functional properties of  $\text{Na}_v1.8$  are altered under conditions of inflammation and nerve damage (see section “ $\text{Na}_v1.8$  in pain”). Expression of  $\text{Na}_v1.8$  has also been reported in cerebellar Purkinje cells during experimental autoimmune encephalomyelitis and human multiple sclerosis (Black et al., 2000a; Damarjian et al., 2004), in conjunction with an increase in p11/annexin 2 expression (Craner et al., 2003b). This dysregulated expression is thought to contribute to the abnormal Purkinje cell activity observed in these conditions (Saab et al., 2004).

#### **1.5.4.1 Modulators of $\text{Na}_v1.8$ expression and properties**

Properties of VGSCs are often investigated by expression of the channel in heterologous expression systems, such as *Xenopus* oocytes, CHO, COS or HEK cells. Many channels require accessory  $\beta$ -subunits for native levels of functional expression. Although the low

functional expression of  $\text{Na}_v1.8$  is increased by co-expression with the  $\beta 1$  subunit (Vijayaragavan et al., 2004b), current densities in *Xenopus* oocytes, CHO, COS-7 and HEK-293 cell lines remains substantially below endogenous levels in DRG (England, 1998), with channels displaying properties different from those in DRG neurons (FitzGerald et al., 1999). Microinjection of  $\text{Na}_v1.8$  cDNA into the nuclei of SCG or  $\text{Na}_v1.8$ -null mutant DRG neurons, however, produces sodium currents with similar properties and magnitude to wild-type DRG neurons (England, 1998), implying that these cells contain additional factors required for endogenous levels of  $\text{Na}_v1.8$  functional expression. With this in mind, Okuse *et al.* (2002) used the yeast two-hybrid system to search for proteins interacting with the intracellular domains of  $\text{Na}_v1.8$ . A range of proteins were identified, including p11, Papin, PAF67, connexin, calmodulin, and  $\beta$ -actin (Malik-Hall et al., 2003). The roles of several of these interactions have been investigated further, with interesting results. p11 increases plasma membrane expression of  $\text{Na}_v1.8$  via an interaction with the N-terminal domain, increasing surface immunoreactivity and TTX-R current density (Okuse et al., 2002; Poon et al., 2004). This interaction is described in more detail elsewhere in this thesis. Papin is a 300kDa protein containing 6 PDZ domains which binds to the intracellular loop between domains II and III of  $\text{Na}_v1.8$ . Nuclear injection of antisense vector to Papin into DRG neurons resulted in a 71% reduction in TTX-R current density, implying a role in functional expression (Shao et al., 2005). PAF67 is a 67kDa protein associated with a subtype of RNA polymerase I, and plays an important role in the initiation of transcription. PAF67 bind to the C-terminal domain of  $\text{Na}_v1.8$ . Antisense downregulation of PAF67 resulted in a 76% reduction in TTX-R current density, while overexpression in CHO cells promoted translocation of  $\text{Na}_v1.8$  to the plasma membrane, resulting in functional channel expression (Shao et al., 2005).

Calmodulin binds directly to ion channels by an IQ motif, present in the C-terminus of all VGSCs, in a  $\text{Ca}^{2+}$ -independent manner (Herzog et al., 2003b; Mori et al., 2000; Rhoads and Friedberg, 1997). The modulation of VGSCs is isoform dependent; that is, disruption of calmodulin binding has differing effects on each isoform (e.g. Herzog et al., 2003a; Young and Caldwell, 2005). Choi et al. (2006d) recently examined the effect of disruption of calmodulin binding to  $\text{Na}_v1.8$  in DRG neurons. In the absence of calmodulin binding,  $\text{Na}_v1.8$  current density was reduced by over 50%, possibly via endocytotic mechanisms, with voltage-dependence of activation and inactivation unchanged. Additionally, frequency-dependent inhibition was significantly enhanced, even at a relatively low frequency of 0.1Hz. The association of calmodulin with  $\text{Na}_v1.8$  can therefore enhance electrogenesis in DRG neurons.

Contactin, a glycosyl-phosphatidylinositol-anchored neuronal cell surface glycoprotein, was not identified in the  $\text{Na}_v1.8$  yeast two-hybrid screen, but was shown by other methods to

regulate  $\text{Na}_v1.8$  functional expression. DRG neurons from contactin-null mice displayed a reduction in  $\text{Na}_v1.8$  (and  $\text{Na}_v1.9$ ) current density of more than 2-fold, but this effect was limited to small-diameter, IB4-positive cells, for reasons that have yet to be explained. Axonal  $\text{Na}_v1.8$  immunoreactivity was also reduced in the contactin-null mice. Contactin may therefore regulate  $\text{Na}_v1.8$  functional expression in a subtype of nociceptive DRG neurons (Rush et al., 2005a).

#### **1.5.4.2 $\text{Na}_v1.8$ in pain**

The expression profile of  $\text{Na}_v1.8$  suggests a specialised role in nociceptive pathways, prompting the investigation of  $\text{Na}_v1.8$  function in a range of pain models. Changes in expression have been observed in conditions in inflammation and nerve damage. During inflammation, NGF causes a modest increase in  $\text{Na}_v1.8$  expression in A but not C-fibres (Fang et al., 2005; Okuse et al., 1997). More striking is the PKA and PKC-mediated phosphorylation of  $\text{Na}_v1.8$  induced by inflammatory mediators such as  $\text{PGE}_2$ , which increases TTX-R currents by shifting the current-voltage relationship and possibly the voltage-dependence of activation (FitzGerald et al., 1999; Gold et al., 1998; Vijayaragavan et al., 2004a). Several groups have investigated changes in  $\text{Na}_v1.8$  expression following various types of nerve injury, with a consensus downregulation being reported. Okuse et al. (1997) reported decreases of 25-80% in  $\text{Na}_v1.8$  transcript levels in various models of sensory nerve damage (including diabetic neuropathy), while Cummins et al. (1997a) observed a substantial decrease in TTX-R currents in axotomised neurons. Following ischaemic injury to the trigeminal nerve in a model of orofacial neuropathic pain,  $\text{Na}_v1.8$  transcript was downregulated (Eriksson et al., 2005), in agreement with observations in DRG. Redistribution of  $\text{Na}_v1.8$  from soma to axon, however, was observed in neuropathic conditions (Novakovic et al., 1998), and the channel was also found to accumulate in painful human neuroma (Kretschmer et al., 2002a), leaving the contribution of the channel to neuropathic pain unclear (although this has now been addressed by other methods).

Akopian et al. (1999) created a null-mutant mouse to investigate the role of  $\text{Na}_v1.8$  in pain pathways, reporting behavioural deficits in nociception in response to acute mechanical and thermal stimuli. Matthews et al. (Matthews et al., 2006) used electrophysiological recordings from the dorsal horn in these mice to show reduced noxious coding in response to mechanical but not thermal (apart from cold) stimuli. Inflammatory pain thresholds following carrageenan injection were unchanged by  $\text{Na}_v1.8$  deletion, although a reduction in pain compared to wild-type animals was observed when given in combination with a low dose of lidocaine, proposed to unmask an effect obscured by compensatory changes in other VGSCs (Akopian et al., 1999).

NGF-induced hyperalgesia was attenuated in the  $Na_v1.8$ -null mouse (Kerr et al., 2001), in conjunction with a small NGF-induced increase in transcript (Okuse et al., 1997). PGE2-mediated phosphorylation can alter the properties of this channel as previously discussed. No differences in neuropathic pain were seen in the  $Na_v1.8$ -null mouse (Kerr et al., 2001). It was speculated that compensatory upregulation of  $Na_v1.7$  was masking the effect of  $Na_v1.8$  deletion on neuropathic pain, but  $Na_v1.7/1.8$  double knockout mice also displayed behaviour similar to wild-type in models of neuropathic pain (Nassar et al., 2005). Studies reporting a downregulation of  $Na_v1.8$  transcript or protein in response to nerve injury support these results (Eriksson et al., 2005; Okuse et al., 1997). Treatment with antisense to  $Na_v1.8$  mRNA, however, substantially reduced neuropathic pain, although this paper did not test selectivity over other VGSCs (Lai et al., 2002). Additionally, the conotoxin MrVIB, a selective blocker of  $Na_v1.8$  reduced allodynia resulting from both neuropathic and chronic inflammatory pain models (Ekberg et al., 2006). The site of action of this conotoxin is not clear, since in this case it was administered by intrathecal injection, raising doubts about access to primary afferent neurons. Finally, the presence of  $Na_v1.8$  was shown to be required for spontaneous activity in damaged sensory neurons, a process which may be important in the generation of neuropathic pain states (Roza et al., 2003). On balance, the data do not appear to support a role for  $Na_v1.8$  in neuropathic pain, although some data do suggest a limited function in this process. Laird et al. (2002) investigated the role of  $Na_v1.8$  in visceral pain, reporting that  $Na_v1.8$ -null mice displayed reduced visceral pain and referred hyperalgesia. It is thus apparent from these studies that  $Na_v1.8$  plays a specialised role in pain pathways, including acute, visceral and inflammatory pain.

### **1.5.5 VGSCs and nociception**

A detailed discussion of the role of VGSCs in pain pathways can be found in a recent review by Wood et al. (2004c). A brief overview is given here.

Small-diameter sensory neurons, representing putative nociceptors, express a sodium current consisting of several pharmacologically- and electrophysiologically distinct components. Correspondingly, several different VGSC transcripts are expressed, as described previously. Several VGSC subtypes have been shown to be important in nociception or in the development of inflammatory and neuropathic pain states, where changes in expression levels can alter neuronal properties.

$Na_v1.3$  is normally absent from the adult peripheral nervous system, but is strongly induced by nerve damage (Hains et al., 2003; Waxman et al., 1994), while this can be reversed by

exogenous GDNF. Nav1.3 is rapidly repriming (Cummins et al., 2001) and therefore suited to a role in the generation of ectopic neuronal activity. A recent study by Nassar et al. (2006), however, found that in Nav1.3 conditional (nociceptor-specific) null mice, the development and extent of neuropathic pain was unaltered, precluding a major role for this channel in neuropathic pain.

Nav1.7 is expressed predominantly in the peripheral nervous system, in both sensory and sympathetic neurons. Immunocytochemical studies support a strong association with nociceptors (Djouhri et al., 2003b), suggesting a role in nociception. Nociceptor-specific Nav1.7 knockout mice show substantial deficits in acute and inflammatory (but not neuropathic) pain (Nassar et al., 2004). The most compelling evidence, however, comes from human genetic studies. A range of heritable painful conditions in humans have been mapped to several different gain-of-function mutations in Nav1.7. The first group of mutations to be identified give rise to erythromelalgia, an autosomal dominant neuropathy characterised by severe burning pain and redness in the extremities in response to mild thermal stimuli. Many different gain-of-function mutations have been associated with this condition, resulting in either hyperpolarising shifts in activation, depolarising shifts in inactivation, increased current amplitude in response to small depolarisations, and other changes in biophysical properties leading to increased neuronal excitability (Choi et al., 2006a; Cummins et al., 2004a; Dib-Hajj et al., 2005b; Han et al., 2006a; Han et al., 2007; Harty et al., 2006b; Lampert et al., 2006a; Sheets et al., 2007b). Another gain-of-function mutation in Nav1.7, resulting in a reduction in fast inactivation and therefore a persistent Na<sup>+</sup> current, was recently shown to be the cause of paroxysmal extreme pain disorder, a genetic disorder resulting in spontaneous pain with some inflammatory character (Fertleman et al., 2006a). Most recently, a heritable disorder resulting in the complete absence of nociception was mapped to 3 distinct nonsense mutations in *SCN9A*, the gene encoding Nav1.7 (Cox et al., 2006b). Surprisingly, no other neurological deficits were described in this group, suggesting that Nav1.7 may be a good therapeutic target for the treatment of pain.

Nav1.9 is expressed in unmyelinated DRG neurons (Amaya et al., 2000a; Dib-Hajj et al., 1998c), although it is also present in some myelinated nociceptive neurons (Fang et al., 2002). Interestingly, it has been localised to nerve endings in the cornea (Black and Waxman, 2002). Together with its role in setting activation thresholds and regulating excitability (Baker et al., 2003; Herzog et al., 2001b), and its upregulation by G-protein pathways (Baker et al., 2003), these data suggest a role in nociception. Two groups generated Nav1.9-null mouse lines to investigate the effect on pain-related behaviour, both describing deficits in inflammatory but not acute or neuropathic pain behaviour. Priest et al. (2005) found deficits in thermal but not mechanical hyperalgesia following inflammation. Amaya et al. (2006b) reported a similar

effect upon administration of pro-inflammatory intraplantar complete Freund's adjuvant, but also described reduced or absent pain hypersensitivity elicited by intraplantar PGE<sub>2</sub>, bradykinin, IL-1 $\beta$  and capsaicin, but not NGF. These results support the hypothesis that Nav1.9 is an effector of the hypersensitivity produced by inflammatory mediators and therefore plays a key role in peripheral sensitisation (Amaya et al., 2006a).

## 1.6 PROJECT OUTLINE

Studies in heterologous expression systems have illustrated the role of p11 in the functional expression of the VGSC Nav1.8 at the plasma membrane. Given the analgesic phenotype of the Nav1.8-null mouse line, the interaction between p11 and Nav1.8 would appear to be a potential target for the development of novel therapeutic interventions for the treatment of pain. The significance of this interaction in pain sensation, however, has yet to be examined. This thesis aims to examine the importance of the p11-Nav1.8 interaction in nociceptive pathways. This will be achieved by the generation and analysis of a nociceptor-specific p11-null mouse line.

Should the p11-Nav1.8 interaction prove to be a valid therapeutic target, a thorough understanding of the nature of the binding sites involved will aid intelligent drug design. This thesis will investigate the residues of the Nav1.8 N-terminus required for its interaction with p11, with a view to producing a model for the interaction.

## **2 MATERIALS AND METHODS**

### **2.1 MOLECULAR BIOLOGY**

#### **2.1.1 Agarose Gel Electrophoresis**

Agarose gel electrophoresis was used to separate DNA/RNA fragments by length. Powdered agarose (Sigma) was added to 1X TAE buffer (Tris-acetate-EDTA pH 8.3, Promega) to a final concentration of 0.6-1.5% (w/v), depending on expected fragment length. After dissolution by heating, the solution was cooled to around 50°C using a water bath. Ethidium bromide (EtBr) (Mercury Reagents) was added to a final concentration of 0.00005% (w/v), and the solution allowed to set in a casting tray (Fisherbrand). The gel was then placed into an electrophoresis tank and covered with 1X TAE. Samples were mixed with 6X loading buffer and loaded into wells, along with an appropriate molecular weight marker. A potential difference of 60-130mV was then applied across the gel until the loading buffer dye approached the end of the gel. The DNA/RNA was visualized using a UV transilluminator, which induces fluorescence in the EtBr intercalated in the nucleic acid minor groove. Images were taken using a camera attached to the transilluminator. Where the DNA was required for subsequent reactions, aluminium foil was used to limit UV-induced damage to the DNA.

#### **2.1.2 Recovery of DNA from agarose gels**

DNA fragments of the required size were cut from gels using a sterile scalpel blade. Stratagene's Strataprep DNA Gel Extraction Kit was used according to instructions to isolate DNA.

#### **2.1.3 The Polymerase Chain Reaction**

The polymerase chain reaction (PCR) allows the exponential amplification of regions of nucleic acid between two defined sites. It can be used for both constructive (amplification of a DNA fragment for cloning) and diagnostic purposes. PCR is dependent on the specific binding of primers to complementary regions of a template, which is influenced by reaction conditions such as annealing temperature and MgCl<sub>2</sub> concentration, the optimal levels of which differ according to primer sequence. Reaction conditions were therefore optimised for each set of primers, to minimise non-specific priming whilst allowing efficient amplification of the target sequence.

As PCR is an amplification reaction, it is sensitive to contamination by other DNA sources. Sterile materials were therefore used where possible. Reactions were carried out in 200µl PCR tubes, using the following mixture as a standard starting point:

10ng template DNA, 400nM each primer, 1X polymerase buffer (dependent on polymerase), 0.5mM MgCl<sub>2</sub>, 0.2mM dNTP and 1 unit KOD HiFi DNA polymerase (constructive PCR) or 2 units Taq polymerase (diagnostic PCR), in deionised water (ddH<sub>2</sub>O). An example amplification protocol is given below:

Initial denaturing:		94°C, 1 min	
Cycle:	Denaturing	94°C, 30 secs	
	Annealing	60°C, 30 secs	
	Extension	72°C, 90 secs	x 30-35
Final extension:		72°C, 1 min	
Final temperature:		4°C, forever	

Annealing temperatures used were typically 2-5°C below the melting temperature,  $T_m$ , for the primer bound to its target sequence. On completion of the PCR reaction, products were subjected to agarose gel electrophoresis before use in subsequent reactions.

#### **2.1.4 Addition of 3'A Overhangs for TOPO-TA Cloning**

For the TOPO-TA cloning reaction, it was necessary to produce fragments with a 3'A overhang following amplification by KOD HiFi DNA polymerase. As KOD is a proofreading polymerase, it does not show 3'-adenylation activity. A further reaction was used for this purpose: 0.4mM dATP and 5 units Taq DNA polymerase were added to the products of the initial PCR reaction, and incubated at 72°C for 10 mins.

#### **2.1.5 TOPO-TA Cloning ®: Insertion of DNA Fragments into pCRII**

TOPO-TA Cloning (Invitrogen) was used as a sub-cloning step, to insert DNA fragments produced by PCR into a high copy number vector for amplification. This system utilises Topoisomerase I, covalently bound to the open vector, to insert fragments possessing a 3' A-overhang.

#### **2.1.6 Transformation of Chemically Competent Bacterial Cells**

For general cloning purposes, One Shot ® TOP10 *E. coli* cells (Invitrogen) were used. BL21 cells (Invitrogen) were used for protein expression. Each cell type was transformed according to instructions, with appropriate selective agent present. Where the pCRII vector was used, 40µl of 40mg/ml X-gal was spread onto each plate to discriminate between insert-containing and empty vectors, and only white colonies used for further steps. Transformation efficiency was generally good.

### **2.1.7 Screening Bacterial Clones by Colony PCR**

Colony PCR was used to identify bacterial clones containing the required construct. This technique allowed the screening of clones before plasmid isolation by miniprep.

50µl of L-broth (Fisher) containing 0.01% (w/v) ampicillin (Sigma) was added to the required number of wells in a 96-well plate (Neptune). Individual bacterial colonies were then picked from an agar plate into separate wells, and the plate sealed. This was then incubated at 37°C, 170 rpm for 1 hour in a shaking incubator (Gallenkamp). 2µl from each well was then used as template for a diagnostic PCR reaction.

### **2.1.8 Isolation of Plasmid DNA by Mini- and Midiprep**

The isolation of plasmid DNA that was to be sequenced was performed using Wizard *Plus* SV Miniprep and Wizard *Plus* Midiprep kits (Promega). All other minipreps were performed using the alkaline lysis method, as described by Sambrook et al. (1989).

### **2.1.9 Restriction Digests**

Digestion of DNA with restriction enzymes was used to remove inserts from plasmids during the cloning process. It was also used in addition to colony PCR as a diagnostic tool, prior to DNA sequencing. For both purposes, the cloning enzymes BamHI and NdeI were used. Digests were carried out in a volume of 20µl, containing 1x Buffer D, 0.5µl of each enzyme and 17µl DNA solution (from miniprep). The reaction was incubated at 37°C for around 1 hour, then run on agarose gel.

### **2.1.10 Ligation of Fragments into pET14b**

The bacterial expression vector pET14b was used to express recombinant proteins. pET14b contains an N-terminal sequence coding for 6 x His, which was required for protein purification (described later), under the control of the bacteriophage T7 promoter. The vector was first opened using the restriction enzymes NdeI and BamHI, then treated with shrimp alkaline phosphatase (SAP) to prevent re-ligation of the empty vector. The desired fragment was isolated from the cloning vector pCRII with the same enzymes, to produce cohesive ends. 2.5µl of pET14b and 7.5µl of the required insert were mixed in a 2ml Eppendorf tube. 1x Quick Ligase Buffer (New England Biolabs) and 1µl Quick Ligase (New England Biolabs) were added, and the mixture incubated for 15 mins at room temperature followed by storage on ice. TOP10 cells were then transformed with 2µl of product as described previously.

### **2.1.11 DNA Sequencing**

DNA sequencing was carried out from miniprep or midiprep by Lark Technologies. Both raw trace data and sequence were received, to allow evaluation of errors in sequence. Primers

based on the T7 and Sp6 promoters were used, depending on vector. Sequencing was started around 100bp from the section of interest to allow for errors in the initial stages of the reaction.

## **2.1.12 Isolation of Genomic DNA from Tissue Samples**

The isolation of genomic DNA from murine tissue samples was required for genotyping and the assessment of Cre activity. DNA was isolated from a small (<2mm) section of tail for genotyping, or from other tissues (most commonly DRG) for other applications. Tissue samples were digested for 1 hour - overnight in tail lysis buffer containing 0.01% Proteinase K, at 55°C. After digestion, samples were vortexed vigorously then centrifuged at 13,000 rpm for 2 mins in a benchtop microcentrifuge to remove debris. The supernatant was transferred to a fresh tube and the DNA precipitated with an equal volume of isopropanol. Following vigorous shaking, after which the DNA was visible, centrifugation (as before) was used to pellet the DNA. The supernatant was discarded, leaving the precipitate DNA. After 2 washes in 70% ethanol, the pellet was briefly dried then resuspended in 200µl TE buffer or ddH<sub>2</sub>O.

## **2.1.13 Southern Blot**

### **2.1.13.1 DNA Separation and Blotting**

Around 10 µg of mouse genomic DNA was digested using a range of restriction enzymes and appropriate buffers. A total volume of 50 µl was incubated for >16 h at either room temperature or 37°C depending on enzyme. Bands were separated by agarose gel electrophoresis, using 0.6-0.8% gels run at 15-30V overnight.

After digestion and separation of DNA, the gel was exposed to short wavelength UV light to fragment the DNA, ensuring complete transfer to the membrane. The DNA was denatured (1 h) (0.5 M NaOH, 1.5 M NaCl) followed by a rinse in distilled water, then neutralised (1 h) (1.0 M Tris-HCl, 1.5M NaCl) followed by another rinse in distilled water.

The DNA was then attached to a Hybond<sup>TM</sup>+ Membrane (Amersham Pharmacia Biotech UK Ltd) by capillary transfer, as follows: a glass plate was placed on top of a tray filled with 10X SSPE (20X stock: 3M NaCl, 0.2M NaH<sub>2</sub>PO<sub>4</sub>, 0.02M EDTA, pH 7.0). A large piece of filter paper was placed over the glass plate with the ends in the SSPE. The gel was then covered with a piece of Hybond<sup>TM</sup>+ Membrane, and a further two layers of soaked filter paper were placed on top, followed by multiple layers of absorbent paper. This setup was left for >6h, after which the SSPE had carried the DNA to the membrane. The DNA was cross-linked (120,000 µJ) to the membrane using a Stratalinker® UV Crosslinker, Stratagene, US.

### **2.1.13.2 Pre-Hybridization**

The membrane was pre-hybridised (blocked) in a glass tube containing hybridization mix (6X SSPE, 5X Denhardt's reagent, 100µg/ml yeast RNA and 0.5-1.0% SDS). The same volume of formamide was added and the membrane incubated at 42°C in a rotary PreHybaid oven for 6 hours. This step reduces non-specific probe binding.

### **2.1.13.3 Probe Labelling and Hybridisation**

For hybridisation, a 0.4-1.0 kb probe was prepared using PCR. After gel separation on 1.0% low melting point agarose gel, the DNA fragment was excised and 3 volumes of water added. The probe was labelled with <sup>32</sup>P using a Prime-it Random Labelling Kit (Stratagene), and purified using Qiagen's Nucleotide Purification Kit, before being denatured for 3 mins at 94°C, then snap-cooled on ice for another 1-3 min. The radioactive probe was then added to the hybridisation solution and incubated with the membrane at 42°C for 6 hours.

### **2.1.13.4 Membrane Washing and Imaging**

After hybridization, any excess probe was removed by washing the membrane in 2X SSPE, 0.1% SDS for 15-30 min at 65°C followed by another wash using 0.2 X SSPE, 0.1% SDS for 5-20 min. The washed membrane was exposed to Kodak film at -80°C for between 1 hr and 5 days, and developed using standard methods.

### **2.1.14 RNA Extraction**

DRG were removed from humanely-killed mice, working quickly on ice. RNA that was to be used for quantitative PCR was extracted immediately with Qiagen's RNeasy Mini Kit, to reduce genomic DNA contamination. RNA for other purposes was extracted as follows: DRG from one mouse were homogenised in 500µl TRIzol and incubated for 5 mins at room temperature. 0.1ml chloroform was added and tubes were shaken vigorously for 15s, incubated for 3 mins at room temperature, followed by centrifugation at 12,000 X g for 15 mins at 4°C. The colourless aqueous phase was taken, and the remainder discarded. RNA was precipitated with 0.25ml isopropanol for 10 mins at room temperature, with the addition of 1µl glycogen to aid precipitation. Following centrifugation at 12,000 X g, 4°C for 10 mins, the supernatant was discarded and the pellet washed twice in 75% ethanol. The pellet was dried for 5 mins at room temperature, before being dissolved in 20µl RNase-free H<sub>2</sub>O. RNA quality was checked by agarose gel electrophoresis, looking for 2 distinct rRNA bands without excessive smearing (from degradation). Quantity and purity were assessed by spectrophotometry, reading A<sub>260</sub> and A<sub>280</sub>. RNA was stored at -80°C.

### 2.1.15 Reverse Transcription Reaction

cDNA was made from RNA using a Bio-Rad iScript kit, or with Invitrogen Superscript II, according to manufacturer's instructions. cDNA was stored at -20°C.

### 2.1.16 Quantitative (Real-Time) PCR

qPCR primers were designed with Beacon Designer 5, using BLAST searches to ensure specificity. Primers were designed to give an amplicon of 80-150 bp, and to overlap an intron where possible, to reduce the effect of potential genomic DNA contamination. Primers were first examined by conventional PCR, to check for specificity. Only primers giving a single distinct band were used for qPCR. Reactions were performed in a volume of 20µl, using Bio-Rad iQ SYBR Green Supermix. Primers were used at 200-400nM. Reaction mixtures were prepared on ice, and run using a Bio-Rad iCycler PCR machine. The following programme was used as a starting point:

Start:	95°C, 3 mins
Cycle (x 40):	95°C, 20s 55°C, 30s
Final denaturing:	95°C, 1 min
Final annealing/extension:	55°C, 1 min
Melt curve (80 steps):	55°C, 10s + 0.5°C/cycle

Primer efficiency was measured using a dilution series of cDNA. The efficiency, E, was calculated using the gradient of a graph of log (template) against threshold cycle,  $C_t$ . Efficiency is given by the formula:  $E = 10^{(-1/\text{gradient})} - 1$ . Only primers with efficiencies of 90-110% were used for RNA quantification.

The Pfaffl method (Pfaffl, 2001) was used for the relative quantification of cDNA levels. This equation takes into account the efficiency of a primer set when calculating relative changes in gene expression. Housekeeping primers for GAPDH and  $\beta$ -actin were used for normalisation of cDNA levels.

## 2.2 PROTEIN BIOLOGY

### 2.2.1 Recombinant Protein Expression

The expression of recombinant proteins in bacteria can in some cases affect bacterial growth or survival. In order to minimise these effects, a repression system was used to prevent protein expression until required. The expression plasmid, pET14b, contained the sequence for expression under the control of the bacteriophage T7 promoter. The BL21 bacterial cells express the T7 phage polymerase under the control of the *lac* promoter, which is repressed by the plasmid pREP4. The addition of isopropyl-beta-D-thiogalactopyranoside (IPTG) removes this repression, allowing expression of T7 polymerase and therefore the recombinant protein. This system allows very low levels of expression “leak” in the absence of IPTG, but high levels of expression after IPTG addition, due to the strength of the T7 promoter. To prevent degradation of the recombinant proteins, protease-deficient BL21 cells were used for expression.

BL21(DE3) cells were co-transformed with pET14b containing the Na<sub>v</sub>1.8 1-120 or p11 sequence, and pREP4, as described, and grown overnight at 37°C on LB agar plates containing 0.01% (w/v) ampicillin and 0.002% (w/v) kanamycin. A colony from these plates was then used to inoculate 200ml L-broth containing 0.01% (w/v) ampicillin and 0.002% (w/v) kanamycin. This was grown overnight at 30°C, 170rpm, in an orbital shaker. The culture was then diluted to 4x 500ml L-broth (0.01% (w/v) ampicillin and 0.002% (w/v) kanamycin) in 2-litre barbed flasks, to ensure sufficient aeration, and grown for 2 hours at 30°C. IPTG was added to 10µM final concentration, and the cultures grown for a further 4 hours. The cells were harvested by centrifugation at 3,800 rpm (Kendro Heraeus Multifuge) for around 40 mins, then stored overnight at -80°C.

### 2.2.2 Purification of Recombinant Proteins

Following the expression of recombinant proteins, purification was achieved using the His-Tag – Ni-NTA (nickel-nitrilotriacetic acid) system. This system uses NTA-chelated Ni<sup>2+</sup> ions attached to agarose resin to bind a 6 x His sequence at the N- or C-terminal end of a peptide, allowing its isolation from cellular lysate. Once the recombinant protein has been isolated from the lysate, it can be released by either a reduction in pH or the addition of imidazole as a competitor.

### **2.2.2.1 Purification of Nav1.8 1-120 (Wild-type & Mutant)**

It was found that the protein “Nav1.8 1-120” and related proteins were confined to inclusion bodies after bacterial expression, due to low cytoplasmic solubility. The extraction and purification of these proteins therefore required denaturing methodologies to be used. Extraction was possible using 8M urea and 2mM  $\beta$ -mercaptoethanol.

The frozen bacterial cell pellets were thawed in Buffer B + 2mM  $\beta$ -mercaptoethanol (used to prevent protein aggregation). 20ml per 2 litre culture was used to resuspend. The mixture was homogenized in a dounce homogenizer (Wheaton, 15ml) using at least 20 up and down strokes (tight pestle), then incubated on a roller incubator for 15 mins at room temperature. This was followed by centrifugation at 10,000 X g for 30 mins, after which the supernatant was taken.

2ml Ni-NTA agarose beads (Novagen), equivalent to 1ml bead volume, were washed with buffer B and added to the supernatant. This was incubated on a roller incubator for 1 hour at room temperature. The beads were centrifuged at 3,800 rpm for 10 mins and the supernatant discarded. The beads were washed with 2x 50ml Buffer C + 2mM  $\beta$ -mercaptoethanol, then loaded into a column cartridge (Evergreen Scientific). After the liquid had run out, the beads were washed with a further 10ml Buffer C + 2mM  $\beta$ -mercaptoethanol. The protein was then eluted with 3ml Buffer E + 2mM  $\beta$ -mercaptoethanol.

### **2.2.2.2 Buffer exchange**

For use in FRET interaction assays, it was necessary to transfer recombinant Nav1.8 1-120 from the 8M urea buffer to the physiological buffer PBS. The 3ml eluate from the purification protocol was concentrated using a Centricon YM-3000 centrifugal concentrator (Millipore). After washing the filter with water then Buffer B + 2mM  $\beta$ -mercaptoethanol, the protein solution was added and concentrated to around 0.5ml (giving a concentration of around 40mg/ml) by centrifugation at 4,000 X g. The concentrated protein was then added dropwise to 4.5ml PBS + 2mM  $\beta$ -mercaptoethanol. The resulting 5ml was taken over 2 PD10 columns (Amersham Biosciences) equilibrated in PBS + 2mM  $\beta$ -mercaptoethanol, giving an eluate of 2 x 3.5ml, which was stored at 4°C.

### **2.2.2.3 Cy3 Labelling of Nav1.8 1-120**

Following buffer exchange, 2.5 ml Nav1.8 1-120 was labelled using 1 vial of Cy3 fluorophore (PA23000, Amersham). 0.5ml of the aliquot was added to 1 vial of Cy3 label, mixed, and returned to the remaining solution. Incubation was carried out at room temperature for 45

mins. The labelled material was then taken over a PD10 column equilibrated in PBS + 2mM  $\beta$ -mercaptoethanol, and 3.5ml eluate collected.

#### **2.2.2.4 Isolation of Pure p11**

In contrast to recombinant Na<sub>v</sub>1.8 1-120, p11 was found to have a high cytoplasmic solubility. This allowed purification in its native state (i.e. in the physiological buffer PBS).

The frozen bacterial cell pellets were thawed in 20ml PBS + 10mM imidazole, 2mM  $\beta$ -mercaptoethanol, the protease inhibitors leupeptin, benzamidine and PMSF, and DNase I. Lysozyme was added to 0.05% (w/v) and Triton X-100 to 1% (w/v) final volume, followed by homogenization in a dounce homogenizer. At least 20 up and down strokes with the tight pestle were performed, followed by incubation at 4°C for 15 mins. The resulting mixture was then spun at 11,000 rpm for 30 mins. The supernatant was taken and incubated with 1ml bead volume Ni-NTA beads for 1 hour, with occasional shaking. The beads were then spun at 3,800 rpm for 30 mins, and the supernatant discarded. The beads were washed sequentially with 50ml PBS + 2mM  $\beta$ -mercaptoethanol, 2x 50ml PBS + 20mM imidazole + 2mM  $\beta$ -mercaptoethanol, and 2x 50ml PBS + 40mM imidazole + 2mM  $\beta$ -mercaptoethanol. After loading into a column cartridge, a further wash of 2x 5ml PBS + 40mM imidazole + 2mM  $\beta$ -mercaptoethanol was performed. Two elutions were carried out using 10ml PBS + 250mM imidazole + 2mM  $\beta$ -mercaptoethanol. The eluate was collected and stored at 4°C. Purity was assessed using SDS-PAGE, and concentration was measured as described.

#### **2.2.2.5 Cy5 Labelling of p11**

5mg of p11 protein in 2.5ml was labelled with 1 vial of Cy5 fluorophore (PA25000, Amersham). Concentration of p11 was adjusted before labelling if necessary, using a centrifugal concentrator. 0.5ml p11 was added to the Cy5 vial, mixed, and returned to the p11 solution. After incubation at room temperature for 30 mins, the labelled material was taken over a PD10 column equilibrated in PBS + 2mM  $\beta$ -mercaptoethanol, and 3.5ml eluate collected.

### **2.2.3 Measurement of Protein Concentration**

A variety of methods have been described for the measurement of protein concentration in solution, each with particular considerations. Biochemical methods, such as the Bradford and Lowry assays, depend on the presence of particular residues, particularly those with aromatic side chains, with which the reagent reacts to form coloured complexes. With complex mixtures

of proteins, such as whole-cell lysates, these methods work well, relying on an averaging effect to normalise aromatic residue variation between proteins. These methods, however, are unsuitable for comparing concentrations of pure proteins with different compositions. In this case, two proteins of equal concentration may appear to be of different concentrations due to differing aromatic content. For solutions of pure proteins, absorbance at 280nm ( $A_{280}$ ) is a more accurate way of comparing concentration. For a known sequence, the extinction coefficient per unit concentration can be calculated using chemical models, allowing adjustment for sequence differences and thus permitting accurate comparisons between proteins of different composition.

### **2.2.3.1 Bradford Assay**

The Bradford assay was used as a quick method to determine approximate protein concentration. 1ml Bradford reagent (Sigma) was added to protein in a volume of less than 10ul in a plastic disposable cuvette. After 10 mins at room temperature, absorbance at 595nm was read. A standard curve (bovine serum albumin, Sigma) and appropriate blanks were used to convert absorbance to concentration.

### **2.2.3.2 Micro Lowry Assay (Peterson's Modification)**

The Lowry method was also used to measure protein concentration. 1ml of Lowry reagent (Sigma) was added to protein in less than 10ul volume, in a plastic disposable cuvette. After 30 mins incubation at room temperature, 0.5ml Folin & Ciocalteu's phenol reagent (Sigma) was added. After a further 30 mins absorbance was read at 595nm. A BSA standard was used.

### **2.2.3.3 Measurement of Protein Concentration by Absorbance at 280nm**

Absorbance at 280nm was used to measure protein concentration. The extinction coefficient for each protein, based on primary structure, was determined using the program ProtParam from the ExPASy Proteomics Server (<http://www.expasy.org/>). The absorbance at 280nm of 1ml of protein was measured by spectrophotometer. The appropriate buffer was used as a blank. Absorbance was converted to concentration using the formula:

$$\text{Concentration (M)} = \frac{\text{Absorbance}}{\text{Path Length (cm)} \times \text{Extinction Coefficient (M}^{-1} \text{ cm}^{-1})}$$

#### 2.2.3.4 BCA Method

The BCA method was performed according to manufacturer's instructions.

#### 2.2.4 Measurement of p11- Na<sub>v</sub>1.8 1-120 Interaction by Fluorescence Resonance Energy Transfer (FRET)

Experiments were carried out in black-bottomed 384 well plates (Fluorotrac 200). A total volume of 50 $\mu$ l was used for each well. Cy-5 labelled p11 was added to all wells, followed by unlabelled competitor if required. Plates were spun at 300rpm for 1 min, then Cy5-labelled Na<sub>v</sub>1.8 1-120 was added. Addition of labelled components was performed using a Matrix Impact 2 multichannel pipette. The plates were spun again before being analysed in an LJL Biosystems Analyst. Analysis was performed immediately, at 5 mins, and at 30 mins. Data were recorded using the program CriterionHost (Molecular Devices). For FRET recording, the wells were excited using light at 525nm, and fluorescence was recorded at 695nm. In each case, wells without labelled p11 or without labelled Na<sub>v</sub>1.8 1-120 were included to quantify "bleed-through" (either excitation of p11-Cy5 by light at 525nm, or emission of light around 695nm by excitation of Na<sub>v</sub>1.8-Cy3). When both were present in a well, the expected emission at 695nm would be the additive of these measurements. Any 695nm fluorescence above this level was therefore taken to be FRET-dependent. FRET was therefore defined as total fluorescence at 695nm after subtraction of bleed-through. Each concentration/condition was present in triplicate. The experimental approach is summarised below:

p11-Cy5	-	+	-	+
Na <sub>v</sub> 1.8-Cy3	-	-	+	+
Function	Background	Bleed-through	Bleed through	FRET

#### 2.2.5 Analysis of FRET Protein Interaction Studies

Data were downloaded from CriterionHost into Microsoft Excel, and converted into the required format. GraphPad Prism was then used for analysis. Interactions between 2 labelled proteins were fit to the One-Site Binding function, while data from competition assays were fit to the One-Site Competition function using non-linear regression. B<sub>Max</sub>, K<sub>d</sub> and IC<sub>50</sub> (denoted in Prism as EC<sub>50</sub>) were the main parameters of interest. Comparisons were performed by Student's *t*-test.

### **2.2.6 SDS-PAGE**

Denaturing SDS Polyacrylamide Gel Electrophoresis (SDS-PAGE) was used to separate proteins by molecular weight. SDS anions impart a uniform charge per unit mass (1.4:1) to the protein, negating the effects of charged amino acids and allowing separation solely by size. Dithiothreitol (DTT) was used to reduce disulphide bonds, allowing proteins to adopt the required random coil configuration.

8-16% acrylamide gels were made in a Hoefer Mighty Small gel caster. Higher percentage gels were used to visualise larger proteins. Running gel was made as follows: for 10ml of 16% gel, 4ml 40% acrylamide/bisacrylamide mix was added to 0.15ml 20% SDS, 3.75ml 1M Tris (pH 8.8), and 2.15ml ddH<sub>2</sub>O. To polymerise the mixture, 0.01ml TEMED and 0.05ml 20% ammonium persulfate were added, and the mixture poured into the caster. A layer of butan-1-ol was used to prevent inhibition of polymerisation by atmospheric oxygen, and to provide a smooth transition between the running and stacking gels. Once the running gel had set, a layer of stacking gel was added. The stacking gel is more porous than the running gel, and causes the accumulation of the proteins in a very thin layer at the interface between the two gel layers. For 10ml stacking gel, the following components were mixed: 1.67ml 40% (v/v) acrylamide/bisacrylamide mix, 0.05ml 20% SDS, 1.25ml 1M Tris (pH 6.8), 7ml ddH<sub>2</sub>O, 0.01ml TEMED and 0.05ml 20% ammonium persulfate.

The gels were then transferred to the electrophoresis apparatus (Hoefer Mighty Small Mini-Vertical Unit), and covered with running buffer. Samples were mixed with 4 x sample buffer (containing DTT) and incubated at 95°C for 3-5 mins. After brief centrifugation, samples were then loaded onto the gel using a Microliter #702 syringe. A constant current of 35mA per gel was applied across the gel for around 1 hour.

### **2.2.7 Coomassie Blue Staining**

Coomassie Blue staining was used to visualise total protein content on SDS-PAGE gels. Immediately after electrophoresis, gels were transferred to a staining and fixing solution containing 0.1% Brilliant Blue R-250, 50% methanol, 10% acetic acid. After staining overnight, gels were de-stained in 50% methanol, 10% acetic acid.

### **2.2.8 Western Blotting**

Western blotting was used to transfer proteins to a nitrocellulose membrane, allowing verification of protein identity by antibody binding. Immediately after SDS-PAGE, gels were transferred to a nitrocellulose membrane (Hybond-C, Amersham Biosciences) in transfer buffer (25mM Tris-HCl pH 8.3, 192mM glycine, 0.1% SDS, 20% methanol) for 1h at 100V. Semi-

dry transfer was used for smaller proteins, but wet transfer used for larger proteins to increase transfer efficiency. The membrane was blocked with 5% non-fat milk in PBS-Tween (0.1%) for 1h at room temperature and then incubated with primary antibody, diluted 1:200-1:1000 in blocking buffer, overnight at 4°C. The membrane was then washed 3 times with PBS-Tween and horseradish peroxidase-conjugated secondary antibody applied at 1:1000 in PBS-Tween for 2h at room temperature. For anti-His-Tag Western blots, the Novagen protocol for His-Tag Monoclonal Antibody was followed. Bound secondary antibody was detected using ECL Detection reagent (Amersham Pharmacia Biotech), exposed to BioMax film (Kodak, Harrow, UK).

Quantification of western blots was performed using the programme ImageJ (National Institutes of Health, USA). Band pixel density was calculated and normalised according to reference gene bands, before comparison to control. The area of analysis was kept constant, and greater than band size, between test and control, to account for effects of differences in band area. Blots were repeated several times for quantitative data.

### **2.2.9 Immunocytochemistry**

DRG were excised and neurons cultured on poly-L-lysine and laminin-coated glass cover slips for 24-48 hours. Cells were fixed using 4% paraformaldehyde for 5 mins at room temperature, washed (3 x 5 mins) in PBS, then blocked and permeabilised in PBS containing 0.1% Triton X-100 and 10% goat serum for 20 mins at room temperature. Cells were incubated with primary antibody diluted 1:100-1:1,000 in blocking solution for 2 hours, washed, then exposed to secondary antibody (Alexa 488 or 595), diluted 1:100, for one hour. Following a final wash, cover slips were mounted on slides with Citifluor (Citifluor, Leicester, UK) to prevent bleaching. Images were obtained using a Zeiss confocal microscope.

### **2.2.10 Immunohistochemistry**

DRG were excised from humanely-killed mice and rapidly frozen in OCT. 12 µm sections were cut by Cryostat and mounted on Superfrost Plus (positively-charged) slides. Following 30-45 mins drying, the slides were fixed in 4% paraformaldehyde for 5mins on ice. Sections were washed and permeabilised in PBS + 0.3% Triton X-100 (3 x 5 mins), then blocked in PBS + 10% goat serum (or appropriate other species) for 1 hour at room temperature. Primary antibody was diluted in blocking buffer (1:200 – 1:1,000) and exposed to the sections for 2 hours at room temperature, or overnight at 4°C. Slides were then washed (3 x 10 mins) in PBS, before addition of secondary antibody (Alexa Fluor 488 or 594) in blocking buffer and

incubation for 1-2 hours in the dark (room temperature). 3 x 5 mins washes reduced background before mounting with CitiFluor™, which helps to prevent photo-bleaching of the fluorophore. Images were obtained using a fluorescence light microscope.

## 2.3 ELECTROPHYSIOLOGY

### 2.3.1 Whole-cell patch-clamp recordings

DRG neuron cultures were prepared from humanely-killed mice aged 4-8 weeks, as described previously (Stirling et al., 2005). Neurons were maintained in culture in the presence of NGF ( $0.25\mu\text{g}\cdot\text{ml}^{-1}$ ) for a maximum of 48 hours. Whole-cell patch-clamp was performed in the absence of TTX, followed by the addition of 250nM TTX by acute local superfusion.

Voltage-clamp recordings were made from single DRG neurons of  $\leq 25\ \mu\text{m}$  diameter, using an Axopatch 200B amplifier controlled by PClamp 9 software (both Axon Instruments, Union City, CA). Neurons were voltage-clamped at  $-80\text{mV}$ , except when a noticeable  $\text{Na}_v1.9$ -mediated current was observed, where the cells were held at  $-60\text{mV}$  to inactivate this channel. Series resistance was compensated for at 70-70%, using a feedback lag of  $12\mu\text{s}$ . Currents were elicited by incremental ( $+10\text{mV}$ ) depolarizing steps (50ms duration), preceded by a hyperpolarizing pulse to  $-100\text{mV}$  to remove any inactivation. Averages of 3 sweeps were taken to form the current records, which were filtered at 5 KHz (8-pole Bessel). TTX-sensitive currents were obtained by digital subtraction of the TTX-resistant current from total current. Current density estimates were made from stable, maximal current amplitudes. All currents included in the analysis displayed appropriate kinetics and voltage dependencies, corresponding to TTX-sensitive or  $-\text{resistant Na}^+$  channels. Current densities were compared using a Mann-Whitney rank sum test, since the current distributions failed normality testing.

Resting potential measurements were made in current-clamp mode. Voltage-clamp mode was used to patch the cell, holding at  $-70\text{mV}$ , then the amplifier configuration was switched. No current was injected, and the resting potential was read immediately. This minimised the effect of dialysis of pipette solution into the cell altering the ionic balance across the membrane. Voltage-clamp was then used to examine the sodium channels present in the cell, to allow grouping of cells by channel expression.

### 2.3.2 *In vivo* recordings from dorsal horn neurons

Measurements of electrical inputs into wide dynamic range neurons in the spinal cord were carried out as described previously (Matthews et al., 2006), in urethane-anaesthetised mice. Single-unit extracellular recordings were made following electrical, mechanical or thermal stimulation of varying magnitude. A- and C-fibre-mediated responses were distinguished by latency relative to initial stimulus. Neuronal responses occurring after the C-fibre latency band of the neuron (250 – 800 ms) were classed as postdischarge, a result of repeated stimulation leading to wind-up neuronal hyperexcitability. The 'input' (non-potentiated response), and the

'wind-up' (potentiated response, evident by increased neuronal excitability to repeated stimulation) were calculated. Input = (action potentials (50 - 800ms) evoked by first pulse at 3 times C-fibre threshold) x total number of pulses (16). Wind-up = (total action potentials (90 - 800ms) after 16 train stimulus at 3 time C-fibre threshold) – Input. Data are presented as mean  $\pm$  S.E.M. Two-factor ANOVA with replication was used for statistical analysis and the level of significance taken to be  $p < 0.05$ .

## **2.4 ANIMAL BREEDING & BEHAVIOURAL ANALYSIS**

Animals were bred at University College London under conditions complying with United Kingdom Home Office guidelines. They were housed in filter cages, with a 12 hour light/dark cycle and were fed standard chow and water *ad libitum*.

All behavioural tests were approved under the United Kingdom Home Office Animals (Scientific Procedures) Act 1986. They were performed in a Home Office designated room at 22±2°C. Experiments were performed on F5 or F6 animals of at least 8 weeks of age. p11 floxed (p11<sup>-/-</sup>), Nav1.8 Cre heterozygote (+/-) animals were compared to Cre-negative littermate controls. Results for male and female animals were combined, unless a significant difference was found in testing. All experiments were performed blind by the same observer.

### **2.4.1 Motor Function**

The Rotarod test (Ugo Basile) was used to assess motor function. Animals were placed on the rod at a constant rate of 20rpm. After one minute the rate of revolution was switched to a progressively increasing mode, reaching a maximum of 36rpm after 2 mins, until the animal fell. A cut-off time of 5 mins was used. Each animal was tested 3 times, with at least 1 hour recovery between tests. The results for the two groups were compared using a Student's *t*-test.

### **2.4.2 Mechanical Withdrawal Thresholds**

Withdrawal thresholds to mechanical stimuli were measured using the Randall-Selitto apparatus and von Frey hairs.

#### **2.4.2.1 Randall-Selitto**

Each animal was placed in a restrainer (IITC) and left to settle for a few minutes until cessation of struggling. An analgesy meter (Ugo Basile) was used to apply an increasing force to the tail, at a point where the tail diameter was just greater than that of the probe. Three tests were performed per animal, each on a different section of the tail. The force at which the animal attempted to withdraw the tail or struggle was recorded. The results for the two groups were compared using an unpaired 2-tailed Student's *t*-test.

#### **2.4.2.2 von Frey**

Animals were acclimatised in individual chambers with a metal mesh floor for 1-2 hours, until exploratory activity had ceased. The up-down method, as described by Chaplan *et al.* (1994),

was used to assess the 50% withdrawal threshold of each mouse. This method has been shown to be more powerful and less labour-intensive than battery methods. Starting from hair 7 (0.6g), hairs were applied until moderate bending occurred. If a response was elicited, the next test used a weaker hair, and *vice-versa*. 6 trials were performed on each mouse, with at least 10 mins between applications. Results were analysed using an unpaired 2-tailed Student's *t*-test.

### **2.4.3 Thermal Thresholds**

Withdrawal thresholds to thermal stimuli were measured using Hargreaves' apparatus and the hot plate.

#### **2.4.3.1 Hargreaves' Apparatus**

Animals were acclimatised to test chambers on a clean Plexiglass plate for at least 1 hour until exploratory activity had ceased. Beam intensity was set to give a latency to withdrawal of around 10-15s. Paw withdrawal latency was measured on the left hindpaw, with 4 repeats per animal and at least 2 mins between tests. Results were compared using an unpaired 2-tailed Student's *t*-test.

#### **2.4.3.2 Hot Plate**

Animals were acclimatised to the hot plate (Ugo Basile) in it in groups of 4-6 for 15 mins, with the plate at room temperature. Latency to hindpaw licking was measured at 50°C and 55°C. Each animal was tested once at each temperature, with tests separated by 24 hrs. Results were compared using an unpaired 2-tailed Student's *t*-test.

### **2.4.4 Inflammatory Pain Models**

#### **2.4.4.1 Intraplantar Nerve Growth Factor**

Baseline thermal withdrawal thresholds for the left hindpaw were measured for each animal using Hargreaves' test. 50ng human-recombinant NGF in 5µl saline carrier (pH 7.0) was delivered subcutaneously to the plantar region of the left hindpaw using a Hamilton syringe with 27g needle. Hargreaves' test was then repeated at intervals for the next 24 hours. Data were expressed for each mouse as relative change from baseline. These data were compared using 2-way repeated measures analysis of variance.

#### **2.4.4.2 Intraplantar Carrageenan**

Baseline thermal withdrawal thresholds for the left hindpaw were measured for each animal using Hargreaves' test. 20µl of 2% carrageenan in saline was injected into the plantar region of

the left hindpaw as before. Thermal withdrawal thresholds were then measured at hourly intervals. Data were expressed for each mouse as relative change from baseline, and were compared using 2-way repeated measures analysis of variance.

#### **2.4.4.3 Intraplantar Formalin**

Animals were acclimatised individually to an observation chamber for around 15 mins, until exploratory activity had ceased. 20 $\mu$ l of 5% formalin (40% formaldehyde) in saline was injected subcutaneously into the plantar region of the left hindpaw, using a Hamilton syringe and 27g needle. The time spent engaged in nocifensive behaviour (licking or biting the injected paw) was recorded in 5 minute sections over the next hour. The first phase of response was defined as 0-10 mins post-injection, while the second phase referred to subsequent behaviour. Comparison was made using an unpaired 2-tailed Student's *t* test.

#### **2.4.5 Neuropathic Pain Model**

A modified version of the Chung method (Kim and Chung, 1992) was used to induce neuropathic pain in the mouse. First, baseline measurements of mechanical and thermal withdrawal thresholds (von Frey and Hargreaves`) were performed on two consecutive days. Animals were then anaesthetised using halothane, and a midline incision made into the skin of the back. The L5 transverse process was removed and the left L5 spinal nerve cut. This surgery was performed by Mohammed Nassar and Bjarke Abrahamsen. Mechanical and thermal withdrawal thresholds were then assessed at intervals, up to 25 days post-surgery. Thresholds were expressed as relative changes compared to pre-surgery baselines, at the level of the individual animal. Results were analysed using 2-way repeated measures analysis of variance.

## **2.5 ANGIOGENESIS ASSAYS**

### **2.5.1 Tumour cell growth**

Cell from the B16 murine melanoma line, derived from the C57BL/6 strain, were cultured in DMEM + 10% FCS. Cultures were passaged 1:10 before confluence, until sufficient numbers were obtained at 30% confluence. Cells were then trypsinised, washed and resuspended at a concentration of 1,000,000 cells/200µl PBS.

### **2.5.2 Melanoma cell injection**

1,000,000 cells, in 200µl PBS, were injected subcutaneously into the dorsal neck region of each mouse. After days, during which time the health of the animals was monitored carefully, the animals were humanely sacrificed and the tumours excised. Tumour volume was measured by multiplying the maximum length, breadth and depth measurements. Tumours were then fixed in 4% PFA overnight, before being subjected to histological analysis.

## 3 MAPPING THE $\text{Na}_v1.8$ -P11 INTERACTION

### 3.1 INTRODUCTION

The intelligent design of pharmacological inhibitors of the p11- $\text{Na}_v1.8$  interaction, which has been proposed as a therapeutic target, requires a detailed understanding of the nature of the domains involved in binding. This chapter explores the residues in the  $\text{Na}_v1.8$  N-terminus required for its interaction with p11.

#### 3.1.1 $\text{Na}_v1.8$ -p11 Interaction

Voltage-gated sodium channels (VGSCs) consist of primary, pore-forming  $\alpha$ -subunits and auxiliary  $\beta$ -subunits. Whilst  $\alpha$ -subunits are sufficient for voltage-gated channel activity,  $\beta$ -subunits are required for cellular localisation, full levels of functional expression and certain aspects of channel kinetics (reviewed in Isom (2000)). Expression of  $\alpha$ -subunits alone in heterologous cell expression systems (including mammalian cell lines) often results in low-level functional expression, with altered voltage-dependence of activation and inactivation (Isom, 2001). When co-expressed with  $\beta$ -subunits, however, the expression levels and kinetics of most VGSCs become closer to those of the endogenous channels (Isom et al., 1994; Isom et al., 1995).

Although functional expression of  $\text{Na}_v1.8$  in *Xenopus* oocytes is increased by co-expression with the  $\beta 1$  subunit, (Vijayaragavan et al., 2004b), current densities remain substantially below endogenous levels in DRG. The functional expression of  $\text{Na}_v1.8$  in CHO, COS-7 and HEK-293 cell lines is poor even in the presence of  $\beta$ -subunits (England, 1998), with channels showing different properties from the endogenous current (FitzGerald et al., 1999). Microinjection of  $\text{Na}_v1.8$  cDNA into the nuclei of SCG or  $\text{Na}_v1.8$ -null mutant DRG neurons, however, produces sodium currents with similar properties and magnitude to wild-type DRG neurons (England, 1998). More recent studies have successfully expressed functional  $\text{Na}_v1.8$  channels in neural cell lines (SH-SY5Y, ND7-23), with properties matching the endogenous current (Dekker et al., 2005; John et al., 2004). These data imply that  $\text{Na}_v1.8$  requires the presence of additional regulatory factors, present in DRG neurons, to achieve endogenous levels of functional expression.

Okuse et al. (2002) used the yeast two-hybrid system to search for proteins interacting with the intracellular domains of  $\text{Na}_v1.8$ . Of the 28 positive clones identified, five were found to code for the S100 protein p11 (Malik-Hall et al., 2003). Co-expression of p11 with  $\text{Na}_v1.8$  in CHO

cells resulted in the translocation of the channel from cytosol to plasma membrane. Co-expression also resulted in the manifestation of a high-threshold TTX-R sodium current similar to that observed in DRG neurons, which was down-regulated by antisense mRNA to p11 (Okuse et al., 2002). Poon et al. (2004) demonstrated that p11 binds directly to the N-terminus of Nav1.8, but not to other VGSCs. The GST pull-down assay was used to map the p11-Nav1.8 interaction to residues 33-78 of p11, and residues 74-103 of Nav1.8, using sequences from the rat. In contrast to the p11-interacting domains of TASK-1 and TRPV5/6 (Girard et al., 2002; van de Graaf et al., 2003), this region of Nav1.8 does not contain a PDZ consensus binding sequence, nor any other readily-identifiable domain. The region has a characteristic cluster of acidic and basic amino acids divided by a putative  $\beta$ -strand, which is well-conserved in other species, including mouse (Poon et al., 2004). Two domains with low homology to other sodium channels have been identified (residues 87-90 and 98-102), which may play a role in binding to p11. Other than these regions, however, a fairly high degree of homology with other VGSCs is seen.

The involvement of annexin 2 in the Nav1.8-p11 interaction has not been investigated. 2 models for the annexin 2-p11 complex, a heterotetramer and a hetero-octamer, have been proposed (Lewit-Bentley et al., 2000). In both cases, the putative binding domains for Nav1.8 are the most peripheral and exposed (Poon et al., 2004). Since annexin 2 is present in higher quantities in the cell than p11 (SE Moss, personal communication), it is likely that annexin 2 forms part of the p11-Nav1.8 complex.

No further localisation of the p11-Nav1.8 interaction has been carried out, possibly due to methodological limitations relating to the sensitivity of the GST pull-down assay. It has been postulated, however, that disruption of this interaction may be a valid target for analgesic drug design (Okuse et al., 2002). For directed (intelligent) design of small molecule inhibitors of this interaction, a more precise definition of the binding region is required. We used fluorescence resonance energy transfer (FRET), in combination with the expression of mutant proteins, as a tool to allow more precise mapping of the p11-Nav1.8 interaction.

### **3.1.2 Identification of binding domains for p11- protein interactions**

The role of p11 in trafficking proteins to the plasma membrane is not restricted to Nav1.8. Since the publication of the requirement of p11 for Nav1.8 functional expression (Okuse et al., 2002), several other membrane proteins which require p11 have been identified. Girard et al. (2002) reported that the interaction of p11 with the 2-pore domain K<sup>+</sup> channel TASK-1 is essential for trafficking to the plasma membrane. The C-terminal sequence Ser-Val-Val of

TASK-1 was found to be required for the association. Binding of p11 to the channel was found to mask an endoplasmic reticulum retention signal, Lys-Arg-Arg, preceding the Ser-Val-Val binding domain. In a subsequent publication, however, Renigunta et al. (2006) found no requirement of this sequence, and instead identified a 40-amino acid region, 120-80 residues from the C-terminus. In this study, p11 was found to cause the retention of TASK-1 in the endoplasmic reticulum, in direct contrast to the previous work (Renigunta et al., 2006). Retention was ascribed to residues on p11 rather than TASK-1, via the putative endoplasmic reticulum retention motif (H/K)<sub>x</sub>K<sub>xxx</sub> at the C-terminal end of p11. No explanation has been found for the discrepancy between these studies with respect to the inferred binding site for p11. The range of techniques used in each investigation was similar (yeast 2-hybrid, co-immunoprecipitation, GST pull-down, whole-cell patch clamp), as were the model systems used. It has been proposed, however, that the stimulatory effect on TASK-1 trafficking observed by Girard et al. (2002) may have been mediated by another TASK-1 interacting protein, 14-3-3, the binding of which may also have been disrupted by deletion of C-terminal amino acids on TASK-1 (Renigunta et al., 2006). The involvement of annexin 2 in the p11-TASK-1 interaction has not been formally tested, but seems unlikely, since the C-terminus of TASK-1 binds to the same or overlapping regions on p11 as annexin 2 (Renigunta et al., 2006).

The functional expression of the epithelial Ca<sup>2+</sup> channels TRPV5 and TRPV6 was also found to require the association of p11 (van de Graaf et al., 2003). These interactions were found to take place via a conserved sequence, VATTV, in the C-terminal tails of TRPV5 and TRPV6. The first threonine of this sequence was found to play a crucial role in the interaction, shown by the analysis of mutant channels. No information was given in this report regarding residues on p11 required for the interaction. Using GST pull-down and co-immunoprecipitation assays, however, the authors were able to demonstrate that annexin 2 is part of the TRPV5-p11 complex. siRNA-mediated downregulation of annexin 2 was shown to inhibit TRPV5/6 mediated currents in HEK cells, although this may be explained by the observation that under normal conditions, annexin 2 upregulates levels of p11 by a post-translational mechanism (Puisieux et al., 1996). This means that downregulation of annexin 2 may act via a reduction in p11 levels rather than directly on TRPV5/6.

ASIC1a (Donier et al., 2005) and 5-HT<sub>1B</sub> (Svenningsson et al., 2006) have also been shown to interact with p11, but investigation of the domains involved in binding has yet to be undertaken.

### 3.1.3 FRET

FRET describes the physical phenomenon whereby energy is transferred non-radiatively from an excited fluorophore to an acceptor molecule. Long-range dipole-dipole coupling occurs over distances between 1-10nm, allowing energy transfer without the emission of a photon (Förster, 1948). The transfer rate is inversely proportional to the 6<sup>th</sup> power of the donor-acceptor separation distance within this range, allowing its use as a “spectroscopic ruler” (Stryer, 1978). These 1-10nm distances are relevant for most biomolecular associations (Jares-Erijman and Jovin, 2003), meaning that in practice FRET can be used as a surrogate measure of molecular interaction, or “binding”. The occurrence of FRET is therefore indicative of protein-protein interaction in this context.

If the acceptor molecule in this system is itself a fluorophore, the occurrence of FRET will cause the emission of photons of a characteristic wavelength. In this instance, excitation of the donor fluorophore will cause emission in the spectrum of the acceptor. This is illustrated in Figure 3.1, using Cy3 and Cy5 as example fluorophores, and Na<sub>v</sub>1.8 and p11 as interacting proteins.

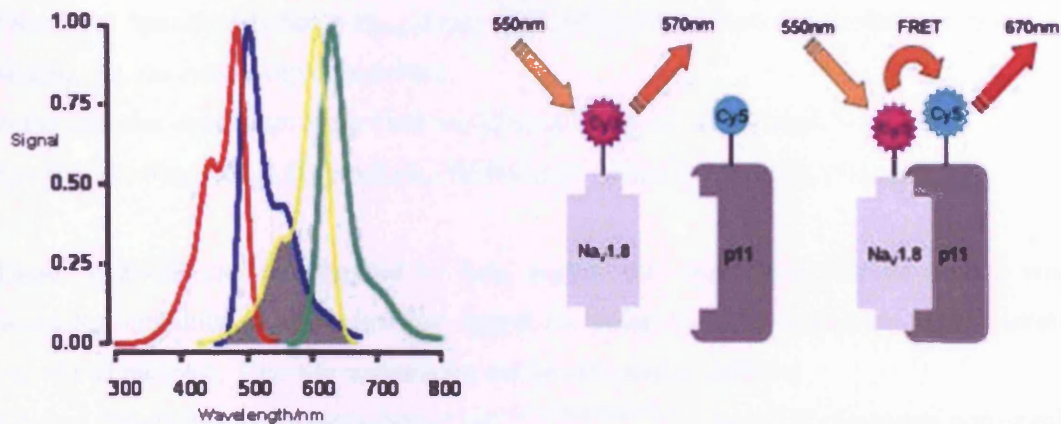


Figure 3.1 Fluorescence resonance energy transfer used to detect protein-protein interactions. Graph: Red line represents Cy3 excitation spectrum, blue Cy3 emission, yellow Cy5 excitation and green Cy5 emission.

FRET can be measured either as quenching of the donor fluorescence (in this example reduction in output at 570nm) or as an increase in acceptor fluorescence (670nm in this example). The former method suffers less from the problem of “bleed-through”, where the acceptor can be made to fluoresce to a small degree by the donor excitation spectrum. The latter method, however, provides a more direct measurement of the interaction process.

### 3.1.4 Protein-protein interaction models

Site-specific protein-protein interactions can be modelled in the same way as ligand-receptor binding, using the principles of the law of mass action. The law of mass action states that the rate of a reaction is proportional to the concentrations of the reactants. For the reaction: Receptor + Ligand  $\rightleftharpoons$  Receptor.Ligand, the rate of forward reaction can be given by:

Rate = [Receptor].[Ligand]. $k_{on}$ , where  $k_{on}$  is the rate constant for the forward reaction. At equilibrium, the rates of forward and reverse reaction are by definition equal, meaning that [Receptor].[Ligand]. $k_{on}$  = [Receptor.Ligand]. $k_{off}$ . Since  $k_{on}$  and  $k_{off}$  are constants, they can be combined into the equilibrium dissociation constant  $K_d$ :

$$K_d = k_{off} \cdot k_{on}^{-1} = [Ligand].[Receptor]/[Ligand.Receptor].$$

$K_d$  thus gives a measure of the affinity of the ligand for the receptor, and is the concentration of ligand required to reach half-maximal receptor occupancy. From this, a model for single-site binding can be derived:

$$\begin{aligned} \text{Fractional Occupancy} &= [Ligand.Receptor]/[Receptor]_{\text{Total}} \\ &= [Ligand.Receptor]/([Ligand.Receptor] + [Receptor]) \\ &= [Ligand]/([Ligand] + ([Ligand].[Receptor]/[Ligand.Receptor])) \\ &= [Ligand]/([Ligand] + K_d) \end{aligned}$$

Therefore: Specific Binding =  $B_{Max} \cdot [Ligand]/(K_d + [Ligand])$ , where  $B_{Max}$  is the maximal binding (i.e. the total receptor number).

In the case that one receptor can bind two ligand molecules, the equation becomes:

$$\text{Specific Binding} = B_{Max1} \cdot [Ligand] \cdot (K_{d1} + [Ligand])^{-1} + B_{Max2} \cdot [Ligand] \cdot (K_{d2} + [Ligand])^{-1}$$

These equations can be extended to form models for competition binding assays, where increasing amounts of unlabelled test ligand are added to fixed concentrations of labelled ligand and receptor. One-site competition can be described as follows:

Binding (labelled) =  $NS + (Max - NS) \cdot (1 + 10^{\text{Log}[Ligand] - \text{Log}[IC_{50}]})^{-1}$ , where NS represents non-specific binding.  $IC_{50}$  is the concentration of unlabelled competitor that is required to block 50% of the specific binding, and is therefore dependent on the affinity of the competitor for the labelled "receptor".  $IC_{50}$  can be converted to a dissociation constant,  $K_i$ , using the Cheng and Prusoff equation (Cheng and Prusoff, 1973):

$$K_i = IC_{50} / (1 + [Ligand^*]/K_d^*)$$

Where [Ligand\*] is the concentration of labelled ligand, and  $K_d^*$  is the corresponding dissociation constant. This is derived as follows:

For the reactions  $A + R \rightleftharpoons AR$  and  $B + R \rightleftharpoons BR$ , where R is a receptor capable of binding A and B, and  $K_A$  and  $K_B$  are the *association* constants for each reaction:

$$\begin{aligned} [R]_{\text{Total}} &= [R] + [AR] + [BR] \\ &= [R] + K_A \cdot [A] \cdot [R] + K_B \cdot [B] \cdot [R] \end{aligned}$$

$$= [R] \cdot (1 + K_A \cdot [A] + K_B \cdot [B])$$

Therefore  $[R] = [R]_{\text{Total}} / (1 + K_A \cdot [A] + K_B \cdot [B])$

Since  $[AR] = K_A \cdot [A] \cdot [R]$ ,

$$[AR] = K_A \cdot [A] \cdot [R]_{\text{Total}} / (1 + K_A \cdot [A] + K_B \cdot [B])$$

Therefore  $[AR] / [R]_{\text{Total}} = K_A \cdot [A] / (1 + K_A \cdot [A] + K_B \cdot [B])$

When  $[A] = IC_{50}$ ,  $[AR] / [R]_{\text{Total}} = 0.5$ , therefore  $0.5 = K_A \cdot IC_{50} / (1 + K_A \cdot IC_{50} + K_B \cdot [B])$

Therefore  $K_A = (1 + K_B \cdot [B]) / IC_{50}$

And  $K_i = IC_{50} / (1 + K_B \cdot [B])$

We employed a combination of site-directed mutagenesis and *in vitro* FRET measurement to map the domains of Na<sub>v</sub>1.8 required for interaction with p11. This approach allowed direct quantitative measurement of the effect of mutations in Na<sub>v</sub>1.8 on its affinity for p11. By identifying the residues critical for interaction, the design of small molecule or peptide inhibitors will be facilitated.

### 3.2 METHODS

Human p11 cDNA was amplified from human a cDNA library (Invitrogen) by PCR, and inserted into the vector pCRII. This construct was made by Lodewijk Dekker. The sequence was then ligated into the expression vector pET14b (containing a 5' His-Tag), and expressed as described previously.

The process of making mutant  $Na_v1.8$  constructs is summarised in Figure 3.2. Human  $Na_v1.8$  N-terminal cDNA was isolated from DRG RNA (Analytical Biological Services), used as a template for Smart<sup>TM</sup> cDNA synthesis, followed by specific amplification based on public sequence information and ligation into the vector pCRII. This was performed by Lodewijk Dekker (Dekker et al., 2005). The resulting amino acid sequence for  $Na_v1.8$  1-120 is:

MEFPIGSLETNNFRRFTPESLVEIEKQIAAKQGTTKAREKHREQKDQEEKPRPQLDLKA  
CNQLPKFYGELPAELIGEPLEDLDPFYSTHRTFMVLNKGRTISRFSATRALWLFSPFNLI  
R

PCR was used to produce three mutant sequences, each with a third of the sequence deleted, and the fragment 41-80. This was intended to confirm previous work on the interaction region. The full sequence was also altered by site-specific primer mismatch mutagenesis, to produce a series of 3-amino acid deletions in the predicted p11-binding region. The constructs created are shown in Table 3.1.

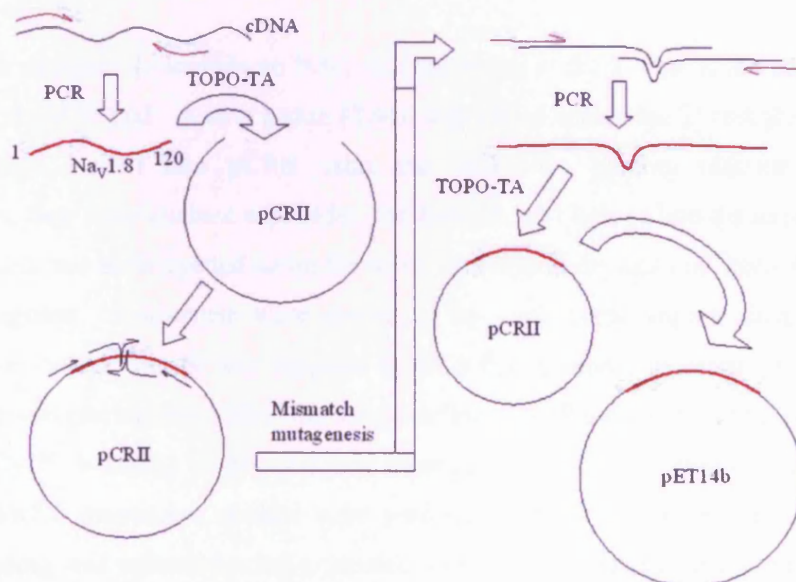


**Figure 3.2 Overview of cloning and generation of mutants for  $Na_v1.8$  1-120.** Human cDNA was used to generate the 1-120 fragment, which was cloned into pCRII. Primer mismatch mutagenesis allowed the production of mutant sequences, which were subcloned into pCRII then cloned into pET14b.

Name	Description
Na <sub>v</sub> 1.8 1-120	DNA coding for amino acids 1-120 of Na <sub>v</sub> 1.8 N-terminus
Na <sub>v</sub> 1.8 41-80	DNA coding for amino acids 41-80 of Na <sub>v</sub> 1.8 N-terminus
Na <sub>v</sub> 1.8 Δ2-40	Na <sub>v</sub> 1.8 1-120 with amino acids 2-40 deleted
Na <sub>v</sub> 1.8 Δ41-80	Na <sub>v</sub> 1.8 1-120 with amino acids 41-80 deleted
Na <sub>v</sub> 1.8 Δ81-120	Na <sub>v</sub> 1.8 1-120 with amino acids 81-120 deleted
Na <sub>v</sub> 1.8 ΔLIG	Na <sub>v</sub> 1.8 1-120 with amino acids LIG (74-76) deleted
Na <sub>v</sub> 1.8 ΔEPL	Na <sub>v</sub> 1.8 1-120 with amino acids EPL (77-79) deleted
Na <sub>v</sub> 1.8 ΔEDL	Na <sub>v</sub> 1.8 1-120 with amino acids EDL (80-82) deleted
Na <sub>v</sub> 1.8 ΔDPF	Na <sub>v</sub> 1.8 1-120 with amino acids DPF (83-85) deleted
Na <sub>v</sub> 1.8 ΔYST	Na <sub>v</sub> 1.8 1-120 with amino acids YST (86-88) deleted
Na <sub>v</sub> 1.8 ΔHRT	Na <sub>v</sub> 1.8 1-120 with amino acids HRT (89-91) deleted
Na <sub>v</sub> 1.8 ΔFMV	Na <sub>v</sub> 1.8 1-120 with amino acids FMV (92-94) deleted
Na <sub>v</sub> 1.8 ΔLNK	Na <sub>v</sub> 1.8 1-120 with amino acids LNK (95-97) deleted
Na <sub>v</sub> 1.8 ΔGRT	Na <sub>v</sub> 1.8 1-120 with amino acids GRT (98-100) deleted
Na <sub>v</sub> 1.8 ΔISR	Na <sub>v</sub> 1.8 1-120 with amino acids ISR (101-103) deleted

**Table 3.1 Mutant proteins produced using the His-Tag bacterial expression/purification system.**

Primers were designed to include an NdeI restriction site at the 5' end of the construct, and a BamHI site at the 3' end. A stop codon (TAG) was added before the 3' restriction site. PCR products were inserted into pCRII using the TOPO-TA cloning reaction. Following amplification, they were excised with NdeI and BamHI, and ligated into the expression vector pET14b, which had been opened using the same restriction enzymes and treated with SAP to prevent re-ligation. Constructs were sequenced by Lark Technologies, then expressed as described previously. Purity was assessed by SDS-PAGE, and concentrations measured by absorption spectrophotometry. Identities were confirmed by Western blot using anti-His-Tag. Following Cy3/5 labelling of proteins (on average, less than one fluorophore per protein molecule), FRET interaction studies were performed, using several experimental designs. Initially, binding was validated using a titration approach, adding increasing concentrations of labelled Na<sub>v</sub>1.8 to a fixed quantity of labelled p11. Mutant proteins were then investigated using a competition binding approach, adding increasing concentrations of unlabelled mutant to fixed quantities of labelled Na<sub>v</sub>1.8 and p11. Finally, small peptides (chemically synthesised) were used in this competition assay, as shown in Table 3.2.

Name	Sequence
Na <sub>v</sub> 1.8 74-103	Residues 74-103 of Na <sub>v</sub> 1.8 N-terminus
Na <sub>v</sub> 1.8 74-88	LIGEPLEDLDPFYST
Na <sub>v</sub> 1.8 89-103	HRTFMVLNKGRTISR
Na <sub>v</sub> 1.8 74-81	LIGEPLED
Na <sub>v</sub> 1.8 82-88	LDPFYST
Na <sub>v</sub> 1.8 89-96	HRTFMVLN
Na <sub>v</sub> 1.8 97-103	KGRTISR

**Table 3.2 Peptides produced by chemical synthesis.**

For each FRET study, bleed-through was measured and subtracted from the FRET reading, to give a measure of sensitised emission. This ensures that the values used represent binding only, and not other fluorescence effects. For details of analysis, see Chapter 2.

### 3.3 RESULTS

#### 3.3.1 $\text{Na}_v1.8$ N-terminus and p11 can be expressed at high levels and purified to >95% purity

##### 3.3.1.1 $\text{Na}_v1.8$ N-terminus

The protein “ $\text{Na}_v1.8$  1-120” and related mutants were extracted and purified in 8M urea, due to their accumulation in inclusion bodies. After purification, these proteins were estimated to be >95% pure, assessed by SDS-PAGE. An example gel is shown in Figure 3.3. Occasionally proteins were found to have contaminants, probably due to errors in the purification process. These proteins were not used in FRET assays. At high concentrations, dimers were often observed. These were not considered to be contaminants.

Protein identity was confirmed by Western blotting, using anti-His-Tag for identification. An example Western blot is shown in Figure 3.3. Concentrations of these proteins (assessed by  $A_{280}$ ) were 50-200 $\mu\text{M}$ . After transfer from 8M urea to PBS, concentrations were 10-100 $\mu\text{M}$ .

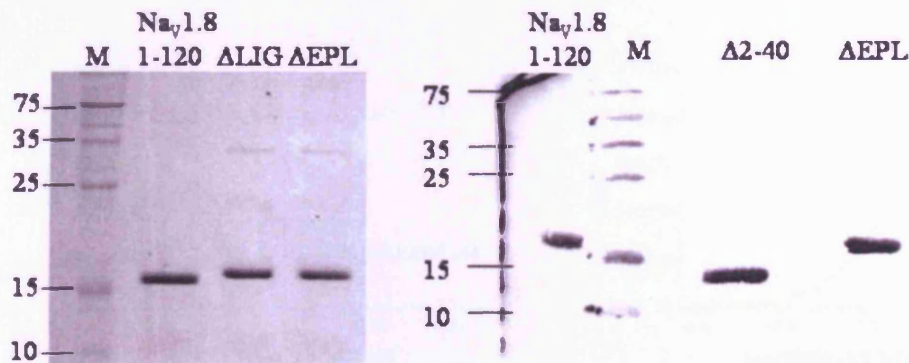


**Figure 3.3 Confirmation of protein identity and purity.** Coomassie blue-stained SDS-PAGE gel (left) and anti-His-Tag Western blot (right). Molecular weight in kDa given on the left of each image. M, marker. Other lanes as labelled.

##### 3.3.1.2 p11

p11 was extracted and purified under native conditions, using PBS as a buffer. 2mM  $\beta$ -mercaptoethanol was found to be sufficient to minimise dimerisation. Following purification, purity was assessed by SDS-PAGE, and found to be in excess of 95%.

p11 identity was confirmed by anti-His-Tag Western blotting. Concentrations of p11 were 200-300 $\mu\text{M}$  after Cy5 labelling.

### 3.3.2 FRET-based assays effectively measure the site-specific interaction between Na<sub>v</sub>1.8 and p11

Before investigating the effects of Na<sub>v</sub>1.8 N-terminal mutations on binding to p11, it was necessary to validate our FRET methodology using wild-type recombinant proteins. The objective of this was to show that the FRET signal was arising from the Na<sub>v</sub>1.8-p11 interaction, and was therefore both selective and site-specific. The reproducibility of interaction parameters was also examined.

Increasing concentrations of Cy3-labelled Na<sub>v</sub>1.8 1-120 were added to a fixed concentration (250ng/well) of Cy5-labelled p11. FRET resulting from the interaction (after subtraction of baseline and bleed-through) was found to fit well to a one-site binding model, shown in Figure 3.4. The K<sub>d</sub> for the interaction was typically around 100nM. A two-site binding model was found to offer no improvement of fit. A clear saturation was evident at high concentrations of Na<sub>v</sub>1.8 1-120, implying that the increase in FRET with Na<sub>v</sub>1.8 1-120 concentration is due to a site-specific protein-protein interaction, rather than a non-specific effect of increasing fluorophore concentrations.

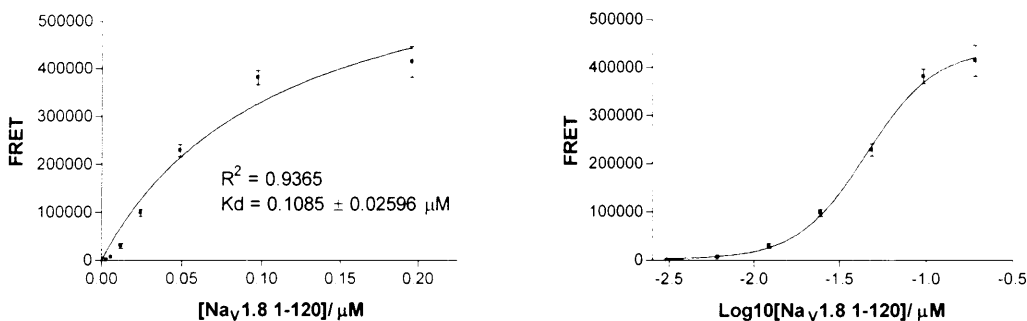


**Figure 3.4 Titration of Cy3-Na<sub>v</sub>1.8 against 250ng Cy5-p11 (conventional and log plots).** The equation for one-site binding was used to model the data: Specific Binding =  $B_{\text{Max}} \cdot [\text{Ligand}] / (K_d + [\text{Ligand}])$ . A K<sub>d</sub> of around 100nM was observed.

A similar experiment was performed titrating increasing concentrations of p11 against a fixed concentration of Na<sub>v</sub>1.8 1-120. The data fit well to a one-site binding model and exhibited saturation at high concentrations of p11, confirming the previous result.

To confirm that the FRET signal observed was due to site-specific protein-protein interactions between p11 and Na<sub>v</sub>1.8 1-120, the ability of unlabelled Na<sub>v</sub>1.8 1-120 to compete with labelled Na<sub>v</sub>1.8 1-120 for the binding site was examined. Increasing concentrations of unlabelled Na<sub>v</sub>1.8 1-120 were added to fixed amounts of labelled Na<sub>v</sub>1.8 1-120 (200nM) and p11. Data

were found to fit well to a one-site competition binding model, as illustrated in Figure 3.5, with  $IC_{50}=0.49\pm 0.03\mu M$  ( $n=67$ ) and therefore  $K_i=160\pm 10nM$ . This affinity is similar to that measured by direct binding assay ( $\sim 100nM$ ).

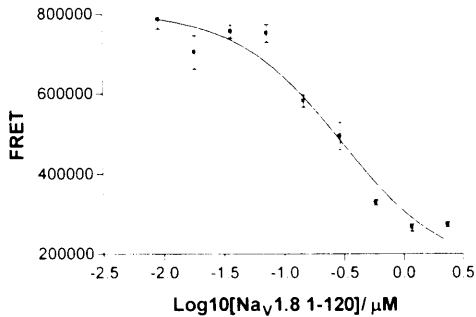


**Figure 3.5** Competition of the Cy3-Na $_v$ 1.8 - Cy5-p11 interaction by unlabelled Na $_v$ 1.8 1-120. The  $IC_{50}$  for this competition, averaged over all tests, was  $0.49\pm 0.03\mu M$  ( $n=67$ ).

As a final proof that the FRET observed was due to a site-specific interaction between p11 and Na $_v$ 1.8, we tested the ability of the annexin 2 (p36) N-terminus (acetyl-1-14) to compete for Na $_v$ 1.8 1-120 binding. Previous work has shown that annexin 2 is unable to bind to Na $_v$ 1.8, but does bind to a distinct site on p11. This means that any reduction in FRET signal observed would be due to non-specific effects. Annexin 2 1-14, however, was unable to decrease the FRET signal in this assay, even at relatively high concentrations. This supports our assertion that the FRET signal originates from site-specific protein-protein interaction between p11 and Na $_v$ 1.8 1-120.

The models and parameters used to describe these interactions apply only if the system is at equilibrium. We therefore investigated equilibration time for binding to ensure that this was the case. Readings were taken immediately and after 5, 10 and 30 mins. No substantial differences were observed, although immediate readings very occasionally appeared to have slightly higher variability. This was ascribed to plate handling procedure. Readings for subsequent experiments were therefore taken after 5-10 mins incubation. Additionally, various reaction volumes were tested. It was found that a total volume of 50 $\mu l$  allowed reproducible and accurate pipetting whilst conserving reagents.

### 3.3.3 Annexin 2 and Na $_v$ 1.8 bind to distinct sites on p11

To determine whether annexin 2 and Na $_v$ 1.8 are likely to bind p11 simultaneously, we investigated whether the binding sites overlap. The N-terminal 14 amino acids of annexin 2 were used for this experiment, using the competition assay format described in the previous

section (note that prevention of simultaneous binding would not prove overlapping sites, but simultaneous binding is unlikely to occur if sites do overlap). Fixed concentrations of labelled p11 and annexin 2 (1-14) were used to generate a FRET signal. Increasing concentrations of unlabelled annexin 2 (1-14) or Na<sub>v</sub>1.8 were used to compete for this interaction, measured by a reduction in FRET signal. Unlabelled annexin 2 (1-14) was able to displace labelled annexin 2 (1-14) from p11, as would be expected (Figure 3.6a), with an IC<sub>50</sub> of 2.5μM. Unlabelled Na<sub>v</sub>1.8 1-120, however, was unable to compete with labelled annexin 2 (1-14) for p11 binding in the concentration range tested (Figure 3.6b).

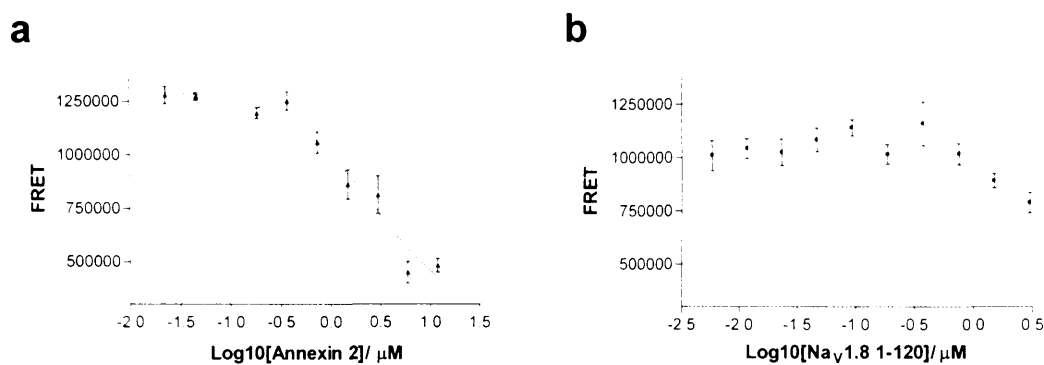


**Figure 3.6 FRET competition assays illustrating distinct binding sites for annexin 2 and Na<sub>v</sub>1.8 on p11.** **a:** Competition for the annexin 2 (1-14)-Cy3 - Cy5-p11 interaction by unlabelled annexin 2. **b:** No competition for this interaction by unlabelled Na<sub>v</sub>1.8 1-120.

### 3.3.4 Amino acids 74-103 of Na<sub>v</sub>1.8 are sufficient to bind p11

Previously it was shown that amino acids 74-103 of Na<sub>v</sub>1.8 are sufficient for binding to p11 (Poon et al., 2004). We tested the ability of the fragment Na<sub>v</sub>1.8 74-103 to compete with labelled Na<sub>v</sub>1.8 1-120 for p11 binding in the FRET assay. Na<sub>v</sub>1.8 74-103 was found to compete effectively with Na<sub>v</sub>1.8 1-120, but displayed a reduced affinity for p11. Figure 3.7 illustrates a typical assay to measure the affinity of unlabelled Na<sub>v</sub>1.8 74-103 for p11, competing for binding against labelled Na<sub>v</sub>1.8 1-120. The IC<sub>50</sub> measured for Na<sub>v</sub>1.8 74-103 was 1.02±0.17μM (therefore K<sub>i</sub>=340±57nM), approximately 2-3 times that of Na<sub>v</sub>1.8 1-120 (p=0.035, 1-tailed t-test). At high concentration, however, Na<sub>v</sub>1.8 74-103 is able to extinguish most non-background FRET, implying that both can not bind simultaneously. A small amount of residual FRET was observed in some assays, particularly in older protein preparations, and is likely to be due to deterioration of the protein over time. This was also observed for older preparations of other Na<sub>v</sub>1.8 fragments.

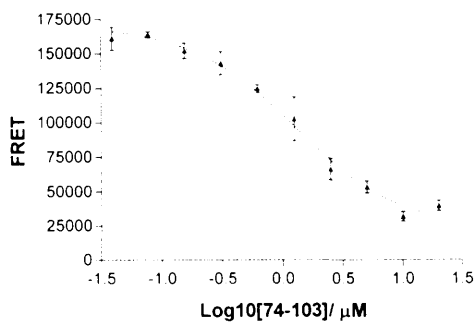


**Figure 3.7** Competition of the Cy3-Na<sub>v</sub>1.8 - Cy5-p11 interaction by unlabelled Na<sub>v</sub>1.8 74-103.

### 3.3.5 Amino acids 2-40 of Na<sub>v</sub>1.8 do not interact with p11

Deletion of amino acids 2-40 had no effect on IC<sub>50</sub> or other parameters (IC<sub>50</sub>: Na<sub>v</sub>1.8 1-120 0.330±0.088μM; Na<sub>v</sub>1.8Δ2-40 0.399±0.092μM; p=0.600) (K<sub>i</sub>: Na<sub>v</sub>1.8 1-120 110±29nM; Na<sub>v</sub>1.8Δ2-40 133±31nM; p=0.600) (Figure 3.8). We therefore conclude that these residues do not take part in the p11-Na<sub>v</sub>1.8 interaction.

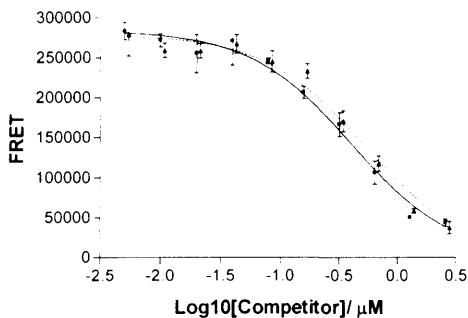


**Figure 3.8** Competition by Δ2-40. Competition of the Cy3-Na<sub>v</sub>1.8 - Cy5-p11 interaction by unlabelled Na<sub>v</sub>1.8 Δ2-40 (dotted line) and Na<sub>v</sub>1.8 1-120 control (solid line).

### 3.3.6 Amino acids 41-80 of Na<sub>v</sub>1.8 interact with p11

Deletion of amino acids 41-80 caused a reduction in affinity for p11 of approximately 3-fold (IC<sub>50</sub> Na<sub>v</sub>1.8 1-120 0.323±0.006μM; Na<sub>v</sub>1.8Δ41-80 1.083±0.091μM; n=4; p=0.003) (K<sub>i</sub>: Na<sub>v</sub>1.8 1-120 108±2nM; Na<sub>v</sub>1.8Δ41-80 361±30nM; n=4; p=0.003). Na<sub>v</sub>1.8Δ41-80, however, retained the ability to bind to p11, and was able to compete with the tracer to the same extent as Na<sub>v</sub>1.8 1-120 at high concentration (Figure 3.9a). The peptide consisting of amino acids 41-80 of Na<sub>v</sub>1.8 (Na<sub>v</sub>1.8 41-80) showed an affinity for p11 comparable to that of full-length Na<sub>v</sub>1.8 1-120 (IC<sub>50</sub> ratio 0.92; n=3; p=0.83) (Figure 3.9b).

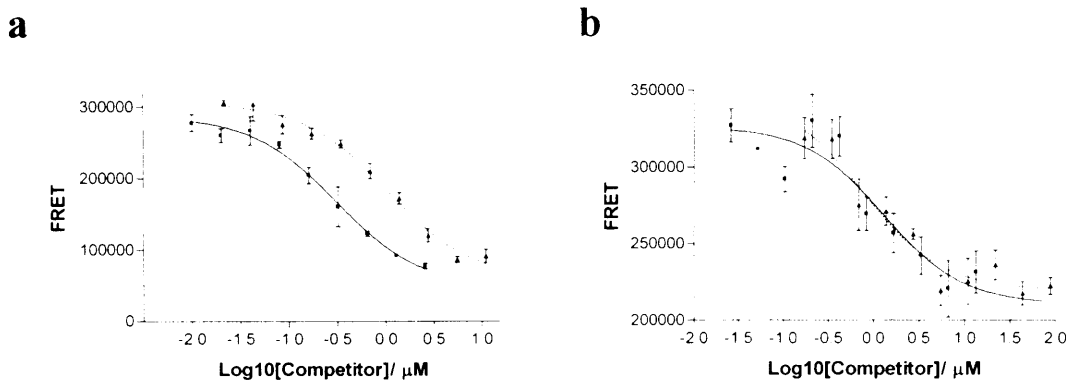


**Figure 3.9 Binding at residues 41-80.** Competition of the Cy3-Na<sub>v</sub>1.8 - Cy5-p11 interaction by: **a:** unlabelled Na<sub>v</sub>1.8 Δ41-80; **b:** Na<sub>v</sub>1.8 41-80. Dotted lines represent fragments, while solid lines show Na<sub>v</sub>1.8 1-120 control.

### 3.3.7 Amino acids 81-120 of Na<sub>v</sub>1.8 inhibit Na<sub>v</sub>1.8 1-120 binding to p11

Amino acids 81-120 were expected to be essential for the p11-Na<sub>v</sub>1.8 interaction, since the predicted binding domain is contained largely within this region. Deletion of these residues, however, caused a noticeable (~5-fold) increase in affinity for p11 ( $IC_{50}$  Na<sub>v</sub>1.8 1-120  $0.398 \pm 0.050 \mu M$ ; Na<sub>v</sub>1.8Δ81-120  $0.081 \pm 0.008 \mu M$ ;  $n=6$ ;  $p=0.001$ ) ( $K_i$ : Na<sub>v</sub>1.8 1-120  $133 \pm 17 nM$ ; Na<sub>v</sub>1.8Δ81-120  $27 \pm 3 nM$ ;  $n=6$ ;  $p=0.001$ ), suggesting an inhibitory or obstructive role for these residues in p11 binding. Figure 3.10a shows the results of a representative competition assay. Since this result was surprising, the data were verified by direct binding assay. Δ81-120 was labelled with Cy3, and was added at increasing concentrations to a fixed amount (250ng/well) of p11, with data shown in Figure 3.10b. This was compared to the binding curve for Na<sub>v</sub>1.8 1-120. The  $K_d$  of Na<sub>v</sub>1.8 81-120 was found to be approximately 4-fold lower (i.e. 4-fold higher affinity) than that of Na<sub>v</sub>1.8 1-120 (81-120  $K_d=26.04 \pm 3.16 nM$ ), consistent with the competition assay results.

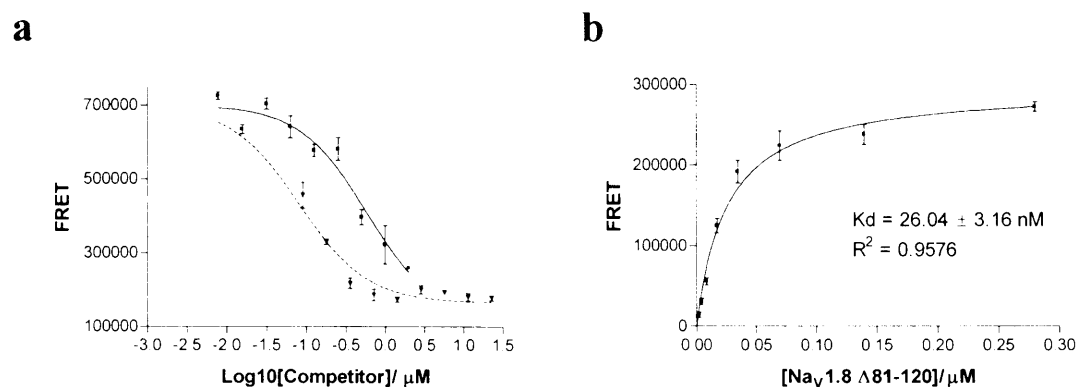


**Figure 3.10 Inhibition of interaction by residues 81-120.** **a:** Competition of the Cy3-Na<sub>v</sub>1.8 - Cy5-p11 interaction by unlabelled Na<sub>v</sub>1.8 Δ81-120 (dotted line) and Na<sub>v</sub>1.8 1-120 control (solid line). **b:** Titration of Cy3-Na<sub>v</sub>1.8 Δ81-120 against 250ng p11.

### 3.3.8 Summary

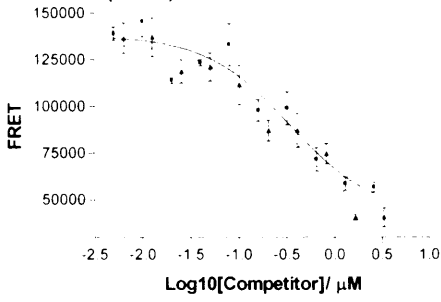
Amino acids 2-40 of Na<sub>v</sub>1.8 do not take part in the Na<sub>v</sub>1.8-p11 interaction, since deletion of these residues has no effect on affinity. Deletion of residues 41-80 reduced affinity for p11 by approximately 3-fold, while residues 41-80 alone were able to bind p11 with affinity comparable to Na<sub>v</sub>1.8 1-120. Deletion of residues 81-120 increased affinity for p11 by 4-5-fold. Residues 74-103 were able to bind to p11, but with an affinity around 2-3 times lower than that of Na<sub>v</sub>1.8 1-120.

### 3.3.9 3-amino acid deletions in the region 74-103 of Na<sub>v</sub>1.8 have subtle effects on affinity for p11, but do not prevent binding

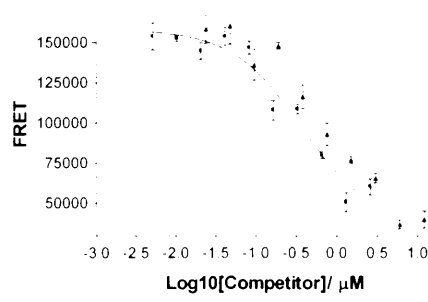
We attempted to locate the residues critical for binding p11 in the proposed interaction domain (74-103) of Na<sub>v</sub>1.8 by deleting sections of 3 amino acids from this region, then examining changes in affinity for p11. In each case, the ability of mutant proteins to displace labelled Na<sub>v</sub>1.8 1-120 was compared to wild-type unlabelled Na<sub>v</sub>1.8 1-120. Example competition assays are shown in Figure 3.11, and the results summarised in Figure 3.12 and Table 3.3. Deletion of residues EPL or DPF was found to decrease affinity for p11 ( $p < 0.05$ ), implying that these residues are involved in the interaction with p11. Deletion of residues YST or GRT increases affinity for p11 ( $p < 0.05$ ), showing that these residues mediate the residue 81-120 inhibition of the interaction. Deletions of the residues between YST and GRT also show a trend towards increased affinity, but this was not found to be significant ( $\Delta$ HRT  $p = 0.138$ ,  $\Delta$ LNK  $p = 0.062$ ). Additionally, deletion of residues LIG or LNK appeared to increase affinity, but this effect was not found to reach significance ( $p = 0.064$ ,  $p = 0.062$  respectively). This may be an allosteric effect via nearby residues, or only a portion of an interacting/inhibitory region may be contained within each deletion.

*t*-tests were performed on raw data rather than on relative (ratio) data, to avoid problems with non-normal distributions of ratios.

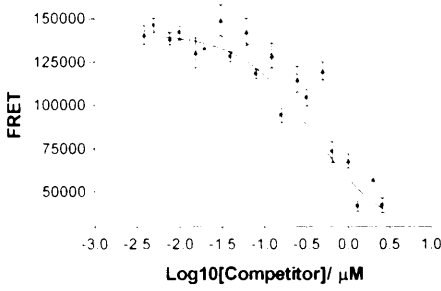
$\Delta 74-76$  (LIG)



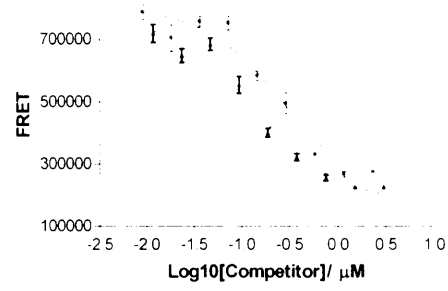
$\Delta 77-79$  (EPL)



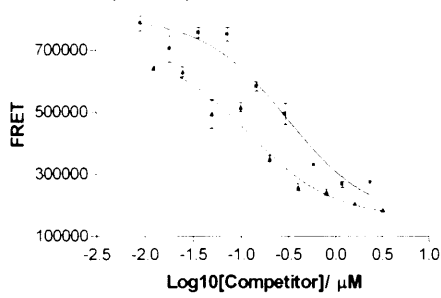
$\Delta 83-85$  (DPF)



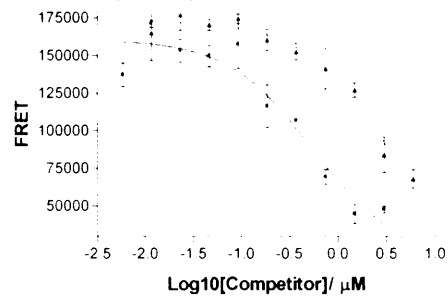
$\Delta 86-88$  (YST)



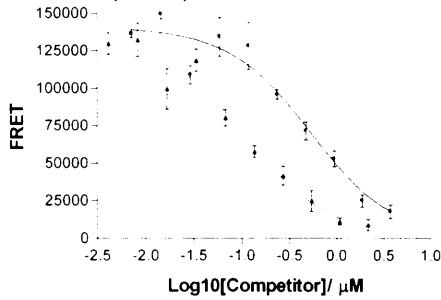
$\Delta 89-91$  (HRT)



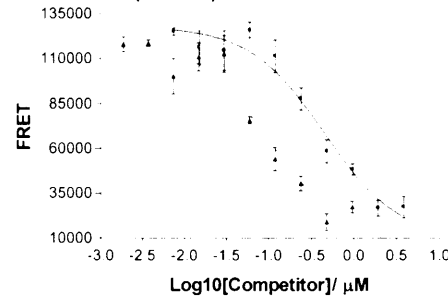
$\Delta 92-94$  (FMV)



$\Delta 95-97$  (LNK)



$\Delta 98-100$  (GRT)



$\Delta 101-103$  (ISR)

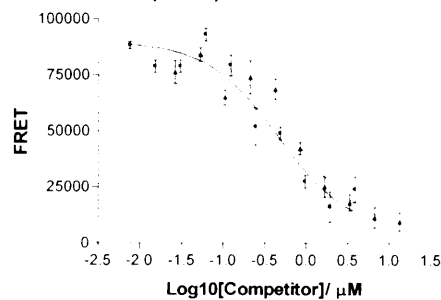


**Figure 3.11 Examples of 3-amino acid deletion assays.** Competition of the Cy3- $\text{Na}_v1.8$  - Cy5-p11 interaction by unlabelled mutant  $\text{Na}_v1.8$  (dotted lines) and  $\text{Na}_v1.8$  1-120 control (solid lines).

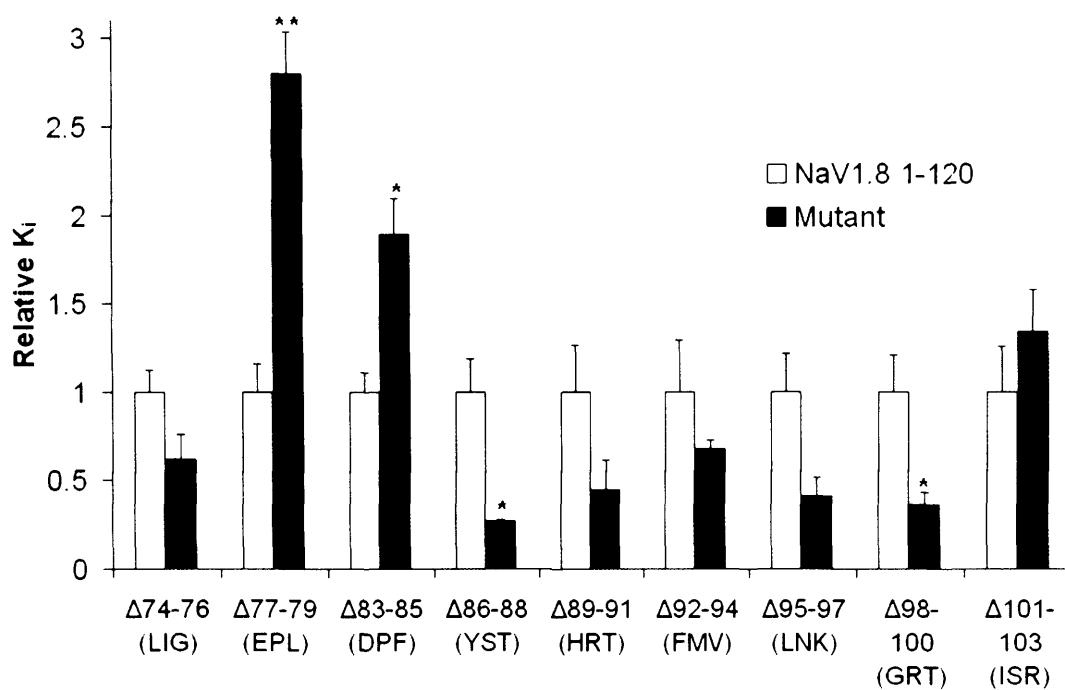


**Figure 3.12 Effects of 3-amino acid deletions.** Summary of the effects of 3-amino acid deletions on affinity for p11, relative to Na<sub>v</sub>1.8 1-120 control. Internal controls were used for each experiment. An increase in relative  $K_i$  indicates a reduction in affinity for p11. \* $p < 0.05$ . \*\* $p < 0.01$ . Error bars represent SEM.

Mutant	Relative $K_i$	SEM
Na <sub>v</sub> 1.8 1-120	1	0.042534
Δ74-76 (LIG)	0.621926	0.140270
Δ77-79 (EPL)	2.801114**	0.233456
Δ 83-85 (DPF)	1.891907*	0.204136
Δ86-88 (YST)	0.270146*	0.012406
Δ89-91 (HRT)	0.448688	0.167565
Δ92-94 (FMV)	0.677061	0.049715
Δ95-97 (LNK)	0.413666	0.099779
Δ98-100 (GRT)	0.361565*	0.071078
Δ101-103 (ISR)	1.340576	0.234789

**Table 3.3 Summary of effects of 3-amino acid deletions.** Summary of the effects of 3-amino acid deletions on affinity for p11, relative to Na<sub>v</sub>1.8 1-120 control. An increase in relative  $K_i$  indicates a reduction in affinity for p11 compared to control. \* $p < 0.05$ . \*\* $p < 0.01$ .

### 3.3.10 Na<sub>v</sub>1.8 74-81 is sufficient to bind p11

The subtle effects of small deletions in the predicted p11-binding domain of Na<sub>v</sub>1.8 prompted the design of an alternative experimental strategy. Rather than searching for a mutation that would prevent the interaction, we attempted to identify the smallest fragment of the predicted binding domain that would retain the capacity to bind p11. The peptide 74-103 was first divided into 2 sections, then each of these divided in half again. Competition binding experiments were performed for each peptide, shown in Figure 3.13a. Na<sub>v</sub>1.8 74-88 retained the ability to interact with p11, with an IC<sub>50</sub> of 7.229±2.012μM (n=4) (K<sub>i</sub>=2.4±0.7μM). Na<sub>v</sub>1.8 89-103, however, did not cause a noticeable reduction in FRET signal in the concentration range tested. This implies either that Na<sub>v</sub>1.8 89-103 is not capable of binding to p11 in a site-specific manner, or that it does so with such reduced affinity that the effect is not apparent within the range of concentrations tested.

Of the smaller fragments tested, only Na<sub>v</sub>1.8 74-81 retained the ability to bind to p11, albeit with a reduced affinity compared to Na<sub>v</sub>1.8 1-120 (Na<sub>v</sub>1.8 74-81 IC<sub>50</sub> 23.641±11.892μM; n=3) (K<sub>i</sub>=7.9±3.9). This is shown in Figure 3.13b. The other small peptides were not able to bind p11 at the concentrations tested.

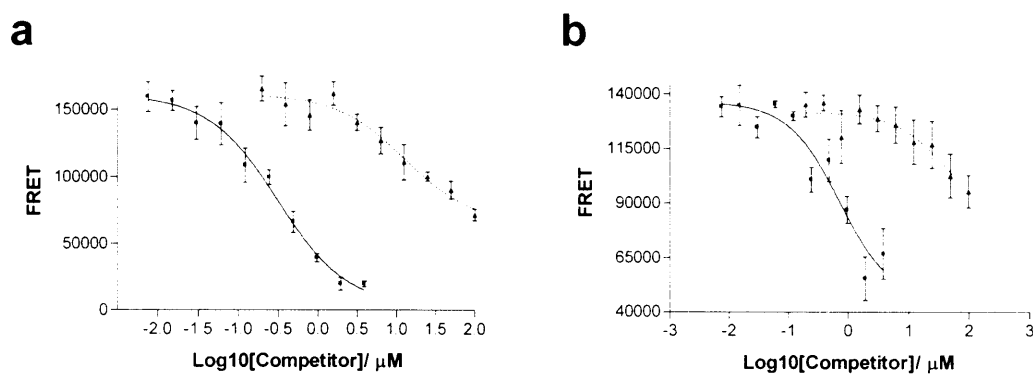


**Figure 3.13 Localisation of binding site to residues 74-81.** **a:** Competition of the Cy3-Na<sub>v</sub>1.8 - Cy5-p11 interaction by unlabelled Na<sub>v</sub>1.8 74-88 (dotted line) and Na<sub>v</sub>1.8 1-120 control (solid line). **b:** Competition of the Cy3-Na<sub>v</sub>1.8 - Cy5-p11 interaction by unlabelled Na<sub>v</sub>1.8 74-81 (dotted line) and Na<sub>v</sub>1.8 1-120 control (solid line).

### 3.3.11 Summary of Results

For ease of comparison, results are summarised in Figure 3.14.

Protein	Relative $K_i$
Na <sub>v</sub> 1.8 1-120	1
Na <sub>v</sub> 1.8 Δ2-40	1.21
Na <sub>v</sub> 1.8 Δ41-80	2.98
Na <sub>v</sub> 1.8 41-80	0.92
Na <sub>v</sub> 1.8 Δ81-120	0.20**
Na <sub>v</sub> 1.8 Δ74-76	0.62
Na <sub>v</sub> 1.8 Δ77-79	2.80**
Na <sub>v</sub> 1.8 Δ80-82	N/A
Na <sub>v</sub> 1.8 Δ83-85	1.89*
Na <sub>v</sub> 1.8 Δ86-88	0.27*
Na <sub>v</sub> 1.8 Δ89-91	0.45
Na <sub>v</sub> 1.8 Δ92-94	0.68
Na <sub>v</sub> 1.8 Δ95-97	0.41
Na <sub>v</sub> 1.8 Δ98-100	0.36*
Na <sub>v</sub> 1.8 Δ101-103	1.34
Na <sub>v</sub> 1.8 74-103	1.82*
Na <sub>v</sub> 1.8 74-88	13.94**
Na <sub>v</sub> 1.8 74-81	19.75**
Na <sub>v</sub> 1.8 89-103	>1,000

**Figure 3.14 Summary of results.** Summary of the involvement of Na<sub>v</sub>1.8 residues on affinity for p11. Relative  $K_i$  is defined as  $K_i$  (protein)/ $K_i$  (Na<sub>v</sub>1.8 1-120). A decrease in relative  $K_i$  corresponds to an increase in affinity for p11. \* $p$ <0.05, \*\* $p$ <0.01 (tests performed on raw data).

## 3.4 DISCUSSION

### 3.4.1 FRET-based assays are suitable for the quantitative investigation of protein-protein interactions

Our data show that this assay system is a powerful tool for the investigation of protein-protein interactions. Traditional (generally antibody-based) methods, such as GST pull-down and immunoprecipitation, are at best considered semi-quantitative with respect to assessment of interaction strength. The detection of interactions is subject to arbitrary factors, such as wash stringency and binding conditions, meaning that only large changes in affinity can be detected reliably. FRET-based *in vitro* binding and competition assays allow more quantitative measurement of interaction affinity, using well-characterised pharmacological analyses. We have found measurements of affinity to be highly reproducible both within and between protein preparations, allowing the detection of changes in affinity of less than 2-fold. Additionally, using FRET to measure interactions *in vitro* allows the assay to be performed in physiological buffers, modelling more closely the conditions under which the interactions occur *in vivo*. The use of highly purified proteins means that non-specific binding is reduced, and the possibility of an alternative interaction influencing results is removed. The lack of intermediary proteins also means that direct interaction can be implied.

In order to be certain that the *in vitro* FRET signal observed was a direct result of a site-specific protein-protein interaction, it was necessary to show that it satisfied the requirements of models resulting from the law of mass action, and could therefore be described in terms of a chemical reaction between the two proteins. Titration curves showed saturation at high concentrations of Na<sub>v</sub>1.8 1-120, implying that p11 levels were limiting the FRET signal. Saturation is a key feature of site-specific interactions, and generally does not occur for non-specific phenomena. Titration curves also fit extremely well to the single-site binding model previously described. This demonstrates that the FRET signal followed the expected behaviour of a site-specific interaction. Titration curves produced from increasing concentrations of p11 against a fixed concentration of Na<sub>v</sub>1.8 1-120 were found to have similar properties. Competition binding assays were also used to show that the FRET signal observed resulted from a site-specific interaction between p11 and Na<sub>v</sub>1.8 1-120. Data from these assays were found to fit the one-site competition model described previously. The ability of unlabelled protein to compete for the interaction site, therefore reducing the FRET signal, is clear evidence that the FRET is due to a specific interaction. The high affinity for this competition ( $K_i \sim 100\text{nM}$ ) supports this observation, since non-specific effects are generally of much lower affinity. Finally, the

inability of annexin 2 to compete for Na<sub>v</sub>1.8 1-120 binding is persuasive evidence of a site-specific interaction. Annexin 2 binds to p11 at a distinct site to Na<sub>v</sub>1.8 (Rety et al., 1999), but is unable to reduce FRET, demonstrating that only proteins binding to a specific site are capable of competition.

### **3.4.2 The Na<sub>v</sub>1.8-p11 interaction is best described by a single-site binding model**

Data from the Na<sub>v</sub>1.8-p11 interaction assays were found to fit well to single-site binding and competition models. The loss of degrees of freedom when switching to 2-site models was found to outweigh any improvement in fit, as shown by *F*-test values. It is important to note, however, that 2-site binding applies to situations where the molar interaction ratio is 1:2. Where a 1:1 interaction occurs via 2 sites on each protein (i.e. the 2 sites are attached), the interaction is best described by a one-site interaction model. In effect, 2 attached domains are modelled as a single site, with affinity given by the sum of affinities of the 2 attached sites. In reality, the situation may be more complex, since binding at the second site may be facilitated by binding at the first. In practice, however, a single-site model remains the best method to describe this type of interaction, since binding at only one site is likely to be an extremely transient process, meaning that the vast majority of proteins will be either free or fully bound, and that partially-bound pairs are unlikely to make a major contribution to the FRET signal. This is supported by the fact that unlabelled fragments of Na<sub>v</sub>1.8 1-120, such as Na<sub>v</sub>1.8 74-103, are able to quench completely the FRET resulting from Na<sub>v</sub>1.8 1-120 – p11 interaction.

### **3.4.3 Amino acids 77-85 of Na<sub>v</sub>1.8 are the critical residues in the 74-103 binding domain**

Poon et al. (2004) identified amino acids 74-103 of Na<sub>v</sub>1.8 as the domain required for binding to p11, using a GST pull-down assay. Our results show that this fragment is capable of binding to p11. Using the FRET assay, however, we were able to discern a significant reduction in affinity for p11 compared with the full length N-terminus (Na<sub>v</sub>1.8 1-120). We employed this assay to characterise the binding site further. The peptide consisting of amino acids 74-88 of Na<sub>v</sub>1.8 retained the ability to interact with p11, whereas the peptide 89-103 did not. The peptide 74-88 was then divided into 2 sections, 74-81 and 82-88, of which only the former was found to retain p11-binding activity. We therefore conclude that amino acids 74-81 of Na<sub>v</sub>1.8 are the p11-binding residues in the Na<sub>v</sub>1.8 N-terminus. The affinity of this peptide, however, was greatly reduced compared to the fragment 74-103. This may suggest that residues other than 74-81 form part of the binding site. It is possible that both fragments 74-81 and 82-88

contain a portion of the binding domain, but that the part retained by the latter is not sufficient for binding to occur at the concentrations tested.

Data from the 3-amino acid deletion proteins appear to support this hypothesis. Residues 77-79 and 83-85 both cause a marked loss of affinity for p11 when deleted (80-82 not tested), and are therefore likely to be involved in the interaction. It is possible that residues 83-85 affect binding via an allosteric mechanism, but the most likely explanation is a direct role in binding p11.

Deletion of residues 74-76 of Na<sub>v</sub>1.8 caused a moderate increase in affinity for p11, which was not found to be statistically significant (p=0.06). Regardless of whether this effect is real or not, the observation precludes a role for these residues in binding p11.

Combining these observations allows us to build a picture of the Na<sub>v</sub>1.8-p11 interaction at residues 74-103. Our evidence identifies residues 77-85 of Na<sub>v</sub>1.8 as those required to interact with p11. These residues possess a characteristic cluster of acidic groups (see Figure 3.15) that are well-conserved in other species (mouse, rat, human and dog). The acidic nature of these amino acids may be important for the Na<sub>v</sub>1.8-p11 interaction, although this has yet to be tested. The region 77-85, however, shows a fairly high degree of homology with other VGSCs, although complete identity is not seen. Evidence from GST pull-down experiments suggests some interaction between the N-termini of other VGSCs and p11, although their relative affinities are not known (Poon et al., 2004).

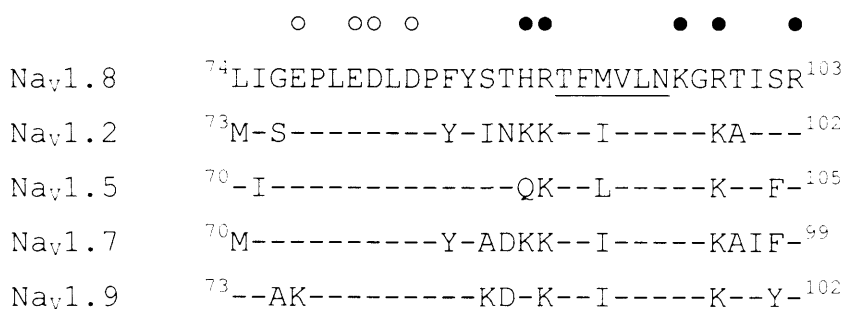


**Figure 3.15 Human Na<sub>v</sub>1.8 74-103: comparison with other VGSCs.** Acidic amino acids (on Na<sub>v</sub>1.8) are marked by white circles, while basic residues are identified by black circles. A putative β-strand is underlined.

### 3.4.4 An additional binding site at residues 41-74

We observed a significant reduction in the affinity of the fragment 74-103 for p11 compared with the full-length  $\text{Na}_v1.8$  N-terminus (1-120). This led us to hypothesise that there may be other residues involved in or capable of binding to p11 in the  $\text{Na}_v1.8$  N-terminus. The fragment 41-80 binds with an affinity identical to that of the full length N-terminus, despite it lacking the major portion of the 77-85 binding site. When residues 41-80 are deleted, affinity for p11 is markedly reduced. Since the fragment 41-80 binds with higher affinity than 74-103, it appears that residues outside the 74-103 region are involved in the binding interaction. The relatively subtle effects of 3-residue deletions in the 77-85 binding domain are most readily explained by an additional interaction outside this region.

The lack of effect of deletion of residues 2-40 allows the localisation of this additional interaction domain to amino acids 41-74. This region was not detected in earlier studies on the p11- $\text{Na}_v1.8$  interaction (Poon et al., 2004), which identified an interaction only in the region 74-103. It is possible that the greater sensitivity of the current study enabled the detection of the additional binding region, whereas methodological factors prevented its discovery previously. For example, the GST pull-down assays used before rely on washing steps of variable stringency to remove background. These steps are often adjusted to give a single, distinct band on the membrane, meaning that the band containing the 41-80 interaction domain may have been removed from the gel as part of the background. Alternatively, this discrepancy may be due to the way in which the full-length construct was divided. Poon et al. (2004) tested the fragments 1-25, 26-50 and 51-127, and subsequently concentrated on the latter region. It is therefore possible that a sequence capable of interaction with p11 in the region 41-80 was divided by this division scheme, rendering each section incapable of interaction. This explanation would require the inclusion of amino acids 50-51 in the interaction domain, which could be investigated in further studies.

Interestingly, the presence of an additional binding site provides a mechanism for the selectivity of p11 for  $\text{Na}_v1.8$  compared to other VGSCs. Since the binding region 77-85 is relatively well conserved, an alternative mechanism for specificity is required. The region 41-80 shows low homology to other VGSCs, as illustrated in Figure 3.16, supporting this hypothesis. Significantly, there are a number of domains common to other VGSCs that are not conserved in  $\text{Na}_v1.8$ , evident in Figure 3.16. These domains may explain the specificity of binding observed.

```

Nav1.8      40 KHREQKDQEEKPRPQLDLKACNQLPKFYGELPAELIGEPLE80
Nav1.1      38 -PDKKD-D-NG-K-NS--E-GKN--FI--DI-P-MVS----78
Nav1.2      39 QE-KDE-D-NG-K-NS--E-GKS--FI--DI-P-MVSV---79
Nav1.3      41 QDN-D-N--K-NS--E-GKN--FI--DI-P-MVS----78
Nav1.4      41 RNKQMEIE-PERK-RS--E-GKN--MI--DP-P-V--I---81
Nav1.5      43 --GLPE--A-----Q-SKK--DL--NP-Q-----81
Nav1.6      44 ---D_-EDS--K-NS--E-GKS--FI--DI-QG-VAV---80
Nav1.7      47 -K-SS--E-GK---FI--DI-PGMVS----76
Nav1.9      34 -SKD-TGEVPQ-----SRK---L--DI-R----K---79
NaX         37 -THNEDHE--DLK-NP--EVGKK--FI--N-SQGMVS----87

-           Identity
Italic     Positives

```

**Figure 3.16 Alignment of protein sequence for human VGSCs.** Generated using NCBI Blast.

The existence of a second binding domain is consistent with the observation that a substantial section (residues 33-78) of p11 is required to bind Na<sub>v</sub>1.8. It was found that the division of this region into smaller fragments, 33-51 and 52-77, prevented the interaction (Poon et al., 2004). This region consists of the loop connecting the 2 EF hands of p11 and the first  $\alpha$ -helix of the second EF hand. While the inactivity of the smaller fragments could be due to the disruption of the binding domain, it is possible that the entire region 33-78 is involved in the interaction, fitting with the presence of 2 binding domains on Na<sub>v</sub>1.8. A hydrogen bond connects residues 48 and 54, which may be important for the p11-Na<sub>v</sub>1.8 interaction, since it is disrupted in the smaller fragments. By analysing the 3D structure of p11, Poon et al. (2004) predicted 2 possible areas for the Na<sub>v</sub>1.8 binding pockets. In the 2-site model proposed here, both of these areas may bind to Na<sub>v</sub>1.8, providing a match for each site on Na<sub>v</sub>1.8.

### 3.4.5 Residues 86-100 of Na<sub>v</sub>1.8 contain an inhibitory domain for the Na<sub>v</sub>1.8-p11 interaction

We found that deletion of residues 81-120 of Na<sub>v</sub>1.8 causes a substantial increase in affinity for p11. If residues 74-103 constituted the binding site for p11, the opposite effect would have been predicted. This was investigated further. Deletion of residues 86-88 or 98-100 was found to produce a statistically significant increase in affinity, although with slightly reduced magnitude. Deletion of the intervening residues 89-91, 92-94 or 95-97 did not produce a

statistically significant difference, but all showed a strong trend towards increased affinity ( $p=0.13$ ,  $0.46$  and  $0.06$  respectively). Since the effect of residue deletion beyond amino acid 103 was not investigated, it remains possible that amino acids 104-120 contribute to the increase in affinity observed on deletion of residues 81-120. The effect of 3-amino acid deletions in the region 86-100, however, is sufficient to account for the increased affinity following residue 81-120 deletion, meaning that the involvement of residues 104-120 is not required to explain this observation. We therefore conclude that it is residues 86-100 of  $\text{Na}_v1.8$  that exert an inhibitory effect on the  $\text{Na}_v1.8$ -p11 interaction.

The mechanism of this inhibition, however, is unclear. The lack of cysteine residues in this region precludes a role for disulfide bonding. 4 of the 15 residues are in a characteristic cluster of basic amino acids, not shared with other VGSCs but well conserved between species (mouse, rat, human and dog), surrounding a putative  $\beta$ -strand (see Figure 3.15). It is possible that acid-base interactions occur between these residues and the acidic residues identified in the predicted binding domain, 77-85, reducing the accessibility of the binding residues to p11. Alternatively, the effect of residues 86-100 may be via an inhibitory effect on the binding domain identified in residues 41-80. The inhibitory residues may act by repelling moieties on p11, altering the Gibbs free energy change upon interaction. Finally, the inhibitory effect may be due to conformational parameters. The presence of residues 86-100 may cause a steric inhibition of binding at residues 77-85, which can be relieved by their deletion. Amino acid substitution experiments may help to define a mechanism for the inhibition.

The inhibition of the  $\text{Na}_v1.8$ -p11 interaction by residues 86-100 also provides an alternative explanation for the increased affinity of  $\text{Na}_v1.8$  41-80 relative to  $\text{Na}_v1.8$  74-103. Rather than the presence of an additional binding domain in the region 41-80, it is possible that the increased affinity is caused by the removal of residue 86-100-mediated inhibition. If this were the case, however,  $\text{Na}_v1.8$  74-103 would be expected to bind to p11 with equal affinity to  $\text{Na}_v1.8$  1-120, since both contain the predicted binding site 77-85 and the inhibitory domain 86-100. The increased affinity of  $\text{Na}_v1.8$  1-120 provides strong evidence for the existence of additional residues involved in the interaction with p11. Additionally, the affinity for p11 of  $\text{Na}_v1.8$  41-80 would be expected to be substantially reduced relative to the full-length protein, due to the deletion of residues 81-85, which are within the predicted binding site, although it is possible that this is outweighed by the reduction in inhibition. If residues 77-85 formed the sole binding site, the effects of the 3-residue deletions in this region would be expected to be far greater than observed, giving added weight to a 2-site interpretation of the data. Overall, a 2-site interaction provides the best explanation for our observations, and is consistent with all results obtained.

### 3.4.6 A 2-site model for the Na<sub>v</sub>1.8-p11 interaction

Integration of the observations made so far allows us to propose a model for the Na<sub>v</sub>1.8-p11 interaction. This model is illustrated in Figure 3.17, and consolidates the localisation of the 74-103 binding domain, the existence of a second binding region, and the presence of inhibitory residues. PKA and PKC phosphorylation sites were predicted using the NetPhosK 1.0 Server (Blom et al., 2004), and provide a putative mechanism of regulation of the interaction. In the FRET assay system, amino acids are unlikely to be phosphorylated, meaning that this is not taken into account. Since no information is available on the structure of this region, the shape shown below is purely hypothetical. In particular, the putative acid-base interactions shown are wholly speculative. The mechanism of inhibition by residues 86-100 is unknown, as discussed previously, and could be via an interaction with one of the binding sites (illustrated in this model), a conformational effect, or steric inhibition of the interaction with p11.

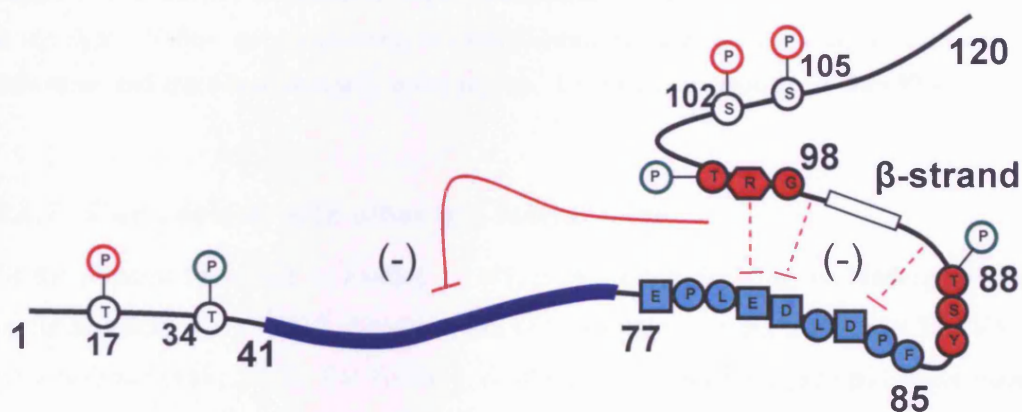


**Figure 3.17** Na<sub>v</sub>1.8 N-terminus domains. p11-binding site 1 shown by dark blue line, site 2 by light blue amino acids, inhibitory site by red amino acids. Circles represent neutral amino acids, squares acidic residues and hexagons basic residues. Phosphorylation sites shown by open circles: Red - PKA; Green - PKC. Putative β-strand shown by white rectangle. Potential inhibitory effects shown by red lines with blocked ends. Hypothetical acid-base interactions shown by dotted lines.

The validity of this model was examined by comparison to predicted secondary structures of the Na<sub>v</sub>1.8 N-terminus. Secondary structure was predicted using an *ab initio* method, HMMSTR, a hidden Markov model based on the I-Sites library of sequence-structure motifs (Bystroff et al., 2000; Bystroff and Shao, 2002). Visualisation of the output from this process was performed using the programme RasTop (<http://www.geneinfinity.org/rastop/>) (Philippe Valadon, 2007). The structure generated appears compatible with the model in Figure 3.17, and is shown in Figure 3.18. In particular, predicted inhibitory residues seem to be in a position compatible with inhibition of binding at the site 77-85.

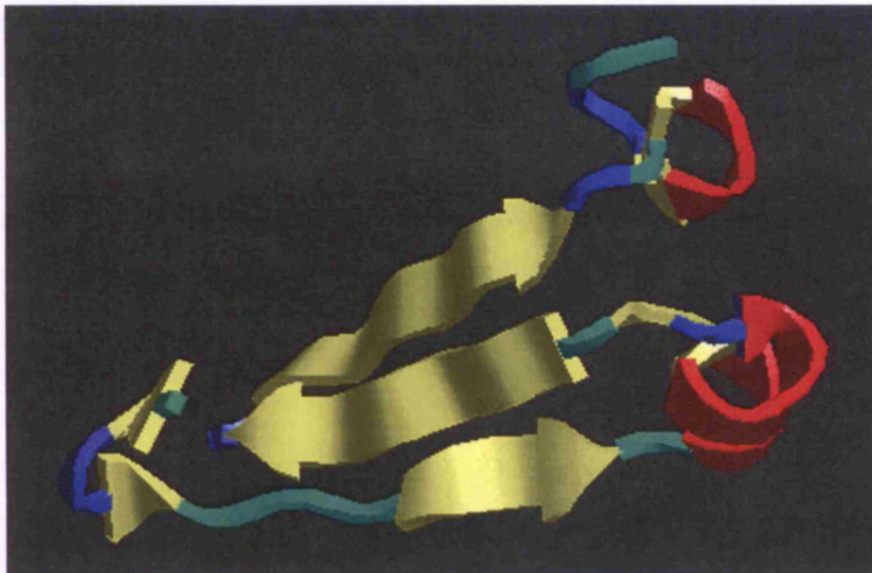


**Figure 3.18 Predicted structure of Na<sub>v</sub>1.8 N-terminus.** Amino acids 71-115 shown, from bottom left to top right. Yellow arrows (pointing towards C-terminus) represent  $\beta$ -sheets, red coils helices, blue lines turns, and green lines randomly coiled regions. The first helix contains residues 82-89.

### 3.4.7 Comparison with other p11 interactions

Of the proteins identified as binding to p11, a detailed analysis of the binding site has been performed only for TASK-1 (Girard et al., 2002; Renigunta et al., 2006) and TRPV5/TRPV6 (van de Graaf et al., 2003). For TASK-1, conflicting evidence implicates p11 in the masking of endoplasmic reticulum retention sites (Girard et al., 2002) or the retention in the endoplasmic reticulum via motifs in the C-terminal region of p11 (Renigunta et al., 2006). The trafficking mechanism for TRPV5 and TRPV6, however, appears to be a more direct effect, with p11 required for channel transfer between a sub-plasma membrane area and the plasma membrane. The effect of p11 on Na<sub>v</sub>1.8 appears to be similar to the effect on TRPV5/TRPV6, with no obvious endoplasmic reticulum localisation in the absence (or presence) of p11 (Okuse et al., 2002).

### 3.4.8 Annexin 2 binds p11 at a site distinct from that of Na<sub>v</sub>1.8

The role of annexin 2 (p36) in the trafficking of Na<sub>v</sub>1.8 is not clear. Current evidence suggests indirectly that annexin 2 is likely to bind p11 at the same time as Na<sub>v</sub>1.8, since the binding domains on p11 do not appear to overlap. Amino acids 33-78 of p11 were found to be responsible for the interaction with Na<sub>v</sub>1.8 (Poon et al., 2004). According to the 3D structure of the annexin 2-p11 complex (Lewit-Bentley et al., 2000), based on both crystallographic and energy-modelling data, these residues are peripheral and exposed. It is therefore likely that p11

can bind both annexin 2 and Nav1.8 simultaneously. In the current study, we found that the Nav1.8 N-terminus was unable to displace annexin 2 from p11, strongly supporting the presence of distinct binding sites on p11 for annexin 2 and Nav1.8. Given the probable molar excess of annexin 2 compared to p11 (Moss SE, personal communication), it is reasonable to predict the occurrence of an annexin 2-p11-Nav1.8 complex. The physiological significance of this, however, is unknown. For example, does annexin 2 play a role in the insertion of Nav1.8 into the plasma membrane? Detailed work on the molecular consequences of the p11-Nav1.8 interaction may yield answers to questions of this nature.

Studies of other p11-interacting membrane proteins do not provide a consistent role for annexin 2 in these complexes. While annexin 2 has been co-immunoprecipitated with TRPV5 and TRPV6 (van de Graaf et al., 2003), the annexin 2 binding site of p11 overlaps with the site for TASK-1 (Renigunta et al., 2006), implying a mutual exclusivity of annexin 2 and TASK-1 binding.

The stoichiometry of the p11-Nav1.8 interaction remains unclear. Although our data support a 1:1 ratio between p11 and Nav1.8, whether the complex exists as a heterodimer, heterotetramer, or other conformation has yet to be deduced. Since p11 generally exists in dimeric form, the existence of a p11-Nav1.8 heterotetramer is plausible, although steric inhibition from the relatively bulky channel may prevent this.

### **3.4.9 Importance of the Nav1.8-p11 interaction to analgesic drug discovery**

The identification of an additional p11-interacting domain in Nav1.8 has important connotations for the drug discovery process. The Nav1.8-p11 interaction has been proposed as a therapeutic target on several occasions (e.g. Okuse et al., 2002). Since Nav1.8 expression is restricted to a subset of primary afferent sensory neurons (Akopian et al., 1996) and plays an important role in nociception (Akopian et al., 1999), pharmacological agents targeted to this channel would be expected to be both specific and efficacious in their physiological effects. The search for a channel blocker specific to Nav1.8, however, has proven troublesome, primarily due to the similarities between Nav1.8 and other VGSCs in the pore domain. Actions at other VGSCs are likely to lead to serious side effects, particularly cardiac arrhythmias and CNS irregularities. Attention then turns to modulators of Nav1.8 function, of which p11 has been studied the most extensively. By disrupting the Nav1.8-p11 interaction, it may be possible to reduce channel function to a level comparable to that of a pore-blocking compound, without affecting other VGSCs, which do not interact with p11.

To allow the intelligent design of small molecule or peptide inhibitors of the  $\text{Na}_V1.8$ -p11 interaction, precise knowledge of the protein domains involved is required. For small molecule inhibitors, this allows the design of chemical entities designed to fit the secondary protein structure, with the positioning of active moieties such that access to the intended amino acids is facilitated. Peptide inhibitors can be modelled on the target sequence, but often exhibit reduced cellular penetration and therefore efficacy as their size increases. It is therefore advantageous to have a precise understanding of the binding domain, allowing the identification of small regions critical for the interaction and therefore the use of smaller, more permeant peptides to disrupt the interaction.

The 2-site + inhibition model proposed, however, does not lend itself well to drug design, due to the need to target multiple sites. Our results suggest that the disruption of a single binding site would be insufficient to achieve a meaningful reduction in binding in the cell. For example, complete ablation of the 74-103 region produces a reduction in affinity of around 2-fold. Even given a highly efficacious block of this site, a clinically-evident reduction in  $\text{Na}_V1.8$  trafficking would be highly unlikely. For an efficacious disruption of the interaction, an inhibitor would be required to act at both sites. Small molecules would be required somehow to disrupt both interactions, possibly by causing a conformational change in the structure of the  $\text{Na}_V1.8$  N-terminus. Peptides could potentially be designed to block both sites, but would be large as a consequence. Since the desired site of action is intracellular, this is likely to prove a barrier to the therapeutic efficacy of a peptide. The use of carrier groups, targeting for example the transferring receptor, to improve transport across the plasma membrane, may be able to overcome this limitation. An alternative strategy would be the combined use of a pair of agents, one targeting each interaction site. This has the limitation of requiring two rounds of the drug screening process, which is both labour- and resource-intensive.

While disruption of the  $\text{Na}_V1.8$ -p11 interaction may not affect other VGSCs, the possibility of unwanted effects due to disturbance of other p11-membrane protein interactions remains. Proteins currently identified as binding to p11, including TASK-1, TRPV5/6, ASIC1a and 5-HT<sub>1B</sub>, play important roles in a variety of physiological processes, as discussed previously. Since the residues of p11 which interact with each of these proteins have yet to be identified, predicting the effect of inhibitors of the p11- $\text{Na}_V1.8$  interaction on these processes is problematic.

### **3.4.10 FRET interaction studies are suitable for use with other proteins**

The FRET assay used in this study was found to be a useful tool for the investigation of protein-protein interactions. Importantly, neither the His-Tag used for protein purification nor the Cy3/5 labelling was found to interfere with the interaction. The assay was performed under near-physiological conditions, allowing proteins to assume their natural conformation and therefore permitting physiologically-relevant interactions to take place. Methods of assessing protein-protein interaction in culture or *ex vivo* often require harsh conditions for protein extraction, especially for membrane-associated proteins, which can disrupt interactions. The use of a bacterial expression system allows the extraction of all types of protein, followed by purification and transfer to a variety of buffers. Additionally, the high purity of the proteins means that problems due to interactions with or interference by other proteins are eliminated. The competition assay format, coupled with the high sensitivity of the FRET signal, allows the detection of relatively small changes in affinity compared to other methods, allowing detailed analysis of interaction sites. This *in vitro* approach will therefore be useful for the study of a variety of protein-protein interactions.

## 4 P11 IN PAIN PATHWAYS

### 4.1 INTRODUCTION

The EF hand superfamily protein p11 exists as a heterotetramer with the  $\text{Ca}^{2+}$ - and phospholipid-binding protein annexin 2. It is unique among S100 proteins in its  $\text{Ca}^{2+}$  independence due to a mutation in its EF hand loops, resulting in a permanently active conformation with respect to annexin binding (for review, see Gerke and Moss, 2002). p11 plays an important role in the trafficking of transmembrane proteins. It binds directly to several channels, regulating the functional expression of the sensory neuron-specific  $\text{Na}^+$  channel  $\text{Na}_v1.8$  (Okuse et al., 2002), the acid-sensing ion channel ASIC1a (Donier et al., 2005), the transient receptor potential vanilloid receptors TRPV5&6 (van de Graaf et al., 2003), the TWIK-related acid-sensitive  $\text{K}^+$  channel TASK-1 (Girard et al., 2002; Renigunta et al., 2006), and the G-protein coupled 5-hydroxytryptamine receptor 5-HT<sub>1B</sub> (Svenningsson et al., 2006). A specialised function in pain pathways has been demonstrated for  $\text{Na}_v1.8$  (Akopian et al., 1999), while ASIC1a and 5-HT<sub>1B</sub> are expressed at high levels in nociceptive DRG neurons, suggesting a role in nociception (Svenningsson et al., 2006; Voilley et al., 2001). We therefore hypothesised that p11 plays a role in nociception through its involvement in trafficking of transmembrane proteins. Since different channels appear to bind to distinct sites on p11, although not all have been mapped, the possibility of co-localisation through interactions with p11 is also raised. There are currently no small-molecule inhibitors of p11 function, precluding the testing of our hypothesis by pharmacological means. We therefore considered the use of genetic technology to address this question.

#### 4.1.1 Genetic technology for the investigation of protein function

Technologies allowing the downregulation of p11 expression include antisense DNA, RNA interference (RNAi) and related techniques, conventional gene deletion in the mouse ("global knockout"), and conditional (tissue-specific) gene deletion. Antisense DNA uses single-stranded DNA complementary to the mRNA of the target gene. Translation of the target mRNA is inhibited by steric inhibition (physical obstruction) of the translation machinery. This effect is stoichiometric; that is, one antisense molecule prevents the translation of a single mRNA. While relatively simple and rapid, this method does not always produce complete downregulation of the target gene, and is highly dose-dependent. As such, it is critical that the antisense DNA can access the target tissue efficiently, which can be problematic for relatively isolated areas, including DRG neurons. The restriction of activity to a particular tissue or cell type, useful for mechanistic information, can be problematic. Specificity is also difficult to

achieve in many cases, especially in the presence of closely related proteins. Even in relatively favourable circumstances, it is likely that limited downregulation of non-target proteins will occur.

RNAi is a naturally-occurring process by which degradation of target mRNA is controlled by short, non-coding RNA sequences. mRNA complementary to these short sequences is degraded by argonaute 2, part of the RNA-induced silencing complex (RISC). This pathway can be harnessed to effect protein downregulation by the introduction of small inhibitory RNA (siRNA) strands complementary to the target mRNA. Longer double-stranded RNA molecules are generally not used in mammalian cells due to the induction of the interferon response. siRNA-mediated gene knockdown is catalytic in nature: one siRNA molecule can degrade multiple copies of the target mRNA, meaning that lower doses are required for efficacy. Specificity remains a problem, although to a lesser extent than with antisense mRNA. With the use of specific design software, it is estimated that around 10% of siRNAs will have substantial off-target effects (Qiu et al., 2005).

Conventional global gene deletion produces mice lacking the gene for the protein of interest, and therefore achieves the complete absence of target protein expression in all cells. This method is obviously efficacious, but does not allow mechanistic insights by restriction of activity to a particular tissue. Additionally, compensatory upregulation of other genes has been reported in several studies (e.g. Akopian et al., 1999), complicating analysis, although the genetic mechanisms behind this are unclear. The process of creating a null-mutant mouse line is relatively slow and resource-intensive compared to other methods of investigation. The process is presently readily available only in the mouse, restricting the range of analysis that can be performed (for example, behavioural analysis of nociceptive thresholds is generally believed to be more sensitive in the rat). Conditional or tissue-specific gene deletion uses a site-specific recombinase under the control of a tissue-specific promoter to effect gene deletion only in the tissue of interest. For proteins with distinct roles in multiple tissues, conditional gene deletion allows the investigation of a function in a single tissue, removing the confounding effects of functions in other tissues. This is dependent on the existence of a suitable recombinase-expressing mouse line, available for a relatively large range of tissues.

The multiple roles of p11 in various tissues and physiological processes, especially its involvement in depression (Svenningsson et al., 2006), suggest that global p11 deletion would give a complex and potentially confounded phenotype. Its sequence similarity to other S100 proteins means that antisense or RNAi would risk significant off-target effects. Since we wish to investigate p11 function in DRG neurons, accessibility is also a limitation of these

technologies. We therefore chose to use conditional gene deletion to delete p11 only from nociceptive sensory neurons, using the Cre-*loxP* system and expressing Cre recombinase under the control of the nociceptor-specific Nav1.8 promoter (Stirling et al., 2005).

#### 4.1.2 Gene targeting and homologous recombination

Gene targeting is defined as the site-specific modification of a gene by homologous recombination (reviewed by Muller, 1999). Homologous recombination is a phenomenon occurring in mammalian cells, whereby two sections of identical (or very similar) DNA “cross over”: the strands break and rejoin to their opposing partners, via an intermediate structure known as a Holliday junction. By designing an exogenous DNA construct with sequences homologous to the desired gene, specific parts of DNA can be replaced with altered sequence. Recombination can occur at any point in the homologous region, and was first investigated in yeast. In mammalian cells, the targeting frequency is reduced due to the alternative pathway of random integration, which is an important consideration when designing targeting constructs. The first successful instance of gene targeting in mammalian cells was described by Lin et al. (1985), using a fibroblast cell line with a selectable locus, and achieved a recombination efficiency of around 1 cell in  $10^6$  (compared to modern methods, which allow an improved efficiency of around 1 in  $10^4$ ). This was followed by gene targeting at the endogenous  $\beta$ -globin gene in erythroleukemia cells (Smithies et al., 1985).

For successful gene targeting, the intelligent design of the targeting construct is essential. There are three essential components of a targeting construct: a region of homology at each end to mediate recombination (“arms of homology”), positive and negative selection markers, and the sequence for replacement, illustrated in Figure 4.1.

The arms of homology play a critical role in determining targeting efficiency. Since homologous recombination is relatively infrequent compared to random, non-homologous vector integration (in mammals), it is important to maximise the rate of homologous recombination. The length of each arm of homology affects recombination frequency, with greater lengths increasing targeting frequency (Hasty et al., 1991; Thomas and Capecchi, 1987). Although recombination has been observed with less than 500bp (Hasty et al., 1991), at least 2kb is desirable (Thomas et al., 1992). Recombination was found to occur in almost all introduced sequences when arms of homology greater than 5kb were used (Thomas and Capecchi, 1987). The degree of homology between construct and endogenous DNA also affects recombination frequency (te et al., 1992). Significant variation between the two sequences involved can dramatically reduce the recombination frequency, due to the

involvement of the DNA mismatch repair system. This is illustrated by the fact that targeting frequencies using non-isogenic vectors in cell lines with non-functional DNA mismatch repair genes are comparable to levels using isogenic constructs in normal cells (de et al., 1995). Choice of the appropriate strain for construct template is therefore important. In addition to length and degree of homology, the absolute frequencies of homologous recombination appear to be locus dependent, perhaps accounting for differences in chromatin structure (Muller, 1999).

Since gene targeting frequency is relatively rare, the molecular screening of all potential transformants is not desirable. The use of enrichment schemes for correctly-targeted cells is therefore advantageous. Positive selection allows enrichment for cells that have stably incorporated the vector DNA. The gene *Neo* is often incorporated into the targeting vector, within the arms of homology, for this purpose. *Neo* encodes the protein neomycin phosphotransferase, which confers resistance to geneticin (G418). Cells unaffected by the presence of geneticin are therefore likely to contain the targeting construct. Since homologous recombination is relatively rare compared to random integration, however, many of the cells surviving geneticin selection will not contain correctly-targeted DNA. To enrich for cells containing the correct targeting event over those where random integration has occurred, negative selection is used. The most commonly used negative selection marker is the *Herpes simplex* thymidine kinase gene. This gene confers sensitivity to gancyclovir. By positioning this gene outside the region enclosed by the arms of homology, the gene will be incorporated by random insertion events, but not by homologous recombination. Cells surviving both selection steps therefore have a greatly increased chance of containing the correct targeting event.

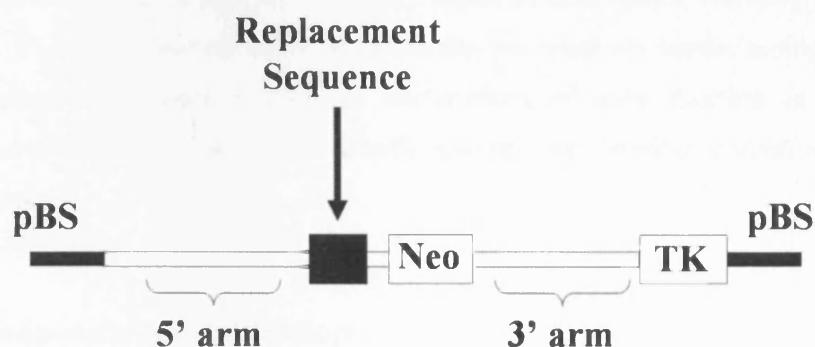


**Figure 4.1. Gene targeting construct design.** This diagram illustrates the general form of gene targeting constructs, with pBS representing pBluescript, a vector used to contain the construct, Neo the positive selection marker, and TK the negative selection marker. 5' arm and 3' arm represent the arms of homology.

### 4.1.3 Production of a mutant mouse

The process of gene targeting can theoretically be used in any cell type capable of homologous recombination. By targeting pluripotent embryonic stem (ES) cells, it is possible to create an entire animal containing the targeted allele. ES cells are derived from the inner cell mass of the blastocysts, and can differentiate into all cell types including, importantly, the gametes. In chimaeric mice, they are capable of contributing to all embryonic tissues. They can also be maintained in culture in an undifferentiated state by the use of appropriate conditions (Evans and Kaufman, 1981; Martin, 1981). Transformed (successfully targeted) ES cells, from a 129 strain (white) can be microinjected into a blastocyst from a C57Bl/6 strain (black), which can then be implanted into the uterus of a pseudopregnant mouse (i.e. a surrogate mother). The chimaeric embryo generated by this process will then develop into an adult chimaera, itself capable of reproduction, and recognisable by coat colour. Since ES cells are capable of forming all tissues, a proportion of the gametes of this mouse will derive from the implanted, transformed cells. If this is the case, the offspring of this chimaera will contain animals derived from the targeted cells, heterozygous for the desired mutation, with a brown coat colour. Homozygotes can then be produced by the use of an appropriate breeding strategy. The 129 strain is most often used for ES cell generation as it is the strain from which ES cells are most easily established, although this is possible for other strains (Kawase et al., 1994).

Gene targeting is often used to produce null-mutant ("knockout") mice. While this approach can be extremely revealing, in some cases problems inherent in the design can prevent the collection of meaningful data (Joyner and Guillemot, 1994). For example, a recent paper examining the role of the sodium channel gene *Scn9a* found that global deletion (from all tissues) caused perinatal lethality (Nassar et al., 2004), preventing phenotypic analysis. Other gene deletions may have developmental effects, leading to gross morphological phenotypes which preclude analysis, or may affect the expression of other genes, resulting in a complex phenotype. Even when the effects of gene deletion are relatively subtle, multiple actions in different tissues can hinder mechanistic explanations of gene function in a particular physiological process. The use of site-specific recombinases provides a solution to many of these limitations.

### 4.1.4 Site-specific recombination

Site-specific recombinase systems have been exploited in numerous studies to delete genes only in specific tissues (e.g. Nassar et al., 2004). Site-specific recombination, in contrast to other forms, requires an enzyme capable of recognising specific DNA sequences on the recombining molecules. Recombination occurs with absolute fidelity, which is important for

several applications of this process. Depending on the relative placement and orientation of the DNA recognition sites, various outcomes are possible as a result of recombination. Where both sites are present on a single molecule of DNA, in the same orientation, the region between the sites is excised as a circular fragment. By placing recombinase recognition sites flanking a particular gene, the action of the recombinase will excise this gene from the genomic DNA. The circular fragment produced is not replicated, and rapidly lost. These permutations are illustrated in Figure 4.2. Insertion of the gene for a recombinase enzyme into the genome of a mouse, under the control of a tissue-specific promoter, allows conditional (tissue-specific) gene deletion to be effected (Takeda et al., 1998; Tsien et al., 1996). This facilitates the investigation of gene function in a particular tissue of interest, without confounding effects from actions of the gene in other tissues. This is particularly useful when global gene deletion is lethal (e.g. Nassar et al., 2004).

The efficiency of site-specific recombination decreases with distance between recognition sites. For example, even using an exceptionally strong CMV promoter to drive Cre recombinase expression, including the addition of a nuclear localisation signal, a 400kb genomic region was excised with around 50% efficiency (Niwa et al., 1991). Although this in itself is impressive, when using site-specific recombinase systems to examine whole-animal behavioural effects, it is vital that the targeted gene is deleted in all cells in which the recombinase is expressed. Since many gene targets are relatively large, it is often not feasible to place recombinase sites flanking the entire gene. To address this problem, the location of recombination sites can often be designed such that the translational ATG (methionine), the major part of protein coding sequence, or a section of DNA essential for protein activity is deleted. In some cases, it is possible to place recombination sites such that a STOP codon is introduced upon excision. The introduction of more than one pair of recognition sites for the same recombinase is not generally desirable, due to the range of recombination scenarios which may occur.

An additional use of site-specific recombinases is the removal of positive selection markers from the genome following targeting. This is important due to the observation that the strong promoter present in the *Neo* cassette can affect the expression of nearby genes. Reduction in expression of the target gene (Fiering et al., 1995), of surrounding genes (Olson et al., 1996), and of genes distant from the site of insertion (Pham et al., 1996) have all been observed. This problem can be circumvented by using a site-specific recombinase to remove the *Neo* cassette before phenotypic analysis. In some cases, however, analysis of the allele with *Neo* remaining can be informative, giving information on the effect of a partial gene “knock-down” (Meyers et al., 1998; Nagy et al., 1998).

#### 4.1.4.1 The Cre/*loxP* recombination system

Cre recombinase is a 38kDa protein produced by the P1 bacteriophage. It is a member of the integrase family of site-specific recombinases, and catalyses recombination between two identical *loxP* recognition sites without the need for additional cofactors or sequences. Recombination is catalysed regardless of cellular environment and properties of DNA, making it a powerful tool for alteration of the mouse genome. The *loxP* (locus of crossover *x* in *P1*) site recognised by Cre is a 34bp consensus sequence, with a core spacer sequence of 8bp flanked by two palindromic 13bp sequences (Figure 4.2). The directionality of the *loxP* site is determined by the orientation of the central spacer sequence. Recombination occurs when one Cre molecule binds to each palindromic sequence of each *loxP* site. The Cre molecules form a tetramer, which brings two *loxP* sites into conjunction (Voziyanov et al., 1999). The enzymatic activity of the recombinases catalyses the DNA cutting, exchange and resealing reactions within the core spacer region, forming a small heteroduplex joint at the point of union. The recombination process is conservative, meaning that the reverse reaction exactly reproduces the original sequences. The rate of the reverse reaction, however, is slow, due to the need for accessory proteins not expressed in mammalian cells.

Importantly, *loxP* sites are sufficiently small that insertion into an intron is unlikely to interfere with normal gene expression in the absence of Cre recombinase. The random occurrence of a 34bp sequence, however, requires a length of DNA of  $10^{18}$ bp (Nagy, 2000). Since the mouse genome is only around  $3 \times 10^9$ bp, the likelihood of an endogenous *loxP* site occurring is small. It was therefore thought that the mouse genome contains no endogenous *loxP* sites. It was shown, however, that Cre can mediate recombination between sequences divergent from the *loxP* site, and that pseudo-*lox* sites exist in the mouse genome (Thyagarajan et al., 2000). For a review of the Cre/*loxP* system in mouse genetics, see Nagy (2000).

5' ATAACCTTCGTATAAT**GTATGCTATACGAAGTTAT** 3'  
 5' TATTGAAGCATATTACATAC**GATATGCTTCAATA** 3'

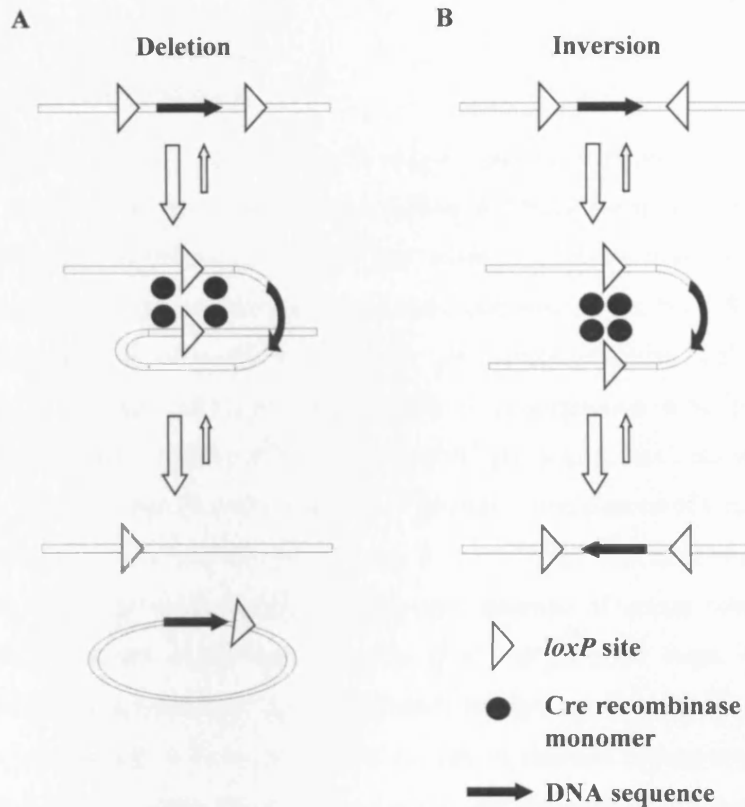


**Figure 4.2 The Cre-*loxP* recombination system.** The *loxP* sequence is shown in the uppermost panel, with the non-palindromic core indicated in bold. **A:** Deletion of intervening sequence between 2 *loxP* sites orientated in the same direction. **B:** Inversion of sequence between 2 inverted *loxP* sites.

#### 4.1.4.2 The Flp/*FRT* recombination system

In many cases, it is desirable to use site-specific recombination for multiple purposes in the same construct, most commonly for effecting excision of the positive selection marker, then deleting the gene under investigation. Although this is possible using partial excision with a single recombinase system, this approach is inconvenient and requires the screening of a large number of ES cells. An alternative is to use different recombinase systems for each process. The recombinase Flp recognises DNA sequences known as *FRT* (Flp recognition target), 8bp of directional core surrounded by inverted 13bp repeats. The Flp/*FRT* system, however, is less efficient than Cre/*loxP* (e.g. Dymecki and Tomasiewicz, 1998). Flp displays a low level of activity at 37°C, due to its origin - Flp is derived from the yeast *Saccharomyces cerevisiae*. A more thermostable Flp derivative (FLPe), made using cycling mutagenesis to emulate an evolutionary process, has since been shown to be 3-5 times more efficient in mammalian cells (Buchholz et al., 1998). Importantly, it was shown that FLPe works with high efficiency in germ cells (Rodriguez et al., 2000). Farley et al. (2000) targeted the constitutively-expressed

ROSA26 locus with the gene for FLPe, creating the mouse strain “FLPeR” (“flipper”), which has become a valuable tool for excision of positive selection markers.

#### **4.1.4.3 The $Na_v1.8$ Cre mouse**

Stirling et al. (2005) recently generated a “knock-in” mouse strain expressing Cre under the control of the  $Na_v1.8$  promoter. The coding sequence for  $Na_v1.8$  was replaced by the gene for Cre, using the initiator methionine of  $Na_v1.8$  and therefore allowing retention of all regulatory elements controlling spatial and temporal expression patterns. Since  $Na_v1.8$  is expressed in a subset of sensory neurons, of which over 85% are nociceptors (Akopian et al., 1996; Djouhri et al., 2003a), this is a useful tool for the investigation of gene function in peripheral nociceptive processes. The expression pattern of  $Na_v1.8$ , discussed previously, has been well-characterised (Djouhri et al., 2003a; Novakovic et al., 1998). The expression pattern of Cre, examined using ROSA26 reporter mice, was found to match exactly that of  $Na_v1.8$ . Onset of expression was at embryonic day 14, in small diameter, unmyelinated neurons of dorsal root, trigeminal and nodose ganglia. Limited expression was also observed in some large, myelinated DRG neurons. CNS and non-neuronal cells were shown to have no Cre expression.  $Na_v1.8$  Cre heterozygotes were found to have no deficits in sodium channel expression, measured using whole-cell patch-clamp. Motor function was normal, and the mice were shown to have normal acute pain thresholds. The development of inflammatory and neuropathic pain was also shown to be unaffected, as predicted by the lack of phenotype of heterozygous  $Na_v1.8$  null-mutants (Akopian et al., 1999). The  $Na_v1.8$ Cre mouse is therefore a suitable tool for nociceptor-specific gene deletion.

#### **4.1.5 Behavioural assessment of nociceptive thresholds**

The use of animal models for human pain is widespread. Human studies are able to use the visual-analogue scale to assess the intensity of pain (including the affective component) evoked by a given stimulus (e.g. Jones et al., 2004). Since this approach is unsuitable for use with non-verbal populations, animal behavioural assays focus on the measurement of thresholds of nociception. In general, a stimulus of increasing intensity is presented, and the intensity at which a response is evoked is taken as the output of the experiment. Different tests of nociception, depending on the particular behaviour being assessed, are likely to involve different amounts of supraspinal processing. For example, Hargreaves’ test, in which a rapid withdrawal of the hind paw is considered an endpoint, is likely to be mediated almost entirely by spinal reflex circuitry. In contrast, the hot plate, in which jumping or other escape behaviour is sometimes measured, requires a more coordinated response and is therefore likely

to involve higher centres of the brain. It is consequently standard practice to perform a range of behavioural tests of nociception when examining the effect of gene deletion.

In humans, acute pain is rare as a clinical presentation, and is generally well-managed. Chronic inflammatory and neuropathic pain states are the most significant clinical problems, and a number of animal models of these pain states have therefore been developed. Neural plasticity, both in the peripheral and central nervous systems, is demonstrated by these models (Dickenson, 1997; Woolf, 1983). Animal models of chronic pain generally rely on the measurement of hyperalgesia or allodynia, requiring the use of acute stimuli to evoke a response. Spontaneous pain, perhaps the most relevant phenomenon from a clinical viewpoint, has proven difficult to quantify in animal models. A recent study from the Lawson group reported progress in this field, presenting several models for spontaneous pain in the rat quantified by spontaneous foot lifting (Djouhri et al., 2006). Despite these limitations, animal models of nociception have been shown to have relevance to human conditions, for example as a predictor of efficacy for many analgesics (Taber, 1973).

Stimulus intensity is a critical parameter in nociceptive behavioural assays. There is a body of evidence to suggest that noxious stimuli of different intensities are differentially processed; for example, different rates of skin heating evoke capsaicin-sensitive C-fibres and capsaicin-insensitive A $\delta$ -fibres (Yeomans et al., 1996; Yeomans and Proudfit, 1996). Interestingly, certain proteins have been found to be involved in the process of nociception within specific intensity ranges. For example, disruption of the gene encoding substance P and a related tachykinin in mice reduced sensitivity to stimuli only in the moderate to intense noxious range (Cao et al., 1998). These findings mean that a range of nociceptive assays, of varying stimulus nature and intensity, must be used to investigate the effects of gene deletion.

Nociceptive testing of genetically-altered mice is complicated by the substantial differences in nociceptive thresholds between strains. Various inbred strains have been compared in a wide range of nociceptive assays, showing 1.2- to 54-fold ranges of sensitivity (Mogil et al., 1999). The genetic background of test mice is therefore an important factor to be considered. Since null-mutant mice are generally derived from 129-C57BL/6 chimeras, resulting in a mixed background, the potential for strain differences to affect results exists. This can be reduced by repeated backcrossing to C57BL/6, but tightly-linked genes are likely to persist (Crusio, 1996), complicating analysis. This effect can be reduced by the use of site-specific recombination, since both test and control mice are derived from the same source. Genes linked to the locus in which the recombinase has been inserted, however, may still interfere with analysis. The recombinase-expressing mouse used in this study was tested extensively before use to ensure

that nociceptive phenotypes were identical to wild-type C57BL/6 (Stirling et al., 2005), removing this concern. Gender has also been shown to affect pain-related behaviour in certain nociceptive assays in mice (Mogil et al., 2006). Results were therefore separated by gender in this study, unless values for each gender were not significantly different.

#### **4.1.5.1 Measurement of noxious mechanical thresholds**

##### *4.1.5.1.1 Randall-Selitto*

The Randall-Selitto test was first described in its current form by Takesue et al. (1969). The basic principle is that an increasing pressure (via increasing force with fixed area) is applied to the tail (mouse) or hind paw (rat) of the animal, until a stimulus is evoked. For the mouse, the area over which the force is applied is typically 2mm diameter, with force at the onset of tail flick/struggling used as the endpoint. Restraint is required for this test, which is likely to be stressful for the mouse, possibly leading to altered nociceptive thresholds, although mice are not tested until calm.

##### *4.1.5.1.2 von Frey*

von Frey hairs are graded filaments of increasing diameter, such that the force applied upon flexion is known for each hair. Typically, each increment is a constant on a logarithmic scale. Filaments are applied sequentially to the plantar aspect of the hind paw through a mesh floor, until a sharp withdrawal of the paw is seen. Many groups have used von Frey hairs to assess noxious mechanical thresholds, particularly for the evaluation of analgesic drugs or models of neuropathic pain (Fuchs et al., 1999; Kim and Chung, 1992; Seltzer et al., 1990). Traditionally, a battery testing approach was used, applying each filament 5-10 times before moving to the next, in order of increasing magnitude. More recently, however, the up-down method was described (Chaplan et al., 1994). This uses a statistical technique, first described by Dixon (1980), which makes greater use of the number of observations obtained (or in practice, to make fewer measurements for a given level of certainty). Here, if a response to a given filament is observed, the subsequent test is performed with the filament one increment below the first, and *vice versa*. The pattern of responses, along with the final filament tested, can be used to calculate an estimate of the 50% withdrawal threshold, that is, the filament to which a response would be expected 50% of the time. Chaplan et al. (1994) demonstrated a good correlation between both methods, despite the reduced labour required for the latter.

In contrast to the Randall-Selitto test, von Frey filaments present a relatively sudden stimulus to the animal. Whilst this has the advantage of allowing the animal to remain in a relaxed state immediately prior to the test, the contribution of the startle reflex to the response must be taken

into account. Gradual presentation of each filament is necessary to ensure that withdrawal is a response to nociception rather than non-noxious mechanosensation. Responses to von Frey filaments are generally considered to be mediated by spinal reflex arcs rather than higher-order processing.

#### **4.1.5.2 Thermal nociception**

##### *4.1.5.2.1 Hargreaves' test*

Hargreaves' test (Hargreaves et al., 1988) uses a focused light source to apply radiant heat to the hind paw, via a plexiglass plate. Animals are not restrained, and the gradually-increasing nature of the stimulus removes any contribution of the startle reflex. Since the response observed is a rapid withdrawal of the paw, this test is considered to involve only the spinal reflex arc. Since the tail is the major organ of thermoregulation in mice, thermal tests using the paw are generally considered more reliable (Hargreaves et al., 1988).

##### *4.1.5.2.2 Hot plate*

The endpoint of the hot plate test is hind paw licking. In contrast to Hargreaves' test, this response involves higher-level processing of the noxious stimulus (Jensen and Yaksh, 1984). This is consistent with the observation of behavioural tolerance for the test: repetition within a 30 minute period results in a marked reduction in latency (Wilson and Mogil, 2001).

#### **4.1.5.3 Inflammatory pain models**

##### *4.1.5.3.1 Formalin*

Formalin is an aqueous solution of 37% formaldehyde. Injection of a 5% solution of formalin is commonly used as a model of nociception, providing a moderate, spontaneous pain caused by damaged tissue (Tjolsen et al., 1992). In this way, it differs from most other pain models, which rely on an external stimulus to evoke pain-related behaviour. Licking and biting of the hind paw is measured, since this is not a frequent component of normal grooming behaviour (Tjolsen et al., 1992), and has been validated as the best behavioural measure for mice (Sufka et al., 1998). Two distinct phases of response are seen following injection of formalin. The early phase, beginning almost immediately and lasting for around 5 mins, is reduced by systemic administration of opioids, paracetamol and aspirin, but not other NSAIDS or corticosteroids (Hunskar and Hole, 1987). The late phase response begins around 15 mins post-injection, lasts for approximately 15 mins, and is blocked by opioids, NSAIDS, corticosteroids, paracetamol and aspirin (Hunskar and Hole, 1987). The differing responses to

pharmacological inhibition suggest differing nociceptive mechanisms for each phase. It is generally believed that the early phase is a result of direct chemical stimulation of C-fibres, while the late phase is dependent on a combination of an inflammatory response and functional changes in the dorsal horn of the spinal cord, probably initiated by the C-fibre afferent barrage during the early phase (Tjolsen et al., 1992).

#### *4.1.5.3.2 Nerve Growth Factor*

The subcutaneous injection of small doses of NGF induces a rapid onset thermal hyperalgesia that persists for many hours. This is thought to be due to a peripheral action, since no contralateral effects are observed (Andreev et al., 1995). Around 40% of DRG primary afferents express trkA, the receptor for NGF, most of which are nociceptors (Averill et al., 1995; McMahon et al., 1994; Verge et al., 1989). While this provides a mechanism for the direct sensitisation of nociceptors by NGF, current evidence suggests that a large component of the sensitisation observed is mediated indirectly, via actions on post-ganglionic sympathetic neurons (Andreev et al., 1995). Sympatholytic treatment was found to reduce NGF-induced hyperalgesia, although there is some evidence that mast cell degranulation also makes a significant contribution to the initial phase of hyperalgesia (Andreev et al., 1995).

Significantly, NGF expression is upregulated in most animal models of inflammation, including Freund's adjuvant and carrageenan (Woolf et al., 1994). This suggests that NGF may act as a mediator of the inflammatory pain produced by these models.

#### *4.1.5.3.3 Carrageenan*

Carrageenan is a collective term for a group of polysaccharides prepared by alkaline extraction from the red seaweed *Rhodophyceae*. The injection of  $\lambda$ -carrageenan produces an inflammatory response, maximal 3-5 hours post-injection, causing hyperalgesia that can be detected by a reduction in mechanical or thermal nociceptive thresholds (Kayser and Guilbaud, 1987). This is in contrast to the formalin test, in which pain is assessed without additional stimuli.

#### **4.1.5.4 Neuropathic pain models**

Traditionally, animal models of neuropathic pain used mechanical damage to the sciatic nerve to elicit allodynia and spontaneous pain. These allowed the predictable localisation of pain to the ipsilateral hindpaw, and demonstrated good levels of reproducibility (e.g. Kim and Chung, 1992). Clinical neuropathic pain, however, rarely arises from purely mechanical nerve damage; more common is nerve damage due to metabolic (e.g. diabetes), viral (e.g. HIV, herpes), or pharmacological (paclitaxel, vincristine) factors. Recent work has focused on the

generation of animal models for specific conditions, with varying success. For example, the intrathecal injection of the HIV envelope glycoprotein gp120 was shown to produce thermal hyperalgesia and mechanical allodynia in the rat (Milligan et al., 2000). Intraperitoneal streptozocin has also been used to model diabetic neuropathy (Courteix et al., 1993). Paclitaxel and vincristine are also used in rodents to generate neuropathic pain resembling that occurring in human chemotherapy (Cavaletti et al., 1995; Nozaki-Taguchi et al., 2001). These models, however, are not generally well-characterised, especially in the mouse. The models described below trade clinical relevance for increased reproducibility, thus improving experimental power.

The most commonly used models of neuropathic pain in the mouse derive from paradigms described by Kim and Chung (1992) in the rat. Two models were described, the first involving the tight ligation of the L<sub>5</sub> and L<sub>6</sub> spinal nerves, and the second requiring the ligation of L<sub>5</sub> alone. Both models produce mechanical hypersensitivity, maximal around one week post-surgery and lasting for around 14 weeks, and thermal hyperalgesia. The Chung model has certain advantages over the earlier models of neuropathic pain, the chronic constriction injury (CCI) (Bennett and Xie, 1988) and sciatic nerve ligation (SNL) (Seltzer et al., 1990) models. The surgical procedure has less scope for variation in ligature tension or number of fibres ligated, meaning that the only major source of variation in the procedure is the normal biological variability in the sciatic nerve. It also allows the contribution of both injured and uninjured fibres to be examined. The behavioural and neurochemical responses to L<sub>5</sub> ligation have been shown to be conserved between rat and mouse, validating this method for use in the mouse (Honore et al., 2000). The Chung model, however, required more invasive surgery than the CCI or SNL models, increasing the inflammatory contribution to altered pain states.

More recently, Decosterd and Woolf (2000) described a new model of neuropathic pain, the spared nerve injury (SNI). This involves a lesion of two of the three terminal branches of the sciatic nerve (tibial and common peroneal nerves) leaving the remaining sural nerve intact and therefore restricting interactions between intact and degenerating axons. In contrast to some models, no changes in thermal thresholds are observed in this model.

Models of neuropathic pain are illustrated in Figure 4.3.

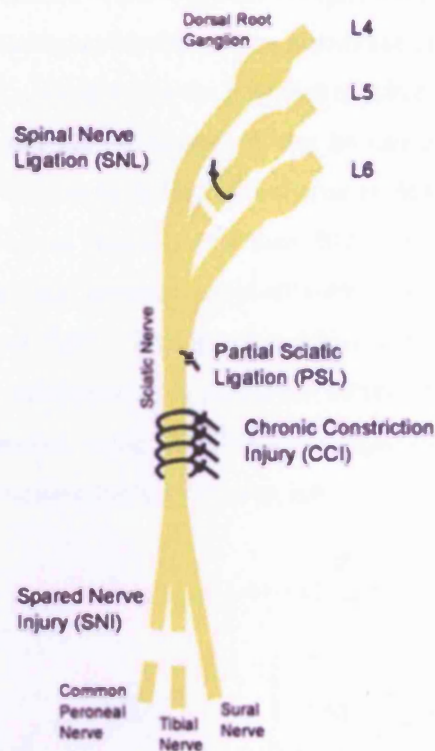


Figure 4.3 Models of neuropathic pain. From Campbell and Meyer (2006).

## 4.1.6 Electrophysiology

While whole-animal behavioural assays allow the assessment of the contribution of a given factor to nociceptive processes, little mechanistic information is revealed by these approaches. Electrophysiological analysis permits the discrimination of actions at different levels of nociceptive pathways, and can provide insights into the effects of gene deletion (and other factors) at the molecular level. Due to the wide range of parameters that can be investigated, it can be useful to hypothesise on the effects that might be expected, and focus analysis accordingly.

### 4.1.6.1 Whole-cell patch-clamp of DRG neurons

The electrophysiological properties of acutely-cultured DRG neurons can be studied by whole-cell patch-clamp, providing information on the effects of gene deletion on primary afferent nociceptor function. The patch-clamp technique (Hamill et al., 1981) allows the recording of membrane currents or voltage, whilst controlling the other. A simplified circuit for a voltage-clamp experiment is shown in Figure 4.4. A high-gain operational amplifier is used to compare the pipette potential ( $V_p$ ) to a pre-determined command potential ( $V_{ref}$ ). A current ( $I_f$ ) is passed through the feedback resistor to maintain the pipette potential at the same level as the reference

potential. Since the input resistance of the amplifier is high (and therefore passes little current), this current is equal to that passing across the plasma membrane ( $I_p$ ). The output voltage of the amplifier is given by  $I_p R_f + V_{ref}$ , since  $I_p R_f$  is the potential required to pass the current  $I_p$  through the resistance  $R_f$ . Since  $R_f$  and  $V_{ref}$  are known,  $I_p$  can be calculated. The amplifier output, however, differs from that at the pipette tip due to the series resistance (access resistance) of the pipette. Since this resistance was typically less than  $5\text{m}\Omega$ , compensated at 70% to give an effective resistance of  $3.5\text{m}\Omega$ , and currents recorded were around  $2\text{nA}$ , the residual IR drop across the pipette was around  $7\text{mV}$ . The junction potential at the interface of the pipette solution and the extracellular solution adds an additional source of error. This can be estimated and thus accounted for, however, using the Henderson equation (Barry and Lynch, 1991), which takes into account the relative mobility of each ion.

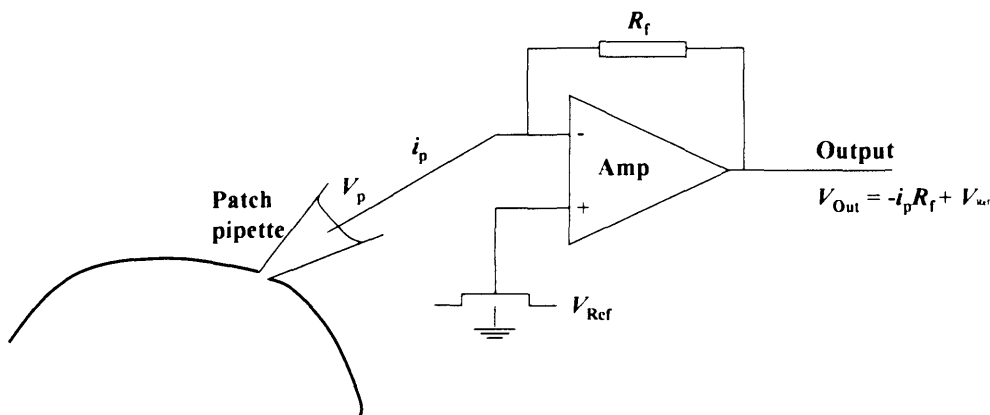


**Figure 4.4 The whole-cell patch-clamp circuit.** Adapted from Aidley and Stanfield (1996). Current passing across the plasma membrane, equal to  $i_p$ , is measured by the voltage drop across the feedback resistor  $R_f$  by the high-gain amplifier Amp.

#### 4.1.6.2 Electrophysiological recording from wide dynamic range neurons of the spinal cord

Whole-cell patch-clamp of DRG neurons is a useful tool for the investigation of neuronal properties, but its physiological relevance is limited by the need to use dissociated cells in culture. Removal of these neurons from their physiological environment and associated growth factors, cellular contacts and support cells is likely to produce at least a degree of phenotypic alteration. *In vivo* recording removes this barrier, and is possible from a range of nervous tissues, both peripheral and central. Single unit extracellular recordings from WDR neurons in the spinal cord (laminae IV-V) allow the measurement of neuronal activity in the native environment. This approach is complementary to that in cultured DRG neurons, assessing effects of gene deletion at a higher point in the sensory circuitry, and allowing the investigation of dorsal horn phenomena such as wind-up and LTP, both of which can play important roles in

chronic pain states. This technique is described in Urch and Dickenson (2003). An added benefit of this approach is that, in contrast to most behavioural assays, quantitative measures of supra-threshold activity can be obtained. Since the majority of clinical pain conditions fall into this category, these measurements are particularly interesting.

#### **4.1.7 Angiogenesis**

p11, through its interaction with tissue plasminogen activator (tPA), is thought to play an important role in angiogenesis. This section gives an overview of this process.

Angiogenesis is the formation of new blood vessels from the pre-existing vasculature (Folkman, 1995a). It involves the migration, proliferation and differentiation of endothelial cells and results in the formation of vascular loops (Risau, 1997). Angiogenesis is required for many physiological processes, including wound healing, and plays a vital role in pathological processes, particularly tumour growth (Folkman, 1995b) and diabetic retinopathy.

The plasma serine protease plasmin degrades fibrin, a fibrillar protein involved in thrombus formation. It also activates collagenases, such as matrix metalloproteases, either directly (Netzel-Arnett et al., 2002) or indirectly (Ramos-DeSimone et al., 1999). Plasmin is produced through the activation of plasminogen, by tissue plasminogen activator (tPA) or urokinase plasminogen activator (uPA) cleavage. Plasmin has been reported to promote angiogenesis, and this appears to be via several mechanisms (Browder et al., 2000). Pro-neoangiogenic programmes of gene expression are activated by plasmin, resulting in migration and proliferation of endothelial cells, and other changes (Tarui et al., 2002). Gene expression changes include the induction of Cyr61, a growth factor-like gene implicated in cell proliferation, adhesion and migration, via MAP kinase pathways (Pendurthi et al., 2002). In addition to fibrin, plasmin degrades substrates such as laminin, fibronectin and the protein core of proteoglycans (Chen and Strickland, 1997; Werb et al., 1980), all components of the extracellular matrix that must be degraded for effective angiogenesis. This degradation may release basic fibroblast growth factor (bFGF) trapped within the extracellular matrix (Falcone et al., 1993), which promotes angiogenesis by both direct effects on endothelial cells and indirectly via upregulation of vascular endothelial growth factor (VEGF) expression (Stavri et al., 1995), which is itself pro-angiogenic. Plasmin also activates transforming growth factor- $\beta$  (TGF- $\beta$ ), a pro-invasive endothelial cell-differentiating factor (Lyons et al., 1990). Importantly, plasmin-generated fibrin degradation products (e.g. A(61), fragment E, angiostatin) may stimulate endothelial cell proliferation (Thompson et al., 1992), while plasmin itself attenuates fibrin-mediated endothelial cell adhesion via specific integrins (Thiagarajan et

al., 1996). Finally, plasmin regulates vascular-endothelial cell cadherin-mediated association (Bach et al., 1998b; Bach et al., 1998a). It is apparent from this multitude of actions that plasmin plays a central role in the regulation of angiogenesis, promoting neovascularisation by a variety of mechanisms.

The formation of plasmin from plasminogen (Figure 4.5) is a central step in angiogenesis. Regulators of this process may thus exert powerful control over angiogenesis, with subsequent effects on tumour growth and other angiogenesis-dependent events.

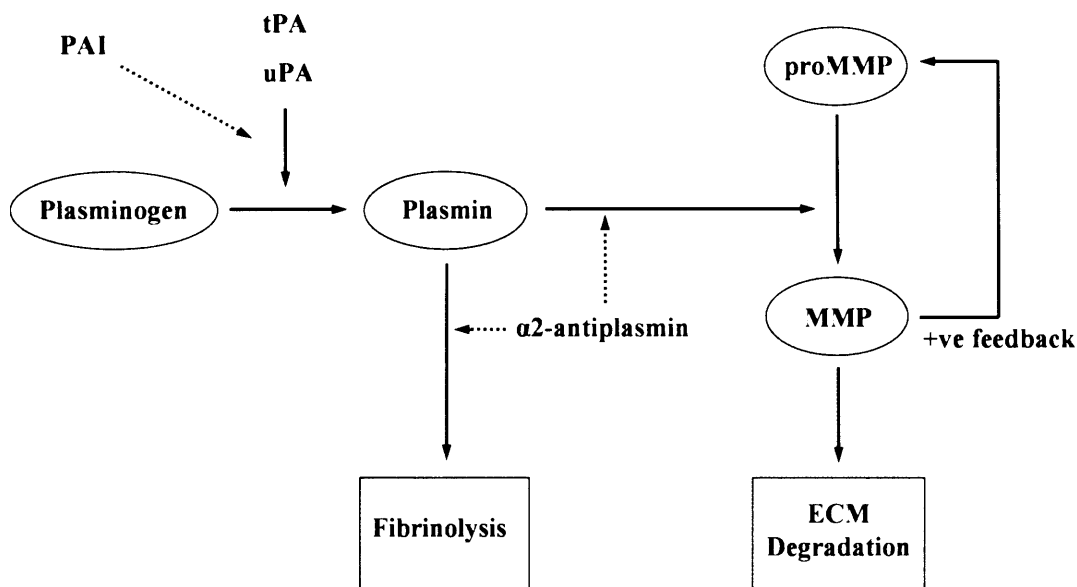


**Figure 4.5 Plasmin formation and downstream effects.** tPA and uPA catalyse the formation of plasmin from plasminogen. Plasmin promotes angiogenesis by fibrin degradation and activation of matrix metalloproteases (MMP), which degrade the extracellular matrix (ECM). PAI: plasminogen activator inhibitor. Solid lines represent stimulatory effects; dotted lines indicate inhibitory actions.

#### 4.1.8 Aims

This section aims to use a tissue-specific p11-null mouse to investigate the role of p11 in nociception. A range of molecular, electrophysiological and behavioural techniques will be used for this purpose. Additionally, a global p11-null mouse line will be used to determine the role of p11 in angiogenesis using a tumour growth model.

## 4.2 METHODS

### 4.2.1 Gene targeting: generation of *loxP*-flanked *S100A10* mice

The design and manufacture of the floxed p11 targeting construct were performed by Mohammed Nassar and Tim Lane.

We chose to control the deletion of the *S100A10* gene using the *Cre-loxP* system. This system allows the deletion of a *loxP*-flanked gene to be restricted to tissues expressing the enzyme Cre recombinase. By placing Cre under the control of a tissue-specific promoter, the floxed gene can be deleted only in the cell type of interest. This system was chosen for several reasons. First, it would allow any phenotype observed to be ascribed to the role of p11 in the particular tissue from which it had been deleted. Second, it allows the generation of test and littermate control mice from a single litter, with no unusable genotypes. Finally, it provides a valuable tool for groups researching the role of p11 in other systems.

When using the *Cre-loxP* system, it is generally not considered possible to delete an entire gene, due to a hypothetical reduction in Cre-mediated recombination efficiency over very large distances. We therefore chose to flox only a single exon of the *S100A10* gene. The exon structure of *S100A10*, as shown in Figure 4.6, shows that the first exon is a 5' untranslated region, with translation beginning at the start of exon 2. We therefore chose to flox exon 2, to minimise the chance of a (potentially functional) truncated fragment being expressed after recombination. This deletion also induces a frame shift in the remaining exons, meaning that any protein expressed would bear little resemblance to p11. A stop codon was also introduced to prevent partial protein expression.

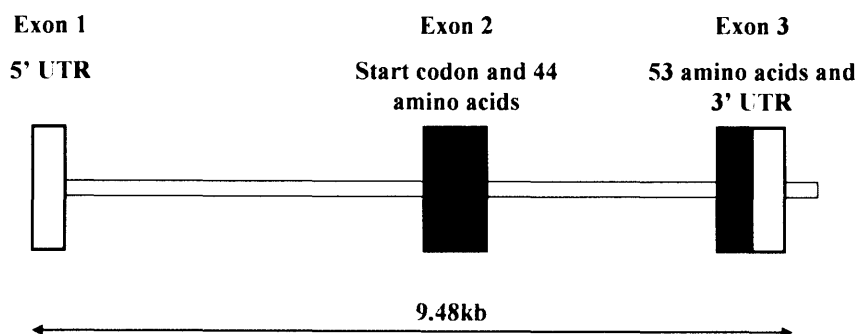


**Figure 4.6.** Exon structure of *S100A10* gene. Non-coding regions shown in white, coding sequence shown in black.

Since the targeting construct would later be electroporated into 129-derived embryonic stem cells, all sequences were based on the 129 strain genome. A 200bp probe for *Sl00A10* was prepared by PCR, using 129-derived embryonic stem cell DNA as a template with primers gccaaactggagcactgtaccccc and ggatacaacaataataaaactcagaagc. This probe was used to identify genomic clones from an RCPI-22 129S6/SvEvTac mouse bacterial artificial chromosome (BAC) library by Southern blotting. The targeting vector was derived from two overlapping *Bam*HI and *Apa*I genomic subclones that contained both exons 2 and 3 of p11. The 5' arm is the 4412 bp *Bam*HI–*Xba*I fragment upstream of exon 2. The *loxP*-flanked (floxed) exon 2 was obtained as a 990 bp *Xba*I–*Apa*I fragment. The 3' arm is the 6422 *Apa*I–*Xma*I fragment downstream of exon 2. The three genomic fragments were inserted into a plasmid containing two *loxP* sites and an FLP recombination target (FRT)-flanked (flrtd) *Neo* cassette (Nassar et al., 2004). The complete targeting vector was linearized and electroporated into 129-derived embryonic stem cells and screened as described by Nassar et al. (2004), using 5' and 3' external probes for Southern blot. Two correctly targeted clones were injected into C57BL/6J blastocysts to generate chimeras. Electroporation and injection were performed by the University of Michigan (Ann Arbor, MI).

#### 4.2.2 Breeding strategy

The chimeras were crossed to C57BL/6 animals. This was followed by a cross to FLPe deleter mice (Farley et al., 2000) to excise the positive selection marker (*Neo*). Correct targeting was confirmed by Southern blot (digestion by *Eco*RI or *Bam*HI) and PCR (primers p11 Sequencing 1 (ccttctctgctgaacttgataatgaa) and p11 Sequencing 4 (tcttgccacagaacatgtaattcttt)), with genomic DNA extracted from tail samples in both cases. These mice were then crossed to mice expressing Cre under the control of the *Nav*1.8 promoter (Stirling et al., 2005). These mice express Cre in small-diameter (<25 $\mu$ m) neurons arising from the DRG, of which >85% are nociceptors (Akopian et al., 1996; Djouhri et al., 2003). Further crosses between floxed mice and floxed mice heterozygous for *Nav*1.8 Cre generated conditional-null mutants and floxed littermate controls for analysis. This ensured an identical genetic background between p11 conditional-null and control animals, which had been backcrossed to F5 on a C57BL/6 background. Genotyping for floxed versus wild-type mice was performed using the primers p11 Sequencing 1 (ccttctctgctgaacttgataatgaa) and p11 Sequencing 4 (tcttgccacagaacatgtaattcttt), whereas the presence of the gene for Cre was detected using the primers Cre 2s (ctgcattaccggctgatgcaacga) and Cre 5a (aaatgttgctggatggttttactgcc). The floxed p11 mice were also crossed to a “global” Cre-expressing strain (Schwenk et al., 1995) to produce a global p11-null animal for certain experiments requiring either complete p11 deletion or p11 deletion in non-neuronal tissues. These p11-null mice were then bred to remove the

gene for Cre. Deletion of p11 was confirmed by PCR, using primers p11 Sequencing 1 (ccttctctgctgaacttgataatgaa) with p11 Sequencing 4 (tcttgccacagaacagtaattcttt), and p11 Sequencing 1 with p11 Sequencing 3 (ttgttctattcatccagcaactaa). p11-null mice were expected to produce no product with primers 1 & 4, and a product of ~450bp with primers 1 & 3. p11 floxed mice yielded a 400bp product from primers 1 & 4, and a product greater than 1.5kb with primers 1 & 3. p11 deletion was confirmed by western blotting, using brain lysate. The mass of p11-null mice was compared to control animals, and fertility was monitored.

### 4.2.3 Confirmation of correct gene targeting

Correct targeting of the *S100A10* gene in the mouse was shown by Southern blotting and PCR, using genomic DNA extracted from the tail. Southern blotting was performed using *EcoRI* and *BamHI* to digest DNA, with 5' and 3' probes respectively. PCR primers were designed either side of a *loxP* site. Primers p11 Sequencing 1 (ccttctctgctgaacttgataatgaa) and p11 Sequencing 4 (tcttgccacagaacatgtaattcttt) were used, with the floxed allele resulting in a band approximately 100bp larger than the wild-type.

### 4.2.4 Proving selective/global deletion

The selective deletion of the *S100A10* gene in cells expressing Nav1.8 was confirmed at the level of genomic DNA, mRNA and protein.

Deletion of exon 2 from genomic DNA was tested using primers p11 Sequencing 1 (ccttctctgctgaacttgataatgaa) and p11 Sequencing 3 (ttgttctattcatccagcaactaa). p11 Sequencing 1 binds to the 5' arm of homology, while p11 Sequencing 3 binds to the 3' arm, a distance of around 1.5kb. Upon deletion of exon 2 of p11, however, the distance between the primers is reduced to approximately 450bp. Confirmation of this result was obtained using primers p11 Sequencing 1 & 4: p11 Sequencing 4 binds to exon 2 of p11, meaning that no band would be expected following deletion. DNA extracted from DRG was compared to that extracted from spinal cord, brain and tail.

Tissue-specific deletion of exon 2 of *S100A10* was confirmed at the level of mRNA, using RT-PCR. cDNA was synthesised from mRNA template extracted from DRG and a variety of other tissues. The primers p11 RT-PCR Fwd 1 (tgtgccagctcttccaagg) and p11 RT-PCR Rev 1 (acaagaagcagtggggcagat) were used in the PCR reaction, giving a band 150bp smaller following deletion of exon 2.

These approaches to verification of tissue-specific deletion, however, are confounded by the fact that each DRG contains a multitude of cell types, some expressing Nav1.8 (and therefore Cre) but many, for example Schwann cells, not. To demonstrate conclusively that p11 was deleted only in cells expressing Nav1.8, we used immunocytochemistry. Dual labelling with antibodies to p11 (a kind gift from Prof. Volker Gerke) and Nav1.8 was used to define precisely from which cells p11 had been deleted.

The global deletion of the *Sl00A10* gene from the mouse was confirmed at the level of genomic DNA and mRNA as above, using a wider range of tissues. Deletion of exon 2 at the level of protein was verified by western blotting, using anti-p11 antibody (R&D Systems) to probe crude brain lysate.

#### **4.2.5 Effect on cell survival**

The effect of p11 deletion on the survival of DRG neurons was investigated, to verify that any phenotype observed was not due to neuronal death. DRG were sectioned and stained with anti-peripherin and the anti-neurofilament antibody N200, identifying small unmyelinated and large myelinated neurons respectively. The number and proportions of these cells were compared between p11 conditional null-mutant and floxed p11 control DRG.

#### **4.2.6 Analysis of p11 conditional-null phenotype**

Trafficking of Nav1.8 to the plasma membrane was investigated by western blotting of membrane preparations from DRG. Functional expression of Nav1.8 was then measured using whole-cell patch-clamp to measure TTX-R Na<sup>+</sup> currents in dissociated small-diameter DRG neurons. Following this, single unit recording were made from wide dynamic range neurons in the dorsal horn of the spinal cord (performed by Dr Elizabeth Matthews). Nociceptive behavioural responses were examined using acute, inflammatory and neuropathic models.

#### **4.2.7 Urine Analysis**

Analysis of urine Ca<sup>2+</sup> and Na<sup>+</sup> levels was performed by the laboratory of Prof. Rene Bindels, Radboud University Nijmegen.

#### **4.2.8 Tumour growth/angiogenesis testing**

Cells from the B16 murine melanoma line, derived from the C57BL/6 strain, were injected subcutaneously into the dorsal neck region of each mouse (1,000,000 cells, in 200µl PBS). After 11 days, during which time the health of the animals was monitored carefully, the animals were humanely sacrificed and the tumours excised. Tumour volume was measured by multiplying the maximum length, breadth and depth measurements.

## 4.3 RESULTS

### 4.3.1 A successful recombination event was detected in 129 embryonic stem cells

The wild-type p11 allele, targeting construct, correct targeting event and effect of Cre-mediated deletion are shown in Figure 4.7.

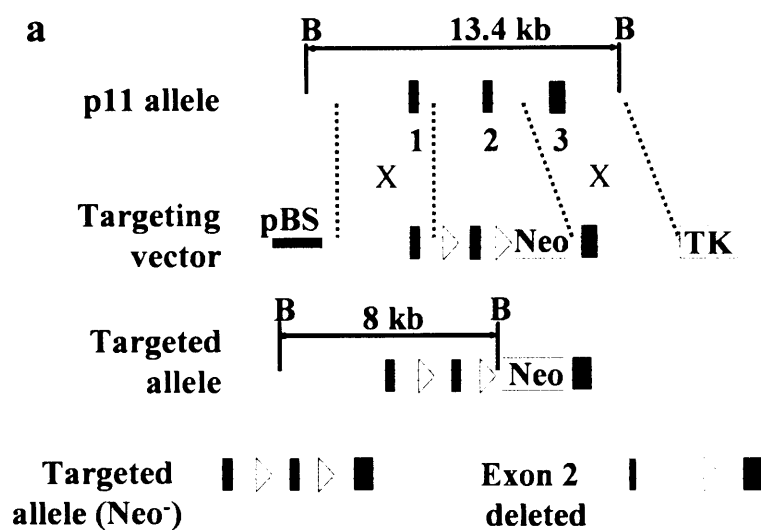


**Figure 4.7 Gene targeting process.** p11 genomic allele, targeting construct, correct targeting event and Cre-mediated excision. *loxP* sites represented by white triangles, exons by black rectangles, positive selection marker Neo and negative selection marker TK. B represents BamHI restriction sites, 1-3 exons 1-3. pBS: pBluescript.

Southern blotting was used to confirm the correct targeting of the p11 locus in 129 ES cells. Both EcoRI and BamHI digests were analysed to detect the correct gene targeting event, using both 5' and 3' external probes. An EcoRI digest probed with a 5' external probe and a BamHI digest probed with a 3' external probe are shown in Figure 4.8. The correct targeting event introduced an additional BamHI site, reducing the fragment size from 13.4kb to 8kb.

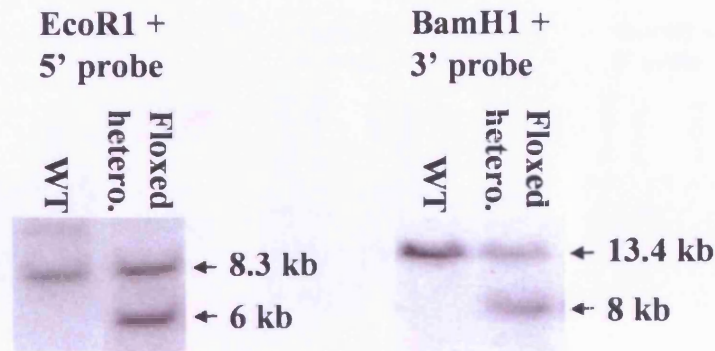


**Figure 4.8 Southern blotting to detect p11-floxed cells.** In each case, insertion of *loxP* sites introduced an additional restriction site, reducing fragment size. Following a successful recombination event, cells are heterozygous for the desired mutation, thus giving 2 bands.

A clone of cells containing the correct targeting event was transplanted into an early-stage blastocyst, which was then implanted into a pseudopregnant surrogate female. The resulting chimaeric offspring were then crossed to wild-type (C57BL/6) animals. This was performed by the University of Michigan.

#### 4.3.2 Embryonic stem cell transplantation produced viable p11 floxed mice

The transplantation of targeted (p11 floxed) 0129 ES cells into C57BL/6 (wild-type) blastocysts produced chimaeric mice, identified by a mixed coat colour due to contributions from 0129 (white) and C57BL/6 (black) cell types. These were crossed with C57BL/6 animals, with the expectation that a proportion of the offspring would be derived from targeted cells (i.e. that germline transmission of the targeted mutation would occur). Mice in which this had occurred were identified by coat colour (brown, from one C57BL/6 and one 0129 allele), and genotyped by PCR using primers p11 Sequencing 1 and p11 Sequencing 4 (Figure 4.9a), confirmed using Southern blot (Figure 4.9b). Germline transmission occurred in a relatively small proportion of offspring (~10%).

The positive selection marker encoded by the *Neo* cassette was excised by crossing p11 floxed animals with transgenic mice constitutively expressing the FLPe gene (Farley et al., 2000). The FLPe recombinase protein recognises the *FRT* sites flanking the *Neo* cassette and deletes the intervening region. This deletion was confirmed by PCR, using the primers p11 Sequencing 2 and p11 Sequencing 3 (data not shown).

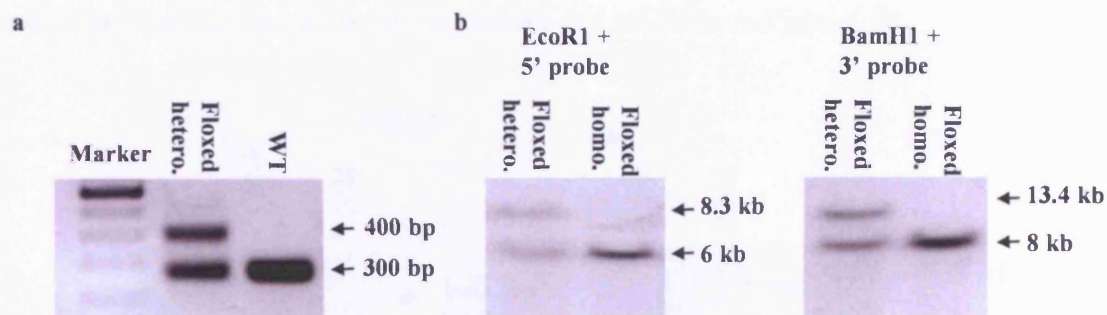


**Figure 4.9 Genotyping of p11 floxed mice.** a: PCR using primers p11 Seq.1 and p11 Seq.4 using DNA from wild-type and heterozygous floxed mice. The larger band represents the floxed p11 allele. b: Southern blotting to confirm genotypes of heterozygous and homozygous floxed p11 mice. The smaller bands represent the floxed p11 allele.

### 4.3.3 Conditional deletion: p11 is deleted from $Na_v1.8$ -expressing neurons, but not from other tissues

Following breeding to obtain homozygous floxed p11 animals, a cross was made with the  $Na_v1.8$ Cre mouse line (Stirling et al., 2005), which expresses Cre recombinase under the control of the  $Na_v1.8$  promoter. Tissues from the resulting offspring were examined at the level of DNA, mRNA and protein, to assess the extent of p11 deletion.

Genomic DNA extracted from DRG, brain and spinal cord was subjected to PCR, using primers p11 Sequencing 1 and p11 Sequencing 3. The deletion of exon 2 of p11 by Cre resulted in a band of around 450bp, while the floxed allele gave a 1.5kb band. DNA extracted from DRG gave both bands, due to the presence of a mixed population of cells, a proportion of which express  $Na_v1.8$  and therefore Cre. The larger band was weaker than the smaller counterpart, probably due to the more efficient amplification of the smaller fragment (Figure 4.10b). DNA from brain (not shown) or spinal cord, or from wild-type DRG, gave only the larger band, due to the absence of Cre expression and thus p11 exon 2 deletion. These results, illustrated in Figure 4.10, demonstrate that p11 is deleted from a subset of cells in the DRG but not from other tissues.

mRNA was extracted from a range of tissues in the p11 floxed  $Na_v1.8$ Cre mouse. The cDNA yielded from subsequent reverse transcriptase reactions was analysed by PCR. cDNA from conditional-null mutant DRG yielded a truncated (290bp) band, in addition to the full length product (440bp). cDNA from other tissues, or from p11 floxed control animals, showed only

the full-length band. These results confirm that p11 is deleted from a subset of DRG cells but not other tissues in the conditional-null mutant, and are shown in Figure 4.10.

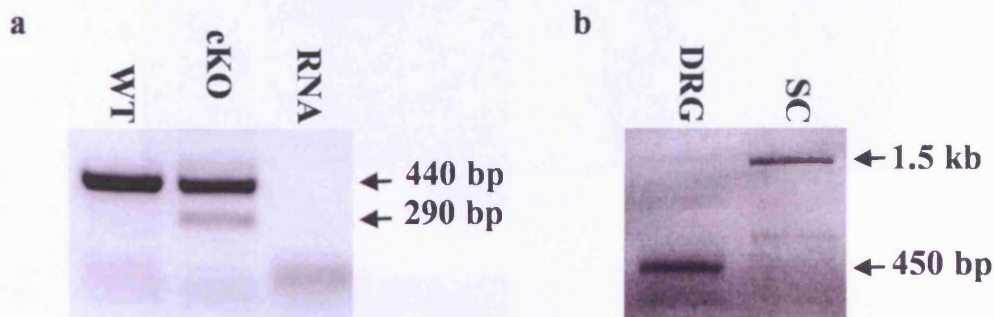


**Figure 4.10 Confirmation of conditional p11 deletion.** **a:** RT-PCR using cDNA from conditional-null DRG. The smaller band represents p11 deletion from Nav1.8-positive cells. **b:** PCR using primers p11 Seq.1 and p11 Seq.3 on genomic DNA from DRG and spinal cord (SC). The smaller band represents p11 deletion.

A monoclonal antibody to p11 was used to define more precisely the subset of cells from which p11 had been deleted in the conditional-null mutant. Attempts to use this antibody on DRG sections were unsuccessful, even following extended optimisation, due to high background reactivity (data not shown). Immunocytochemistry on acute DRG cultures, however, was more successful. In acute DRG cultures from control (floxed p11) animals, more than 85% of neurons displayed an intense staining with a distinct membrane localisation, consistent with the expected subcellular localisation of p11. In conditional-null mutant mice, however, fewer than 30% of neurons displayed anti-p11 immunoreactivity, although non-neuronal cells (defined by morphology) were generally stained. These results are illustrated in Figure 4.11, and show that p11 is deleted from a subset of DRG neurons in the conditional-null animal.

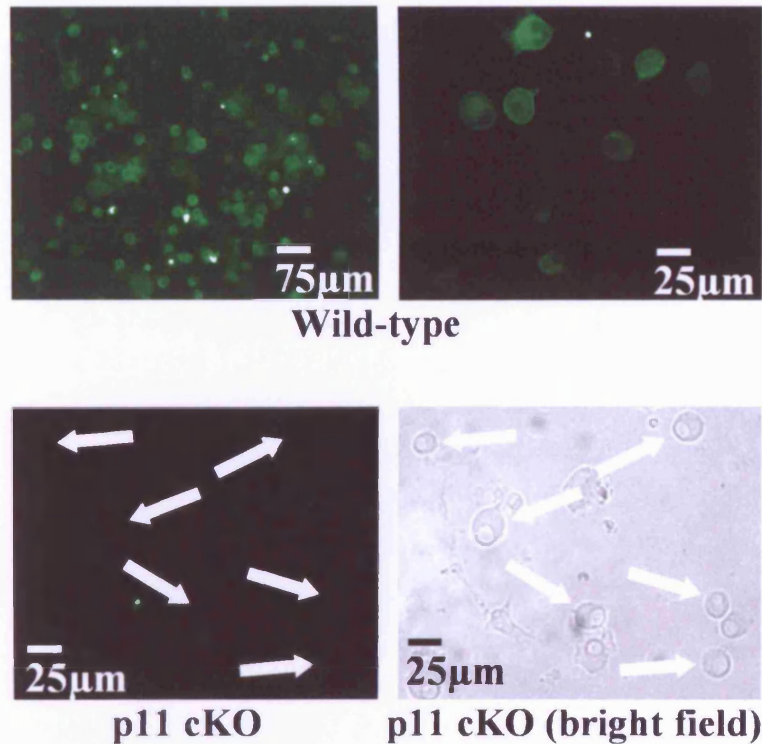


**Figure 4.11 Conditional deletion of p11.** Acutely-cultured DRG neurons are labelled with a monoclonal antibody to p11. Many more p11-positive cells are seen in wild-type cultures than in the conditional knockout (cKO). The bright field image is of the same field as the p11 cKO image, demonstrating the presence of neurons (white arrows) but not p11 immunoreactivity.

To define more precisely the subpopulation of DRG neurons from which p11 was deleted, co-staining with anti-Nav1.8 was performed. Deletion of p11 would be expected to show a precise correlation with Nav1.8 expression, since Cre expression is controlled by Nav1.8 regulatory sequences. In conditional-null cultures, p11 and Nav1.8 immunoreactivity were mutually exclusive. p11 immunoreactivity was absent from all Nav1.8-positive cells, while all cells which continued to express p11 did not display Nav1.8 immunoreactivity. In control cultures, however, many cells displayed both p11 and Nav1.8 immunoreactivity. A small proportion of cells in both control and conditional-null cultures displayed neither Nav1.8 nor p11 immunoreactivity. The proportion of cells in this category was similar between control and conditional-null cultures, and therefore is likely to represent a naturally-occurring neuronal subset. This is supported by *in situ* hybridisation data from previous studies (Okuse et al., 2002n). Figure 4.12 shows representative neurons from control and conditional-null DRG cultures labelled with anti-p11 and anti-Nav1.8.

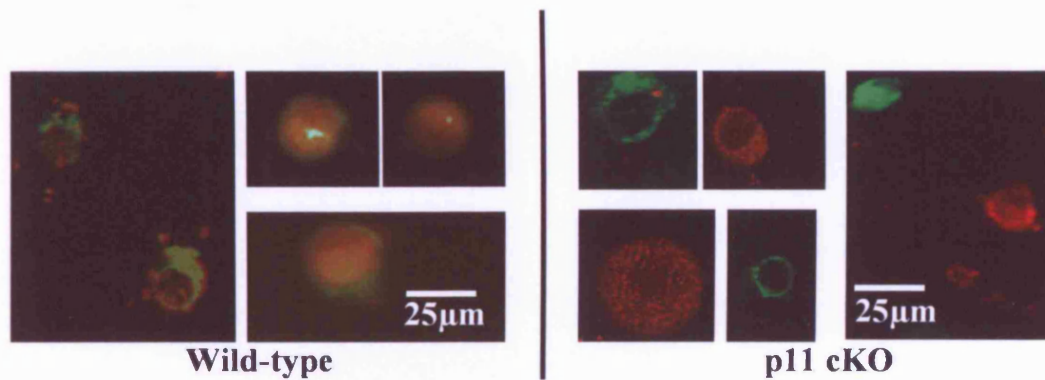


**Figure 4.12 Distribution of p11-null neurons in the conditional-null animal.** Acutely-cultured DRG neurons labelled with anti-p11 (green) and anti- $\text{Na}_v1.8$  (red). Colocalisation is evident in wild-type neurons. In conditional-null (cKO) cultures, labelling is mutually exclusive: cells are either green or red (or neither), but not both.

#### 4.1.8 Conditional p11 deletion does not affect the survival of DRG neurons

Whole sectioned DRG were examined to test for effects of p11 deletion on neuronal survival. The purpose of this was to ensure that any phenotype observed was not due to loss of neurons, but due to a more subtle action of p11. Small unmyelinated cells, most of which are nociceptors, were labelled with an antibody to peripherin. Larger myelinated neurons (less likely to express  $\text{Na}_v1.8$ ) were labelled with the anti-neurofilament antibody N200. Sections from control and conditional-null DRG appeared normal, showing a characteristic ring of small-diameter peripherin-positive cells surrounding larger N200-positive neurons (Figure 4.13). The proportions of peripherin- and N200-positive neurons were not significantly different between control and conditional-null animals (Figure 4.13).

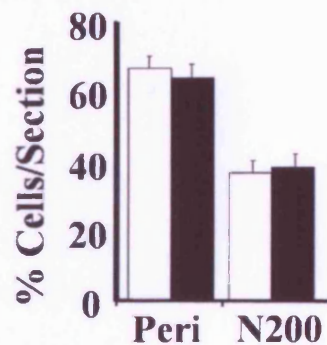
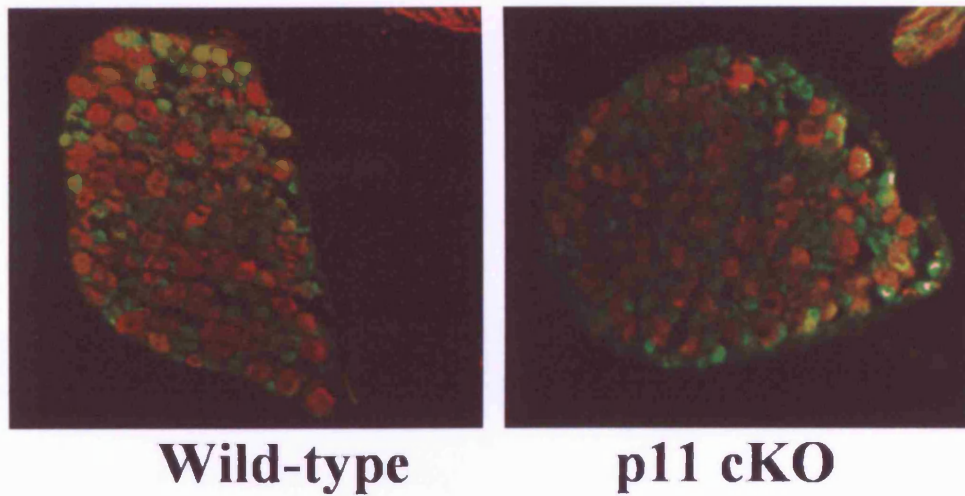


**Figure 4.13 Conditional deletion of p11 does not affect neuronal survival.** DRG sections from floxed p11 littermate control (wild-type) and p11 conditional-null (cKO) animals labelled with peripherin (green) and N200 (red). No difference in ratio was observed between littermate control ( $n=11$ ) and p11 conditional-null ( $n=24$ ) sections. Peripherin control (Peri),  $67\pm 3\%$ ; p11 conditional-null,  $64\pm 4\%$ ; N-200 control,  $37\pm 3\%$ ; p11 conditional-null,  $38\pm 4\%$ . Error bars represent mean $\pm$ SEM.

The cell size distribution of DRG neurons in culture was examined as a further check that p11 deletion did not affect the survival of certain groups of neurons. It should be noted that the culture methods used tend to favour smaller-diameter cells and therefore may not be representative of actual size distributions *in vivo*. Since p11 is primarily deleted from small- to medium-diameter cells in the conditional-null mutant, however, this was not considered to affect the validity of this exercise. Cultures from both control and conditional-null lines yielded a similar cell density. The mean diameter of control neurons ( $22.55\pm 0.65\mu\text{m}$ ,  $n=180$ ) was not significantly different to p11 conditional-null neurons ( $21.76\pm 0.75\mu\text{m}$ ,  $n=190$ ). Additionally, the proportion of cells with diameter  $\leq 25\mu\text{m}$  (considered to represent  $\text{Na}_v1.8$ -expressing cells) was similar between groups (control 70.55%,  $n=180$ , conditional-null 73.16%,  $n=190$ ). These results are illustrated in Figure 4.14.

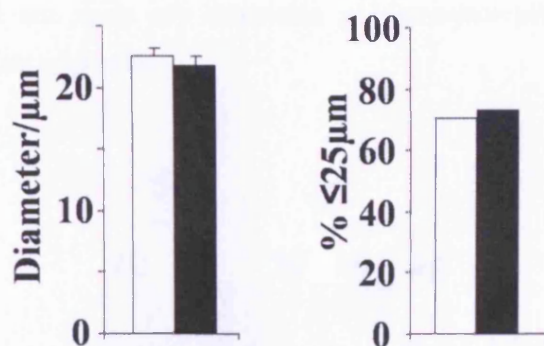


**Figure 4.14** Effect of p11 deletion on neuron size. Neuronal diameter was measured for floxed p11 littermate control (white) and p11 conditional-null animals (black), and expressed as mean diameter (left graph; error bars represent SEM), or % of neurons  $\leq 25\mu\text{m}$ , taken to represent  $\text{Nav}1.8$ -expressing cells (right graph). No significant differences were seen between p11 conditional-null and control with either presentation.

### 4.3.5 Global deletion: p11 is deleted from all tissues

A global p11 null mouse was produced by crossing the p11 floxed line with a global Cre strain (Schwenk et al., 1995) for use in certain experiments. p11 deletion was confirmed by RT-PCR, using mRNA extracted from a variety of tissues. p11 was found to be deleted from all tissues tested (Figure 4.15).

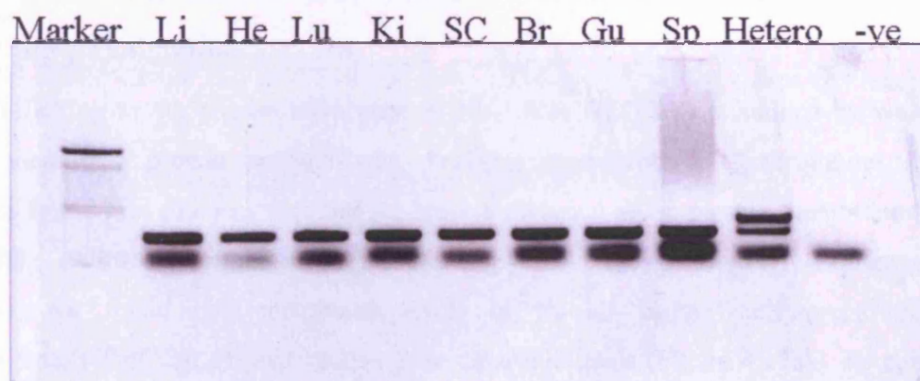


**Figure 4.15** p11 is deleted from all tissues in the global-null mouse line. RT-PCR using RNA extracted from liver (Li), heart (He), lungs (Lu), kidney (Ki), spinal cord (SC), brain (Br), gut (Gu) and spleen (Sp). The heterozygous reference shows 2 bands, while all tissues show only the smaller band, representing the deleted allele. The lowest band represents primer dimers, also seen in the negative control (no template).

Tissues from the global-null mouse were tested for p11 expression by Western blot (Figure 4.16). Brain lysate from control animals gave a distinct 11kDa band, whereas that from p11

global-null mice did not show any detectable p11 immunoreactivity, even when loading relatively large amounts of protein.

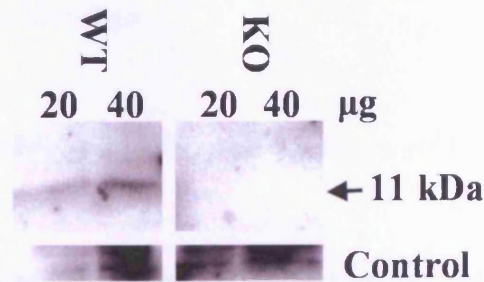


**Figure 4.16 Global deletion of p11.** Western blot using brain lysate from floxed p11 control (WT) and global-null animals (KO). The 11kDa band seen in the WT but not KO preparations represents p11 protein. “Control” represents Na<sup>+</sup>/K<sup>+</sup> ATPase loading control.

p11 global-null mice were apparently healthy, with no gross morphological differences from wild-type animals. Mass and litter size were not found to differ significantly from floxed p11 control animals, although a higher proportion of breeding pairs did not produce any litters among the p11-null population.

#### **4.3.6 Plasma membrane trafficking of Na<sub>v</sub>1.8 in DRG neurons is reduced by p11 deletion**

The trafficking to the plasma membrane of Na<sub>v</sub>1.8 in DRG was examined by western blot, using membrane protein preparations. Previous experiments in heterologous expression systems found that p11 was required for Na<sub>v</sub>1.8 presence at the plasma membrane (Okuse et al., 2002). Following normalisation to a reference protein, the constitutively-expressed Na<sup>+</sup>/K<sup>+</sup>-ATPase, we found that membrane levels of Na<sub>v</sub>1.8 in p11-null preparations were approximately half that of preparations from control animals (Figure 4.17a). To confirm that this difference was attributable to trafficking and not to changes in expression levels of Na<sub>v</sub>1.8, western blots were performed on total DRG cell lysates. No difference was observed between control and p11-null preparations (Figure 4.17b).

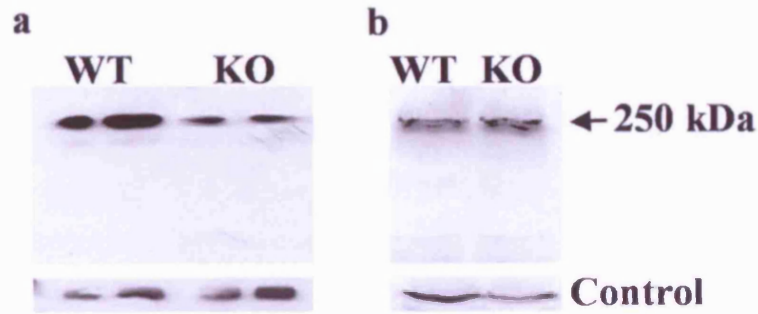


**Figure 4.17 Plasma membrane trafficking of  $\text{Na}_V1.8$ , assessed by western blot.** **a:** Anti- $\text{Na}_V1.8$  (250kDa) and reference  $\text{Na}^+/\text{K}^+$ -ATPase (Control) staining of membrane preparations from p11 global-null (KO; 20, 40 $\mu\text{g}$ ) and control (WT; 20, 40 $\mu\text{g}$ ) animals. A reduction in membrane levels was observed upon p11 deletion (KO range 50-65% of WT, following normalisation to reference gene). **b:** As a, but using total cell lysates. No changes in total  $\text{Na}_V1.8$  cellular expression were observed.

We attempted to corroborate this result using immunocytochemistry in acutely-cultured DRG neurons. Anti- $\text{Na}_V1.8$  staining was evident in a subset of small- to medium-diameter neurons, as expected. As previously reported, however, the majority of  $\text{Na}_V1.8$  immunoreactivity appears to be cytoplasmic (or at least non-plasma membrane), with the result that staining at the plasma membrane is difficult to distinguish. Normally this could be addressed by the use of non-permeabilised cultures, but the  $\text{Na}_V1.8$  antibody is directed against a cytoplasmic region of the channel, meaning that in non-permeabilised cells the required antigen is not accessible. These results, however, do confirm that the expression of  $\text{Na}_V1.8$  is not reduced by p11 deletion. Representative pictures are shown in Figure 4.18.

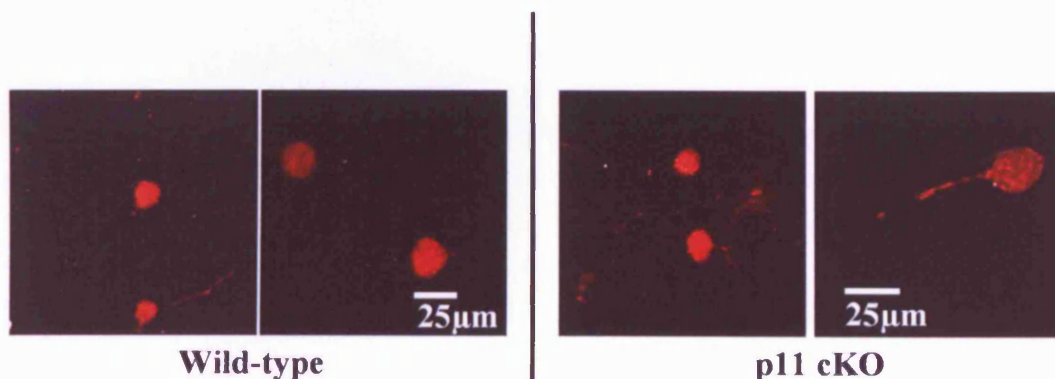


**Figure 4.18 Anti- $\text{Na}_V1.8$  immunocytochemistry.** Acutely-cultured DRG neurons from floxed p11 littermate control (wild-type) and p11 conditional-null (cKO) animals. No changes were obvious from this preparation.

#### 4.1.11 No changes in plasma membrane trafficking of annexin 2, ASIC1 or 5-HT<sub>1B</sub> in DRG neurons were seen following deletion of p11

p11 forms a heterotetramer with annexin 2. It is likely that the majority of cellular functions of p11 are mediated by this complex. To exclude the possibility that effects of p11 deletion were mediated by annexin 2 membrane downregulation, we examined levels of annexin 2 in DRG membrane preparations from p11 global-null mice. Following normalisation to reference protein (Na<sup>+</sup>/K<sup>+</sup>-ATPase) levels, no significant differences in membrane levels of annexin 2 were observed (Figure 4.19b). This result was confirmed using immunocytochemistry. Acutely-cultured DRG neurons from p11-null or littermate control animals were stained with an antibody to annexin 2. A characteristic membrane localisation was observed (Figure 4.19a), in agreement with previous reports. No differences were seen between p11-null and control neurons.

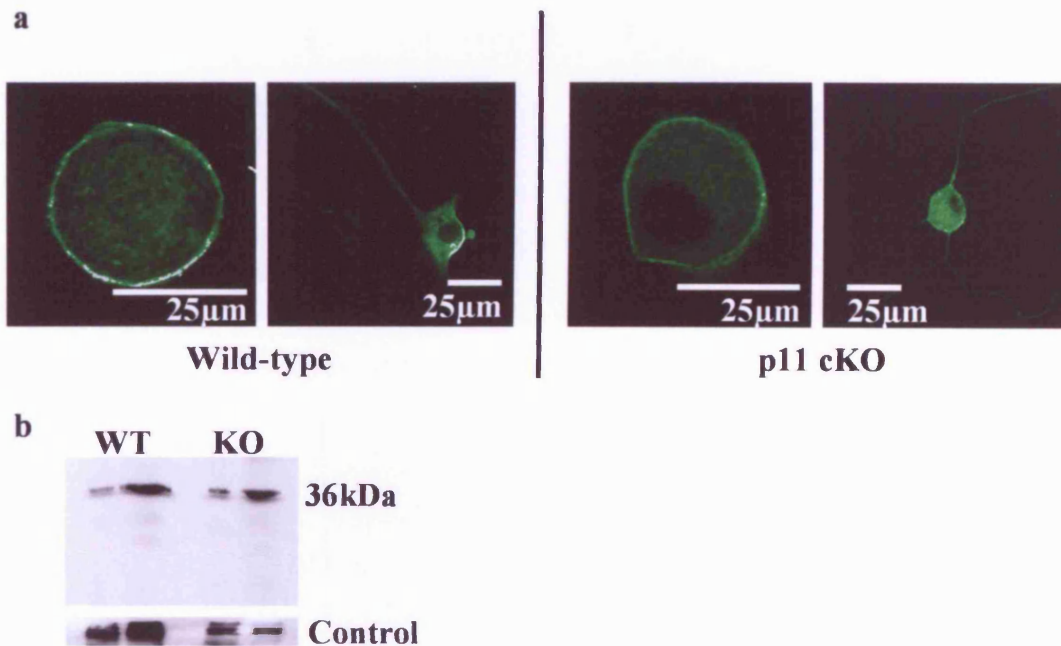


**Figure 4.19 Plasma membrane trafficking of annexin 2.** **a:** Immunocytochemistry using anti-annexin 2 on cultured DRG neurons from control (wild-type) and p11 conditional-null (cKO) animals. No differences in membrane localisation were observed. **b:** Western blot using anti-annexin 2 (36kDa) and anti-Na<sup>+</sup>/K<sup>+</sup>-ATPase (Control) on membrane preparations from floxed p11 (WT; 20, 40µg) and p11 global-null (KO; 20, 40µg) DRG. No differences in annexin 2 trafficking were seen.

p11 has been shown to mediate plasma membrane trafficking of ASIC1a and 5-HT<sub>1B</sub>. We therefore examined the effect of p11 deletion on plasma membrane levels of these proteins by western blot on DRG membrane preparations. Global-null mice were used to avoid the confounding effects of non-Cre-expressing cell populations. Following normalisation to

reference protein ( $\text{Na}^+/\text{K}^+$ -ATPase) levels, no significant differences in membrane levels of these proteins were observed (Figure 4.20). In this case, however, membrane preparations may represent not only the plasma membrane but also internal cellular membranes, including endoplasmic reticulum. This means that changes in plasma membrane levels may be masked by channel presence in other membrane bodies. These results do not therefore contradict previous studies showing an effect of p11 on plasma membrane trafficking of proteins.

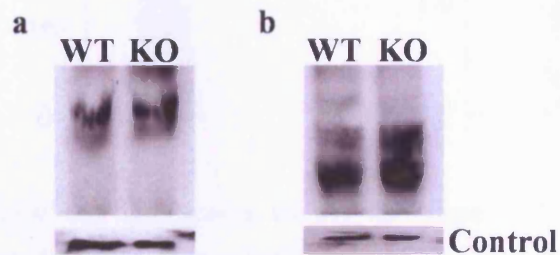


**Figure 4.20. Plasma membrane trafficking assessed by western blot.** DRG membrane preparations from control (WT; 20, 40 $\mu\text{g}$ ) and p11 global-null (KO; 20, 40 $\mu\text{g}$ ) mice, probed with a: anti-5-HT<sub>1B</sub> and b: anti-ASIC1. Anti-  $\text{Na}^+/\text{K}^+$ -ATPase was used as a loading control. No differences in membrane trafficking were observed.

#### 4.3.8 p11 deletion does not affect $\text{Ca}^{2+}$ excretion

Since p11 is required for TRPV5&6 trafficking, and these channels are involved in  $\text{Ca}^{2+}$  transport in the kidney, we measured  $\text{Ca}^{2+}$  and  $\text{Na}^+$  levels in urine from p11-null mice. Measurement of concentrations was performed by staff in the laboratory of Rene Bindels. Concentrations were normalised to creatinine levels. p11 deletion had no effect on  $\text{Ca}^{2+}$  excretion:  $\text{Ca}^{2+}$  levels in p11-null mice were  $2.1 \pm 0.3 \text{ mM Ca}^{2+}/\text{mM creatinine}$  ( $n=11$ ), compared to  $2.0 \pm 0.4 \text{ mM Ca}^{2+}/\text{mM creatinine}$  ( $n=8$ ) in floxed p11 control animals. This is illustrated in Figure 4.21.

A trend towards increased  $\text{Na}^+$  excretion was observed in p11-null mice, although significance was not reached.  $\text{Na}^+$  levels in p11-null mice were  $55.8 \pm 14.0 \text{ mM Na}^+/\text{mM creatinine}$  ( $n=11$ ), compared to  $29.7 \pm 4.0 \text{ mM Na}^+/\text{mM creatinine}$  ( $n=8$ ) in floxed p11 control animals. This is illustrated in Figure 4.21.

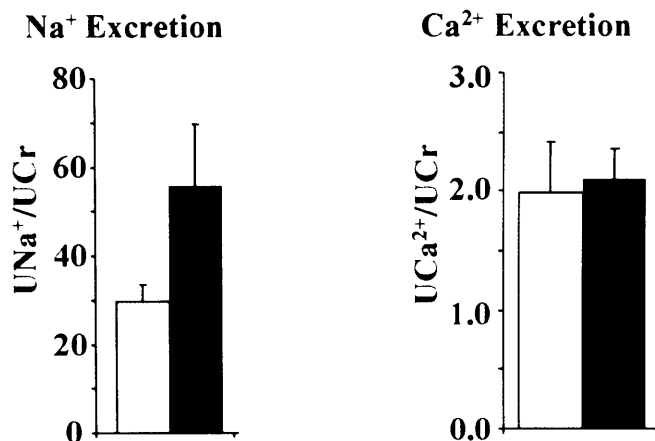


**Figure 4.21** Excretion of Ca<sup>2+</sup> and Na<sup>+</sup> in the p11-null mouse. White bars represent floxed p11 control, black bars p11-null animals. Mean  $\pm$  SEM.

#### **4.3.9 TTX-R Na<sup>+</sup> current density is reduced in p11 conditional-null mutants**

Voltage-activated sodium currents were recorded from acutely-cultured DRG neurons, from p11-null and floxed p11 littermate control mice. Voltage recordings were subject to a junction potential between intra- and extracellular solutions, calculated to be -3.7mV (using the method described by Barry and Lynch (1991)), but were not adjusted to compensate. A series of steps of increasing voltage were applied to each neuron, and the peak current recorded. Capacitance was taken as a measure of cell size, allowing the calculation of current density. Neurons of <25 $\mu$ m diameter were chosen, taken to be Cre-expressing nociceptors. Currents arising from channel subpopulations were discriminated between using TTX. Both TTX-R and TTX-S currents appeared similar between p11-null and control neurons, each showing a distinctive shape. Example traces are shown in Figure 4.22.

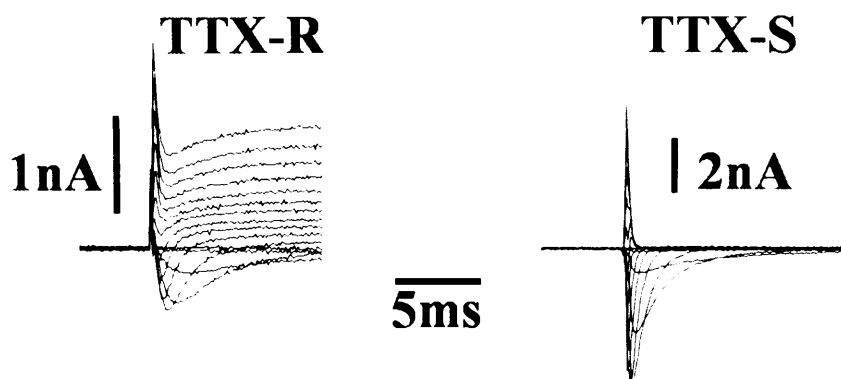


**Figure 4.22** Electrophysiology of p11-null DRG neurons. Example TTX-R and TTX-S currents in acutely-cultured DRG neurons from p11-null mice. Currents appeared similar in floxed p11 controls.

Deletion of p11 caused a statistically significant reduction in TTX-R  $\text{Na}^+$  current density of approximately 50%, compared to control neurons (Figure 4.23) (p11-null  $0.037 \pm 0.0056 \text{ nA/pF}$ ,  $n=42$ ; control  $0.071 \pm 0.016 \text{ nA/pF}$ ,  $n=26$ ;  $p=0.016$ , Mann-Whitney Rank Sum test). TTX-S current densities, however, were not significantly different between p11-null and control neurons (p11-null  $0.14 \pm 0.017 \text{ nA/pF}$ ,  $n=42$ ; control  $0.11 \pm 0.024 \text{ nA/pF}$ ,  $n=22$ ;  $p=0.19$ ). A slight increase in mean current density was observed in p11-null neurons, although this was not statistically significant (Figure 4.23). Results for both TTX-R and TTX-S current densities in floxed p11 control neurons corresponded well with those obtained from wild-type mice (C57BL/6) in previous studies (Nassar et al., 2004).

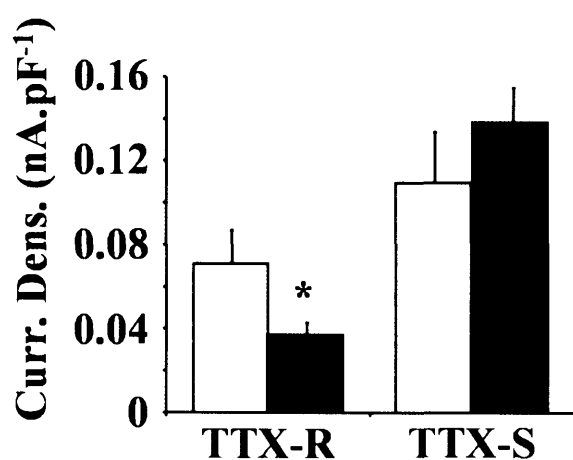


**Figure 4.23** Current densities in small-diameter DRG neurons. Whole-cell voltage clamp: TTX-sensitive (TTX-S) and TTX-resistant (TTX-R) peak sodium current densities in floxed p11 (white;  $n=24$ ) and p11-null (black;  $n=42$ ) mice. A significant decrease in TTX-R sodium current density was observed in the p11-null mice. ( $p=0.016$ ; Mann-Whitney Rank Sum test). No significant difference was observed in TTX-S current density. Data expressed as mean  $\pm$  SEM. \*  $p<0.05$ .

To determine whether the reduction in TTX-R current density was due to a reduction in channel membrane density or effects of p11 on the biophysical properties of  $\text{Na}_v1.8$ , TTX-R current-voltage relationships were examined. Comparable current-voltage relationships were observed in p11-null (n=7) and floxed p11 control (n=7) neurons (Figure 4.24). This shows that the increased current density observed is likely due to the presence of more functional channels at the membrane, rather than a shift in channel voltage-dependence.

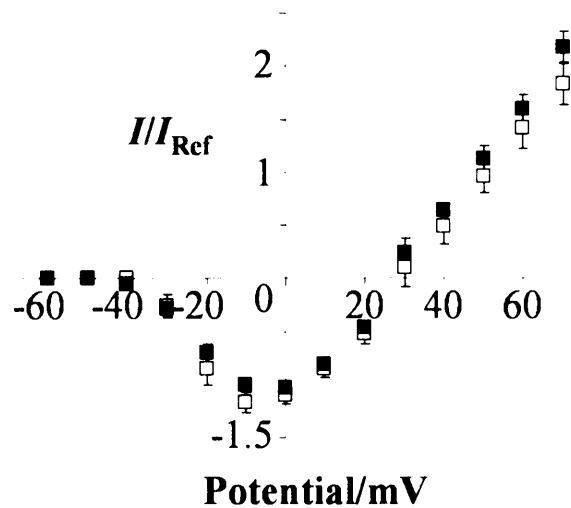


**Figure 4.24** Current-voltage relationship for TTX-R currents in small-diameter DRG neurons. No differences were observed between floxed p11 control (white: n=7) and p11-null (black: n=7) neurons. Data expressed as mean  $\pm$  SEM.

Since p11 is known to interact with the  $\text{K}^+$  channel TASK-1, which may have a role in setting neuronal resting potentials, the effect of p11 deletion on resting potential was investigated. Using physiological solutions, DRG neurons were found to fall into two groups: one with a resting potential around -50mV, the other around -70mV. This is consistent with previous research in DRG neurons (Renganathan et al., 2001), and may be related to the expression of  $\text{Na}_v1.9$  in a subset of sensory neurons (Herzog et al., 2001c). No significant differences, however, were seen in resting potentials between p11-null and control neurons (Figure 4.25). Control neurons had mean resting potentials of  $-49.68 \pm 1.54\text{mV}$  (n=12) and  $-73.30 \pm 3.40\text{mV}$  (n=7), while values for p11-null neurons were  $-47.92 \pm 1.27\text{mV}$  (n=17) and  $-68.43 \pm 4.12\text{mV}$  (n=4). The proportion of neurons in the -50mV group was greater than that in the -70mV group, consistent with the relatively infrequent occurrence of  $\text{Na}_v1.9$ -mediated currents observed in voltage-clamp recordings.

Attempts to record ASIC-mediated currents, by whole-cell and perforated-patch techniques were unsuccessful, matching experiences of other groups working on these channels in mouse DRG neurons (personal communications).

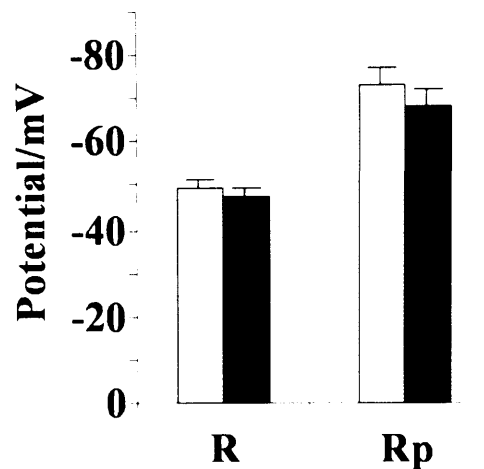


**Figure 4.25 Resting potentials of cultured DRG neurons.** No significant differences in resting potential were observed between floxed p11 control (white; n=19) and p11-null (black; n=21) neurons. Cells were grouped according to Herzog et al. (2001a). Data expressed as mean  $\pm$  SEM.

#### **4.3.10 Wide dynamic range neurons in the spinal cord show deficits in noxious somatosensory coding following p11 deletion**

Electrophysiological recordings from the dorsal horn were performed by Dr Elizabeth Matthews. Recordings were made from a total of 22 WDR neurons in p11 conditional-null (n=11) and littermate control floxed p11 (n=11) mice. The mean depths of the neurons from the surface of the spinal cord were  $471 \pm 30 \mu\text{m}$  and  $508 \pm 39 \mu\text{m}$  respectively, corresponding to the deep laminae.

Single-unit neuronal responses evoked by a range of stimuli were reduced in p11 conditional-null mice compared to littermate controls. p11 conditional-null mice showed deficits in both mechanical coding in the noxious range (above the behavioural withdrawal threshold (0.6-0.8g in this study)) compared to control (Figure 4.26a). This difference was found to be statistically significant when expressed as total evoked neuronal activity ( $p < 0.05$ , ANOVA) (Figure 4.26b). Responses to lower intensity mechanical stimuli (up to 1g von Frey) were not significantly different from control animals. p11 conditional-null mice also showed deficits in thermal coding, statistically significant when expressed as total neuronal activity ( $p < 0.05$ , ANOVA). Additionally, p11 conditional-null mice showed a statistically significant reduction in dorsal horn neuronal activity in response to noxious pinch stimuli ( $p < 0.05$ ) (Figure 4.26e&f). WDR neuronal responses to cold ( $0^\circ\text{C}$  water) and non-noxious tactile (brush) or thermal stimulation were not significantly different between p11 conditional-null and control animals (Figure 4.26e&f).

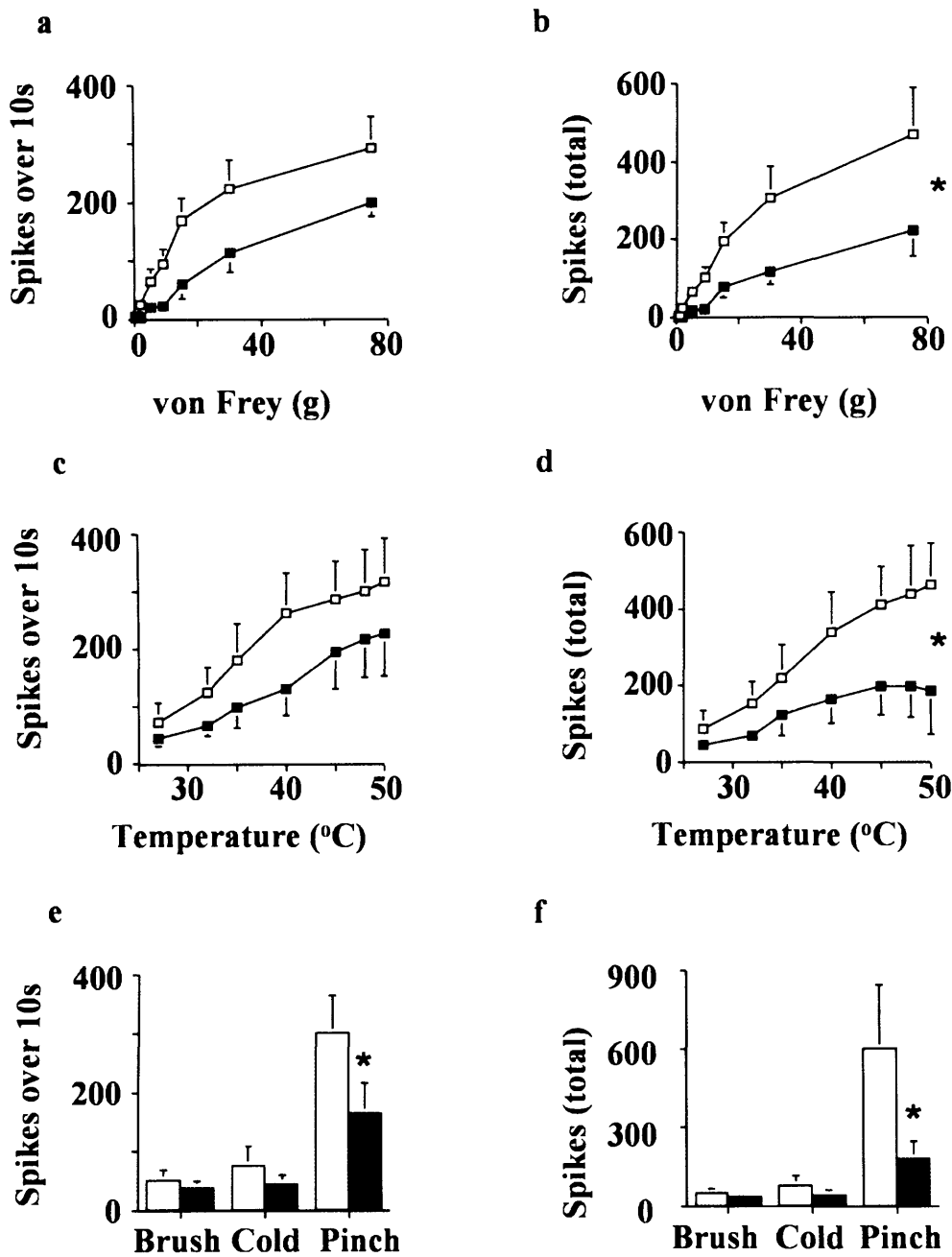


**Figure 4.26** Electrophysiological recordings from WDR neurons in the dorsal horn. **a,b:** p11 conditional-null mice (black boxes) display marked deficits in mechanically-evoked dorsal horn neuronal activity compared with littermate controls (white boxes). WDR neurons recorded from p11-null mice ( $n=11$ ) show significantly reduced activity ( $p<0.05$ ) to punctate mechanical von Frey stimuli. Data are shown during stimulus application (**a**) and for total evoked activity to the stimulus (**b**) compared with littermate control mice ( $n=11$ ). **c,d:** The same neurons show significantly reduced response ( $p<0.05$ ) to thermal stimuli (water jet). Data are shown during stimulus application (**c**) and for total evoked activity to the stimulus (**d**). **e,f:** These neurons also show significantly reduced activity to noxious pinch stimuli ( $p<0.05$ ), but not to brush or noxious cold ( $1^{\circ}\text{C}$ ) when compared with controls for the duration of the stimuli (**e**) and for total evoked activity to the stimulus (**f**). Stimuli were applied for 10s to the peripheral receptive field of the neuron on the hindpaw. Data are expressed as mean  $\pm$  SEM; \* $p<0.05$ .

Evoked responses to transcutaneous electrical stimulation of the peripheral receptive field were measured to examine effects of p11 deletion on axonal transmission properties, post-discharge and wind-up. No differences in electrical threshold for activation of A- and C-fibre afferents were observed. No differences in electrically-evoked neuronal responses or related input or wind-up parameters were observed between p11 conditional-null and wild-type animals. Spontaneous ongoing firing occurrence and rate were similar between groups. A significant reduction in post-discharge, however, was observed in p11 conditional-null animals compared to control (p11 conditional null  $34.4 \pm 11.0$ ,  $n=12$ ; control  $6.2 \pm 2.9$ ,  $n=10$ ;  $p=0.028$ ,  $t$ -test)

#### **4.3.11 p11 conditional-null mice show no gross abnormalities**

p11 conditional-null mice were healthy, fertile and apparently normal. They showed no overt differences from floxed p11 littermates in appearance or spontaneous behaviour. Weight (age- and sex-matched) was found to be comparable between p11 conditional-null and p11 floxed littermates (control male  $27.25 \pm 1.13$ g,  $n=6$ ; p11 conditional-null male  $26.38 \pm 0.82$ g,  $n=4$ ; control female  $22.04 \pm 0.50$ g,  $n=8$ ; p11 conditional-null female  $22.49 \pm 0.43$ g,  $n=11$ ). Genotype frequencies followed Mendelian ratios as expected.

To ensure that p11 conditional-null mice had normal motor coordination, allowing differences in response to noxious stimuli to be ascribed to sensory rather than motor deficits, the Rotarod test was used. Motor coordination performance on this apparatus was comparable between p11 conditional-null animals and littermate controls (p11 conditional-null  $189 \pm 8.21$ s,  $n=12$ ; control  $205 \pm 12.85$ s,  $n=12$ ).

#### **4.3.12 p11 conditional-null mice show behavioural deficits in noxious mechanosensation**

Behavioural responses to noxious mechanical stimuli were assessed using von Frey hairs and the Randall-Selitto test. No difference in withdrawal threshold to von Frey hairs was observed between p11 conditional-null and control animals (Figure 4.27a). Thresholds were comparable to previous studies undertaken in this group (floxed p11 control  $0.059 \pm 0.008$ g,  $n=5$ ; p11 conditional-null  $0.067 \pm 0.010$ g,  $n=7$ ).

The Randall-Selitto test, in contrast, revealed a deficit in behavioural responses to noxious blunt mechanical stimulation of the tail in p11 conditional-null mice (Figure 4.27b). A significant increase in withdrawal/response threshold was observed in p11 conditional-null mice compared to littermate controls (floxed p11 control  $0.0026 \pm 0.00025$ N,  $n=13$ ; p11

conditional-null  $0.0019 \pm 0.00012\text{N}$ ,  $n=13$ ;  $p=0.013$ ). A deficit in one model of mechanosensation but not another has been observed in a number of studies, for example in the analysis of the  $\text{Nav}1.8$ -null mouse line by Akopian et al.(1999), and is probably due to differences in the nature of the stimulus (blunt pressure increasing gradually compared to sharp, sudden and punctate).

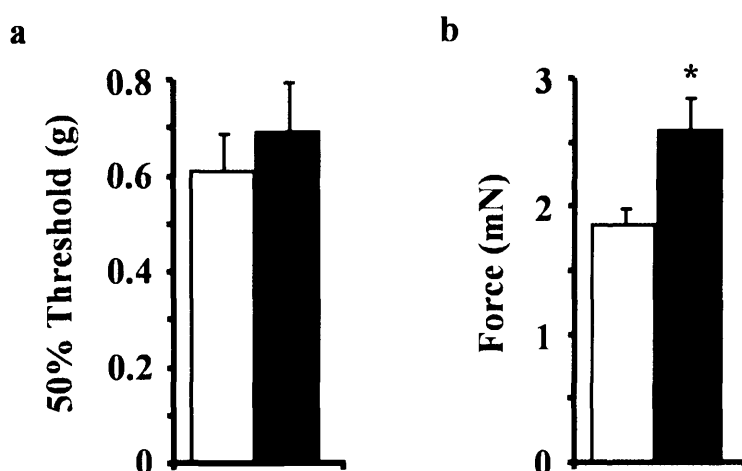


**Figure 4.27** Acute mechanical pain behaviour in p11 conditional-null and littermate control (floxed p11) mice. **a:** Response to mechanical stimulation using von Frey hairs was not significantly different between littermate control floxed p11 (white;  $n=5$ ) and p11 conditional-null (black;  $n=7$ ) mice. **b:** p11 conditional-null mice (black;  $n=13$ ) showed partial analgesia to noxious mechanical pressure applied to the tail using the Randall–Selitto apparatus compared with littermate controls (white;  $n=13$ ) ( $p=0.013$ , Student’s *t*-test). All results are shown as mean  $\pm$  SEM; \*  $p<0.05$ .

#### 4.3.13 p11 conditional-null mice do not show behavioural deficits in noxious thermosensation

Responses to noxious thermal stimuli were assessed using Hargreaves’ apparatus and the hot plate test. Paw withdrawal latency in Hargreaves’ test was not altered by p11 conditional deletion (Figure 4.28a) (control  $7.41 \pm 0.35\text{s}$ ,  $n=11$ ; p11 conditional-null  $8.28 \pm 0.50\text{s}$ ,  $n=12$ ). There were no significant differences in latency to response on the hot plate at either 50 or 55°C (Figure 4.28b) (50°C: control  $22.4 \pm 1.9\text{s}$ ,  $n=14$ ; p11 conditional-null  $25.1 \pm 2.4\text{s}$ ,  $n=15$ ;  $p=0.38$ ) (55°C: control  $10.9 \pm 0.6\text{s}$ ,  $n=14$ ; p11 conditional-null  $13.1 \pm 1.3\text{s}$ ,  $n=15$ ;  $p=0.12$ ). In each test, however, p11 conditional-null mice showed a trend towards increased latency of response, suggesting that there may be a slight tendency to thermal analgesia, similar to that observed in the  $\text{Nav}1.8$  null-mutant mouse (Akopian et al., 1999).

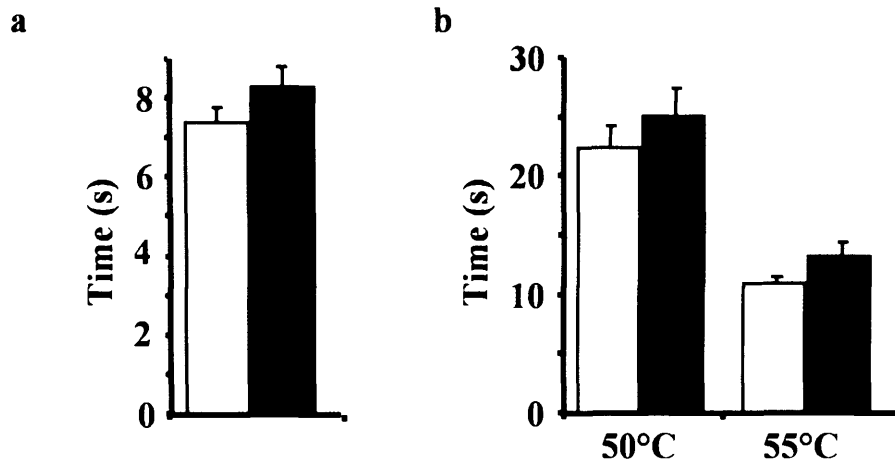


**Figure 4.28** Acute thermal pain behaviour in p11 conditional-null and littermate control (floxed p11) mice. **a:** Noxious thermal stimulation using Hargreaves' apparatus. No significant difference in latency of hindpaw withdrawal was observed between littermate control (white;  $n=11$ ) and p11 conditional-null (black;  $n=12$ ) mice. **b:** Response to noxious thermal stimulation using the hotplate apparatus was not significantly different between littermate control (white;  $n=14$ ) and p11 conditional-null (black;  $n=15$ ) mice. At 50°C,  $p=0.38$  (Student's  $t$ -test). At 55°C,  $p=0.12$  (Student's  $t$ -test). All results are shown as mean  $\pm$  SEM.

#### 4.3.14 p11 conditional-null mice show no deficits in response to noxious cold

Behavioural responses to noxious cold were assessed using the cold plate at 0°C. Substantial variation in response was seen between individual animals, with some consistently displaying higher or lower responses. This variation, however, was found to be distributed evenly between p11 conditional-null and control animals. No significant differences were seen between p11 conditional-null and littermate control animals (Figure 4.29). Previous studies have on occasion observed differences in response between male and female groups; results were separated on this basis. Results, expressed as the number of hind paw lifts or jumps over 5 mins, were as follows: Male: p11 conditional-null  $35.4 \pm 4.37s$ ,  $n=15$ ; control  $27.19 \pm 6.54s$ ,  $n=8$ ;  $p=0.31$ . Female: p11 conditional-null  $17.29 \pm 4.50$ ,  $n=7$ ; control  $27.73 \pm 4.45$ ,  $n=11$ ;  $p=0.12$ .

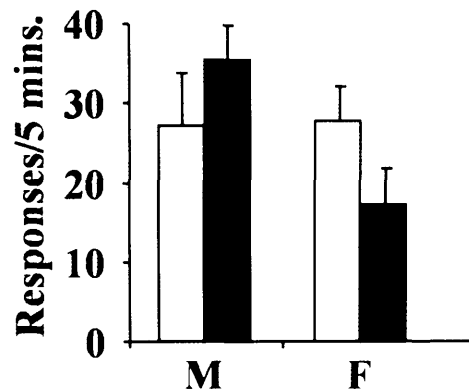


**Figure 4.29** Acute cold pain behaviour in p11 conditional-null and littermate control (floxed p11) mice. No significant differences were seen between floxed p11 littermate control (white) or p11 conditional-null (black) animals, in either males (M) or females (F).

#### **4.3.15 p11 conditional-null mice show no deficits in models of inflammatory pain**

Inflammatory pain behaviour was assessed using Hargreaves' test to measure thermal hyperalgesia in response to intraplantar carrageenan and NGF. Spontaneous inflammatory pain behaviour was assessed using the intraplantar formalin model.

Following intraplantar injection of carrageenan, profound thermal hyperalgesia was observed from 1h post-injection, persisting for at least 6h. Both baseline latencies and the extent of hyperalgesia were similar between p11 conditional-null animals (n=6) and littermate controls (n=6) (Figure 4.30a). Values obtained were comparable to those from previous studies (Akopian et al., 1999).

Intraplantar injection of NGF produced a thermal hyperalgesia with similar qualities to that induced by carrageenan, although with a slightly reduced magnitude. No significant differences were observed between p11 conditional-null animals (n=7) and littermate controls (n=5) (Figure 4.30b).

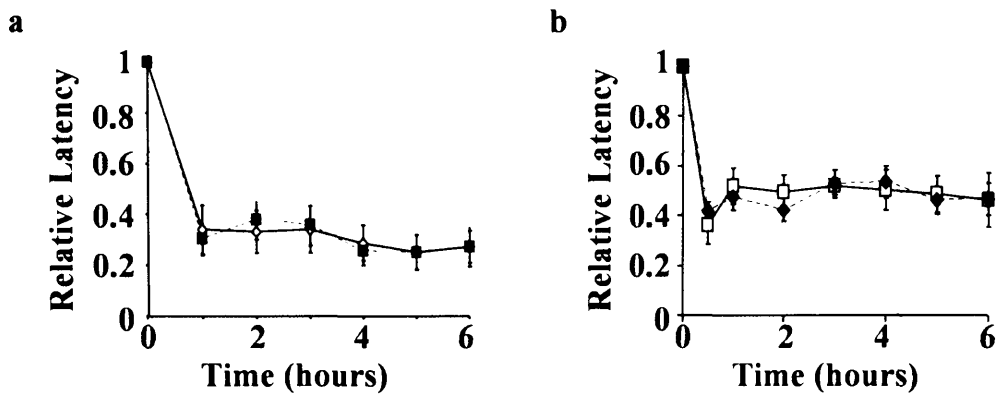


**Figure 4.30 Inflammatory pain behaviour in p11 conditional-null and littermate control (floxed p11) mice.** **a:** Thermal hyperalgesia, tested using Hargreaves' apparatus, after intraplantar injection of 2% carrageenan (20 $\mu$ l). Both floxed p11 littermate control (white;  $n=6$ ) and p11 conditional-null (black;  $n=6$ ) mice developed pronounced hyperalgesia, with no significant difference between genotypes. **b:** NGF-induced hyperalgesia. Both littermate control (white;  $n=5$ ) and p11 conditional-null (black;  $n=7$ ) mice developed profound thermal hyperalgesia.

The formalin model produced a characteristic biphasic response, eliciting spontaneous nocifensive behaviour. The second phase of response in this model is believed to model chronic pain, including a centrally-driven component. The total pain behaviour in each phase was not significantly different between p11 conditional-null animals and littermate controls (Figure 4.31a) (1<sup>st</sup> phase: p11 conditional-null  $100.6 \pm 22.2$ s,  $n=5$ ; control  $87.4 \pm 5.3$ s,  $n=7$ ) (2<sup>nd</sup> phase: p11 conditional-null  $283.2 \pm 43.2$ s,  $n=5$ ; control  $286.8 \pm 33.9$ s,  $n=7$ ). This is consistent with results obtained for  $Na_v1.8$ -null mice (Nassar et al., 2005). When viewed on a more detailed level, it appears that the 2<sup>nd</sup> phase occurs slightly earlier, and to a higher maximum level, in p11 conditional-null mice, before subsiding more rapidly (Figure 4.31b). This is a purely qualitative change, however, and was not found to be statistically significant. Environmental or observer-related parameters may be responsible for this slight difference.

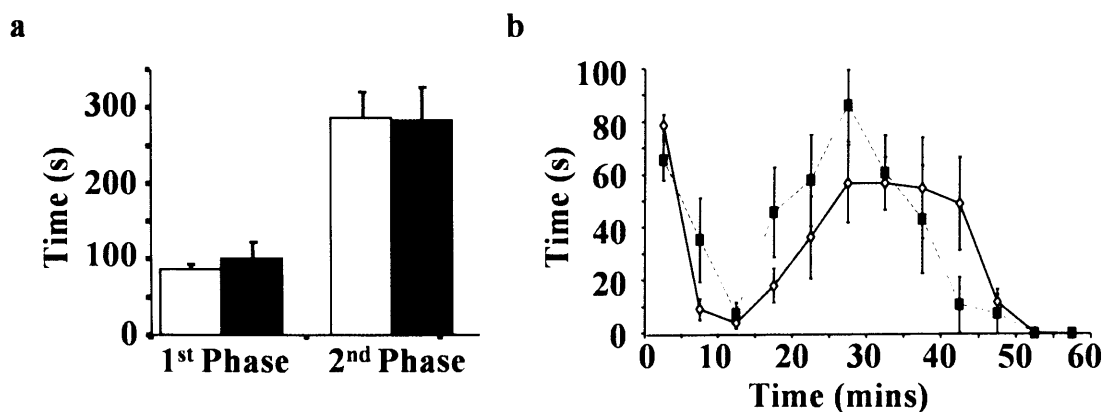


**Figure 4.31 Formalin-induced inflammatory pain behaviour in p11 conditional-null and littermate control (floxed p11) mice.** Behaviour following intraplantar injection of 20 $\mu$ l of 5% formalin. **a:** Time spent licking/biting the injected hindpaw was recorded in 5 min sections. No significant reduction in time of pain behaviour was seen at Phase 1 (0–10 mins) or at Phase 2 (10–55 mins) between littermate control (white;  $n=7$ ) and p11 conditional-null (black;  $n=5$ ) mice. **b:** Time course of the formalin test. A characteristic biphasic response was observed, with no significant differences between p11 conditional-null (black) and littermate controls (white).

#### 4.3.16 p11 conditional-null mice display reduced neuropathic pain behaviour

The Chung model (injury to the L5 spinal nerve) was used to assess the effect of p11 deletion on the development and maintenance of neuropathic pain. Surgery was performed by Bjarke Abrahamsen and Mohammed Nassar. von Frey hairs were used to measure mechanical allodynia. p11 conditional-null animals displayed similar baseline thresholds to littermate controls. Floxed p11 control animals showed a substantial decrease in mechanical threshold, to around 25% of baseline by Day 5, which gradually returned towards baseline levels, to a value of around 65% at Day 25. Thresholds for p11 conditional-null animals, in contrast, did not drop below 50% of baseline, and generally remained around 60% before recovery to around 80% at day 25. These results are shown in Figure 4.32. Overall mechanical allodynia was significantly greater in floxed p11 littermate controls ( $n=5$ ) than in p11 conditional-null ( $n=7$ ) mice ( $p=0.031$ , 2-way repeated measures ANOVA). A number of individual time points were also found to be significantly different between groups (Days 6 & 7,  $p<0.05$ ).

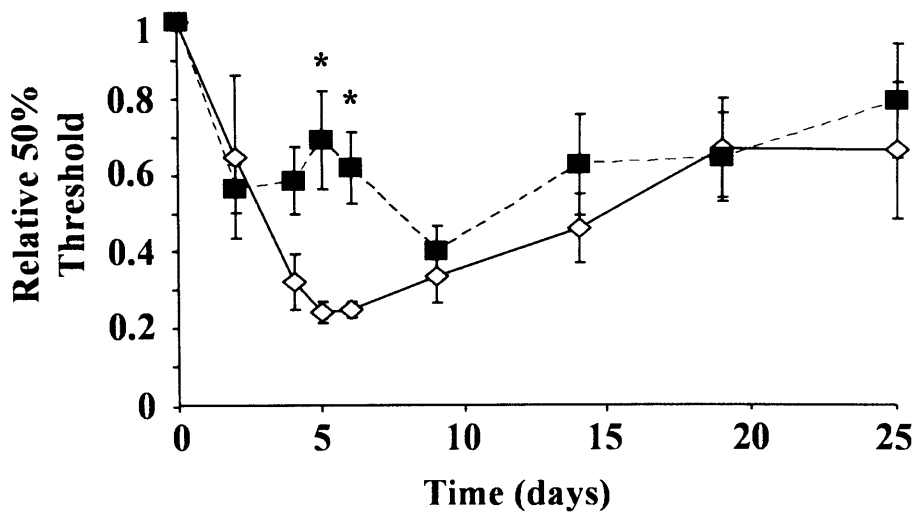


**Figure 4.32** Neuropathic pain behaviour in p11 conditional-null and littermate control (floxed p11) mice. Mechanical allodynia, measured by using von Frey hairs, resulting from the Chung model of neuropathic pain. A significant reduction in mechanical allodynia ( $p=0.031$ ; two-way repeated measures ANOVA) was observed overall in the p11 conditional-null (black;  $n=7$ ) when compared with the littermate control (white;  $n=5$ ) mice. Data are expressed as mean  $\pm$  SEM; \*  $p<0.05$  (individual points).

### 4.3.17 p11 plays a complex role in neoangiogenesis and tumour growth

To assess the role of p11 in neoangiogenesis, we used a model of tumour growth. The size to which the tumour grows is dependent on the extent of neoangiogenesis.  $10^6$  cells from a melanoma-derived cell line (B16F0) were injected subcutaneously under the dorsal surface of p11-null and floxed p11 control animals. After 11 days, the mice were culled and tumours excised. p11-null animals were found to have significantly greater tumour volumes than p11 floxed control mice (Figure 4.33).

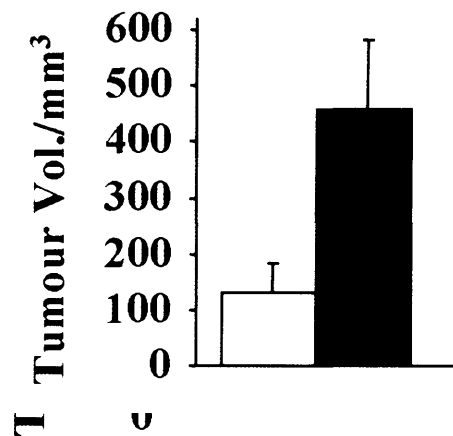


**Figure 4.33** Effect of p11 deletion on tumour growth. Melanoma growth over 11 days following subcutaneous injection of  $1 \times 10^6$  B16F0 cells in p11-null (black,  $n=10$ ; mean volume  $131.3 \pm 51.9 \text{ mm}^3$ ) and floxed p11 littermate control (white,  $n=10$ ; mean volume  $456.2 \pm 124.6 \text{ mm}^3$ ) mice.  $p=0.033$  (2-tailed  $t$ -test, unequal variance).

Blood vessel morphology was examined histologically in skin samples and in sections from the tumour. Preliminary results suggest an abnormal morphology in p11-null animals, although this will be confirmed in subsequent studies.

## 4.4 DISCUSSION

Previous studies suggested a role for p11 in the detection of noxious stimuli in peripheral sensory neurons. In particular, effects on pain thresholds via regulation of the nociceptor-specific VGSC  $Na_v1.8$  were predicted (Okuse et al., 2002). We investigated this hypothesis using p11-null mutant mice. p11 is broadly expressed in a range of tissues and has been implicated in many cellular processes, meaning that a global-null mutant would be expected to display a complex phenotype, precluding a definitive analysis of its role in nociceptive processes in DRG neurons. In particular, recently described effects on depression-related behaviour (Svenningsson et al., 2006) would be likely to confound the interpretation of nociceptive behavioural phenotypes. We therefore created a conditional (tissue-specific) p11-null mutant mouse to examine the role of p11 in nociceptive sensory neurons.

Exon 2 of p11 was deleted, since this contains the translational start codon (ATG) required for protein expression. Figure 4.34 shows the amino acids encoded by exon 2.

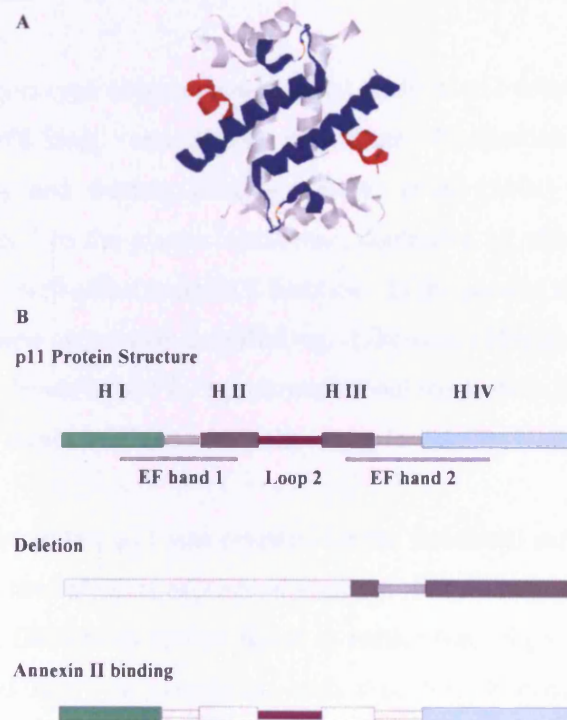


**Figure 4.34 Deleted regions of p11.** **A:** 3-D structure of the p11 dimer. Deleted residues 1-54 in white, remaining residues 55-96 in blue, annexin 2 N-terminus in red. **B:** p11 protein linear structure, illustrating deleted region and annexin 2 binding site. H I-IV represent helices I-IV.

In this study, we demonstrated a role for p11 in nociception in DRG neurons. Deletion of p11 resulted in reduced  $\text{Na}_V1.8$  expression and thus TTX-R current density in cultured sensory neurons. Deficits in noxious coding were observed at the dorsal horn, and behaviour in response to noxious mechanical stimuli was attenuated. No effects on inflammatory pain behaviour were observed, but reduced allodynia was observed in a model of neuropathic pain.

#### **4.4.1 Effects of p11 deletion on protein trafficking and nociceptor properties**

To investigate the role of p11 in nociception, a conditional p11-null mouse was created. p11 is known to show anti-apoptotic activity via its interaction and interference with the pro-apoptotic BAD (Bcl-xL/Bcl-2-Associated Death Promoter) (Hsu et al., 1997a). It was therefore possible that p11-null cells would undergo apoptosis, precluding meaningful analysis of the conditional-null mouse. The effect of p11 deletion on cell survival was therefore examined carefully. p11-null cells did not appear to undergo premature apoptosis, nor were the numbers or proportions of cells different between the p11 conditional-null animal and littermate controls. Additionally, p11 global-null mice survived and were viable. The phenotype of p11 conditional-null mice could thus be described.

To ensure that any phenotype observed was a direct result of p11 deletion, rather than an effect on annexin 2 trafficking, annexin 2 membrane localisation was assessed using immunocytochemistry and western blotting. Deora et al. (2004) reported p11-dependent trafficking of annexin 2 to the plasma membrane, controlled by phosphorylation, suggesting that p11 deletion may well affect annexin 2 function. In the present study, however, we found no effect of p11 deletion on annexin 2 trafficking. Likewise, although the presence of annexin 2 upregulates cellular levels of p11 by a posttranslational mechanism (Puisieux et al., 1996), no changes in annexin 2 levels were observed following p11 deletion (see Figure 4.19).

Okuse et al. (2002) found that p11 was essential for the functional expression of  $\text{Na}_V1.8$  at the plasma membrane in heterologous expression systems. In the study presented in this chapter, deletion of p11 from DRG neurons was found to reduce  $\text{Na}_V1.8$  protein levels at the plasma membrane by around half. In correlation with this,  $\text{Na}_V1.8$ -mediated  $\text{Na}^+$  currents were reduced by a similar level. While a reduction in  $\text{Na}_V1.8$  membrane trafficking is in agreement with the previous work, it is interesting to note that  $\text{Na}_V1.8$  functional expression was not completely abolished by p11 deletion. This observation can be explained in one of two ways: either  $\text{Na}_V1.8$  is capable of functional expression in the absence of accessory factors, or that a protein other than p11 can perform this function. In a previous study, CHO cell stable

transfection with Na<sub>v</sub>1.8 cDNA did not produce a TTX-R current, despite displaying immunoreactivity associated with the plasma membrane (Okuse et al., 2002), suggesting that Na<sub>v</sub>1.8 alone is not capable of functional expression. Antisense mRNA knockdown of p11 in cultured DRG neurons produced a reduction in TTX-R current density of around 3-fold, leaving a detectable Na<sub>v</sub>1.8-mediated current and showing that the presence of p11 is not an absolute requirement for Na<sub>v</sub>1.8 functional expression in DRG neurons (Okuse et al., 2002). These results suggest that the remaining Na<sub>v</sub>1.8 functional expression following p11 deletion is due to trafficking by other factors present in DRG neurons but not CHO cells. Candidates for Na<sub>v</sub>1.8 trafficking include those identified by yeast two-hybrid screening, such as Papin or PAF67 (Malik-Hall et al., 2003). Both Papin and PAF67 (but not calmodulin) have recently been shown to promote functional expression of Na<sub>v</sub>1.8 (Shao et al., 2005). Contactin was also shown to regulate TTX-R current density (Rush et al., 2005c). Alternatively, p11 homologues may bind to Na<sub>v</sub>1.8 under conditions of high local Ca<sup>2+</sup> concentration (binding thus not detected in the yeast two-hybrid assay), allowing for control of nociceptive thresholds by intracellular signalling pathways. The S100 protein S100A11 shares the putative Na<sub>v</sub>1.8 binding site of p11, and thus may be capable of Na<sub>v</sub>1.8 trafficking (Poon et al., 2004).

The reduction in VGSC functional expression appears to be specific to Na<sub>v</sub>1.8, since TTX-S currents were not reduced by p11 deletion. A non-significant trend towards increased TTX-S current density was observed in p11-null neurons. This may represent a degree of functional compensation, perhaps via reduced competition for insertion into membrane microdomains. Alternatively, this difference may represent nothing more than the natural variation between cells.

The regulation of Na<sub>v</sub>1.8 functional expression by p11 provides a mechanism for the control of noxious thresholds. It has been shown that Na<sub>v</sub>1.8 contributes substantially to electrogenesis in small DRG neurons, and maintains excitability in the presence of modest depolarisation (Renganathan et al., 2001), acting as a key determinant of excitability under these conditions due to its resistance to inactivation (Rush et al., 2006b). This means that relatively subtle changes in channel density at the membrane may produce sizeable changes in neuronal properties. Additionally, Na<sub>v</sub>1.8 channels have been shown to cluster at nerve termini (Brock et al., 1998a) and in neuroma (Kretschmer et al., 2002d), perhaps requiring p11. This localisation is thought to set thresholds of depolarisation at free nerve endings (Akopian et al., 1999). It is possible that further sublocalisation exists, but this has yet to be addressed. Acute cultures of DRG neurons, which do not show this morphology, may therefore underestimate the effect of p11 deletion on local neuronal properties *in vivo*.

Interactions of p11 with other membrane proteins appear to show similar variability in p11 requirement. For example, ASIC1a is expressed (functionally) in the absence of p11, but at relatively low levels. p11 causes an increase in membrane levels of ASIC1a, but does not appear to be essential for its functional expression (Donier et al., 2005). In contrast, p11 has reported to be essential for the trafficking of TASK-1 to the plasma membrane (Girard et al., 2002), although this has been disputed in a subsequent study (Renigunta et al., 2006), and for the functional expression of TRPV5&6 (van de Graaf et al., 2003). These mixed results imply that either p11 acts via several different mechanisms to promote trafficking, or that in some cases other proteins are capable of substituting for p11 function.

No changes in resting potentials were observed upon p11 deletion. It had been hypothesised that TASK-1-mediated effects could alter neuronal excitability by this method, although given the current contradictory data on the p11-TASK interaction, the direction expected was unclear. It appears that either deletion of p11 does not affect TASK-1 functional expression, or that any effects are not sufficiently large to be detectable.

The ion channels TRPV5 and TRPV6 are the most  $\text{Ca}^{2+}$ -selective of the TRP family, and constitute the rate limiting step in the  $\text{Ca}^{2+}$  influx required for reabsorption in kidney, proximal intestine and placenta (Hoenderop et al., 2001a;Hoenderop et al., 2002). TRPV5 is expressed along the apical membrane of the distal convoluted and collecting tubules (Hoenderop et al., 2001b;Loffing et al., 2001b), while TRPV6 is expressed at the brush-border membrane of duodenum, and both are prominently expressed in placenta and pancreas. A significant amount of TRPV5 is localised subapically in the distal tubules of the kidney, suggesting a shuttling mechanism for regulation of functional channel density (Loffing et al., 2001a). The p11 global-null mouse did not show deficits in epithelial  $\text{Ca}^{2+}$  transport, measured by urine  $\text{Ca}^{2+}$  excretion. This indicates that functional compensation is able to counter a reduction in p11-induced channel trafficking to restore normal levels of  $\text{Ca}^{2+}$  flux. This compensation may be a result of TRPV5/6 trafficking by another molecule, perhaps a member of the S100 protein family. In particular, S100B and S100A11 show similarities to p11, with S100A11 capable of annexin 2 binding (Rintala-Dempsey et al., 2006b). Alternatively, increased activity of other epithelial  $\text{Ca}^{2+}$ -permeant channels may be sufficient for physiological compensation, allowing physiological levels of  $\text{Ca}^{2+}$  excretion. Other members of the TRP family may fulfil this role, although many have reduced permeability to  $\text{Ca}^{2+}$ .

It is possible that the p11-null mouse displays a more subtle phenotype with respect to TRPV5/6 trafficking. The  $\text{Ca}^{2+}$  excretion assay presented here is relatively crude, and does not take into account urine volume, meaning that smaller changes in  $\text{Ca}^{2+}$  excretion are unlikely to

be detected. Nevertheless, the substantial effect of p11 deletion predicted by previous studies was not observed.

A non-statistically significant increase in  $\text{Na}^+$  excretion was observed in the p11-null mouse. While this may be a non-meaningful variation, as suggested by the statistical analysis, the relatively low power of the study means that a real difference may underlie this observation. Although TRPV5 and TRPV6 allow  $\text{Na}^+$  flux, it is likely that other channels mediate alterations in  $\text{Na}^+$  excretion, due to the lack of effect of p11 deletion on  $\text{Ca}^{2+}$  excretion. Epithelial  $\text{Na}^+$  channels are not among the proteins currently identified as interacting with p11, although this remains possible. Alternatively, changes in  $\text{K}^+$  currents resulting from altered membrane trafficking of TASK-1 in the absence of p11 (Girard et al., 2002; Renigunta et al., 2006) may influence the activity of  $\text{Na}^+$ - $\text{K}^+$  exchange processes, resulting in reduced  $\text{Na}^+$  excretion through an indirect mechanism.

The physiological significance of p11 deletion from nociceptive DRG neurons was examined by recording electrical activity from wide dynamic range neurons in the dorsal horn. This was performed *in vivo*, meaning that any effects of  $\text{Na}_v1.8$  clustering were included. Since this procedure is performed in anaesthetised mice, responses to supra-threshold stimuli can be assessed. This is an advantage over behavioural assessment of noxious thresholds, since most clinically-occurring pain is of this nature. This may account for differences between behavioural and electrophysiological data. Neurons innervated by p11-null C-fibres showed reduced activity in response to thermal and mechanical stimuli (including pinch but not brush), particularly in the noxious range, while results from floxed littermate control animals correlated well with those from previous studies (Matthews et al., 2006). This reflects a reduction in the sensitivity of noxious transduction, as might be expected as a result of reduced functional  $\text{Na}_v1.8$  expression. These results, however, differ from those obtained in the  $\text{Na}_v1.8$ -null mouse line, where deficits in mechanical but not thermal nociception were observed (Matthews et al., 2006). It is not clear why one modality but not another was affected in the  $\text{Na}_v1.8$ -null study, although the authors propose a possible restriction of  $\text{Na}_v1.8$  expression to mechano- but not heat-sensitive primary afferents. Further evidence to support this hypothesis, however, has yet to be produced. While this disparity between the two studies may be due to experimental factors, it provides the first hint that p11 may affect nociceptor properties by mechanisms additional to  $\text{Na}_v1.8$  trafficking. Candidate mechanisms include trafficking of other channels such as TASK-1 or ASIC1a. Additionally, similar magnitudes of effect were seen in the p11- and  $\text{Na}_v1.8$ -null mouse lines (for mechanical stimuli), despite the observation that p11 deletion reduces trafficking of the channel by only around 50% (based on electrophysiological and immunological data). No deficits in response to noxious cold were observed in the p11

conditional-null mouse, despite electrophysiological and (unpublished) behavioural evidence for a critical role of  $\text{Na}_v1.8$  in cold nociception (Matthews et al., 2006). The most probable explanation for this discrepancy is that the remaining population of  $\text{Na}_v1.8$  channels in the plasma membrane is sufficient to allow the transmission of noxious cold, with any differences being below the sensitivity of the experimental procedures.

p11 conditional-null mice showed no difference from control animals in response to electrical stimulation of neuronal peripheral receptive fields. This result was also seen in  $\text{Na}_v1.8$ -null mice, and is consistent with the localisation of  $\text{Na}_v1.8$  channels at peripheral termini of sensory neurons (Brock et al., 1998c). These findings support the hypothesis that  $\text{Na}_v1.8$  is closely associated with transducers of noxious stimuli, providing the initial VGSC-mediated current which subsequently activates TTX-S channels along the axon. As a result, direct electrical excitation of neurons is unaffected by changes in  $\text{Na}_v1.8$  levels. Other measures of neuronal properties, input, wind-up and post-discharge, were also assessed in p11 conditional-null mice. While no differences in input or wind-up were observed, post-stimulus electrical discharge was significantly attenuated. Post-discharge is generally regarded as postsynaptic in origin, involving relief of  $\text{Mg}^{2+}$  block of spinal NMDA receptors (Matthews et al., 2006). In this case, however, the conditional (primary afferents only) deletion of p11 allows the attribution of this observation to presynaptic mechanisms. p11 may act, perhaps in conjunction with annexin 2, on processes underlying presynaptic components of synaptic plasticity. Alternatively, it is possible that the role of  $\text{Na}_v1.8$  in determining excitability under conditions of sustained depolarisation may explain this finding (Renganathan et al., 2001; Rush et al., 2006a). Since this effect was not observed in the  $\text{Na}_v1.8$ -null mouse, however, another action of p11 is likely to underlie this observation. ASIC1a, the functional expression of which is enhanced by p11 (Donier et al., 2005), is involved in synaptic plasticity and fear conditioning in the brain (Wemmie et al., 2002; Wemmie et al., 2003), with loss of ASIC associated with impaired hippocampal long-term potentiation. Reduced trafficking of ASIC1a in the p11 conditional-null mouse may therefore explain this observation. It is uncommon for an effect on post-discharge to be observed in the absence of effects on wind-up, since both are a consequence of removal of  $\text{Mg}^{2+}$  block from NMDA receptors. This can be explained, however, by an effect upon sustained firing of peripheral nerves in the p11 conditional-null animal. To calculate wind-up, it is assumed that input is constant over the course of stimulation (16 trains), using the equation: Wind-up = total action potentials (16 trains) - action potentials from first train x 16. If the actual input is different from the calculation of input (first train x 16), the value generated for wind-up may be inaccurate. An effect of p11 deletion on the ability of peripheral nerves to fire repeatedly in response to trains of pulses may therefore explain the discrepancy between wind-up and post-discharge results.

The rate and occurrence of spontaneous firing was normal in p11 conditional-null mice. Since a decrease in occurrence of spontaneous firing was observed in Nav1.8-null mice, it is possible that TASK-1-mediated effects partially compensated for this change, although no change in resting potential was seen. Alternatively, small changes could be below the threshold of detection for this study.

In conclusion, this work has shown a reduction in Nav1.8 functional expression as a result of p11 deletion. While no differences in membrane levels of other proteins trafficked by p11 were observed, direct functional tests were not performed, meaning that p11 deletion may affect functional expression of ASIC1a, TASK-1, 5-HT<sub>1B</sub> or TRPV5/6 in the DRG, as proposed by previous studies. Electrophysiological recordings from wide dynamic range neurons in the spinal cord revealed deficits in noxious somatosensory coding as a result of conditional p11 deletion. While the majority of this observation can be explain through actions of p11 on Nav1.8, certain phenomena were seen that were not present in the Nav1.8-null mouse. These are therefore ascribed to actions of p11 through other effector molecules, perhaps including ASIC1a, some of which may be currently unidentified.

#### **4.4.2 Effects of p11 deletion on pain behaviour**

p11 conditional-null mice appeared healthy and were found to show no motor deficits, allowing their use in assays of nociception. As predicted by the electrophysiological results described previously, conditional-null mice were found to have deficits in certain aspects of pain-related behaviour. p11 conditional-null mice displayed increased behavioural thresholds to acute noxious mechanical stimuli in the Randall-Selitto test, similar to the deficits observed in the Nav1.8-null mouse (Akopian et al., 1999). The magnitude of analgesia in the absence of p11 was ~50% of that seen in the Nav1.8-null mutant, correlating with the reduction in TTX-R Na<sup>+</sup> currents observed in the p11-null. This suggests that the mechanical analgesia observed in the p11 conditional-null mouse is mediated by reduced trafficking of Nav1.8 to the plasma membrane. An involvement of ASIC1a is unlikely, since this was shown not to contribute to cutaneous mechanoreceptor function (Page et al., 2004a), and a mechanism for the involvement of other channels trafficked by p11 is lacking. No differences in mechanical thresholds, however were observed between p11 conditional-null and littermate controls when assessed using von Frey hairs. Although this seems to conflict with the results obtained from the Randall-Selitto test, this was not unexpected: a similar discrepancy was observed in both Nav1.8-null and Nav1.7 conditional-null mice (Akopian et al., 1999; Nassar et al., 2004), and is likely to be due to low- versus high-intensity, or other qualitative differences in the stimulus. It is likely that the Randall-Selitto apparatus requires a higher intensity stimulus for behavioural

response than graded von Frey hairs due to the experimental design (continuous versus sudden pressure). Additionally, the blunt pressure applied by the Randall-Selitto apparatus contrasts with the punctate nature of von Frey hair stimulation. It is possible that the behavioural response to low-intensity von Frey hairs represents a non-nociceptive process, or that Randall-Selitto and von Frey methods assess differing nociceptive pathways. For example, the Randall-Selitto stimulus is of much higher intensity than that of the von Frey method, and is applied over a larger area, to a different body region. The diminished response to von Frey hair stimulation detected by spinal cord recording can be explained by the use of high intensity, supra-threshold stimulation in this model, in contrast to the threshold-detection behavioural approach.

No deficits in noxious thermosensation were observed in the p11 conditional-null mouse. The modality-specific effect of p11 deletion may be explained via its effects on Nav1.8 trafficking, since Nav1.8-null mice were found to show only minor thermal analgesia: the ~50% reduction in expression achieved by p11 deletion would not be likely to cause a detectable effect using behavioural methods (although a slight increase in threshold (non-significant) was seen in all tests). The modality-specific effect of Nav1.8 deletion, however, has not been explained. It may imply that Nav1.8 is not highly-expressed in neurons that detect noxious heat, as suggested by Matthews et al. (2006). Alternatively, coupling to a specific transducer of mechanical stimuli is possible, but perhaps unlikely. It has been noted that handling elevates body temperature in mice, partially confounding thermal assays of nociception (Hole and Tjolsen, 1993), which may explain the difference in results between behavioural and electrophysiological thermal nociception assays. Reduced visceral pain and referred hyperalgesia were observed in the Nav1.8-null mouse (Laird et al., 2002). It would therefore be interesting to test p11 conditional-null mice in models of visceral pain.

p11 is upregulated by a variety of inflammatory mediators, including NGF (Masiakowski and Shooter, 1988) and interferon- $\gamma$  (anti-inflammatory) (Huang et al., 2003b), suggesting a role in inflammatory pain processes. Glucocorticoids and nitric oxide, induced during inflammation, also upregulate p11 (Pawliczak et al., 2001; Yao et al., 1999c). Additionally, NGF-induced hyperalgesia has been shown to be strongly dependent on the presence of Nav1.8 (Kerr et al., 2001), which is upregulated by NGF (Okuse et al., 1997), and ASIC1a channels on sensory neurons may respond to local acidification occurring during inflammation. Nav1.8 has also been found to contribute to PGE<sub>2</sub>-induced hyperalgesia through PKA- and PKC-mediated phosphorylation causing changes in biophysical properties, increasing excitability (FitzGerald et al., 1999; Gold et al., 1998). These factors suggest that p11 deletion from nociceptors may result in reduced hyperalgesia in models of inflammatory pain. Surprisingly, no differences

from control were observed in three models (intraplantar NGF, carrageenan and formalin) of inflammatory pain. This implies that the upregulation of  $\text{Na}_v1.8$  function by NGF is independent of p11, perhaps involving channel phosphorylation or increased trafficking by another molecule. An alternative explanation is that the study by Kerr et al. (2001) used a systemic injection of NGF to induce inflammation, in contrast to the local subcutaneous delivery used in the p11 conditional-null mutant, which may produce inflammatory hyperalgesia through subtly different mechanisms. The  $\text{Na}_v1.8$ -null mouse did not show any resistance to carrageenan-induced thermal hyperalgesia until a phenotype was “unmasked” using lidocaine, in agreement with the lack of effect of p11 deletion. It thus appears that neither p11-mediated  $\text{Na}_v1.8$  trafficking nor any other actions of p11 in primary afferent neurons are required for inflammatory hyperalgesia. This finding is in agreement with a recent paper using nociceptor-specific gene deletion to show that  $\text{Na}_v1.7$  plays a major role in inflammatory pain (Nassar et al., 2004). Since p11 does not interact with  $\text{Na}_v1.7$  (Okuse et al., 2002), any minor role of p11 would likely be hidden by the much larger contribution of this channel.

A marked reduction in neuropathic pain was observed in the p11 conditional-null mouse, despite the observation that p11 mRNA was not found to be upregulated in an orofacial neuropathic pain model (Eriksson et al., 2005). During the initial period (days 2-10), a substantial difference was seen between groups, which reduced over time. The generation and maintenance of neuropathic pain are often considered as distinct processes, with a primary afferent barrage generating conditions under which chronic central sensitisation can occur, prolonging hypersensitivity beyond the duration of primary input (e.g. Coull et al., 2003b; Coull et al., 2005c). Our result therefore can be interpreted as illustrating the contribution of p11-containing primary afferent nociceptors to the generation, but not maintenance of neuropathic pain. The downstream effectors through which this action of p11 is mediated have yet to be identified; it is not clear if previously identified p11 interactors, such as  $\text{Na}_v1.8$ , ASIC1a, TASK-1, 5-HT<sub>1B</sub> and TRPV5/6 are responsible, or if these effects are mediated by as yet unidentified proteins.

The role of  $\text{Na}_v1.8$  in neuropathic pain has been scrutinised by several groups, using a variety of experimental approaches. Initial investigations by Okuse et al. (1997) described a substantial downregulation of  $\text{Na}_v1.8$  transcript and membrane associated immunoreactivity following neuropathic nerve damage, supported by a later investigation studying trigeminal ganglia in an orofacial neuropathic pain model (Eriksson et al., 2005). A similar downregulation was observed in animal models of diabetic neuropathy, although a significant increase in both TTX-S and TTX-R currents was reported, possibly via post-translational

(phosphorylation) mechanisms (Hong et al., 2004). Kerr et al. (2001) used the  $Na_v1.8$ -null mouse to show a lack of contribution to neuropathic pain, using the Seltzer model of partial sciatic nerve injury (Seltzer et al., 1990), although this was subjected to the criticism that the compensatory upregulation of  $Na_v1.7$  observed by Akopian et al. (1999) may have masked any effects of  $Na_v1.8$  deletion. This was addressed subsequently when a double knockout of  $Na_v1.7$  and  $Na_v1.8$  also failed to show deficits in the Chung model of neuropathic pain (Nassar et al., 2005). A reduction in neuropathic pain behaviour was reported after antisense mRNA knockdown of  $Na_v1.8$  (Lai et al., 2002), although strangely no changes in acute thresholds were seen. It is likely that the reduction in neuropathic pain observed here was due to actions of the antisense mRNA on other targets, perhaps including TTX-S  $Na^+$  channels, since no data was provided to demonstrate specificity. The hypothesis that redistribution of  $Na_v1.8$  from cell body to axon in uninjured neurons was proposed by the same group (Gold et al., 2003), although this remains incompatible with the results observed in the  $Na_v1.7/Na_v1.8$  double knockout (Nassar et al., 2005). Deletion of  $Na_v1.8$ , however, did prevent spontaneous activity in damaged sensory axons, and reduced late-phase ectopic discharge in neuroma C-fibres (Roza et al., 2003). This may be due to a role of  $Na_v1.8$  in determining excitability under depolarising conditions (Renganathan et al., 2001; Rush et al., 2006c).  $Na_v1.8$  and  $Na_v1.7$  have also been shown to accumulate in painful human neuromas, although the contribution of this to the pain observed is not clear (Kretschmer et al., 2002c). Recently, the discovery of the conotoxin MrVIB, a specific blocker of  $Na_v1.8$  channels, was reported, along with the observation that its intrathecal administration reduced neuropathic pain behaviour in the rat (Ekberg et al., 2006). The authors report, however, a lack of selectivity of the toxin for TTX-R currents in mouse DRG neurons, raising doubts about the mechanism through which the toxin acts. Additionally, it is unclear how the intrathecal administration of a peptide toxin could result in activity at  $Na_v1.8$ , which is expressed solely in the periphery: a combination of low membrane permeability and rapid degradation would render concentrations low in primary afferent neurons. Overall, the published data do not support a major role for  $Na_v1.8$  in neuropathic pain, although there limited evidence for a contribution to spontaneous activity in damaged fibres. On balance, therefore, it is likely that the effect of p11 deletion on neuropathic pain does not result from attenuated trafficking of  $Na_v1.8$ , but from the interaction of p11 with another protein.

The roles of TASK-1, 5-HT<sub>1B</sub> or TRPV5/6 in neuropathic pain have not been examined. The contribution of TASK channels to the resting membrane potential suggests a mechanism for TASK-1-mediated regulation of neuronal excitability. Although no change in resting potential was observed in acutely-cultured DRG neurons upon p11 deletion, it remains possible that p11-mediated changes in TASK-1 membrane levels become significant following nerve damage.

Conflicting data on the role of p11 in TASK-1 trafficking, however, make the probable effect of p11 deletion on K<sup>+</sup> currents unclear (Girard et al., 2002; Renigunta et al., 2006). The physiological function of 5-HT<sub>1B</sub> in primary afferent neurons has not been described, and a mechanism by which altered trafficking could reduce neuropathic pain is not obvious. Coupling of the receptor to the inhibitory G-protein G<sub>i</sub> allows manipulation of second messenger pathways, but little research exists on the role of 5-HT in nociceptors during neuropathic pain. There are no data on the expression or possible role of TRPV5/6 in DRG neurons.

ASIC1a mRNA has been shown to be downregulated in several models of neuropathic pain, with corresponding reduced functional expression (Poirot et al., 2006). The authors of this paper suggest an inhibitory contribution of ASIC1a-related currents in neuropathic pain, via an inhibitory effect on actively firing neurons (Vukicevic and Kellenberger, 2004). This is inconsistent with a role for ASIC1a in p11-enhanced neuropathic pain behaviour. Although ASIC2 and ASIC3 have been shown to have an involvement in nociception, these channels do not bind p11, and are therefore not responsible for the effects of p11 deletion.

Neuropathic pain involves complex interactions between damaged and intact neuron, either axonally or at the level of the DRG (Boucher and McMahon, 2001a). In particular, the release of signalling molecules by degenerating nerves may underlie a proportion of the hypersensitivity observed following nerve damage (Boucher and McMahon, 2001b). Since p11 interferes with BAD-induced apoptosis (Hsu et al., 1997c), it is possible that p11-null damaged neurons undergo apoptosis more readily than wild-type damaged neurons. This would reduce the extent to which cell contents were released, possibly reducing the effect of nerve damage on uninjured neurons and therefore neuropathic pain.

Finally, certain effects of p11 may be mediated through brain-derived neurotrophic factor (BDNF). The extracellular protease plasmin was reported to convert the BDNF precursor proBDNF into active BDNF, and was shown to be required for hippocampal long-term potentiation (Pang et al., 2004a). Since p11 regulates the production of plasmin by tPA (Kassam et al., 1998d), it is reasonable to suggest that p11 deletion would reduce levels of BDNF. BDNF released from microglia in the spinal cord has been shown to play a central role in the development of neuropathic pain, through shifts in Cl<sup>-</sup> gradients (Coull et al., 2003a; Coull et al., 2005b). In the present study, however, p11 was deleted only from a subset of primary afferent neurons, precluding an effect on microglial BDNF release. Deletion of BDNF from the same subset of neurons was reported to reduce inflammatory pain and secondary hyperalgesia, but was found to have no effect on the development of neuropathic

pain (Zhao et al., 2006). Although it is possible that nociceptor-derived plasmin may be required for the generation of active BDNF in the spinal cord, it is likely that the effect of p11 deletion on neuropathic pain is best explained by another mechanism. The observation that p11 deletion from nociceptors does not attenuate inflammatory pain would suggest that BDNF levels are not significantly altered in the p11 conditional-null mouse line.

A definitive mechanism for the involvement of p11 in the generation of neuropathic pain has yet to be determined. While several molecules identified as interacting with p11 are plausible effectors, a lack of information of the mechanisms behind the generation of neuropathic pain makes further speculation difficult. It remains possible that the effect of p11 deletion on neuropathic pain is orchestrated not through interaction with a specific transmembrane protein, but through effects on membrane microdomain organisation. p11, via the annexin 2 heterotetramer, has been proposed to organise microdomains in the cell membrane through the formation of cholesterol-stabilised phosphatidylinositol 4,5-bisphosphate clusters (Gokhale et al., 2005). These lipid domains may organise channel distribution to affect neuronal excitability, allowing not only trafficking to the membrane but subsequent membrane localisations to be determined by p11. Disruption of this organisation may provide an alternative explanation for the effect of p11 deletion on neuropathic pain. Actin dynamics are regulated by the annexin 2-p11 heterotetramer (Hayes et al., 2006b), resulting in the stabilisation of actin-rich lipid rafts (Hayes et al., 2004) and raising the possibility of their disruption in sensory nerve termini upon p11 deletion. The annexin 2 heterotetramer also interacts with the protein AHNAK to regulate plasma membrane cytoarchitecture in epithelial cells (Benaud et al., 2004; De et al., 2006b), which may also occur in neurons, producing a more general effect of p11 deletion. Likewise, the inhibition of phospholipase A2 by p11 (Bailleux et al., 2004a) may result in alterations in second messenger pathways in the absence of p11, although this is likely to support a pro-inflammatory result of p11 deletion (Wu et al., 1997a).

Effective pharmacological agents for the treatment of neuropathic pain are currently scarce. The present study does not explicitly identify a novel therapeutic target, but does highlight the role of  $Na_v1.8$ -containing neurons in the generation of neuropathic pain. Although small-molecule inhibition of total p11 function would be likely to result in substantial adverse effects, future research to identify the effector through which p11 deletion reduces neuropathic pain may permit the development of therapies targeted towards a specific interaction between p11 and this molecule.

The effects of conditional p11 deletion reported here must be viewed in light of the expression profile of the Cre recombinase used for this deletion. While over 85% of  $Na_v1.8$ -positive cells

are reported to be nociceptors (Akopian et al., 1996; Djouhri et al., 2003a), it is not clear that all nociceptors express Nav1.8; indeed, it is likely that a subset of nociceptors do not express Nav1.8 (Djouhri et al., 2003a). This means that although the neurons from which p11 has been deleted are likely nociceptors, a population of nociceptors in which p11 is present may remain. This study may thus underestimate the importance of p11 in nociception. This nociceptor population, however, has yet to be characterised, making a more precise prediction difficult. It would therefore be interesting to investigate the role of p11 in nociception using other Cre-expressing mouse lines, especially one expressing Cre in all DRG neurons. If the effects of p11 deletion on nociception were mediated solely by attenuated trafficking of Nav1.8, this issue would not arise, but our data in combination with the pre-existing literature suggests that this may not be the case.

#### **4.4.3 Sources of compensation for p11 deletion**

Compensatory changes in gene expression are a commonly-cited limitation of transgenic studies. Additionally, a degree of functional redundancy between proteins can limit the effect of gene deletion. In this study, we observed a 50% reduction in Nav1.8 functional expression following p11 deletion, whereas previous work in heterologous expression systems found Nav1.8-mediated currents to be almost negligible in the absence of p11. This suggests that in DRG neurons, other molecules are capable of Nav1.8 trafficking in place of p11: there is a degree of functional redundancy. A variety of proteins have been identified as capable of binding to Nav1.8, either by yeast two-hybrid studies (Malik-Hall et al., 2003) or by more directed approaches (e.g. Choi et al., 2006e). Of proteins identified by yeast two-hybrid screening, Papin and PAF67 appear capable of Nav1.8 trafficking in heterologous cells (Shao et al., 2005). Choi et al. (2006c) recently demonstrated that calmodulin binds to the C-terminus of Nav1.8 and increases current density, without altering voltage-dependency of activation or inactivation, although this result was not replicated in heterologous expression systems (Shao et al., 2005). The same group also reported a role for contactin, a neuronal cell surface glycoprotein, in the trafficking of Nav1.8 and Nav1.9, showing reduced immunostaining and TTX-R current density in DRG neurons from contactin-null mice (Rush et al., 2005b). Alternatively, Nav1.8 trafficking in the absence of p11 may be carried out by other S100 proteins, especially S100A11, which shares the putative Nav1.8 binding site (Poon et al., 2004) and can bind to annexin 2 (Rintala-Dempsey et al., 2006a) and may therefore be capable of Nav1.8 trafficking under conditions of high Ca<sup>2+</sup> concentration.

Candidates for compensatory actions in the trafficking of other proteins are less well defined. The 14-3-3 family of proteins have been shown to promote plasma membrane expression of

TASK-1 (Renigunta et al., 2006), and incidentally have similar anti-apoptotic actions to p11 through interference with BAD (Hsu et al., 1997d). S100 proteins that share conserved binding site residues with p11 may be able to replace p11 functions in the presence of high  $\text{Ca}^{2+}$  concentration, although this has not been tested.

In conclusion, we have demonstrated for the first time the importance of the S100 protein p11 in nociceptive pathways in primary sensory neurons. A proportion of the phenotype observed upon p11 deletion is due to attenuated  $\text{Na}_v1.8$  trafficking, but certain aspects are proposed to be due to other actions of p11 in nociceptors. We have also created a powerful tool in the p11-floxed mouse line for the tissue-specific investigation of p11 function.

#### **4.4.4 p11 deletion enhances tumour growth and neoangiogenesis**

Since p11 catalyses the formation of plasmin, required for the formation of new vasculature, it was predicted that p11-null mice would display decreased neoangiogenesis. Reduced tumour growth was expected as a direct consequence, since oxygen and nutrient supply would limit cell growth. We tested tumour growth following the injection of a melanoma-derived cell line as a surrogate model of angiogenesis. Surprisingly, tumour volume at the end of the test period was found to be substantially greater in p11-null animals than in floxed p11 controls. Additionally, blood vessel morphology was found to be abnormal in preliminary investigations, although this will be investigated in more detail in subsequent studies. A mechanism for p11-mediated suppression of tumour growth is not immediately apparent from the current literature. Since the injected cell line was not p11-null, effects of p11 deletion on the tumour cells themselves are excluded. Cells in the host system, particularly endothelial cells, must therefore be the focus of p11 action in this assay.

It is possible that the formation of plasmin is not critical for neoangiogenesis under these conditions, a hypothesis which will be investigated in subsequent studies using Matrigel assays as a more direct measure of angiogenesis. This appears unlikely, however, since annexin 2-null mice, which displayed fibrin deposition as a result of reduced plasmin activity, also displayed markedly attenuated angiogenesis in a variety of assay systems (Ling et al., 2004). From this study, annexin 2 (heterotetramer)-dependent plasmin formation appears to be essential for neoangiogenesis. A lack of consequences of decreased plasmin production is therefore unlikely to explain the increased tumour growth in p11-null mice. An alternative explanation is that plasmin formation by uPA is more important than formation by tPA in this assay, or that increased uPA activity can compensate for the reduction in p11-catalysed tPA function. Aside from a lack of evidence to support this hypothesis, the reduced angiogenesis observed in the annexin 2-null mouse would seem to preclude this explanation. Differences in models of

angiogenesis used, and in the angiogenic mechanisms responsible, may account for this, however. In support of this, uPA is generally thought to be involved in pericellular proteolysis during cell migration, wound healing and tissue remodelling, while tPA mediates mainly intravascular fibrinolysis (Kwon et al., 2005b). The tumour growth model may be more dependent on uPA activity than tPA, in contrast to angiogenesis assays used in the annexin 2-null study.

Perhaps the most likely explanation for the pro-tumour growth effect of p11 deletion is an anti-angiogenic action of p11 in endothelial cells. Several mechanisms have been suggested for this by previous studies. The annexin 2-p11 heterotetramer was reported to act as a plasmin reductase via cysteine residues on p11, resulting in plasmin autoproteolysis (Kwon et al., 2002). Aside from reducing the local concentration of active plasmin, this proteolysis results in the formation of A(61), an angiostatin-like protein with anti-angiogenic activity (Kassam et al., 2001). Angiostatin may also be released from this process, likewise inhibiting angiogenesis. The annexin 2-p11 heterotetramer also acts more directly to inhibit angiogenesis, inhibiting plasmin-dependent fibrinolysis (Choi et al., 1998b; Choi et al., 2001). p11 is thus capable of inhibiting plasmin-mediated fibrinolysis and subsequent angiogenesis, in addition to its pro-angiogenic activity. The possible anti-angiogenic actions of p11 are summarised in Figure 4.35.

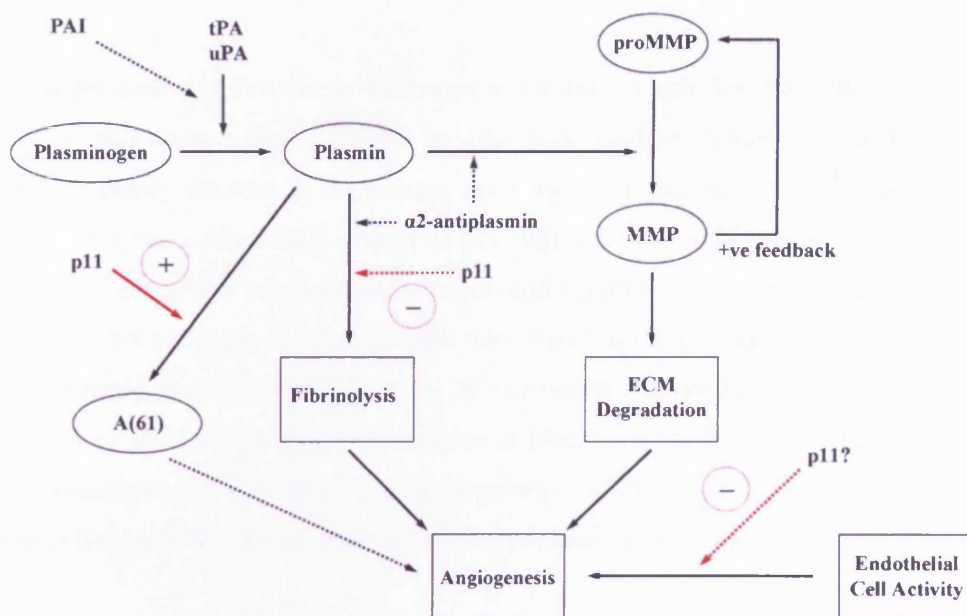


**Figure 4.35 Anti-angiogenic effects of p11.** Red arrows represent effects of p11. Solid lines represent a positive (stimulatory) effect, dotted lines inhibition. p11 acts as a plasmin reductase, reducing plasmin levels and catalysing the formation of A(61), an anti-angiogenic plasmin fragment. p11 also inhibits plasmin-dependent fibrinolysis, and may have anti-angiogenic activity in endothelial cells (although this is purely hypothetical). MMP: matrix metalloproteases; ECM: extracellular matrix; PAI: plasminogen activator inhibitor.

Although preliminary and far from complete, our data suggest an anti-angiogenic role of p11 in endothelial cells in tumour growth models. Previously reported pro-tumour (through effects on invasion and metastasis) discussed previously therefore appear to be due to actions of p11 in the tumour cells themselves. In our study, p11 was not deleted from the implanted tumour cells, meaning that this effect was not observed. This distinction, once confirmed and investigated mechanistically, may have implications for the design of novel anti-cancer therapies targeting p11.

## 5 SUMMARY

The work presented in this thesis describes a specialised role for the S100 protein p11 in nociceptive pathways. The *Cre-loxP* system was used to delete p11 exclusively from nociceptive sensory neurons in the mouse, allowing the investigation of p11 function in this system without the confounding effects of p11 deletion from other tissues. This mouse line displayed deficits in noxious mechanosensation and neuropathic pain behaviour. A proportion of these effects were likely to be due to the role of p11 in the plasma membrane trafficking of the voltage-gated sodium channel  $\text{Na}_v1.8$ . We therefore examined the p11- $\text{Na}_v1.8$  interaction on a molecular level to find key determinants of binding. Finally, global p11-null mice were used to investigate the role of p11 in angiogenesis. Global-null mutants showed enhanced angiogenesis-dependent tumour growth and altered vascular morphology.

Deletion of p11 from nociceptors reduced plasma membrane levels of  $\text{Na}_v1.8$ , consistent with previous studies in heterologous expression systems (Okuse et al., 2002). This effect was detectable in terms of both protein levels and electrophysiological current density, indicating the functional significance of this reduction. Since  $\text{Na}_v1.8$  has been shown to have a specialised function in pain pathways (Akopian et al., 1999), reduced functional expression via blockade of its interaction with p11 may be a valid therapeutic target. Although the plasma membrane expression of  $\text{Na}_v1.8$  was reduced by deletion of p11, however, it was not completely abolished. This implies that p11 is not the sole modulator of  $\text{Na}_v1.8$  plasma membrane trafficking, and that DRG neurons must therefore contain other proteins capable of this process. Currently-identified candidates include Papin and PAF-67 (Malik-Hall et al., 2003; Shao et al., 2005), S100A11 (Poon et al., 2004), and the 14-3-3 proteins (Rajan et al., 2002a). A more detailed understanding of the proteins involved in the functional expression of  $\text{Na}_v1.8$  will not only increase our understanding of ion channel trafficking, but may also provide novel therapeutic strategies for the treatment of pain.

Nociceptor-specific p11-null mice displayed deficits in noxious coding in recordings from wide dynamic range projection neurons in the spinal cord. Consistent with this, behavioural deficits in noxious mechanosensation, but not inflammatory pain, were observed. This phenotype is qualitatively similar to that reported for the  $\text{Na}_v1.8$ -null mouse (Akopian et al., 1999), suggesting that reduced trafficking of  $\text{Na}_v1.8$  may be responsible for the effect of p11 deletion. Significant deficits in mechanical allodynia in a model of neuropathic pain were seen in the nociceptor-specific p11-null mouse. The  $\text{Na}_v1.8$ -null mouse, in contrast, developed neuropathic pain comparable to wild-type animals (Kerr et al., 2001). In combination with

subtle electrophysiological differences observed between these mice, these data provide evidence that p11 deletion affects pain behaviour through both  $\text{Na}_v1.8$ -dependent and -independent mechanisms. Since neuropathic pain is a significant clinical problem,  $\text{Na}_v1.8$ -independent effects of p11 in nociceptors are of great interest. The most plausible mechanisms for these effects may include trafficking of ASIC1a (Donier et al., 2005), which is involved in synaptic plasticity (Wemmie et al., 2003; Wemmie et al., 2004), or of TASK-1, which may affect neuronal excitability (Girard et al., 2002; Renigunta et al., 2006). Subsequent studies may also reveal novel targets of p11 through which effects on neuropathic pain are mediated. Investigation of the mechanisms by which the  $\text{Na}_v1.8$ -independent effects of p11 on pain pathways are produced may yield results useful to the understanding and treatment of neuropathic pain.

To aid the process of intelligent drug design, the interaction of p11 and  $\text{Na}_v1.8$  was examined at a molecular level. Using FRET to measure protein-protein affinities *in vitro*, two distinct p11-binding sites were identified in the  $\text{Na}_v1.8$  N-terminus. Previous studies, using less sensitive methods, had detected only one of these regions (Poon et al., 2004). Additionally, the FRET assay was able to locate an autoinhibitory domain, the deletion of which increased affinity for p11. The complex nature of this interaction, occurring in two sections over a relatively large distance, may preclude the intelligent design of small-molecule inhibitors. The inhibition of more general properties of p11, such as its expression or interaction with annexin 2, would be prone to substantial adverse effects, including those related to angiogenesis. Future studies of the nature of interactions between p11 and its specific targets may therefore prove beneficial, allowing targeting of therapies towards specific actions of p11.

Previous studies have suggested a role for p11 in angiogenesis, via the plasmin formation process (Kassam et al., 1998c). We used the global p11-null mouse for a preliminary investigation using a model of angiogenesis-dependent tumour growth. These mice display enhanced tumour growth, and altered vascular morphology. Subsequent studies will investigate this effect in more detail. An understanding of the role of p11 in angiogenesis may inform the development of novel anti-cancer therapies.

In the floxed p11 mouse line, we have created a valuable tool for investigation of p11 function. The use of other tissue-specific Cre mice will allow detailed study of the roles of p11 in specific tissue types, without interference from confounding effects in other tissues. Several collaborations have been initiated to ensure the exploitation of this novel resource. In particular, the use of endothelial Cre mice will allow a more comprehensive investigation of the role of p11 in plasmin formation and related angiogenic phenomena.

## 6 REFERENCES

Ahluwalia J, Rang H, Nagy I (2002) The putative role of vanilloid receptor-like protein-1 in mediating high threshold noxious heat-sensitivity in rat cultured primary sensory neurons. *Eur J Neurosci* 16: 1483-1489.

Aidley DJ, Stanfield PR (1996) *Ion Channels: Molecules in Action*. Cambridge University Press.

Akiba S, Hatazawa R, Ono K, Hayama M, Matsui H, Sato T (2000b) Transforming growth factor-alpha stimulates prostaglandin generation through cytosolic phospholipase A(2) under the control of p11 in rat gastric epithelial cells. *Br J Pharmacol* 131: 1004-1010.

Akiba S, Hatazawa R, Ono K, Hayama M, Matsui H, Sato T (2000a) Transforming growth factor-alpha stimulates prostaglandin generation through cytosolic phospholipase A(2) under the control of p11 in rat gastric epithelial cells. *Br J Pharmacol* 131: 1004-1010.

Akopian AN, Sivilotti L, Wood JN (1996) A tetrodotoxin-resistant voltage-gated sodium channel expressed by sensory neurons. *Nature* 379: 257-262.

Akopian AN, Souslova V, England S, Okuse K, Ogata N, Ure J, Smith A, Kerr BJ, McMahon SB, Boyce S, Hill R, Stanfa LC, Dickenson AH, Wood JN (1999) The tetrodotoxin-resistant sodium channel SNS has a specialized function in pain pathways. *Nat Neurosci* 2: 541-548.

Amaya F, Decosterd I, Samad TA, Plumpton C, Tate S, Mannion RJ, Costigan M, Woolf CJ (2000a) Diversity of expression of the sensory neuron-specific TTX-resistant voltage-gated sodium ion channels SNS and SNS2. *Mol Cell Neurosci* 15: 331-342.

Amaya F, Decosterd I, Samad TA, Plumpton C, Tate S, Mannion RJ, Costigan M, Woolf CJ (2000b) Diversity of expression of the sensory neuron-specific TTX-resistant voltage-gated sodium ion channels SNS and SNS2. *Mol Cell Neurosci* 15: 331-342.

Amaya F, Wang H, Costigan M, Allchorne AJ, Hatcher JP, Egerton J, Stean T, Morisset V, Grose D, Gunthorpe MJ, Chessell IP, Tate S, Green PJ, Woolf CJ (2006a) The voltage-gated sodium channel Na(v)1.9 is an effector of peripheral inflammatory pain hypersensitivity. *J Neurosci* 26: 12852-12860.

Amaya F, Wang H, Costigan M, Allchorne AJ, Hatcher JP, Egerton J, Stean T, Morisset V, Grose D, Gunthorpe MJ, Chessell IP, Tate S, Green PJ, Woolf CJ (2006b) The voltage-gated sodium channel Na(v)1.9 is an effector of peripheral inflammatory pain hypersensitivity. *J Neurosci* 26: 12852-12860.

Andreev NY, Dimitrieva N, Koltzenburg M, McMahon SB (1995) Peripheral administration of nerve growth factor in the adult rat produces a thermal hyperalgesia that requires the presence of sympathetic post-ganglionic neurones. *Pain* 63: 109-115.

Armstrong CM (1981b) Sodium channels and gating currents. *Physiol Rev* 61: 644-683.

Armstrong CM (1981a) Sodium channels and gating currents. *Physiol Rev* 61: 644-683.

Averill S, McMahon SB, Clary DO, Reichardt LF, Priestley JV (1995) Immunocytochemical localization of trkA receptors in chemically identified subgroups of adult rat sensory neurons. *Eur J Neurosci* 7: 1484-1494.

Babes A, Zorzon D, Reid G (2006) A novel type of cold-sensitive neuron in rat dorsal root ganglia with rapid adaptation to cooling stimuli. *Eur J Neurosci* 24: 691-698.

Babiychuk EB, Monastyrskaya K, Burkhard FC, Wray S, Draeger A (2002) Modulating signaling events in smooth muscle: cleavage of annexin 2 abolishes its binding to lipid rafts. *FASEB J* 16: 1177-1184.

Bach TL, Barsigian C, Chalupowicz DG, Busler D, Yaen CH, Grant DS, Martinez J (1998a) VE-Cadherin mediates endothelial cell capillary tube formation in fibrin and collagen gels. *Exp Cell Res* 238: 324-334.

Bach TL, Barsigian C, Yaen CH, Martinez J (1998b) Endothelial cell VE-cadherin functions as a receptor for the beta15-42 sequence of fibrin. *J Biol Chem* 273: 30719-30728.

Bailleux A, Wendum D, Audubert F, Jouniaux AM, Koumanov K, Trugnan G, Masliah J (2004a) Cytosolic phospholipase A2-p11 interaction controls arachidonic acid release as a function of epithelial cell confluence. *Biochem J* 378: 307-315.

Bailleux A, Wendum D, Audubert F, Jouniaux AM, Koumanov K, Trugnan G, Masliah J (2004b) Cytosolic phospholipase A2-p11 interaction controls arachidonic acid release as a function of epithelial cell confluence. *Biochem J* 378: 307-315.

Baker MD, Chandra SY, Ding Y, Waxman SG, Wood JN (2003) GTP-induced tetrodotoxin-resistant Na<sup>+</sup> current regulates excitability in mouse and rat small diameter sensory neurones. *J Physiol* 548: 373-382.

Barry PH, Lynch JW (1991) Liquid junction potentials and small cell effects in patch-clamp analysis. *J Membr Biol* 121: 101-117.

Bautista DM, Jordt SE, Nikai T, Tsuruda PR, Read AJ, Poblete J, Yamoah EN, Basbaum AI, Julius D (2006d) TRPA1 mediates the inflammatory actions of environmental irritants and proalgesic agents. *Cell* 124: 1269-1282.

Bautista DM, Jordt SE, Nikai T, Tsuruda PR, Read AJ, Poblete J, Yamoah EN, Basbaum AI, Julius D (2006a) TRPA1 mediates the inflammatory actions of environmental irritants and proalgesic agents. *Cell* 124: 1269-1282.

Bautista DM, Jordt SE, Nikai T, Tsuruda PR, Read AJ, Poblete J, Yamoah EN, Basbaum AI, Julius D (2006b) TRPA1 mediates the inflammatory actions of environmental irritants and proalgesic agents. *Cell* 124: 1269-1282.

Bautista DM, Jordt SE, Nikai T, Tsuruda PR, Read AJ, Poblete J, Yamoah EN, Basbaum AI, Julius D (2006c) TRPA1 mediates the inflammatory actions of environmental irritants and proalgesic agents. *Cell* 124: 1269-1282.

Bayliss DA, Talley EM, Sirois JE, Lei Q (2001) TASK-1 is a highly modulated pH-sensitive 'leak' K(+) channel expressed in brainstem respiratory neurons. *Respir Physiol* 129: 159-174.

Benaud C, Gentil BJ, Assard N, Court M, Garin J, Delphin C, Baudier J (2004) AHNAK interaction with the annexin 2/S100A10 complex regulates cell membrane cytoarchitecture. *J Cell Biol* 164: 133-144.

Bennett DL, Boucher TJ, Armanini MP, Poulsen KT, Michael GJ, Priestley JV, Phillips HS, McMahon SB, Shelton DL (2000) The glial cell line-derived neurotrophic factor family receptor components are differentially regulated within sensory neurons after nerve injury. *J Neurosci* 20: 427-437.

Bennett GJ, Xie YK (1988) A peripheral mononeuropathy in rat that produces disorders of pain sensation like those seen in man. *Pain* 33: 87-107.

Benson CJ, Xie J, Wemmie JA, Price MP, Henss JM, Welsh MJ, Snyder PM (2002) Heteromultimers of DEG/ENaC subunits form H<sup>+</sup>-gated channels in mouse sensory neurons. *Proc Natl Acad Sci U S A* 99: 2338-2343.

Bernard JF, Bester H, Besson JM (1996) Involvement of the spino-parabrachio -amygdaloid and -hypothalamic pathways in the autonomic and affective emotional aspects of pain. *Prog Brain Res* 107: 243-255.

Bester H, Chapman V, Besson JM, Bernard JF (2000) Physiological properties of the lamina I spinoparabrachial neurons in the rat. *J Neurophysiol* 83: 2239-2259.

Bevan S, Geppetti P (1994) Protons: small stimulants of capsaicin-sensitive sensory nerves. *Trends Neurosci* 17: 509-512.

Bevan S, Yeats J (1991) Protons activate a cation conductance in a sub-population of rat dorsal root ganglion neurones. *J Physiol* 433: 145-161.

Bird AP (1986) CpG-rich islands and the function of DNA methylation. *Nature* 321: 209-213.

Black JA, Cummins TR, Plumpton C, Chen YH, Hormuzdiar W, Clare JJ, Waxman SG (1999) Upregulation of a silent sodium channel after peripheral, but not central, nerve injury in DRG neurons. *J Neurophysiol* 82: 2776-2785.

Black JA, Dib-Hajj S, Baker D, Newcombe J, Cuzner ML, Waxman SG (2000a) Sensory neuron-specific sodium channel SNS is abnormally expressed in the brains of mice with experimental allergic encephalomyelitis and humans with multiple sclerosis. *Proc Natl Acad Sci U S A* 97: 11598-11602.

Black JA, Dib-Hajj S, Baker D, Newcombe J, Cuzner ML, Waxman SG (2000b) Sensory neuron-specific sodium channel SNS is abnormally expressed in the brains of mice with experimental allergic encephalomyelitis and humans with multiple sclerosis. *Proc Natl Acad Sci U S A* 97: 11598-11602.

Black JA, Waxman SG (2002) Molecular identities of two tetrodotoxin-resistant sodium channels in corneal axons. *Exp Eye Res* 75: 193-199.

Blackburn-Munro G, Fleetwood-Walker SM (1999) The sodium channel auxiliary subunits beta1 and beta2 are differentially expressed in the spinal cord of neuropathic rats. *Neuroscience* 90: 153-164.

Blair NT, Bean BP (2002) Roles of tetrodotoxin (TTX)-sensitive Na<sup>+</sup> current, TTX-resistant Na<sup>+</sup> current, and Ca<sup>2+</sup> current in the action potentials of nociceptive sensory neurons. *J Neurosci* 22: 10277-10290.

Blom N, Sicheritz-Ponten T, Gupta R, Gammeltoft S, Brunak S (2004) Prediction of post-translational glycosylation and phosphorylation of proteins from the amino acid sequence. *Proteomics* 4: 1633-1649.

Borgonovo B, Cocucci E, Racchetti G, Podini P, Bachi A, Meldolesi J (2002) Regulated exocytosis: a novel, widely expressed system. *Nat Cell Biol* 4: 955-962.

Boucher TJ, McMahon SB (2001a) Neurotrophic factors and neuropathic pain. *Curr Opin Pharmacol* 1: 66-72.

Boucher TJ, McMahon SB (2001b) Neurotrophic factors and neuropathic pain. *Curr Opin Pharmacol* 1: 66-72.

Boucher TJ, McMahon SB (2001c) Neurotrophic factors and neuropathic pain. *Curr Opin Pharmacol* 1: 66-72.

Boucher TJ, Okuse K, Bennett DL, Munson JB, Wood JN, McMahon SB (2000) Potent analgesic effects of GDNF in neuropathic pain states. *Science* 290: 124-127.

Brock JA, McLachlan EM, Belmonte C (1998c) Tetrodotoxin-resistant impulses in single nociceptor nerve terminals in guinea-pig cornea. *J Physiol* 512 ( Pt 1): 211-217.

Brock JA, McLachlan EM, Belmonte C (1998d) Tetrodotoxin-resistant impulses in single nociceptor nerve terminals in guinea-pig cornea. *J Physiol* 512 ( Pt 1): 211-217.

Brock JA, McLachlan EM, Belmonte C (1998a) Tetrodotoxin-resistant impulses in single nociceptor nerve terminals in guinea-pig cornea. *J Physiol* 512 ( Pt 1): 211-217.

Brock JA, McLachlan EM, Belmonte C (1998b) Tetrodotoxin-resistant impulses in single nociceptor nerve terminals in guinea-pig cornea. *J Physiol* 512 ( Pt 1): 211-217.

Browder T, Folkman J, Pirie-Shepherd S (2000) The hemostatic system as a regulator of angiogenesis. *J Biol Chem* 275: 1521-1524.

Buchholz F, Angrand PO, Stewart AF (1998) Improved properties of FLP recombinase evolved by cycling mutagenesis. *Nat Biotechnol* 16: 657-662.

Buck MR, Karustis DG, Day NA, Honn KV, Sloane BF (1992) Degradation of extracellular-matrix proteins by human cathepsin B from normal and tumour tissues. *Biochem J* 282 ( Pt 1): 273-278.

Burgard EC, Niforatos W, van BT, Lynch KJ, Touma E, Metzger RE, Kowaluk EA, Jarvis MF (1999) P2X receptor-mediated ionic currents in dorsal root ganglion neurons. *J Neurophysiol* 82: 1590-1598.

Burgess GM, Mullaney I, McNeill M, Dunn PM, Rang HP (1989a) Second messengers involved in the mechanism of action of bradykinin in sensory neurons in culture. *J Neurosci* 9: 3314-3325.

Burgess GM, Mullaney I, McNeill M, Dunn PM, Rang HP (1989b) Second messengers involved in the mechanism of action of bradykinin in sensory neurons in culture. *J Neurosci* 9: 3314-3325.

Bystroff C, Shao Y (2002) Fully automated ab initio protein structure prediction using I-SITES, HMMSTR and ROSETTA. *Bioinformatics* 18 Suppl 1: S54-S61.

Bystroff C, Thorsson V, Baker D (2000) HMMSTR: a hidden Markov model for local sequence-structure correlations in proteins. *J Mol Biol* 301: 173-190.

Caldwell JH, Schaller KL, Lasher RS, Peles E, Levinson SR (2000) Sodium channel Na(v)1.6 is localized at nodes of ranvier, dendrites, and synapses. *Proc Natl Acad Sci U S A* 97: 5616-5620.

Camilleri M, Andrews CN, Bharucha AE, Carlson PJ, Ferber I, Stephens D, Smyrk TC, Urrutia R, Aerssens J, Thielemans L, Gohlmann H, van dW, I, Coulie B (2007) Alterations in expression of p11 and SERT in mucosal biopsy specimens of patients with irritable bowel syndrome. *Gastroenterology* 132: 17-25.

Campbell JN, Meyer RA (2006) Mechanisms of neuropathic pain. *Neuron* 52: 77-92.

Campo E, Munoz J, Miquel R, Palacin A, Cardesa A, Sloane BF, Emmert-Buck MR (1994) Cathepsin B expression in colorectal carcinomas correlates with tumor progression and shortened patient survival. *Am J Pathol* 145: 301-309.

Cao YQ, Mantyh PW, Carlson EJ, Gillespie AM, Epstein CJ, Basbaum AI (1998) Primary afferent tachykinins are required to experience moderate to intense pain. *Nature* 392: 390-394.

Caterina MJ, Leffler A, Malmberg AB, Martin WJ, Trafton J, Petersen-Zeitz KR, Koltzenburg M, Basbaum AI, Julius D (2000d) Impaired nociception and pain sensation in mice lacking the capsaicin receptor. *Science* 288: 306-313.

Caterina MJ, Leffler A, Malmberg AB, Martin WJ, Trafton J, Petersen-Zeitze KR, Koltzenburg M, Basbaum AI, Julius D (2000c) Impaired nociception and pain sensation in mice lacking the capsaicin receptor. *Science* 288: 306-313.

Caterina MJ, Leffler A, Malmberg AB, Martin WJ, Trafton J, Petersen-Zeitze KR, Koltzenburg M, Basbaum AI, Julius D (2000b) Impaired nociception and pain sensation in mice lacking the capsaicin receptor. *Science* 288: 306-313.

Caterina MJ, Leffler A, Malmberg AB, Martin WJ, Trafton J, Petersen-Zeitze KR, Koltzenburg M, Basbaum AI, Julius D (2000e) Impaired nociception and pain sensation in mice lacking the capsaicin receptor. *Science* 288: 306-313.

Caterina MJ, Leffler A, Malmberg AB, Martin WJ, Trafton J, Petersen-Zeitze KR, Koltzenburg M, Basbaum AI, Julius D (2000f) Impaired nociception and pain sensation in mice lacking the capsaicin receptor. *Science* 288: 306-313.

Caterina MJ, Leffler A, Malmberg AB, Martin WJ, Trafton J, Petersen-Zeitze KR, Koltzenburg M, Basbaum AI, Julius D (2000a) Impaired nociception and pain sensation in mice lacking the capsaicin receptor. *Science* 288: 306-313.

Caterina MJ, Rosen TA, Tominaga M, Brake AJ, Julius D (1999a) A capsaicin-receptor homologue with a high threshold for noxious heat. *Nature* 398: 436-441.

Caterina MJ, Rosen TA, Tominaga M, Brake AJ, Julius D (1999b) A capsaicin-receptor homologue with a high threshold for noxious heat. *Nature* 398: 436-441.

Caterina MJ, Schumacher MA, Tominaga M, Rosen TA, Levine JD, Julius D (1997a) The capsaicin receptor: a heat-activated ion channel in the pain pathway. *Nature* 389: 816-824.

Caterina MJ, Schumacher MA, Tominaga M, Rosen TA, Levine JD, Julius D (1997b) The capsaicin receptor: a heat-activated ion channel in the pain pathway. *Nature* 389: 816-824.

Catterall WA (2000) From ionic currents to molecular mechanisms: the structure and function of voltage-gated sodium channels. *Neuron* 26: 13-25.

Cavaletti G, Tredici G, Braga M, Tazzari S (1995) Experimental peripheral neuropathy induced in adult rats by repeated intraperitoneal administration of taxol. *Exp Neurol* 133: 64-72.

Cesare P, Dekker LV, Sardini A, Parker PJ, McNaughton PA (1999) Specific involvement of PKC-epsilon in sensitization of the neuronal response to painful heat. *Neuron* 23: 617-624.

Cesare P, McNaughton P (1996) A novel heat-activated current in nociceptive neurons and its sensitization by bradykinin. *Proc Natl Acad Sci U S A* 93: 15435-15439.

Cestele S, Qu Y, Rogers JC, Rochat H, Scheuer T, Catterall WA (1998) Voltage sensor-trapping: enhanced activation of sodium channels by beta-scorpion toxin bound to the S3-S4 loop in domain II. *Neuron* 21: 919-931.

Chahine M, Ziane R, Vijayaragavan K, Okamura Y (2005) Regulation of Na<sup>v</sup> channels in sensory neurons. *Trends Pharmacol Sci* 26: 496-502.

Chaplan SR, Bach FW, Pogrel JW, Chung JM, Yaksh TL (1994) Quantitative assessment of tactile allodynia in the rat paw. *J Neurosci Methods* 53: 55-63.

Chaplan SR, Guo HQ, Lee DH, Luo L, Liu C, Kuei C, Velumian AA, Butler MP, Brown SM, Dubin AE (2003a) Neuronal hyperpolarization-activated pacemaker channels drive neuropathic pain. *J Neurosci* 23: 1169-1178.

Chaplan SR, Guo HQ, Lee DH, Luo L, Liu C, Kuei C, Velumian AA, Butler MP, Brown SM, Dubin AE (2003b) Neuronal hyperpolarization-activated pacemaker channels drive neuropathic pain. *J Neurosci* 23: 1169-1178.

Chen C, Bharucha V, Chen Y, Westenbroek RE, Brown A, Malhotra JD, Jones D, Avery C, Gillespie PJ, III, Kazen-Gillespie KA, Kazarinova-Noyes K, Shrager P, Saunders TL, Macdonald RL, Ransom BR, Scheuer T, Catterall WA, Isom LL (2002a) Reduced sodium channel density, altered voltage dependence of inactivation, and increased susceptibility to seizures in mice lacking sodium channel beta 2-subunits. *Proc Natl Acad Sci U S A* 99: 17072-17077.

Chen C, Westenbroek RE, Xu X, Edwards CA, Sorenson DR, Chen Y, McEwen DP, O'Malley HA, Bharucha V, Meadows LS, Knudsen GA, Vilaythong A, Noebels JL, Saunders TL, Scheuer T, Shrager P, Catterall WA, Isom LL (2004) Mice lacking sodium channel beta1 subunits display defects in neuronal excitability, sodium channel expression, and nodal architecture. *J Neurosci* 24: 4030-4042.

Chen CC, Akopian AN, Sivilotti L, Colquhoun D, Burnstock G, Wood JN (1995) A P2X purinoceptor expressed by a subset of sensory neurons. *Nature* 377: 428-431.

Chen CC, Zimmer A, Sun WH, Hall J, Brownstein MJ, Zimmer A (2002b) A role for ASIC3 in the modulation of high-intensity pain stimuli. *Proc Natl Acad Sci U S A* 99: 8992-8997.

Chen CC, Zimmer A, Sun WH, Hall J, Brownstein MJ, Zimmer A (2002c) A role for ASIC3 in the modulation of high-intensity pain stimuli. *Proc Natl Acad Sci U S A* 99: 8992-8997.

Chen CC, Zimmer A, Sun WH, Hall J, Brownstein MJ, Zimmer A (2002d) A role for ASIC3 in the modulation of high-intensity pain stimuli. *Proc Natl Acad Sci U S A* 99: 8992-8997.

Chen DS, Barraclough R (1996) Regulatory elements in the first intron of the rat S100A4 (p9Ka) gene. *Biochem Soc Trans* 24: 352S.

Chen ZL, Strickland S (1997) Neuronal death in the hippocampus is promoted by plasmin-catalyzed degradation of laminin. *Cell* 91: 917-925.

Cheng Y, Prusoff WH (1973) Relationship between the inhibition constant ( $K_i$ ) and the concentration of inhibitor which causes 50 per cent inhibition ( $I_{50}$ ) of an enzymatic reaction. *Biochem Pharmacol* 22: 3099-3108.

Chetcuti A, Margan SH, Russell P, Mann S, Millar DS, Clark SJ, Rogers J, Handelsman DJ, Dong Q (2001a) Loss of annexin II heavy and light chains in prostate cancer and its precursors. *Cancer Res* 61: 6331-6334.

Chetcuti A, Margan SH, Russell P, Mann S, Millar DS, Clark SJ, Rogers J, Handelsman DJ, Dong Q (2001b) Loss of annexin II heavy and light chains in prostate cancer and its precursors. *Cancer Res* 61: 6331-6334.

Choi JS, Dib-Hajj SD, Waxman SG (2006b) Inherited erythralgia: limb pain from an S4 charge-neutral Na channelopathy. *Neurology* 67: 1563-1567.

Choi JS, Dib-Hajj SD, Waxman SG (2006a) Inherited erythralgia: limb pain from an S4 charge-neutral Na channelopathy. *Neurology* 67: 1563-1567.

Choi JS, Hudmon A, Waxman SG, Dib-Hajj SD (2006c) Calmodulin regulates current density and frequency-dependent inhibition of sodium channel Nav1.8 in DRG neurons. *J Neurophysiol* 96: 97-108.

Choi JS, Hudmon A, Waxman SG, Dib-Hajj SD (2006e) Calmodulin regulates current density and frequency-dependent inhibition of sodium channel Nav1.8 in DRG neurons. *J Neurophysiol* 96: 97-108.

Choi JS, Hudmon A, Waxman SG, Dib-Hajj SD (2006d) Calmodulin regulates current density and frequency-dependent inhibition of sodium channel Nav1.8 in DRG neurons. *J Neurophysiol* 96: 97-108.

Choi KS, Fitzpatrick SL, Filipenko NR, Fogg DK, Kassam G, Magliocco AM, Waisman DM (2001) Regulation of plasmin-dependent fibrin clot lysis by annexin II heterotetramer. *J Biol Chem* 276: 25212-25221.

Choi KS, Fogg DK, Yoon CS, Waisman DM (2003) p11 regulates extracellular plasmin production and invasiveness of HT1080 fibrosarcoma cells. *FASEB J* 17: 235-246.

Choi KS, Ghuman J, Kassam G, Kang HM, Fitzpatrick SL, Waisman DM (1998a) Annexin II tetramer inhibits plasmin-dependent fibrinolysis. *Biochemistry* 37: 648-655.

Choi KS, Ghuman J, Kassam G, Kang HM, Fitzpatrick SL, Waisman DM (1998b) Annexin II tetramer inhibits plasmin-dependent fibrinolysis. *Biochemistry* 37: 648-655.

Chung CY, Erickson HP (1994) Cell surface annexin II is a high affinity receptor for the alternatively spliced segment of tenascin-C. *J Cell Biol* 126: 539-548.

Cockayne DA, Dunn PM, Zhong Y, Rong W, Hamilton SG, Knight GE, Ruan HZ, Ma B, Yip P, Nunn P, McMahon SB, Burnstock G, Ford AP (2005) P2X2 knockout mice and P2X2/P2X3 double knockout mice reveal a role for the P2X2 receptor subunit in mediating multiple sensory effects of ATP. *J Physiol* 567: 621-639.

Cockayne DA, Hamilton SG, Zhu QM, Dunn PM, Zhong Y, Novakovic S, Malmberg AB, Cain G, Berson A, Kassotakis L, Hedley L, Lachnit WG, Burnstock G, McMahon SB, Ford AP (2000a) Urinary bladder hyporeflexia and reduced pain-related behaviour in P2X3-deficient mice. *Nature* 407: 1011-1015.

Cockayne DA, Hamilton SG, Zhu QM, Dunn PM, Zhong Y, Novakovic S, Malmberg AB, Cain G, Berson A, Kassotakis L, Hedley L, Lachnit WG, Burnstock G, McMahon SB, Ford AP (2000b) Urinary bladder hyporeflexia and reduced pain-related behaviour in P2X3-deficient mice. *Nature* 407: 1011-1015.

Cohn MA, Hjelmso I, Wu LC, Guldborg P, Lukanidin EM, Tulchinsky EM (2001) Characterization of Sp1, AP-1, CBF and KRC binding sites and minisatellite DNA as functional elements of the metastasis-associated mts1/S100A4 gene intronic enhancer. *Nucleic Acids Res* 29: 3335-3346.

Cook SP, Vulchanova L, Hargreaves KM, Elde R, McCleskey EW (1997) Distinct ATP receptors on pain-sensing and stretch-sensing neurons. *Nature* 387: 505-508.

Corey DP, Garcia-Anoveros J, Holt JR, Kwan KY, Lin SY, Vollrath MA, Amalfitano A, Cheung EL, Derfler BH, Duggan A, Geleoc GS, Gray PA, Hoffman MP, Rehm HL,

Tamasauskas D, Zhang DS (2004a) TRPA1 is a candidate for the mechanosensitive transduction channel of vertebrate hair cells. *Nature* 432: 723-730.

Corey DP, Garcia-Anoveros J, Holt JR, Kwan KY, Lin SY, Vollrath MA, Amalfitano A, Cheung EL, Derfler BH, Duggan A, Geleoc GS, Gray PA, Hoffman MP, Rehm HL, Tamasauskas D, Zhang DS (2004b) TRPA1 is a candidate for the mechanosensitive transduction channel of vertebrate hair cells. *Nature* 432: 723-730.

Costigan M, Befort K, Karchewski L, Griffin RS, D'Urso D, Allchorne A, Sitarski J, Mannion JW, Pratt RE, Woolf CJ (2002) Replicate high-density rat genome oligonucleotide microarrays reveal hundreds of regulated genes in the dorsal root ganglion after peripheral nerve injury. *BMC Neurosci* 3: 16.

Coull JA, Beggs S, Boudreau D, Boivin D, Tsuda M, Inoue K, Gravel C, Salter MW, De KY (2005c) BDNF from microglia causes the shift in neuronal anion gradient underlying neuropathic pain. *Nature* 438: 1017-1021.

Coull JA, Beggs S, Boudreau D, Boivin D, Tsuda M, Inoue K, Gravel C, Salter MW, De KY (2005a) BDNF from microglia causes the shift in neuronal anion gradient underlying neuropathic pain. *Nature* 438: 1017-1021.

Coull JA, Beggs S, Boudreau D, Boivin D, Tsuda M, Inoue K, Gravel C, Salter MW, De KY (2005b) BDNF from microglia causes the shift in neuronal anion gradient underlying neuropathic pain. *Nature* 438: 1017-1021.

Coull JA, Boudreau D, Bachand K, Prescott SA, Nault F, Sik A, De KP, De KY (2003a) Trans-synaptic shift in anion gradient in spinal lamina I neurons as a mechanism of neuropathic pain. *Nature* 424: 938-942.

Coull JA, Boudreau D, Bachand K, Prescott SA, Nault F, Sik A, De KP, De KY (2003b) Trans-synaptic shift in anion gradient in spinal lamina I neurons as a mechanism of neuropathic pain. *Nature* 424: 938-942.

Coull JA, Boudreau D, Bachand K, Prescott SA, Nault F, Sik A, De KP, De KY (2003c) Trans-synaptic shift in anion gradient in spinal lamina I neurons as a mechanism of neuropathic pain. *Nature* 424: 938-942.

Courteix C, Eschalier A, Lavarenne J (1993) Streptozocin-induced diabetic rats: behavioural evidence for a model of chronic pain. *Pain* 53: 81-88.

Cox JJ, Reimann F, Nicholas AK, Thornton G, Roberts E, Springell K, Karbani G, Jafri H, Mannan J, Raashid Y, Al-Gazali L, Hamamy H, Valente EM, Gorman S, Williams R, McHale DP, Wood JN, Gribble FM, Woods CG (2006a) An SCN9A channelopathy causes congenital inability to experience pain. *Nature* 444: 894-898.

Cox JJ, Reimann F, Nicholas AK, Thornton G, Roberts E, Springell K, Karbani G, Jafri H, Mannan J, Raashid Y, Al-Gazali L, Hamamy H, Valente EM, Gorman S, Williams R, McHale DP, Wood JN, Gribble FM, Woods CG (2006b) An SCN9A channelopathy causes congenital inability to experience pain. *Nature* 444: 894-898.

Craner MJ, Lo AC, Black JA, Baker D, Newcombe J, Cuzner ML, Waxman SG (2003b) Annexin II/p11 is up-regulated in Purkinje cells in EAE and MS. *Neuroreport* 14: 555-558.

Craner MJ, Lo AC, Black JA, Baker D, Newcombe J, Cuzner ML, Waxman SG (2003a) Annexin II/p11 is up-regulated in Purkinje cells in EAE and MS. *Neuroreport* 14: 555-558.

Crowley C, Spencer SD, Nishimura MC, Chen KS, Pitts-Meek S, Armanini MP, Ling LH, McMahon SB, Shelton DL, Levinson AD. (1994) Mice lacking nerve growth factor display perinatal loss of sensory and sympathetic neurons yet develop basal forebrain cholinergic neurons. *Cell* 76: 1001-1011.

Crusio WE (1996) Gene-targeting studies: new methods, old problems. *Trends Neurosci* 19: 186-187.

Cummins TR, Aglieco F, Renganathan M, Herzog RI, Dib-Hajj SD, Waxman SG (2001) Nav1.3 sodium channels: rapid repriming and slow closed-state inactivation display quantitative differences after expression in a mammalian cell line and in spinal sensory neurons. *J Neurosci* 21: 5952-5961.

Cummins TR, Dib-Hajj SD, Waxman SG (2004a) Electrophysiological properties of mutant Nav1.7 sodium channels in a painful inherited neuropathy. *J Neurosci* 24: 8232-8236.

Cummins TR, Dib-Hajj SD, Waxman SG (2004b) Electrophysiological properties of mutant Nav1.7 sodium channels in a painful inherited neuropathy. *J Neurosci* 24: 8232-8236.

Cummins TR, Waxman SG (1997a) Downregulation of tetrodotoxin-resistant sodium currents and upregulation of a rapidly repriming tetrodotoxin-sensitive sodium current in small spinal sensory neurons after nerve injury. *J Neurosci* 17: 3503-3514.

Cummins TR, Waxman SG (1997b) Downregulation of tetrodotoxin-resistant sodium currents and upregulation of a rapidly repriming tetrodotoxin-sensitive sodium current in small spinal sensory neurons after nerve injury. *J Neurosci* 17: 3503-3514.

Czirjak G, Fischer T, Spat A, Lesage F, Enyedi P (2000) TASK (TWIK-related acid-sensitive K<sup>+</sup> channel) is expressed in glomerulosa cells of rat adrenal cortex and inhibited by angiotensin II. *Mol Endocrinol* 14: 863-874.

Damarjian TG, Craner MJ, Black JA, Waxman SG (2004) Upregulation and colocalization of p75 and Nav1.8 in Purkinje neurons in experimental autoimmune encephalomyelitis. *Neurosci Lett* 369: 186-190.

Davis JB, Gray J, Gunthorpe MJ, Hatcher JP, Davey PT, Overend P, Harries MH, Latcham J, Clapham C, Atkinson K, Hughes SA, Rance K, Grau E, Harper AJ, Pugh PL, Rogers DC, Bingham S, Randall A, Sheardown SA (2000b) Vanilloid receptor-1 is essential for inflammatory thermal hyperalgesia. *Nature* 405: 183-187.

Davis JB, Gray J, Gunthorpe MJ, Hatcher JP, Davey PT, Overend P, Harries MH, Latcham J, Clapham C, Atkinson K, Hughes SA, Rance K, Grau E, Harper AJ, Pugh PL, Rogers DC, Bingham S, Randall A, Sheardown SA (2000a) Vanilloid receptor-1 is essential for inflammatory thermal hyperalgesia. *Nature* 405: 183-187.

De LM, Van Eldik LJ, Shooter EM (1991) Differential regulation of S100 beta and mRNAs coding for S100-like proteins (42A and 42C) during development and after lesion of rat sciatic nerve. *J Neurosci Res* 29: 155-162.

De SS, Benaud C, Assard N, Khediri S, Gerke V, Baudier J, Delphin C (2006b) Identification of an AHNAK binding motif specific for the Annexin2/S100A10 tetramer. *J Biol Chem* 281: 35030-35038.

De SS, Benaud C, Assard N, Khediri S, Gerke V, Baudier J, Delphin C (2006a) Identification of an AHNAK binding motif specific for the Annexin2/S100A10 tetramer. *J Biol Chem* 281: 35030-35038.

de WN, Dekker M, Berns A, Radman M, te RH (1995) Inactivation of the mouse Msh2 gene results in mismatch repair deficiency, methylation tolerance, hyperrecombination, and predisposition to cancer. *Cell* 82: 321-330.

Decosterd I, Ji RR, Abdi S, Tate S, Woolf CJ (2002) The pattern of expression of the voltage-gated sodium channels Na(v)1.8 and Na(v)1.9 does not change in uninjured primary sensory neurons in experimental neuropathic pain models. *Pain* 96: 269-277.

Decosterd I, Woolf CJ (2000) Spared nerve injury: an animal model of persistent peripheral neuropathic pain. *Pain* 87: 149-158.

Dekker LV, Daniels Z, Hick C, Elsegood K, Bowden S, Szestak T, Burley JR, Southan A, Cronk D, James IF (2005) Analysis of human Nav1.8 expressed in SH-SY5Y neuroblastoma cells. *Eur J Pharmacol* 528: 52-58.

Dempsey AC, Walsh MP, Shaw GS (2003) Unmasking the annexin I interaction from the structure of Apo-S100A11. *Structure* 11: 887-897.

Deora AB, Kreitzer G, Jacovina AT, Hajjar KA (2004) An annexin 2 phosphorylation switch mediates p11-dependent translocation of annexin 2 to the cell surface. *J Biol Chem* 279: 43411-43418.

Devor M (2006) Sodium channels and mechanisms of neuropathic pain. *J Pain* 7: S3-S12.

Dib-Hajj S, Black JA, Felts P, Waxman SG (1996) Down-regulation of transcripts for Na channel alpha-SNS in spinal sensory neurons following axotomy. *Proc Natl Acad Sci U S A* 93: 14950-14954.

Dib-Hajj SD, Rush AM, Cummins TR, Hisama FM, Novella S, Tyrrell L, Marshall L, Waxman SG (2005a) Gain-of-function mutation in Nav1.7 in familial erythromelalgia induces bursting of sensory neurons. *Brain* 128: 1847-1854.

Dib-Hajj SD, Rush AM, Cummins TR, Hisama FM, Novella S, Tyrrell L, Marshall L, Waxman SG (2005b) Gain-of-function mutation in Nav1.7 in familial erythromelalgia induces bursting of sensory neurons. *Brain* 128: 1847-1854.

Dib-Hajj SD, Tyrrell L, Black JA, Waxman SG (1998b) NaN, a novel voltage-gated Na channel, is expressed preferentially in peripheral sensory neurons and down-regulated after axotomy. *Proc Natl Acad Sci U S A* 95: 8963-8968.

Dib-Hajj SD, Tyrrell L, Black JA, Waxman SG (1998c) NaN, a novel voltage-gated Na channel, is expressed preferentially in peripheral sensory neurons and down-regulated after axotomy. *Proc Natl Acad Sci U S A* 95: 8963-8968.

Dib-Hajj SD, Tyrrell L, Black JA, Waxman SG (1998a) NaN, a novel voltage-gated Na channel, is expressed preferentially in peripheral sensory neurons and down-regulated after axotomy. *Proc Natl Acad Sci U S A* 95: 8963-8968.

Dickenson AH (1997) Plasticity: implications for opioid and other pharmacological interventions in specific pain states. *Behav Brain Sci* 20: 392-403.

Dirajlal S, Pauers LE, Stucky CL (2003) Differential response properties of IB(4)-positive and -negative unmyelinated sensory neurons to protons and capsaicin. *J Neurophysiol* 89: 513-524.

Dixon WJ (1980) Efficient analysis of experimental observations. *Annu Rev Pharmacol Toxicol* 20: 441-462.

Djoughri L, Bleazard L, Lawson SN (1998a) Association of somatic action potential shape with sensory receptive properties in guinea-pig dorsal root ganglion neurones. *J Physiol* 513 ( Pt 3): 857-872.

Djoughri L, Bleazard L, Lawson SN (1998b) Association of somatic action potential shape with sensory receptive properties in guinea-pig dorsal root ganglion neurones. *J Physiol* 513 ( Pt 3): 857-872.

Djoughri L, Fang X, Okuse K, Wood JN, Berry CM, Lawson SN (2003a) The TTX-resistant sodium channel Nav1.8 (SNS/PN3): expression and correlation with membrane properties in rat nociceptive primary afferent neurons. *J Physiol* 550: 739-752.

Djoughri L, Koutsikou S, Fang X, McMullan S, Lawson SN (2006) Spontaneous pain, both neuropathic and inflammatory, is related to frequency of spontaneous firing in intact C-fiber nociceptors. *J Neurosci* 26: 1281-1292.

Djoughri L, Newton R, Levinson SR, Berry CM, Carruthers B, Lawson SN (2003b) Sensory and electrophysiological properties of guinea-pig sensory neurones expressing Nav 1.7 (PN1) Na<sup>+</sup> channel alpha subunit protein. *J Physiol* 546: 565-576.

Domoto T, Miyama Y, Suzuki H, Teratani T, Arai K, Sugiyama T, Takayama T, Mugiya S, Ozono S, Nozawa R (2006b) Evaluation of S100A10, annexin II and B-FABP expression as markers for renal cell carcinoma. *Cancer Sci*.

Domoto T, Miyama Y, Suzuki H, Teratani T, Arai K, Sugiyama T, Takayama T, Mugiya S, Ozono S, Nozawa R (2006a) Evaluation of S100A10, annexin II and B-FABP expression as markers for renal cell carcinoma. *Cancer Sci*.

Donato R (1986a) S-100 proteins. *Cell Calcium* 7: 123-145.

Donato R (1986b) S-100 proteins. *Cell Calcium* 7: 123-145.

Donato R (2001) S100: a multigenic family of calcium-modulated proteins of the EF-hand type with intracellular and extracellular functional roles. *Int J Biochem Cell Biol* 33: 637-668.

Donato R (2003) Intracellular and extracellular roles of S100 proteins. *Microsc Res Tech* 60: 540-551.

Donier E, Rugiero F, Okuse K, Wood JN (2005) Annexin II Light Chain p11 Promotes Functional Expression of Acid-sensing Ion Channel ASIC1a. *J Biol Chem* 280: 38666-38672.

Doyle CA, Hunt SP (1999) Substance P receptor (neurokinin-1)-expressing neurons in lamina I of the spinal cord encode for the intensity of noxious stimulation: a c-Fos study in rat. *Neuroscience* 89: 17-28.

Drew LJ, Rohrer DK, Price MP, Blaver KE, Cockayne DA, Cesare P, Wood JN (2004) Acid-sensing ion channels ASIC2 and ASIC3 do not contribute to mechanically activated currents in mammalian sensory neurones. *J Physiol* 556: 691-710.

Drew LJ, Wood JN (2007b) FM1-43 is a permeant blocker of mechanosensitive ion channels in sensory neurons and inhibits behavioural responses to mechanical stimuli. *Mol Pain* 3: 1.

Drew LJ, Wood JN (2007a) FM1-43 is a permeant blocker of mechanosensitive ion channels in sensory neurons and inhibits behavioural responses to mechanical stimuli. *Mol Pain* 3: 1.

Drew LJ, Wood JN, Cesare P (2002) Distinct mechanosensitive properties of capsaicin-sensitive and -insensitive sensory neurons. *J Neurosci* 22: RC228.

Dube GR, Lehto SG, Breese NM, Baker SJ, Wang X, Matulenko MA, Honore P, Stewart AO, Moreland RB, Brioni JD (2005) Electrophysiological and in vivo characterization of A-317567, a novel blocker of acid sensing ion channels. *Pain* 117: 88-96.

Duda T, Goraczniak RM, Sharma RK (1996) Molecular characterization of S100A1-S100B protein in retina and its activation mechanism of bovine photoreceptor guanylate cyclase. *Biochemistry* 35: 6263-6266.

Duprat F, Lesage F, Fink M, Reyes R, Heurteaux C, Lazdunski M (1997) TASK, a human background K<sup>+</sup> channel to sense external pH variations near physiological pH. *EMBO J* 16: 5464-5471.

Dymecki SM, Tomaszewicz H (1998) Using Flp-recombinase to characterize expansion of Wnt1-expressing neural progenitors in the mouse. *Dev Biol* 201: 57-65.

Ekberg J, Adams DJ (2006) Neuronal voltage-gated sodium channel subtypes: key roles in inflammatory and neuropathic pain. *Int J Biochem Cell Biol* 38: 2005-2010.

Ekberg J, Jayamanne A, Vaughan CW, Aslan S, Thomas L, Mould J, Drinkwater R, Baker MD, Abrahamsen B, Wood JN, Adams DJ, Christie MJ, Lewis RJ (2006)  $\mu$ O-conotoxin MrVIB selectively blocks Nav1.8 sensory neuron specific sodium channels and chronic pain behavior without motor deficits. *Proc Natl Acad Sci U S A* 103: 17030-17035.

Elliott AA, Elliott JR (1993) Characterization of TTX-sensitive and TTX-resistant sodium currents in small cells from adult rat dorsal root ganglia. *J Physiol* 463: 39-56.

Emmert-Buck MR, Roth MJ, Zhuang Z, Campo E, Rozhin J, Sloane BF, Liotta LA, Stetler-Stevenson WG (1994) Increased gelatinase A (MMP-2) and cathepsin B activity in invasive tumor regions of human colon cancer samples. *Am J Pathol* 145: 1285-1290.

England S, Okuse K, Ogata N, & Wood J. N. Heterologous expression of the sensory neurone-specific sodium channel (SNS)  $\alpha$ -subunit in rat sympathetic neurones. *J Physiol*. [511, 124P]. 1998.

Ref Type: Generic

Eriksson J, Jablonski A, Persson AK, Hao JX, Kouya PF, Wiesenfeld-Hallin Z, Xu XJ, Fried K (2005) Behavioral changes and trigeminal ganglion sodium channel regulation in an orofacial neuropathic pain model. *Pain* 119: 82-94.

Ernstrom GG, Chalfie M (2002) Genetics of sensory mechanotransduction. *Annu Rev Genet* 36: 411-453.

Evans MJ, Kaufman MH (1981) Establishment in culture of pluripotential cells from mouse embryos. *Nature* 292: 154-156.

Falcone DJ, McCaffrey TA, Haimovitz-Friedman A, Vergilio JA, Nicholson AC (1993) Macrophage and foam cell release of matrix-bound growth factors. Role of plasminogen activation. *J Biol Chem* 268: 11951-11958.

Fang X, Djouhri L, Black JA, Dib-Hajj SD, Waxman SG, Lawson SN (2002) The presence and role of the tetrodotoxin-resistant sodium channel Na(v)1.9 (NaN) in nociceptive primary afferent neurons. *J Neurosci* 22: 7425-7433.

Fang X, Djouhri L, McMullan S, Berry C, Okuse K, Waxman SG, Lawson SN (2005) trkA is expressed in nociceptive neurons and influences electrophysiological properties via Nav1.8 expression in rapidly conducting nociceptors. *J Neurosci* 25: 4868-4878.

Farley FW, Soriano P, Steffen LS, Dymecki SM (2000) Widespread recombinase expression using FLPeR (flipper) mice. *Genesis* 28: 106-110.

Ferreira J, Santos AR, Calixto JB (1999) Antinociception produced by systemic, spinal and supraspinal administration of amiloride in mice. *Life Sci* 65: 1059-1066.

Fertleman CR, Baker MD, Parker KA, Moffatt S, Elmslie FV, Abrahamsen B, Ostman J, Klugbauer N, Wood JN, Gardiner RM, Rees M (2006a) SCN9A mutations in paroxysmal extreme pain disorder: allelic variants underlie distinct channel defects and phenotypes. *Neuron* 52: 767-774.

Fertleman CR, Baker MD, Parker KA, Moffatt S, Elmslie FV, Abrahamsen B, Ostman J, Klugbauer N, Wood JN, Gardiner RM, Rees M (2006b) SCN9A mutations in paroxysmal extreme pain disorder: allelic variants underlie distinct channel defects and phenotypes. *Neuron* 52: 767-774.

Fiering S, Epner E, Robinson K, Zhuang Y, Telling A, Hu M, Martin DI, Enver T, Ley TJ, Groudine M (1995) Targeted deletion of 5'HS2 of the murine beta-globin LCR reveals that it is not essential for proper regulation of the beta-globin locus. *Genes Dev* 9: 2203-2213.

FitzGerald EM, Okuse K, Wood JN, Dolphin AC, Moss SJ (1999) cAMP-dependent phosphorylation of the tetrodotoxin-resistant voltage-dependent sodium channel SNS. *Journal of Physiology-London* 516: 433-446.

Fjell J, Cummins TR, Davis BM, Albers KM, Fried K, Waxman SG, Black JA (1999a) Sodium channel expression in NGF-overexpressing transgenic mice. *J Neurosci Res* 57: 39-47.

Fjell J, Cummins TR, Dib-Hajj SD, Fried K, Black JA, Waxman SG (1999b) Differential role of GDNF and NGF in the maintenance of two TTX-resistant sodium channels in adult DRG neurons. *Brain Res Mol Brain Res* 67: 267-282.

Fogg DK, Bridges DE, Cheung KK, Kassam G, Filipenko NR, Choi KS, Fitzpatrick SL, Nesheim M, Waisman DM (2002) The p11 subunit of annexin II heterotetramer is regulated by basic carboxypeptidase. *Biochemistry* 41: 4953-4961.

Folkman J (1995a) Angiogenesis in cancer, vascular, rheumatoid and other disease. *Nat Med* 1: 27-31.

Folkman J (1995b) Angiogenesis in cancer, vascular, rheumatoid and other disease. *Nat Med* 1: 27-31.

Förster, T. Intermolecular energy migration and fluorescence. *Ann.Phys.* 2, 55-75. 1-1-1948.

Ref Type: Generic

Frosch BA, Berquin I, Emmert-Buck MR, Moin K, Sloane BF (1999) Molecular regulation, membrane association and secretion of tumor cathepsin B. *APMIS* 107: 28-37.

Fuchs PN, Roza C, Sora I, Uhl G, Raja SN (1999) Characterization of mechanical withdrawal responses and effects of mu-, delta- and kappa-opioid agonists in normal and mu-opioid receptor knockout mice. *Brain Res* 821: 480-486.

Ganju P, O'Bryan JP, Der C, Winter J, James IF (1998) Differential regulation of SHC proteins by nerve growth factor in sensory neurons and PC12 cells. *Eur J Neurosci* 10: 1995-2008.

Garcia-Anoveros J, Samad IA, Zúvela-Jelaska L, Woolf CJ, Corey DP (2001) Transport and localization of the DEGENERIN ion channel BNaClalpha to peripheral mechanosensory terminals of dorsal root ganglia neurons. *J Neurosci* 21: 2678-2686.

Gerke V, Moss SE (2002) Annexins: from structure to function. *Physiol Rev* 82: 331-371.

Gerke V, Weber K (1984) Identity of p36K phosphorylated upon Rous sarcoma virus transformation with a protein purified from brush borders: calcium-dependent binding to non-erythroid spectrin and F-actin. *EMBO J* 3: 227-233.

Gerke V, Weber K (1985c) The regulatory chain in the p36-kd substrate complex of viral tyrosine-specific protein kinases is related in sequence to the S-100 protein of glial cells. *EMBO J* 4: 2917-2920.

Gerke V, Weber K (1985a) The regulatory chain in the p36-kd substrate complex of viral tyrosine-specific protein kinases is related in sequence to the S-100 protein of glial cells. *EMBO J* 4: 2917-2920.

Gerke V, Weber K (1985b) The regulatory chain in the p36-kd substrate complex of viral tyrosine-specific protein kinases is related in sequence to the S-100 protein of glial cells. *EMBO J* 4: 2917-2920.

Gingrich JA, Hen R (2001) Dissecting the role of the serotonin system in neuropsychiatric disorders using knockout mice. *Psychopharmacology (Berl)* 155: 1-10.

Girard C, Tinel N, Terrenoire C, Romey G, Lazdunski M, Borsotto M (2002) p11, an annexin II subunit, an auxiliary protein associated with the background K<sup>+</sup> channel, TASK-1. *EMBO J* 21: 4439-4448.

Gladwin MF, Yao XL, Cowan M, Huang XL, Schneider R, Grant LR, Logun C, Shelhamer JH (2000) Retinoic acid reduces p11 protein levels in bronchial epithelial cells by a posttranslational mechanism. *Am J Physiol Lung Cell Mol Physiol* 279: L1103-L1109.

Gokhale NA, Abraham A, Digman MA, Gratton E, Cho W (2005) Phosphoinositide specificity of and mechanism of lipid domain formation by annexin A2-p11 heterotetramer. *J Biol Chem* 280: 42831-42840.

Gold MS, Levine JD, Correa AM (1998) Modulation of TTX-R(Na) by PKC and PKA and their role in PGE<sub>2</sub>-induced sensitization of rat sensory neurons in vitro. *Journal of Neuroscience* 18: 10345-10355.

Gold MS, Shuster MJ, Levine JD (1996) Characterization of six voltage-gated K<sup>+</sup> currents in adult rat sensory neurons. *J Neurophysiol* 75: 2629-2646.

Gold MS, Weinreich D, Kim CS, Wang RZ, Treanor J, Porreca F, Lai J (2003) Redistribution of Na(V)1.8 in uninjured axons enables neuropathic pain. *Journal of Neuroscience* 23: 158-166.

Goldstein ME, House SB, Gainer H (1991) NF-L and peripherin immunoreactivities define distinct classes of rat sensory ganglion cells. *J Neurosci Res* 30: 92-104.

Graeser R, Gannon J, Poon RY, Dubois T, Aitken A, Hunt T (2002) Regulation of the CDK-related protein kinase PCTAIRE-1 and its possible role in neurite outgrowth in Neuro-2A cells. *J Cell Sci* 115: 3479-3490.

Green BG (1992) The sensory effects of l-menthol on human skin. *Somatosens Mot Res* 9: 235-244.

Green GM, Scarth J, Dickenson A (2000) An excitatory role for 5-HT in spinal inflammatory nociceptive transmission: state-dependent actions via dorsal horn 5-HT<sub>3</sub> receptors in the anaesthetized rat. *Pain* 89: 81-88.

Gureje O, Von KM, Simon GE, Gater R (1998) Persistent pain and well-being: a World Health Organization Study in Primary Care. *JAMA* 280: 147-151.

Haase H, Podzuweit T, Lutsch G, Hohaus A, Kostka S, Lindschau C, Kott M, Kraft R, Morano I (1999) Signaling from beta-adrenoceptor to L-type calcium channel: identification of a novel cardiac protein kinase A target possessing similarities to AHNAK. *FASEB J* 13: 2161-2172.

Hains BC, Klein JP, Saab CY, Craner MJ, Black JA, Waxman SG (2003) Upregulation of sodium channel Nav1.3 and functional involvement in neuronal hyperexcitability associated with central neuropathic pain after spinal cord injury. *J Neurosci* 23: 8881-8892.

Hajjar KA, Jacovina AT, Chaeko J (1994) An endothelial cell receptor for plasminogen/tissue plasminogen activator. I. Identity with annexin II. *J Biol Chem* 269: 21191-21197.

Halachmi D, Eilam Y (1993) Calcium homeostasis in yeast cells exposed to high concentrations of calcium. Roles of vacuolar H(+)-ATPase and cellular ATP. *FEBS Lett* 316: 73-78.

Hamill OP, Marty A, Neher E, Sakmann B, Sigworth FJ (1981) Improved patch-clamp techniques for high-resolution current recording from cells and cell-free membrane patches. *Pflugers Arch* 391: 85-100.

Han C, Lampert A, Rush AM, Dib-Hajj SD, Wang X, Yang Y, Waxman SG (2007) Temperature dependence of erythromelalgia mutation L858F in sodium channel Nav1.7. *Mol Pain* 3: 3.

Han C, Rush AM, Dib-Hajj SD, Li S, Xu Z, Wang Y, Tyrrell L, Wang X, Yang Y, Waxman SG (2006b) Sporadic onset of erythromelalgia: a gain-of-function mutation in Nav1.7. *Ann Neurol* 59: 553-558.

Han C, Rush AM, Dib-Hajj SD, Li S, Xu Z, Wang Y, Tyrrell L, Wang X, Yang Y, Waxman SG (2006a) Sporadic onset of erythromelalgia: a gain-of-function mutation in Nav1.7. *Ann Neurol* 59: 553-558.

Han HC, Lee DH, Chung JM (2000) Characteristics of ectopic discharges in a rat neuropathic pain model. *Pain* 84: 253-261.

Harder T, Kube E, Gerke V (1992) Cloning and characterization of the human gene encoding p11: structural similarity to other members of the S-100 gene family. *Gene* 113: 269-274.

Hargreaves K, Dubner R, Brown F, Flores C, Joris J (1988) A new and sensitive method for measuring thermal nociception in cutaneous hyperalgesia. *Pain* 32: 77-88.

Harty TP, Dib-Hajj SD, Tyrrell L, Blackman R, Hisama FM, Rose JB, Waxman SG (2006a) Na(V)1.7 mutant A863P in erythromelalgia: effects of altered activation and steady-state inactivation on excitability of nociceptive dorsal root ganglion neurons. *J Neurosci* 26: 12566-12575.

Harty TP, Dib-Hajj SD, Tyrrell L, Blackman R, Hisama FM, Rose JB, Waxman SG (2006b) Na(V)1.7 mutant A863P in erythromelalgia: effects of altered activation and steady-state inactivation on excitability of nociceptive dorsal root ganglion neurons. *J Neurosci* 26: 12566-12575.

Hasty P, Rivera-Perez J, Chang C, Bradley A (1991) Target frequency and integration pattern for insertion and replacement vectors in embryonic stem cells. *Mol Cell Biol* 11: 4509-4517.

Hayes MJ, Rescher U, Gerke V, Moss SE (2004) Annexin-actin interactions. *Traffic* 5: 571-576.

Hayes MJ, Shao D, Bailly M, Moss SE (2006a) Regulation of actin dynamics by annexin 2. *EMBO J* 25: 1816-1826.

Hayes MJ, Shao D, Bailly M, Moss SE (2006b) Regulation of actin dynamics by annexin 2. *EMBO J* 25: 1816-1826.

Hebert SC, Desir G, Giebisch G, Wang W (2005) Molecular diversity and regulation of renal potassium channels. *Physiol Rev* 85: 319-371.

Heinemann SH, Terlau H, Stuhmer W, Imoto K, Numa S (1992) Calcium channel characteristics conferred on the sodium channel by single mutations. *Nature* 356: 441-443.

HENSEL H, ZOTTERMAN Y (1951) The effect of menthol on the thermoreceptors. *Acta Physiol Scand* 24: 27-34.

Herzog RI, Cummins TR, Waxman SG (2001a) Persistent TTX-resistant Na<sup>+</sup> current affects resting potential and response to depolarization in simulated spinal sensory neurons. *J Neurophysiol* 86: 1351-1364.

Herzog RI, Cummins TR, Waxman SG (2001c) Persistent TTX-resistant Na<sup>+</sup> current affects resting potential and response to depolarization in simulated spinal sensory neurons. *J Neurophysiol* 86: 1351-1364.

Herzog RI, Cummins TR, Waxman SG (2001b) Persistent TTX-resistant Na<sup>+</sup> current affects resting potential and response to depolarization in simulated spinal sensory neurons. *J Neurophysiol* 86: 1351-1364.

Herzog RI, Liu C, Waxman SG, Cummins TR (2003a) Calmodulin binds to the C terminus of sodium channels Nav1.4 and Nav1.6 and differentially modulates their functional properties. *J Neurosci* 23: 8261-8270.

Herzog RI, Liu C, Waxman SG, Cummins TR (2003b) Calmodulin binds to the C terminus of sodium channels Nav1.4 and Nav1.6 and differentially modulates their functional properties. *J Neurosci* 23: 8261-8270.

Hoenderop JG, Nilius B, Bindels RJ (2002) Molecular mechanism of active Ca<sup>2+</sup> reabsorption in the distal nephron. *Annu Rev Physiol* 64: 529-549.

Hoenderop JG, Vennekens R, Muller D, Prenen J, Droogmans G, Bindels RJ, Nilius B (2001b) Function and expression of the epithelial Ca(2+) channel family: comparison of mammalian ECaC1 and 2. *J Physiol* 537: 747-761.

Hoenderop JG, Vennekens R, Muller D, Prenen J, Droogmans G, Bindels RJ, Nilius B (2001a) Function and expression of the epithelial Ca(2+) channel family: comparison of mammalian ECaC1 and 2. *J Physiol* 537: 747-761.

Hoenderop JG, Vennekens R, Muller D, Prenen J, Droogmans G, Bindels RJ, Nilius B (2001d) Function and expression of the epithelial Ca(2+) channel family: comparison of mammalian ECaC1 and 2. *J Physiol* 537: 747-761.

Hoenderop JG, Vennekens R, Muller D, Prenen J, Droogmans G, Bindels RJ, Nilius B (2001e) Function and expression of the epithelial Ca(2+) channel family: comparison of mammalian ECaC1 and 2. *J Physiol* 537: 747-761.

Hohaus A, Person V, Behlke J, Schaper J, Morano I, Haase H (2002) The carboxyl-terminal region of ahnak provides a link between cardiac L-type Ca<sup>2+</sup> channels and the actin-based cytoskeleton. *FASEB J* 16: 1205-1216.

Hole K, Tjolsen A (1993) The tail-flick and formalin tests in rodents: changes in skin temperature as a confounding factor. *Pain* 53: 247-254.

Hong S, Morrow TJ, Paulson PE, Isom LL, Wiley JW (2004) Early painful diabetic neuropathy is associated with differential changes in tetrodotoxin-sensitive and -resistant sodium channels in dorsal root ganglion neurons in the rat. *J Biol Chem* 279: 29341-29350.

Honore P, Rogers SD, Schwei MJ, Salak-Johnson JL, Luger NM, Sabino MC, Clohisey DR, Mantyh PW (2000) Murine models of inflammatory, neuropathic and cancer pain each generates a unique set of neurochemical changes in the spinal cord and sensory neurons. *Neuroscience* 98: 585-598.

Hsu SY, Kaipia A, Zhu L, Hsueh AJ (1997c) Interference of BAD (Bcl-xL/Bcl-2-associated death promoter)-induced apoptosis in mammalian cells by 14-3-3 isoforms and P11. *Mol Endocrinol* 11: 1858-1867.

Hsu SY, Kaipia A, Zhu L, Hsueh AJ (1997a) Interference of BAD (Bcl-xL/Bcl-2-associated death promoter)-induced apoptosis in mammalian cells by 14-3-3 isoforms and P11. *Mol Endocrinol* 11: 1858-1867.

Hsu SY, Kaipia A, Zhu L, Hsueh AJ (1997e) Interference of BAD (Bcl-xL/Bcl-2-associated death promoter)-induced apoptosis in mammalian cells by 14-3-3 isoforms and P11. *Mol Endocrinol* 11: 1858-1867.

Hsu SY, Kaipia A, Zhu L, Hsueh AJ (1997b) Interference of BAD (Bcl-xL/Bcl-2-associated death promoter)-induced apoptosis in mammalian cells by 14-3-3 isoforms and P11. *Mol Endocrinol* 11: 1858-1867.

Hsu SY, Kaipia A, Zhu L, Hsueh AJ (1997d) Interference of BAD (Bcl-xL/Bcl-2-associated death promoter)-induced apoptosis in mammalian cells by 14-3-3 isoforms and P11. *Mol Endocrinol* 11: 1858-1867.

Huang X, Pawliczak R, Yao XL, Madara P, Alsaaty S, Shelhamer JH, Cowan MJ (2003a) Characterization of the human p11 promoter sequence. *Gene* 310: 133-142.

Huang XL, Pawliczak R, Cowan MJ, Gladwin MT, Madara P, Logun C, Shelhamer JH (2002) Epidermal growth factor induces p11 gene and protein expression and down-regulates calcium ionophore-induced arachidonic acid release in human epithelial cells. *J Biol Chem* 277: 38431-38440.

Huang XL, Pawliczak R, Yao XL, Cowan MJ, Gladwin MT, Walter MJ, Holtzman MJ, Madara P, Logun C, Shelhamer JH (2003b) Interferon-gamma induces p11 gene and protein expression in human epithelial cells through interferon-gamma-activated sequences in the p11 promoter. *J Biol Chem* 278: 9298-9308.

Hunnskaar S, Hole K (1987) The formalin test in mice: dissociation between inflammatory and non-inflammatory pain. *Pain* 30: 103-114.

Hunt SP, Mantyh PW (2001a) The molecular dynamics of pain control. *Nat Rev Neurosci* 2: 83-91.

Hunt SP, Mantyh PW (2001b) The molecular dynamics of pain control. *Nat Rev Neurosci* 2: 83-91.

Ikebuchi NW, Waisman DM (1990) Calcium-dependent regulation of actin filament bundling by lipocortin-85. *J Biol Chem* 265: 3392-3400.

Immke DC, McCleskey EW (2001) Lactate enhances the acid-sensing Na<sup>+</sup> channel on ischemia-sensing neurons. *Nat Neurosci* 4: 869-870.

Inoue M, Ueda H (2000a) Protein kinase C-mediated acute tolerance to peripheral mu-opioid analgesia in the bradykinin-nociception test in mice. *J Pharmacol Exp Ther* 293: 662-669.

Inoue M, Ueda H (2000b) Protein kinase C-mediated acute tolerance to peripheral mu-opioid analgesia in the bradykinin-nociception test in mice. *J Pharmacol Exp Ther* 293: 662-669.

Isom LL (2000) I. Cellular and molecular biology of sodium channel beta-subunits: therapeutic implications for pain? I. Cellular and molecular biology of sodium channel beta-subunits: therapeutic implications for pain? *Am J Physiol Gastrointest Liver Physiol* 278: G349-G353.

Isom LL (2001) Sodium channel beta subunits: anything but auxiliary. *Neuroscientist* 7: 42-54.

Isom LL, Catterall WA (1996) Na<sup>+</sup> channel subunits and Ig domains. *Nature* 383: 307-308.

Isom LL, De Jongh KS, Catterall WA (1994) Auxiliary subunits of voltage-gated ion channels. *Neuron* 12: 1183-1194.

Isom LL, De Jongh KS, Patton DE, Reber BF, Offord J, Charbonneau H, Walsh K, Goldin AL, Catterall WA (1992) Primary structure and functional expression of the beta 1 subunit of the rat brain sodium channel. *Science* 256: 839-842.

Isom LL, Scheuer T, Brownstein AB, Ragsdale DS, Murphy BJ, Catterall WA (1995) Functional co-expression of the beta 1 and type IIA alpha subunits of sodium channels in a mammalian cell line. *J Biol Chem* 270: 3306-3312.

Jares-Erijman EA, Jovin TM (2003) FRET imaging. *Nat Biotechnol* 21: 1387-1395.

Jensen TS, Yaksh TL (1984) Effects of an intrathecal dopamine agonist, apomorphine, on thermal and chemical evoked noxious responses in rats. *Brain Res* 296: 285-293.

Ji RR, Samad TA, Jin SX, Schmoll R, Woolf CJ (2002) p38 MAPK activation by NGF in primary sensory neurons after inflammation increases TRPV1 levels and maintains heat hyperalgesia. *Neuron* 36: 57-68.

John VH, Main MJ, Powell AJ, Gladwell ZM, Hick C, Sidhu HS, Clare JJ, Tate S, Trezise DJ (2004) Heterologous expression and functional analysis of rat Nav1.8 (SNS) voltage-gated

sodium channels in the dorsal root ganglion neuroblastoma cell line ND7-23. *Neuropharmacology* 46: 425-438.

Jones NG, Slater R, Cadiou H, McNaughton P, McMahon SB (2004) Acid-induced pain and its modulation in humans. *J Neurosci* 24: 10974-10979.

Jordt SE, Bautista DM, Chuang HH, McKemy DD, Zygmunt PM, Hogestatt ED, Meng ID, Julius D (2004) Mustard oils and cannabinoids excite sensory nerve fibres through the TRP channel ANKTM1. *Nature* 427: 260-265.

Jordt SE, Tominaga M, Julius D (2000) Acid potentiation of the capsaicin receptor determined by a key extracellular site. *Proc Natl Acad Sci U S A* 97: 8134-8139.

Joyner AL, Guillemot F (1994) Gene targeting and development of the nervous system. *Curr Opin Neurobiol* 4: 37-42.

Julius D, Basbaum AI (2001d) Molecular mechanisms of nociception. *Nature* 413: 203-210.

Julius D, Basbaum AI (2001b) Molecular mechanisms of nociception. *Nature* 413: 203-210.

Julius D, Basbaum AI (2001a) Molecular mechanisms of nociception. *Nature* 413: 203-210.

Julius D, Basbaum AI (2001c) Molecular mechanisms of nociception. *Nature* 413: 203-210.

Kassam G, Choi KS, Ghuman J, Kang HM, Fitzpatrick SL, Zackson T, Zackson S, Toba M, Shinomiya A, Waisman DM (1998a) The role of annexin II tetramer in the activation of plasminogen. *J Biol Chem* 273: 4790-4799.

Kassam G, Choi KS, Ghuman J, Kang HM, Fitzpatrick SL, Zackson T, Zackson S, Toba M, Shinomiya A, Waisman DM (1998b) The role of annexin II tetramer in the activation of plasminogen. *J Biol Chem* 273: 4790-4799.

Kassam G, Kwon M, Yoon CS, Graham KS, Young MK, Gluck S, Waisman DM (2001) Purification and characterization of A61. An angiostatin-like plasminogen fragment produced by plasmin autodigestion in the absence of sulfhydryl donors. *J Biol Chem* 276: 8924-8933.

Kassam G, Le BH, Choi KS, Kang HM, Fitzpatrick SL, Louie P, Waisman DM (1998d) The p11 subunit of the annexin II tetramer plays a key role in the stimulation of t-PA-dependent plasminogen activation. *Biochemistry* 37: 16958-16966.

Kassam G, Le BH, Choi KS, Kang HM, Fitzpatrick SL, Louie P, Waisman DM (1998e) The p11 subunit of the annexin II tetramer plays a key role in the stimulation of t-PA-dependent plasminogen activation. *Biochemistry* 37: 16958-16966.

Kassam G, Le BH, Choi KS, Kang HM, Fitzpatrick SL, Louie P, Waisman DM (1998e) The p11 subunit of the annexin II tetramer plays a key role in the stimulation of t-PA-dependent plasminogen activation. *Biochemistry* 37: 16958-16966.

Kawase E, Suemori H, Takahashi N, Okazaki K, Hashimoto K, Nakatsuji N (1994) Strain difference in establishment of mouse embryonic stem (ES) cell lines. *Int J Dev Biol* 38: 385-390.

Kayser V, Guilbaud G (1987) Local and remote modifications of nociceptive sensitivity during carrageenin-induced inflammation in the rat. *Pain* 28: 99-107.

Kazen-Gillespie KA, Ragsdale DS, D'Andrea MR, Mattei LN, Rogers KE, Isom LL (2000) Cloning, localization, and functional expression of sodium channel beta1A subunits. *J Biol Chem* 275: 1079-1088.

Kerr BJ, Souslova V, McMahon SB, Wood JN (2001) A role for the TTX-resistant sodium channel Nav 1.8 in NGF-induced hyperalgesia, but not neuropathic pain. *Neuroreport* 12: 3077-3080.

Kidd BL, Urban LA (2001) Mechanisms of inflammatory pain. *Br J Anaesth* 87: 3-11.

Kim SH, Chung JM (1992) An experimental model for peripheral neuropathy produced by segmental spinal nerve ligation in the rat. *Pain* 50: 355-363.

Kligman D, Hilt DC (1988) The S100 protein family. *Trends Biochem Sci* 13: 437-443.

Kobayashi H, Schmitt M, Goretzki L, Chucholowski N, Calvete J, Kramer M, Gunzler WA, Janicke F, Graeff H (1991) Cathepsin B efficiently activates the soluble and the tumor cell receptor-bound form of the proenzyme urokinase-type plasminogen activator (Pro-uPA). *J Biol Chem* 266: 5147-5152.

Kobayashi K, Fukuoka T, Obata K, Yamanaka H, Dai Y, Tokunaga A, Noguchi K (2005) Distinct expression of TRPM8, TRPA1, and TRPV1 mRNAs in rat primary afferent neurons with adelta/c-fibers and colocalization with trk receptors. *J Comp Neurol* 493: 596-606.

Kontis KJ, Rounaghi A, Goldin AL (1997) Sodium channel activation gating is affected by substitutions of voltage sensor positive charges in all four domains. *J Gen Physiol* 110: 391-401.

Kretschmer T, Happel LT, England JD, Nguyen DH, Tiel RL, Beuerman RW, Kline DG (2002c) Accumulation of PN1 and PN3 sodium channels in painful human neuroma-evidence from immunocytochemistry. *Acta Neurochir (Wien)* 144: 803-810.

Kretschmer T, Happel LT, England JD, Nguyen DH, Tiel RL, Beuerman RW, Kline DG (2002a) Accumulation of PN1 and PN3 sodium channels in painful human neuroma-evidence from immunocytochemistry. *Acta Neurochir (Wien)* 144: 803-810.

Kretschmer T, Happel LT, England JD, Nguyen DH, Tiel RL, Beuerman RW, Kline DG (2002d) Accumulation of PN1 and PN3 sodium channels in painful human neuroma-evidence from immunocytochemistry. *Acta Neurochir (Wien)* 144: 803-810.

Kretschmer T, Happel LT, England JD, Nguyen DH, Tiel RL, Beuerman RW, Kline DG (2002b) Accumulation of PN1 and PN3 sodium channels in painful human neuroma-evidence from immunocytochemistry. *Acta Neurochir (Wien)* 144: 803-810.

Kube E, Becker T, Weber K, Gerke V (1992) Protein-protein interaction studied by site-directed mutagenesis. Characterization of the annexin II-binding site on p11, a member of the S100 protein family. *J Biol Chem* 267: 14175-14182.

Kudoh J, Wang Y, Minoshima S, Hashimoto T, Amagai M, Nishikawa T, Shtivelman E, Bishop JM, Shimizu N (1995) Localization of the human AHNAK/desmoyokin gene (AHNAK) to chromosome band 11q12 by somatic cell hybrid analysis and fluorescence in situ hybridization. *Cytogenet Cell Genet* 70: 218-220.

Kwan KY, Allehorne AJ, Vollrath MA, Christensen AP, Zhang DS, Woolf CJ, Corey DP (2006f) TRPA1 contributes to cold, mechanical, and chemical nociception but is not essential for hair-cell transduction. *Neuron* 50: 277-289.

Kwan KY, Allehorne AJ, Vollrath MA, Christensen AP, Zhang DS, Woolf CJ, Corey DP (2006a) TRPA1 contributes to cold, mechanical, and chemical nociception but is not essential for hair-cell transduction. *Neuron* 50: 277-289.

Kwan KY, Allehorne AJ, Vollrath MA, Christensen AP, Zhang DS, Woolf CJ, Corey DP (2006c) TRPA1 contributes to cold, mechanical, and chemical nociception but is not essential for hair-cell transduction. *Neuron* 50: 277-289.

Kwan KY, Allehorne AJ, Vollrath MA, Christensen AP, Zhang DS, Woolf CJ, Corey DP (2006b) TRPA1 contributes to cold, mechanical, and chemical nociception but is not essential for hair-cell transduction. *Neuron* 50: 277-289.

Kwan KY, Allehorne AJ, Vollrath MA, Christensen AP, Zhang DS, Woolf CJ, Corey DP (2006e) TRPA1 contributes to cold, mechanical, and chemical nociception but is not essential for hair-cell transduction. *Neuron* 50: 277-289.

Kwan KY, Allehorne AJ, Vollrath MA, Christensen AP, Zhang DS, Woolf CJ, Corey DP (2006d) TRPA1 contributes to cold, mechanical, and chemical nociception but is not essential for hair-cell transduction. *Neuron* 50: 277-289.

Kwon M, Caplan JF, Filipenko NR, Choi KS, Fitzpatrick SL, Zhang L, Waisman DM (2002) Identification of annexin II heterotetramer as a plasmin reductase. *J Biol Chem* 277: 10903-10911.

Kwon M, Macleod TJ, Zhang Y, Waisman DM (2005a) S100A10, annexin A2, and annexin a2 heterotetramer as candidate plasminogen receptors. *Front Biosci* 10: 300-325.

Kwon M, Yoon CS, Jeong W, Rhee SG, Waisman DM (2005b) Annexin A2-S100A10 heterotetramer, a novel substrate of thioredoxin. *J Biol Chem* 280: 23584-23592.

Lah TT, Buck MR, Honn KV, Crissman JD, Rao NC, Liotta LA, Sloane BF (1989) Degradation of laminin by human tumor cathepsin B. *Clin Exp Metastasis* 7: 461-468.

Lai J, Gold MS, Kim CS, Bian D, Ossipov MH, Hunter JC, Porreca F (2002) Inhibition of neuropathic pain by decreased expression of the tetrodotoxin-resistant sodium channel, Nav1.8. *Pain* 95: 143-152.

Laird JM, Souslova V, Wood JN, Cervero F (2002) Deficits in visceral pain and referred hyperalgesia in Nav1.8 (SNS/PN3)-null mice. *J Neurosci* 22: 8352-8356.

Lampert A, Dib-Hajj SD, Tyrrell L, Waxman SG (2006a) Size matters: Erythromelalgia mutation S241T in Nav1.7 alters channel gating. *J Biol Chem* 281: 36029-36035.

Lampert A, Dib-Hajj SD, Tyrrell L, Waxman SG (2006b) Size matters: Erythromelalgia mutation S241T in Nav1.7 alters channel gating. *J Biol Chem* 281: 36029-36035.

Lauritzen I, Zanzouri M, Honore E, Duprat F, Ehrengruber MU, Lazdunski M, Patel AJ (2003) K<sup>+</sup>-dependent cerebellar granule neuron apoptosis. Role of task leak K<sup>+</sup> channels. *J Biol Chem* 278: 32068-32076.

Lawson SN (1979) The postnatal development of large light and small dark neurons in mouse dorsal root ganglia: a statistical analysis of cell numbers and size. *J Neurocytol* 8: 275-294.

Lawson SN (2002) Phenotype and function of somatic primary afferent nociceptive neurones with C-, Adelta- or Aalpha/beta-fibres. *Exp Physiol* 87: 239-244.

Lawson SN, Harper AA, Harper EI, Garson JA, Anderton BH (1984) A monoclonal antibody against neurofilament protein specifically labels a subpopulation of rat sensory neurones. *J Comp Neurol* 228: 263-272.

Le BF, Capdevielle J, Guillemot JC, Sladeczek F (1998) Characterization of brain PCTAIRE-1 kinase immunoreactivity and its interactions with p11 and 14-3-3 proteins. *Eur J Biochem* 257: 112-120.

Lesage F, Lazdunski M (2000) Molecular and functional properties of two-pore-domain potassium channels. *Am J Physiol Renal Physiol* 279: F793-F801.

Lewin GR, Mendell LM (1994) Regulation of cutaneous C-fiber heat nociceptors by nerve growth factor in the developing rat. *J Neurophysiol* 71: 941-949.

Lewis C, Neidhart S, Holy C, North RA, Buell G, Surprenant A (1995) Coexpression of P2X2 and P2X3 receptor subunits can account for ATP-gated currents in sensory neurons. *Nature* 377: 432-435.

Lewit-Bentley A, Rety S, Sopkova-de Oliveira SJ, Gerke V (2000) S100-annexin complexes: some insights from structural studies. *Cell Biol Int* 24: 799-802.

Liedtke W, Choe Y, Marti-Renom MA, Bell AM, Denis CS, Sali A, Hudspeth AJ, Friedman JM, Heller S (2000b) Vanilloid receptor-related osmotically activated channel (VR-OAC), a candidate vertebrate osmoreceptor. *Cell* 103: 525-535.

Liedtke W, Choe Y, Marti-Renom MA, Bell AM, Denis CS, Sali A, Hudspeth AJ, Friedman JM, Heller S (2000a) Vanilloid receptor-related osmotically activated channel (VR-OAC), a candidate vertebrate osmoreceptor. *Cell* 103: 525-535.

Liedtke W, Friedman JM (2003) Abnormal osmotic regulation in *trpv4*<sup>-/-</sup> mice. *Proc Natl Acad Sci U S A* 100: 13698-13703.

Lin FL, Sperle K, Sternberg N (1985) Recombination in mouse L cells between DNA introduced into cells and homologous chromosomal sequences. *Proc Natl Acad Sci U S A* 82: 1391-1395.

Ling Q, Jacovina AT, Deora A, Febbraio M, Simantov R, Silverstein RL, Hempstead B, Mark WH, Hajjar KA (2004) Annexin II regulates fibrin homeostasis and neoangiogenesis in vivo. *J Clin Invest* 113: 38-48.

Lingueglia E, de W, Jr., Bassilana F, Heurteaux C, Sakai H, Waldmann R, Lazdunski M (1997b) A modulatory subunit of acid sensing ion channels in brain and dorsal root ganglion cells. *J Biol Chem* 272: 29778-29783.

Lingueglia E, de W, Jr., Bassilana F, Heurteaux C, Sakai H, Waldmann R, Lazdunski M (1997a) A modulatory subunit of acid sensing ion channels in brain and dorsal root ganglion cells. *J Biol Chem* 272: 29778-29783.

Liu Y, Cheng K, Gong K, Fu AK, Ip NY (2006) Petaire1 phosphorylates N-ethylmaleimide-sensitive fusion protein: implications in the regulation of its hexamerization and exocytosis. *J Biol Chem* 281: 9852-9858.

Löffing J, Löffing-Cueni D, Valderrabano V, Klausli L, Hebert SC, Rossier BC, Hoenderop JG, Bindels RJ, Kaissling B (2001a) Distribution of transcellular calcium and sodium transport pathways along mouse distal nephron. *Am J Physiol Renal Physiol* 281: F1021-F1027.

Löffing J, Löffing-Cueni D, Valderrabano V, Klausli L, Hebert SC, Rossier BC, Hoenderop JG, Bindels RJ, Kaissling B (2001b) Distribution of transcellular calcium and sodium transport pathways along mouse distal nephron. *Am J Physiol Renal Physiol* 281: F1021-F1027.

Lumb BM, Lovick TA (1993) The rostral hypothalamus: an area for the integration of autonomic and sensory responsiveness. *J Neurophysiol* 70: 1570-1577.

Lumpkin EA, Caterina MJ (2007) Mechanisms of sensory transduction in the skin. *Nature* 445: 858-865.

Luo ZD, Calcutt NA, Higuera ES, Valder CR, Song YH, Svensson CI, Myers RR (2002) Injury type-specific calcium channel alpha 2 delta-1 subunit up-regulation in rat neuropathic pain models correlates with antiallodynic effects of gabapentin. *J Pharmacol Exp Ther* 303: 1199-1205.

Lyons RM, Gentry LE, Purchio AF, Moses HL (1990) Mechanism of activation of latent recombinant transforming growth factor beta 1 by plasmin. *J Cell Biol* 110: 1361-1367.

Macleod TJ, Kwon M, Filipenko NR, Waisman DM (2003) Phospholipid-associated annexin A2-S100A10 heterotetramer and its subunits: characterization of the interaction with tissue plasminogen activator, plasminogen, and plasmin. *J Biol Chem* 278: 25577-25584.

Mai J, Finley RL, Jr., Waisman DM, Sloane BF (2000) Human procathepsin B interacts with the annexin II tetramer on the surface of tumor cells. *J Biol Chem* 275: 12806-12812.

Malik-Hall M, Poon WY, Baker MD, Wood JN, Okuse K (2003) Sensory neuron proteins interact with the intracellular domains of sodium channel Nav1.8. *Brain Res Mol Brain Res* 110: 298-304.

Maroteaux L, Saudou F, Amlaiky N, Boscchert U, Plassat JL, Hen R (1992) Mouse 5HT1B serotonin receptor: cloning, functional expression, and localization in motor control centers. *Proc Natl Acad Sci U S A* 89: 3020-3024.

Marsden BJ, Shaw GS, Sykes BD (1990) Calcium binding proteins. Elucidating the contributions to calcium affinity from an analysis of species variants and peptide fragments. *Biochem Cell Biol* 68: 587-601.

Martin GR (1981) Isolation of a pluripotent cell line from early mouse embryos cultured in medium conditioned by teratocarcinoma stem cells. *Proc Natl Acad Sci U S A* 78: 7634-7638.

Masiakowski P, Shooter EM (1988) Nerve growth factor induces the genes for two proteins related to a family of calcium-binding proteins in PC12 cells. *Proc Natl Acad Sci U S A* 85: 1277-1281.

Masiakowski P, Shooter EM (1990) Changes in PC12 cell morphology induced by transfection with  $\alpha 2C$  cDNA, coding for a member of the S-100 protein family. *J Neurosci Res* 27: 264-269.

Matsuda Y, Yoshida S, Yonezawa T (1978) Tetrodotoxin sensitivity and Ca component of action potentials of mouse dorsal root ganglion cells cultured in vitro. *Brain Res* 154: 69-82.

Matthews EA, Wood JN, Dickenson AH (2006) Nav 1.8-null mice show stimulus-dependent deficits in spinal neuronal activity. *Mol Pain* 2: 5.

McCarthy PW, Lawson SN (1997) Differing action potential shapes in rat dorsal root ganglion neurones related to their substance P and calcitonin gene-related peptide immunoreactivity. *J Comp Neurol* 388: 541-549.

McKemy DD, Neuhausser WM, Julius D (2002b) Identification of a cold receptor reveals a general role for TRP channels in thermosensation. *Nature* 416: 52-58.

McKemy DD, Neuhausser WM, Julius D (2002a) Identification of a cold receptor reveals a general role for TRP channels in thermosensation. *Nature* 416: 52-58.

McMahon SB, Armanini MP, Ling LH, Phillips HS (1994) Expression and coexpression of Trk receptors in subpopulations of adult primary sensory neurons projecting to identified peripheral targets. *Neuron* 12: 1161-1171.

Menke M, Gerke V, Steinem C (2005) Phosphatidylserine membrane domain clustering induced by annexin A2/S100A10 heterotetramer. *Biochemistry* 44: 15296-15303.

Merrifield CJ, Rescher U, Almers W, Proust J, Gerke V, Sechi AS, Moss SE (2001) Annexin 2 has an essential role in actin-based macropinoctytic rocketing. *Curr Biol* 11: 1136-1141.

Meuser T, Pietruck C, Radbruch L, Stute P, Lehmann KA, Grond S (2001) Symptoms during cancer pain treatment following WHO-guidelines: a longitudinal follow-up study of symptom prevalence, severity and etiology. *Pain* 93: 247-257.

Meuth SG, Budde T, Kanyshkova T, Broicher T, Munsch T, Pape HC (2003) Contribution of TWIK-related acid-sensitive K<sup>+</sup> channel 1 (TASK1) and TASK3 channels to the control of activity modes in thalamocortical neurons. *J Neurosci* 23: 6460-6469.

Meyer RA, Davis KD, Cohen RH, Treede RD, Campbell JN (1991) Mechanically insensitive afferents (MIAs) in cutaneous nerves of monkey. *Brain Res* 561: 252-261.

Meyers EN, Lewandoski M, Martin GR (1998) An *Egf8* mutant allelic series generated by Cre- and Fip-mediated recombination. *Nat Genet* 18: 136-141.

Michaelis M, Habler HJ, Jaenig W (1996) Silent afferents: a separate class of primary afferents? *Clin Exp Pharmacol Physiol* 23: 99-105.

Millar JA, Barratt L, Southan AP, Page KM, Fyffe RE, Robertson B, Mathie A (2000b) A functional role for the two-pore domain potassium channel TASK-1 in cerebellar granule neurons. *Proc Natl Acad Sci U S A* 97: 3614-3618.

Millar JA, Barratt L, Southan AP, Page KM, Fyffe RE, Robertson B, Mathie A (2000c) A functional role for the two-pore domain potassium channel TASK-1 in cerebellar granule neurons. *Proc Natl Acad Sci U S A* 97: 3614-3618.

Millar JA, Barratt L, Southan AP, Page KM, Fyffe RE, Robertson B, Mathie A (2000a) A functional role for the two-pore domain potassium channel TASK-1 in cerebellar granule neurons. *Proc Natl Acad Sci U S A* 97: 3614-3618.

Milligan ED, Mehmert KK, Hinde JL, Harvey LO, Martin D, Tracey KJ, Maier SF, Watkins LR (2000) Thermal hyperalgesia and mechanical allodynia produced by intrathecal

administration of the human immunodeficiency virus-1 (HIV-1) envelope glycoprotein, gp120. *Brain Res* 861: 105-116.

Mogil JS, Breese NM, Witty MF, Ritchie J, Rainville ML, Ase A, Abbadi N, Stucky CL, Seguela P (2005) Transgenic expression of a dominant-negative ASIC3 subunit leads to increased sensitivity to mechanical and inflammatory stimuli. *J Neurosci* 25: 9893-9901.

Mogil JS, Ritchie J, Sotocinal SG, Smith SB, Croteau S, Levitin DJ, Naumova AK (2006) Screening for pain phenotypes: analysis of three congenic mouse strains on a battery of nine nociceptive assays. *Pain* 126: 24-34.

Mogil JS, Wilson SG, Bon K, Lee SE, Chung K, Raber P, Pieper JO, Hain HS, Belknap JK, Hubert L, Elmer GI, Chung JM, Devor M (1999) Heritability of nociception I: responses of 11 inbred mouse strains on 12 measures of nociception. *Pain* 80: 67-82.

Molliver DC, Snider WD (1997) Nerve growth factor receptor TrkA is down-regulated during postnatal development by a subset of dorsal root ganglion neurons. *J Comp Neurol* 381: 428-438.

Molliver DC, Wright DE, Leitner ML, Parsadanian AS, Doster K, Wen D, Yan Q, Snider WD (1997) IB4-binding DRG neurons switch from NGF to GDNF dependence in early postnatal life. *Neuron* 19: 849-861.

Moret C, Briley M (2000a) The possible role of 5-HT(1B/D) receptors in psychiatric disorders and their potential as a target for therapy. *Eur J Pharmacol* 404: 1-12.

Moret C, Briley M (2000b) The possible role of 5-HT(1B/D) receptors in psychiatric disorders and their potential as a target for therapy. *Eur J Pharmacol* 404: 1-12.

Morgan K, Stevens EB, Shah B, Cox PJ, Dixon AK, Lee K, Pinnock RD, Hughes J, Richardson PJ, Mizuguchi K, Jackson AP (2000) beta 3: an additional auxiliary subunit of the voltage-sensitive sodium channel that modulates channel gating with distinct kinetics. *Proc Natl Acad Sci U S A* 97: 2308-2313.

Mori M, Konno T, Ozawa T, Murata M, Imoto K, Nagayama K (2000) Novel interaction of the voltage-dependent sodium channel (VDSC) with calmodulin: does VDSC acquire calmodulin-mediated Ca<sup>2+</sup>-sensitivity? *Biochemistry* 39: 1316-1323.

Morris CE, Horn R (1991) Failure to elicit neuronal macroscopic mechanosensitive currents anticipated by single-channel studies. *Science* 251: 1246-1249.

Muller U (1999) Ten years of gene targeting: targeted mouse mutants, from vector design to phenotype analysis. *Mech Dev* 82: 3-21.

Munns C, Alqatari M, Koltzenburg M (2006) Many cold sensitive peripheral neurons of the mouse do not express TRPM8 or TRPA1. *Cell Calcium*.

Nagata K, Duggan A, Kumar G, Garcia-Anoveros J (2005) Nociceptor and hair cell transducer properties of TRPA1, a channel for pain and hearing. *J Neurosci* 25: 4052-4061.

Nagy A (2000) Cre recombinase: the universal reagent for genome tailoring. *Genesis* 26: 99-109.

Nagy A, Moens C, Ivanyi E, Pawling J, Gertsenstein M, Hadjantonakis AK, Pirity M, Rossant J (1998) Dissecting the role of N-myc in development using a single targeting vector to generate a series of alleles. *Curr Biol* 8: 661-664.

Nagy I, Rang H (1999) Noxious heat activates all capsaicin-sensitive and also a sub-population of capsaicin-insensitive dorsal root ganglion neurons. *Neuroscience* 88: 995-997.

Nassar MA, Baker MD, Levato A, Ingram R, Mallucci G, McMahon SB, Wood JN (2006) Nerve injury induces robust allodynia and ectopic discharges in Nav1.3 null mutant mice. *Mol Pain* 2: 33.

Nassar MA, Levato A, Stirling LC, Wood JN (2005) Neuropathic pain develops normally in mice lacking both Nav1.7 and Nav1.8. *Mol Pain* 1: 24.

Nassar MA, Stirling LC, Forlani G, Baker MD, Matthews EA, Dickenson AH, Wood JN (2004) Nociceptor-specific gene deletion reveals a major role for Nav1.7 (PN1) in acute and inflammatory pain. *Proc Natl Acad Sci U S A* 101: 12706-12711.

Netzel-Arnett S, Mitola DJ, Yamada SS, Chrysovergis K, Holmbeck K, Birkedal-Hansen H, Bugge TH (2002) Collagen dissolution by keratinocytes requires cell surface plasminogen activation and matrix metalloproteinase activity. *J Biol Chem* 277: 45154-45161.

Nilius B, Prenen J, Hoenderop JG, Vennekens R, Hoefs S, Weidema AF, Droogmans G, Bindels RJ (2002) Fast and slow inactivation kinetics of the Ca<sup>2+</sup> channels ECaC1 and ECaC2 (TRPV5 and TRPV6). Role of the intracellular loop located between transmembrane segments 2 and 3. *J Biol Chem* 277: 30852-30858.

Nilius B, Prenen J, Vennekens R, Hoenderop JG, Bindels RJ, Droogmans G (2001) Modulation of the epithelial calcium channel, ECaC, by intracellular Ca<sup>2+</sup>. *Cell Calcium* 29: 417-428.

Niwa H, Yamamura K, Miyazaki J (1991) Efficient selection for high-expression transfectants with a novel eukaryotic vector. *Gene* 108: 193-199.

Noda M, Suzuki H, Numa S, Stuhmer W (1989) A single point mutation confers tetrodotoxin and saxitoxin insensitivity on the sodium channel II. *FEBS Lett* 259: 213-216.

Novakovic SD, Tzoumaka E, McGivern JG, Haraguchi M, Sangameswaran L, Gogas KR, Eglén RM, Hunter JC (1998) Distribution of the tetrodotoxin-resistant sodium channel PN3 in rat sensory neurons in normal and neuropathic conditions. *J Neurosci* 18: 2174-2187.

Nozaki-Taguchi N, Chaplan SR, Higuera ES, Ajakwe RC, Yaksh TL (2001) Vincristine-induced allodynia in the rat. *Pain* 93: 69-76.

Obata K, Katsura H, Mizushima T, Yamanaka H, Kobayashi K, Dai Y, Fukuoka T, Tokunaga A, Tominaga M, Noguchi K (2005) TRPA1 induced in sensory neurons contributes to cold hyperalgesia after inflammation and nerve injury. *J Clin Invest* 115: 2393-2401.

Okuse K, Chaplan SR, McMahon SB, Luo ZD, Calcutt NA, Scott BP, Akopian AN, Wood JN (1997) Regulation of expression of the sensory neuron-specific sodium channel SNS in inflammatory and neuropathic pain. *Mol Cell Neurosci* 10: 196-207.

Okuse K, Malik-Hall M, Baker MD, Poon WY, Kong H, Chao MV, Wood JN (2002) Annexin II light chain regulates sensory neuron-specific sodium channel expression. *Nature* 417: 653-656.

Olson EN, Arnold HH, Rigby PW, Wold BJ (1996) Know your neighbors: three phenotypes in null mutants of the myogenic bHLH gene MRF4. *Cell* 85: 1-4.

Ozaki T, Sakiyama S (1993) Molecular cloning of rat calpactin I heavy-chain cDNA whose expression is induced in v-src-transformed rat culture cell lines. *Oncogene* 8: 1707-1710.

Page AJ, Brierley SM, Martin CM, Martinez-Salgado C, Wemmie JA, Brennan TJ, Symonds E, Omari T, Lewin GR, Welsh MJ, Blackshaw LA (2004a) The ion channel ASIC1 contributes to visceral but not cutaneous mechanoreceptor function. *Gastroenterology* 127: 1739-1747.

Page AJ, Brierley SM, Martin CM, Martinez-Salgado C, Wemmie JA, Brennan TJ, Symonds E, Omari T, Lewin GR, Welsh MJ, Blackshaw LA (2004b) The ion channel ASIC1 contributes to visceral but not cutaneous mechanoreceptor function. *Gastroenterology* 127: 1739-1747.

Pang PT, Teng HK, Zaitsev E, Woo NT, Sakata K, Zhen S, Teng KK, Yung WH, Hempstead BL, Lu B (2004a) Cleavage of proBDNF by tPA/plasmin is essential for long-term hippocampal plasticity. *Science* 306: 487-491.

Pang PT, Teng HK, Zaitsev E, Woo NT, Sakata K, Zhen S, Teng KK, Yung WH, Hempstead BL, Lu B (2004b) Cleavage of proBDNF by tPA/plasmin is essential for long-term hippocampal plasticity. *Science* 306: 487-491.

Pang PT, Teng HK, Zaitsev E, Woo NT, Sakata K, Zhen S, Teng KK, Yung WH, Hempstead BL, Lu B (2004c) Cleavage of proBDNF by tPA/plasmin is essential for long-term hippocampal plasticity. *Science* 306: 487-491.

Paoletti P, Ascher P (1994) Mechanosensitivity of NMDA receptors in cultured mouse central neurons. *Neuron* 13: 645-655.

Passmore GM, Selyanko AA, Mistry M, Al-Qatari M, Marsh SJ, Matthews EA, Dickenson AH, Brown TA, Burbidge SA, Main M, Brown DA (2003) KCNQ/M currents in sensory neurons: significance for pain therapy. *J Neurosci* 23: 7227-7236.

Pawliczak R, Cowan MJ, Huang X, Nanavaty UB, Alsaaty S, Logun C, Shelhamer JH (2001) p11 expression in human bronchial epithelial cells is increased by nitric oxide in a cGMP-dependent pathway involving protein kinase G activation. *J Biol Chem* 276: 44613-44621.

Peier AM, Moqrich A, Hergarden AC, Reeve AJ, Andersson DA, Story GM, Earley TJ, Dragoni I, McIntyre P, Bevan S, Patapoutian A (2002) A TRP channel that senses cold stimuli and menthol. *Cell* 108: 705-715.

Pendurthi UR, Ngyuen M, Andrade-Gordon P, Petersen LC, Rao LV (2002) Plasmin induces Cyr61 gene expression in fibroblasts via protease-activated receptor-1 and p44/42 mitogen-activated protein kinase-dependent signaling pathway. *Arterioscler Thromb Vasc Biol* 22: 1421-1426.

Perl ER (1992) Function of Dorsal Root Ganglion Neurons. In: *Sensory Neurons. Diversity, Development, and Plasticity* (Scott SA, ed). New York: Oxford University Press.

Peterson EA, Sutherland MR, Nesheim ME, Pryzdial EL (2003) Thrombin induces endothelial cell-surface exposure of the plasminogen receptor annexin 2. *J Cell Sci* 116: 2399-2408.

Pfaffl MW (2001) A new mathematical model for relative quantification in real-time RT-PCR. *Nucleic Acids Res* 29: e45.

Pham CT, MacIvor DM, Hug BA, Heusel JW, Ley TJ (1996) Long-range disruption of gene expression by a selectable marker cassette. *Proc Natl Acad Sci U S A* 93: 13090-13095.

Poirot O, Berta T, Decosterd I, Kellenberger S (2006) Distinct ASIC currents are expressed in rat putative nociceptors and are modulated by nerve injury. *J Physiol*.

Poon WY, Malik-Hall M, Wood JN, Okuse K (2004) Identification of binding domains in the sodium channel Na(V)1.8 intracellular N-terminal region and annexin II light chain p11. *FEBS Lett* 558: 114-118.

Price DD (2000) Psychological and neural mechanisms of the affective dimension of pain. *Science* 288: 1769-1772.

Price MP, Lewin GR, Mellwrath SL, Cheng C, Xie J, Heppenstall PA, Stucky CL, Mannsfeldt AG, Brennan TJ, Drummond HA, Qiao J, Benson CJ, Tarr DE, Hrstka RF, Yang B, Williamson RA, Welsh MJ (2000b) The mammalian sodium channel BNC1 is required for normal touch sensation. *Nature* 407: 1007-1011.

Price MP, Lewin GR, Mellwrath SL, Cheng C, Xie J, Heppenstall PA, Stucky CL, Mannsfeldt AG, Brennan TJ, Drummond HA, Qiao J, Benson CJ, Tarr DE, Hrstka RF, Yang B, Williamson RA, Welsh MJ (2000a) The mammalian sodium channel BNC1 is required for normal touch sensation. *Nature* 407: 1007-1011.

Price MP, Mellwrath SL, Xie J, Cheng C, Qiao J, Tarr DE, Sluka KA, Brennan TJ, Lewin GR, Welsh MJ (2001d) The DRASIC cation channel contributes to the detection of cutaneous touch and acid stimuli in mice. *Neuron* 32: 1071-1083.

Price MP, Mellwrath SL, Xie J, Cheng C, Qiao J, Tarr DE, Sluka KA, Brennan TJ, Lewin GR, Welsh MJ (2001a) The DRASIC cation channel contributes to the detection of cutaneous touch and acid stimuli in mice. *Neuron* 32: 1071-1083.

Price MP, Mellwrath SL, Xie J, Cheng C, Qiao J, Tarr DE, Sluka KA, Brennan TJ, Lewin GR, Welsh MJ (2001c) The DRASIC cation channel contributes to the detection of cutaneous touch and acid stimuli in mice. *Neuron* 32: 1071-1083.

Price MP, Mellwrath SL, Xie J, Cheng C, Qiao J, Tarr DE, Sluka KA, Brennan TJ, Lewin GR, Welsh MJ (2001b) The DRASIC cation channel contributes to the detection of cutaneous touch and acid stimuli in mice. *Neuron* 32: 1071-1083.

Priest BT, Murphy BA, Lindia JA, Diaz C, Abbadie C, Ritter AM, Liberator P, Iyer LM, Kash SF, Kohler MG, Kaczorowski GJ, MacIntyre DE, Martin WJ (2005) Contribution of the

tetrodotoxin-resistant voltage-gated sodium channel NaV1.9 to sensory transmission and nociceptive behavior. *Proc Natl Acad Sci U S A* 102: 9382-9387.

Puisieux A, Ji J, Ozturk M (1996) Annexin II up-regulates cellular levels of p11 protein by a post-translational mechanisms. *Biochem J* 313 ( Pt 1): 51-55.

Pullarkat SR, Mysels DJ, Tan M, Cowen DS (1998) Coupling of serotonin 5-HT1B receptors to activation of mitogen-activated protein kinase (ERK-2) and p70 S6 kinase signaling systems. *J Neurochem* 71: 1059-1067.

Qiu S, Adema CM, Lane T (2005) A computational study of off-target effects of RNA interference. *Nucleic Acids Res* 33: 1834-1847.

Rajan S, Preisig-Muller R, Wischmeyer E, Nehring R, Hanley PJ, Renigunta V, Musset B, Schlichthorl G, Derst C, Karschin A, Daut J (2002b) Interaction with 14-3-3 proteins promotes functional expression of the potassium channels TASK-1 and TASK-3. *J Physiol* 545: 13-26.

Rajan S, Preisig-Muller R, Wischmeyer E, Nehring R, Hanley PJ, Renigunta V, Musset B, Schlichthorl G, Derst C, Karschin A, Daut J (2002a) Interaction with 14-3-3 proteins promotes functional expression of the potassium channels TASK-1 and TASK-3. *J Physiol* 545: 13-26.

Ramos-DeSimone N, Hahn-Dantona E, Siple J, Nagase H, French DL, Quigley JP (1999) Activation of matrix metalloproteinase-9 (MMP-9) via a converging plasmin/stromelysin-1 cascade enhances tumor cell invasion. *J Biol Chem* 274: 13066-13076.

Reid G, Babes A, Pluteanu F (2002) A cold- and menthol-activated current in rat dorsal root ganglion neurones: properties and role in cold transduction. *J Physiol* 545: 595-614.

Reid G, Flonta M (2001b) Cold transduction by inhibition of a background potassium conductance in rat primary sensory neurones. *Neurosci Lett* 297: 171-174.

Reid G, Flonta M (2001a) Cold transduction by inhibition of a background potassium conductance in rat primary sensory neurones. *Neurosci Lett* 297: 171-174.

Reid G, Flonta ML (2001c) Physiology. Cold current in thermoreceptive neurons. *Nature* 413: 480.

Rempel SA, Rosenblum ML, Mikkelsen T, Yan PS, Ellis KD, Golembieski WA, Sameni M, Rozhin J, Ziegler G, Sloane BF (1994) Cathepsin B expression and localization in glioma progression and invasion. *Cancer Res* 54: 6027-6031.

Renganathan M, Cummins TR, Waxman SG (2001) Contribution of Na(v)1.8 sodium channels to action potential electrogenesis in DRG neurons. *J Neurophysiol* 86: 629-640.

Renigunta V, Yuan H, Zuzarte M, Rinne S, Koch A, Wischmeyer E, Schlichthorl G, Gao Y, Karschin A, Jacob R, Schwappach B, Daut J, Preisig-Muller R (2006) The retention factor p11 confers an endoplasmic reticulum-localization signal to the potassium channel TASK-1. *Traffic* 7: 168-181.

Rety S, Sopkova J, Renouard M, Osterloh D, Gerke V, Tabaries S, Russo-Marie F, Lewit-Bentley A (1999) The crystal structure of a complex of p11 with the annexin II N-terminal peptide. *Nat Struct Biol* 6: 89-95.

Rhoads AR, Friedberg F (1997) Sequence motifs for calmodulin recognition. *FASEB J* 11: 331-340.

Rintala-Dempsey AC, Santamaria-Kisiel L, Liao Y, Lajoie G, Shaw GS (2006a) Insights into S100 target specificity examined by a new interaction between S100A11 and annexin A2. *Biochemistry* 45: 14695-14705.

Rintala-Dempsey AC, Santamaria-Kisiel L, Liao Y, Lajoie G, Shaw GS (2006b) Insights into S100 target specificity examined by a new interaction between S100A11 and annexin A2. *Biochemistry* 45: 14695-14705.

Risau W (1997) Mechanisms of angiogenesis. *Nature* 386: 671-674.

Ritter AM, Mendell LM (1992) Somal membrane properties of physiologically identified sensory neurons in the rat: effects of nerve growth factor. *J Neurophysiol* 68: 2033-2041.

Rodriguez CI, Buchholz F, Galloway J, Sequerra R, Kasper J, Ayala R, Stewart AF, Dymecki SM (2000) High-efficiency deleter mice show that FLPe is an alternative to Cre-loxP. *Nat Genet* 25: 139-140.

Rogers JC, Qu Y, Tanada TN, Scheuer T, Catterall WA (1996) Molecular determinants of high affinity binding of alpha-scorpion toxin and sea anemone toxin in the S3-S4 extracellular loop in domain IV of the Na<sup>+</sup> channel alpha subunit. *J Biol Chem* 271: 15950-15962.

Roza C, Laird JM, Souslova V, Wood JN, Cervero F (2003) The tetrodotoxin-resistant Na<sup>+</sup> channel Nav1.8 is essential for the expression of spontaneous activity in damaged sensory axons of mice. *J Physiol* 550: 921-926.

Ruse M, Lambert A, Robinson N, Ryan D, Shon KJ, Eckert RL (2001) S100A7, S100A10, and S100A11 are transglutaminase substrates. *Biochemistry* 40: 3167-3173.

Rush AM, Craner MJ, Kageyama T, Dib-Hajj SD, Waxman SG, Ranscht B (2005b) Contactin regulates the current density and axonal expression of tetrodotoxin-resistant but not tetrodotoxin-sensitive sodium channels in DRG neurons. *Eur J Neurosci* 22: 39-49.

Rush AM, Craner MJ, Kageyama T, Dib-Hajj SD, Waxman SG, Ranscht B (2005c) Contactin regulates the current density and axonal expression of tetrodotoxin-resistant but not tetrodotoxin-sensitive sodium channels in DRG neurons. *Eur J Neurosci* 22: 39-49.

Rush AM, Craner MJ, Kageyama T, Dib-Hajj SD, Waxman SG, Ranscht B (2005a) Contactin regulates the current density and axonal expression of tetrodotoxin-resistant but not tetrodotoxin-sensitive sodium channels in DRG neurons. *Eur J Neurosci* 22: 39-49.

Rush AM, Dib-Hajj SD, Liu S, Cummins TR, Black JA, Waxman SG (2006c) A single sodium channel mutation produces hyper- or hypoexcitability in different types of neurons. *Proc Natl Acad Sci U S A* 103: 8245-8250.

Rush AM, Dib-Hajj SD, Liu S, Cummins TR, Black JA, Waxman SG (2006b) A single sodium channel mutation produces hyper- or hypoexcitability in different types of neurons. *Proc Natl Acad Sci U S A* 103: 8245-8250.

Rush AM, Dib-Hajj SD, Liu S, Cummins TR, Black JA, Waxman SG (2006a) A single sodium channel mutation produces hyper- or hypoexcitability in different types of neurons. *Proc Natl Acad Sci U S A* 103: 8245-8250.

Rust R, Visser L, van der LJ, Harms G, Blokzijl T, Deloulme JC, van d. V, Kamps W, Kok K, Lim M, Poppema S, van den BA (2005b) High expression of calcium-binding proteins, S100A10, S100A11 and CALM2 in anaplastic large cell lymphoma. *Br J Haematol* 131: 596-608.

Rust R, Visser L, van der LJ, Harms G, Blokzijl T, Deloulme JC, van d. V, Kamps W, Kok K, Lim M, Poppema S, van den BA (2005a) High expression of calcium-binding proteins, S100A10, S100A11 and CALM2 in anaplastic large cell lymphoma. *Br J Haematol* 131: 596-608.

Saab CY, Craner MJ, Kataoka Y, Waxman SG (2004) Abnormal Purkinje cell activity in vivo in experimental allergic encephalomyelitis. *Exp Brain Res* 158: 1-8.

Sambrook J, Fritsch EF, Maniatis T (1989) *Molecular Cloning: A Laboratory Manual*. Cold Spring Harbour Laboratory.

Sangameswaran L, Delgado SG, Fish LM, Koch BD, Jakeman LB, Stewart GR, Sze P, Hunter JC, Eglen RM, Herman RC (1996) Structure and function of a novel voltage-gated, tetrodotoxin-resistant sodium channel specific to sensory neurons. *J Biol Chem* 271: 5953-5956.

Santamaria-Kisiel L, Rintala-Dempsey AC, Shaw GS (2006) Calcium-dependent and -independent interactions of the S100 protein family. *Biochem J* 396: 201-214.

Saris CJ, Kristensen T, D'Eustachio P, Hicks LJ, Noonan DJ, Hunter T, Tack BF (1987a) cDNA sequence and tissue distribution of the mRNA for bovine and murine p11, the S100-related light chain of the protein-tyrosine kinase substrate p36 (calpactin I). *J Biol Chem* 262: 10663-10671.

Saris CJ, Kristensen T, D'Eustachio P, Hicks LJ, Noonan DJ, Hunter T, Tack BF (1987b) cDNA sequence and tissue distribution of the mRNA for bovine and murine p11, the S100-related light chain of the protein-tyrosine kinase substrate p36 (calpactin I). *J Biol Chem* 262: 10663-10671.

Satin J, Kyle JW, Chen M, Bell P, Cribbs LL, Fozzard HA, Rogart RB (1992) A mutant of TTX-resistant cardiac sodium channels with TTX-sensitive properties. *Science* 256: 1202-1205.

Saudou F, Amara DA, Dierich A, LeMeur M, Ramboz S, Segu L, Buhot MC, Hen R (1994) Enhanced aggressive behavior in mice lacking 5-HT<sub>1B</sub> receptor. *Science* 265: 1875-1878.

Schafer BW, Heizmann CW (1996a) The S100 family of EF-hand calcium-binding proteins: functions and pathology. *Trends Biochem Sci* 21: 134-140.

Schafer BW, Heizmann CW (1996b) The S100 family of EF-hand calcium-binding proteins: functions and pathology. *Trends Biochem Sci* 21: 134-140.

Schlieff T, Schonherr R, Imoto K, Heinemann SH (1996) Pore properties of rat brain II sodium channels mutated in the selectivity filter domain. *Eur Biophys J* 25: 75-91.

Schwenk F, Baron U, Rajewsky K (1995) A cre-transgenic mouse strain for the ubiquitous deletion of loxP-flanked gene segments including deletion in germ cells. *Nucleic Acids Res* 23: 5080-5081.

Seltzer Z, Dubner R, Shir Y (1990) A novel behavioral model of neuropathic pain disorders produced in rats by partial sciatic nerve injury. *Pain* 43: 205-218.

Seth D, Leo MA, McGuinness PH, Lieber CS, Brennan Y, Williams R, Wang XM, McCaughan GW, Gorrell MD, Haber PS (2003) Gene expression profiling of alcoholic liver disease in the baboon (*Papio hamadryas*) and human liver. *Am J Pathol* 163: 2303-2317.

Shah BS, Stevens EB, Gonzalez MI, Bramwell S, Pinnock RD, Lee K, Dixon AK (2000) beta3, a novel auxiliary subunit for the voltage-gated sodium channel, is expressed preferentially in sensory neurons and is upregulated in the chronic constriction injury model of neuropathic pain. *Eur J Neurosci* 12: 3985-3990.

Shao, D., Baker, M. D., Poon, W. Y., Malik-Hall, M., Aktar S, Wood, J. N., and Okuse, K. Novel expression regulators for the sensory neuron-specific sodium channel Nav1.8. 11th World Congress on Pain, International Association for the Study of Pain, Sydney , 2005.

Ref Type: Abstract

Sharma MR, Koltowski L, Ownbey RT, Tuszynski GP, Sharma MC (2006a) Angiogenesis-associated protein annexin II in breast cancer: selective expression in invasive breast cancer and contribution to tumor invasion and progression. *Exp Mol Pathol* 81: 146-156.

Sharma MR, Rothman V, Tuszynski GP, Sharma MC (2006b) Antibody-directed targeting of angiostatin's receptor annexin II inhibits Lewis Lung Carcinoma tumor growth via blocking of plasminogen activation: possible biochemical mechanism of angiostatin's action. *Exp Mol Pathol* 81: 136-145.

Sheets PL, Jackson II JO, Waxman SG, Dib-Hajj S, Cummins TR (2007a) A Nav1.7 Channel Mutation Associated with Hereditary Erythromelalgia Contributes to Neuronal Hyperexcitability and Displays Reduced Lidocaine Sensitivity. *J Physiol*.

Sheets PL, Jackson II JO, Waxman SG, Dib-Hajj S, Cummins TR (2007b) A Nav1.7 Channel Mutation Associated with Hereditary Erythromelalgia Contributes to Neuronal Hyperexcitability and Displays Reduced Lidocaine Sensitivity. *J Physiol*.

Shtivelman E, Bishop JM (1993b) The human gene AHNAK encodes a large phosphoprotein located primarily in the nucleus. *J Cell Biol* 120: 625-630.

Shtivelman E, Bishop JM (1993a) The human gene AHNAK encodes a large phosphoprotein located primarily in the nucleus. *J Cell Biol* 120: 625-630.

Shtivelman E, Cohen FE, Bishop JM (1992) A human gene (AHNAK) encoding an unusually large protein with a 1.2-microns polyionic rod structure. *Proc Natl Acad Sci U S A* 89: 5472-5476.

Simone DA, Kajander KC (1997b) Responses of cutaneous A-fiber nociceptors to noxious cold. *J Neurophysiol* 77: 2049-2060.

Simone DA, Kajander KC (1997a) Responses of cutaneous A-fiber nociceptors to noxious cold. *J Neurophysiol* 77: 2049-2060.

Sindrup SH, Jensen TS (1999) Efficacy of pharmacological treatments of neuropathic pain: an update and effect related to mechanism of drug action. *Pain* 83: 389-400.

Sladeczek F, Camonis JH, Burnol AF, Le BF (1997) The Cdk-like protein PCTAIRE-1 from mouse brain associates with p11 and 14-3-3 proteins. *Mol Gen Genet* 254: 571-577.

Smith GD, Gunthorpe MJ, Kelsell RE, Hayes PD, Reilly P, Facer P, Wright JE, Jerman JC, Walhin JP, Ooi L, Egerton J, Charles KJ, Smart D, Randall AD, Anand P, Davis JB (2002a) TRPV3 is a temperature-sensitive vanilloid receptor-like protein. *Nature* 418: 186-190.

Smith GD, Gunthorpe MJ, Kelsell RE, Hayes PD, Reilly P, Facer P, Wright JE, Jerman JC, Walhin JP, Ooi L, Egerton J, Charles KJ, Smart D, Randall AD, Anand P, Davis JB (2002b) TRPV3 is a temperature-sensitive vanilloid receptor-like protein. *Nature* 418: 186-190.

Smithies O, Gregg RG, Boggs SS, Koralewski MA, Kucherlapati RS (1985) Insertion of DNA sequences into the human chromosomal beta-globin locus by homologous recombination. *Nature* 317: 230-234.

Sopkova-de Oliveira SJ, Oling FK, Rety S, Brisson A, Smith JC, Lewit-Bentley A (2000) S100 protein-annexin interactions: a model of the (Anx2-p11)(2) heterotetramer complex. *Biochim Biophys Acta* 1498: 181-191.

Souslova VA, Fox M, Wood JN, Akopian AN (1997) Cloning and characterization of a mouse sensory neuron tetrodotoxin-resistant voltage-gated sodium channel gene, *Scn10a*. *Genomics* 41: 201-209.

Spray DC (1986) Cutaneous temperature receptors. *Annu Rev Physiol* 48: 625-638.

Stavri GT, Zachary IC, Baskerville PA, Martin JF, Erusalimsky JD (1995) Basic fibroblast growth factor upregulates the expression of vascular endothelial growth factor in vascular smooth muscle cells. Synergistic interaction with hypoxia. *Circulation* 92: 11-14.

Steen KH, Issberner U, Reeh PW (1995) Pain due to experimental acidosis in human skin: evidence for non-adapting nociceptor excitation. *Neurosci Lett* 199: 29-32.

Steen KH, Reeh PW, Anton F, Handwerker HO (1992) Protons selectively induce lasting excitation and sensitization to mechanical stimulation of nociceptors in rat skin, *in vitro*. *J Neurosci* 12: 86-95.

Stirling LC, Forlani G, Baker MD, Wood JN, Matthews EA, Dickenson AH, Nassar MA (2005) Nociceptor-specific gene deletion using heterozygous Nav1.8-Cre recombinase mice. *Pain* 113: 27-36.

Story GM, Gereau RW (2006) Numbing the senses: role of TRPA1 in mechanical and cold sensation. *Neuron* 50: 177-180.

Story GM, Peier AM, Reeve AJ, Eid SR, Mosbacher J, Hricik TR, Earley TJ, Hergarden AC, Andersson DA, Hwang SW, McIntyre P, Jegla T, Bevan S, Patapoutian A (2003) ANKTM1, a TRP-like channel expressed in nociceptive neurons, is activated by cold temperatures. *Cell* 112: 819-829.

Strotmann R, Harteneck C, Nunnenmacher K, Schultz G, Plant TD (2000a) OTRPC4, a nonselective cation channel that confers sensitivity to extracellular osmolarity. *Nat Cell Biol* 2: 695-702.

Strotmann R, Harteneck C, Nunnenmacher K, Schultz G, Plant TD (2000b) OTRPC4, a nonselective cation channel that confers sensitivity to extracellular osmolarity. *Nat Cell Biol* 2: 695-702.

Stryer L (1978) Fluorescence energy transfer as a spectroscopic ruler. *Annu Rev Biochem* 47: 819-846.

Stucky CL, Lewin GR (1999) Isolectin B(4)-positive and -negative nociceptors are functionally distinct. *J Neurosci* 19: 6497-6505.

Stuhmer W, Conti F, Suzuki H, Wang XD, Noda M, Yahagi N, Kubo H, Numa S (1989) Structural parts involved in activation and inactivation of the sodium channel. *Nature* 339: 597-603.

Sufka KJ, Watson GS, Nothdurft RE, Mogil JS (1998) Scoring the mouse formalin test: validation study. *Eur J Pain* 2: 351-358.

Sun YM, Favre I, Schild L, Moczydlowski E (1997) On the structural basis for size-selective permeation of organic cations through the voltage-gated sodium channel. Effect of alanine mutations at the DEKA locus on selectivity, inhibition by Ca<sup>2+</sup> and H<sup>+</sup>, and molecular sieving. *J Gen Physiol* 110: 693-715.

Suzuki M, Mizuno A, Kodaira K, Imai M (2003) Impaired pressure sensation in mice lacking TRPV4. *J Biol Chem* 278: 22664-22668.

Suzuki R, Rahman W, Hunt SP, Dickenson AH (2004) Descending facilitatory control of mechanically evoked responses is enhanced in deep dorsal horn neurones following peripheral nerve injury. *Brain Res* 1019: 68-76.

Svenningsson P, Chergui K, Rachleff I, Flajolet M, Zhang X, El Yacoubi M, Vaugeois JM, Nomikos GG, Greengard P (2006) Alterations in 5-HT<sub>1B</sub> receptor function by p11 in depression-like states. *Science* 311: 77-80.

Svenningsson P, Greengard P (2007) p11 (S100A10)--an inducible adaptor protein that modulates neuronal functions. *Curr Opin Pharmacol* 7: 27-32.

Taber RI (1973) Predictive value of analgesic assays in mice and rats. *Adv Biochem Psychopharmacol* 8: 191-211.

Takahashi N, Kikuchi S, Dai Y, Kobayashi K, Fukuoka T, Noguchi K (2003) Expression of auxiliary beta subunits of sodium channels in primary afferent neurons and the effect of nerve injury. *Neuroscience* 121: 441-450.

Takeda K, Kaisho T, Yoshida N, Takeda J, Kishimoto T, Akira S (1998) Stat3 activation is responsible for IL-6-dependent T cell proliferation through preventing apoptosis: generation and characterization of T cell-specific Stat3-deficient mice. *J Immunol* 161: 4652-4660.

Takesue EI, Schaefer W, Jukniewicz E (1969) Modification of the Randall-Selitto analgesic apparatus. *J Pharm Pharmacol* 21: 788-789.

Talley EM, Lei Q, Sirois JE, Bayliss DA (2000a) TASK-1, a two-pore domain K<sup>+</sup> channel, is modulated by multiple neurotransmitters in motoneurons. *Neuron* 25: 399-410.

Talley EM, Lei Q, Sirois JE, Bayliss DA (2000b) TASK-1, a two-pore domain K<sup>+</sup> channel, is modulated by multiple neurotransmitters in motoneurons. *Neuron* 25: 399-410.

Tarui T, Majumdar M, Miles LA, Ruf W, Takada Y (2002) Plasmin-induced migration of endothelial cells. A potential target for the anti-angiogenic action of angiostatin. *J Biol Chem* 277: 33564-33570.

te RH, Maandag ER, Berns A (1992) Highly efficient gene targeting in embryonic stem cells through homologous recombination with isogenic DNA constructs. *Proc Natl Acad Sci U S A* 89: 5128-5132.

Thiagarajan P, Rippon AJ, Farrell DH (1996) Alternative adhesion sites in human fibrinogen for vascular endothelial cells. *Biochemistry* 35: 4169-4175.

Thomas KR, Capecchi MR (1987) Site-directed mutagenesis by gene targeting in mouse embryo-derived stem cells. *Cell* 51: 503-512.

Thomas KR, Deng C, Capecchi MR (1992) High-fidelity gene targeting in embryonic stem cells by using sequence replacement vectors. *Mol Cell Biol* 12: 2919-2923.

Thompson WD, Smith EB, Stirk CM, Marshall FI, Stout AJ, Kocchar A (1992) Angiogenic activity of fibrin degradation products is located in fibrin fragment E. *J Pathol* 168: 47-53.

Thyagarajan B, Guimaraes MJ, Groth AC, Calos MP (2000) Mammalian genomes contain active recombinase recognition sites. *Gene* 244: 47-54.

Tjolsen A, Berge OG, Hunskaar S, Rosland JH, Hole K (1992) The formalin test: an evaluation of the method. *Pain* 51: 5-17.

Toledo-Aral JJ, Moss BL, He ZJ, Koszowski AG, Whisenand T, Levinson SR, Wolf JJ, Silos-Santiago I, Halegoua S, Mandel G (1997) Identification of PN1, a predominant voltage-dependent sodium channel expressed principally in peripheral neurons. *Proc Natl Acad Sci U S A* 94: 1527-1532.

Tominaga M, Caterina MJ, Malmberg AB, Rosen TA, Gilbert H, Skinner K, Raumann BE, Basbaum AI, Julius D (1998d) The cloned capsaicin receptor integrates multiple pain-producing stimuli. *Neuron* 21: 531-543.

Tominaga M, Caterina MJ, Malmberg AB, Rosen TA, Gilbert H, Skinner K, Raumann BE, Basbaum AI, Julius D (1998e) The cloned capsaicin receptor integrates multiple pain-producing stimuli. *Neuron* 21: 531-543.

Tominaga M, Caterina MJ, Malmberg AB, Rosen TA, Gilbert H, Skinner K, Raumann BE, Basbaum AI, Julius D (1998c) The cloned capsaicin receptor integrates multiple pain-producing stimuli. *Neuron* 21: 531-543.

Tominaga M, Caterina MJ, Malmberg AB, Rosen TA, Gilbert H, Skinner K, Raumann BE, Basbaum AI, Julius D (1998b) The cloned capsaicin receptor integrates multiple pain-producing stimuli. *Neuron* 21: 531-543.

Tominaga M, Caterina MJ, Malmberg AB, Rosen TA, Gilbert H, Skinner K, Raumann BE, Basbaum AI, Julius D (1998a) The cloned capsaicin receptor integrates multiple pain-producing stimuli. *Neuron* 21: 531-543.

Treede RD, Meyer RA, Campbell JN (1998) Myelinated mechanically insensitive afferents from monkey hairy skin: heat-response properties. *J Neurophysiol* 80: 1082-1093.

Tsien JZ, Chen DF, Gerber D, Tom C, Mercier EH, Anderson DJ, Mayford M, Kandel ER, Tonegawa S (1996) Subregion- and cell type-restricted gene knockout in mouse brain. *Cell* 87: 1317-1326.

Ueda H, Matsunaga S, Inoue M, Yamamoto Y, Hazato T (2000) Complete inhibition of purinoceptor agonist-induced nociception by spinorphin, but not by morphine. *Peptides* 21: 1215-1221.

Upton AL, Moss SE (1994) Molecular cloning of a novel N-terminal variant of annexin II from rat basophilic leukaemia cells. *Biochem J* 302 ( Pt 2): 425-428.

Urch CE, Dickenson AH (2003) In vivo single unit extracellular recordings from spinal cord neurones of rats. *Brain Res Brain Res Protoc* 12: 26-34.

van de Graaf SF, Hoenderop JG, Gkika D, Lamers D, Prenen J, Rescher U, Gerke V, Staub O, Nilius B, Bindels RJ (2003) Functional expression of the epithelial Ca(2+) channels (TRPV5 and TRPV6) requires association of the S100A10-annexin 2 complex. *EMBO J* 22: 1478-1487.

Vassilev P, Scheuer T, Catterall WA (1989) Inhibition of inactivation of single sodium channels by a site-directed antibody. *Proc Natl Acad Sci U S A* 86: 8147-8151.

Vassilev PM, Scheuer T, Catterall WA (1988) Identification of an intracellular peptide segment involved in sodium channel inactivation. *Science* 241: 1658-1661.

Verge VM, Richardson PM, Benoit R, Riopelle RJ (1989) Histochemical characterization of sensory neurons with high-affinity receptors for nerve growth factor. *J Neurocytol* 18: 583-591.

Viana F, de la PE, Belmonte C (2002a) Specificity of cold thermotransduction is determined by differential ionic channel expression. *Nat Neurosci* 5: 254-260.

Viana F, de la PE, Belmonte C (2002b) Specificity of cold thermotransduction is determined by differential ionic channel expression. *Nat Neurosci* 5: 254-260.

Vijayaragavan K, Boutjdir M, Chahine M (2004a) Modulation of Nav1.7 and Nav1.8 peripheral nerve sodium channels by protein kinase A and protein kinase C. *J Neurophysiol* 91: 1556-1569.

Vijayaragavan K, Powell AJ, Kinghorn IJ, Chahine M (2004b) Role of auxiliary beta1-, beta2-, and beta3-subunits and their interaction with Na(v)1.8 voltage-gated sodium channel. *Biochem Biophys Res Commun* 319: 531-540.

Virginio C, Robertson G, Surprenant A, North RA (1998) Trinitrophenyl-substituted nucleotides are potent antagonists selective for P2X1, P2X3, and heteromeric P2X2/3 receptors. *Mol Pharmacol* 53: 969-973.

Voilley N (2004a) Acid-sensing ion channels (ASICs): new targets for the analgesic effects of non-steroid anti-inflammatory drugs (NSAIDs). *Curr Drug Targets Inflamm Allergy* 3: 71-79.

Voilley N (2004b) Acid-sensing ion channels (ASICs): new targets for the analgesic effects of non-steroid anti-inflammatory drugs (NSAIDs). *Curr Drug Targets Inflamm Allergy* 3: 71-79.

Voilley N, de Weille J, Mamet J, Lazdunski M (2001) Nonsteroid anti-inflammatory drugs inhibit both the activity and the inflammation-induced expression of acid-sensing ion channels in nociceptors. *J Neurosci* 21: 8026-8033.

Voziyanov Y, Pathania S, Jayaram M (1999) A general model for site-specific recombination by the integrase family recombinases. *Nucleic Acids Res* 27: 930-941.

Vukicevic M, Kellenberger S (2004) Modulatory effects of acid-sensing ion channels on action potential generation in hippocampal neurons. *Am J Physiol Cell Physiol* 287: C682-C690.

Wall PD, Melzack R (1999) *Textbook of Pain*. Churchill Livingstone.

Wasner G, Schattschneider J, Binder A, Baron R (2004) Topical menthol--a human model for cold pain by activation and sensitization of C nociceptors. *Brain* 127: 1159-1171.

Watanabe H, Davis JB, Smart D, Jerman JC, Smith GD, Hayes P, Vriens J, Cairns W, Wissenbach U, Prenen J, Flockerzi V, Droogmans G, Benham CD, Nilius B (2002a) Activation

of TRPV4 channels (hVRL-2/mTRP12) by phorbol derivatives. *J Biol Chem* 277: 13569-13577.

Watanabe H, Vriens J, Suh SH, Benham CD, Droogmans G, Nilius B (2002b) Heat-evoked activation of TRPV4 channels in a HEK293 cell expression system and in native mouse aorta endothelial cells. *J Biol Chem* 277: 47044-47051.

Waxman SG, Kocsis JD, Black JA (1994) Type III sodium channel mRNA is expressed in embryonic but not adult spinal sensory neurons, and is reexpressed following axotomy. *J Neurophysiol* 72: 466-470.

Welch JM, Simon SA, Reinhart PH (2000) The activation mechanism of rat vanilloid receptor 1 by capsaicin involves the pore domain and differs from the activation by either acid or heat. *Proc Natl Acad Sci U S A* 97: 13889-13894.

Wemmie JA, Askwith CC, Lamani E, Cassell MD, Freeman JH, Jr., Welsh MJ (2003) Acid-sensing ion channel 1 is localized in brain regions with high synaptic density and contributes to fear conditioning. *J Neurosci* 23: 5496-5502.

Wemmie JA, Chen J, Askwith CC, Hruska-Hageman AM, Price MP, Nolan BC, Yoder PG, Lamani E, Hoshi T, Freeman JH, Jr., Welsh MJ (2002) The acid-activated ion channel ASIC contributes to synaptic plasticity, learning, and memory. *Neuron* 34: 463-477.

Wemmie JA, Coryell MW, Askwith CC, Lamani E, Leonard AS, Sigmund CD, Welsh MJ (2004) Overexpression of acid-sensing ion channel 1a in transgenic mice increases acquired fear-related behavior. *Proc Natl Acad Sci U S A* 101: 3621-3626.

Werb Z, Banda MJ, Jones PA (1980) Degradation of connective tissue matrices by macrophages. I. Proteolysis of elastin, glycoproteins, and collagen by proteinases isolated from macrophages. *J Exp Med* 152: 1340-1357.

West JW, Patton DE, Scheuer T, Wang Y, Goldin AL, Catterall WA (1992) A cluster of hydrophobic amino acid residues required for fast Na(+)-channel inactivation. *Proc Natl Acad Sci U S A* 89: 10910-10914.

Wetzel C, Hu J, Riethmacher D, Benckendorff A, Harder L, Eilers A, Moshourab R, Kozlenkov A, Labuz D, Caspani O, Erdmann B, Machelska H, Heppenstall PA, Lewin GR (2007a) A stomatin-domain protein essential for touch sensation in the mouse. *Nature* 445: 206-209.

Wetzel C, Hu J, Riethmacher D, Benckendorff A, Harder L, Eilers A, Moshourab R, Kozlenkov A, Labuz D, Caspani O, Erdmann B, Machelska H, Heppenstall PA, Lewin GR (2007b) A stomatin-domain protein essential for touch sensation in the mouse. *Nature* 445: 206-209.

Wilson SG, Mogil JS (2001) Measuring pain in the (knockout) mouse: big challenges in a small mammal. *Behav Brain Res* 125: 65-73.

Wirl G, Schwartz-Albiez R (1990) Collagen-binding proteins of mammary epithelial cells are related to Ca<sup>2+</sup>(+)- and phospholipid-binding annexins. *J Cell Physiol* 144: 511-522.

Woo YC, Park SS, Subieta AR, Brennan TJ (2004) Changes in tissue pH and temperature after incision indicate acidosis may contribute to postoperative pain. *Anesthesiology* 101: 468-475.

Wood JN (2000) *Molecular Basis of Pain Transduction*. Wiley-Liss.

Wood JN, Boorman JP, Okuse K, Baker MD (2004a) Voltage-gated sodium channels and pain pathways. *J Neurobiol* 61: 55-71.

Wood JN, Boorman JP, Okuse K, Baker MD (2004c) Voltage-gated sodium channels and pain pathways. *J Neurobiol* 61: 55-71.

Wood JN, Boorman JP, Okuse K, Baker MD (2004b) Voltage-gated sodium channels and pain pathways. *J Neurobiol* 61: 55-71.

Woodbury CJ, Zwick M, Wang S, Lawson JJ, Caterina MJ, Koltzenburg M, Albers KM, Koerber HR, Davis BM (2004) Nociceptors lacking TRPV1 and TRPV2 have normal heat responses. *J Neurosci* 24: 6410-6415.

Woolf CJ (1983) Evidence for a central component of post-injury pain hypersensitivity. *Nature* 306: 686-688.

Woolf CJ, Safieh-Garabedian B, Ma QP, Crilly P, Winter J (1994) Nerve growth factor contributes to the generation of inflammatory sensory hypersensitivity. *Neuroscience* 62: 327-331.

Wu T, Angus CW, Yao XL, Logun C, Shelhamer JH (1997a) P11, a unique member of the S100 family of calcium-binding proteins, interacts with and inhibits the activity of the 85-kDa cytosolic phospholipase A2. *J Biol Chem* 272: 17145-17153.

Wu T, Angus CW, Yao XL, Logun C, Shelhamer JH (1997b) P11, a unique member of the S100 family of calcium-binding proteins, interacts with and inhibits the activity of the 85-kDa cytosolic phospholipase A2. *J Biol Chem* 272: 17145-17153.

Wu T, Angus CW, Yao XL, Logun C, Shelhamer JH (1997c) P11, a unique member of the S100 family of calcium-binding proteins, interacts with and inhibits the activity of the 85-kDa cytosolic phospholipase A2. *J Biol Chem* 272: 17145-17153.

Wu T, Angus CW, Yao XL, Logun C, Shelhamer JH (1997d) P11, a unique member of the S100 family of calcium-binding proteins, interacts with and inhibits the activity of the 85-kDa cytosolic phospholipase A2. *J Biol Chem* 272: 17145-17153.

Xie J, Price MP, Berger AL, Welsh MJ (2002) DRASIC contributes to pH-gated currents in large dorsal root ganglion sensory neurons by forming heteromultimeric channels. *J Neurophysiol* 87: 2835-2843.

Xiong ZG, Zhu XM, Chu XP, Minami M, Hey J, Wei WL, MacDonald JF, Wemmie JA, Price MP, Welsh MJ, Simon RP (2004) Neuroprotection in ischemia: blocking calcium-permeable acid-sensing ion channels. *Cell* 118: 687-698.

Xu GY, Huang LY, Zhao ZQ (2000) Activation of silent mechanoreceptive cat C and Adelta sensory neurons and their substance P expression following peripheral inflammation. *J Physiol* 528 Pt 2: 339-348.

Xu H, Ramsey IS, Kotecha SA, Moran MM, Chong JA, Lawson D, Ge P, Lilly J, Silos-Santiago I, Xie Y, DiStefano PS, Curtis R, Clapham DE (2002) TRPV3 is a calcium-permeable temperature-sensitive cation channel. *Nature* 418: 181-186.

Xu H, Zhao H, Tian W, Yoshida K, Roullet JB, Cohen DM (2003) Regulation of a transient receptor potential (TRP) channel by tyrosine phosphorylation. SRC family kinase-dependent tyrosine phosphorylation of TRPV4 on TYR-253 mediates its response to hypotonic stress. *J Biol Chem* 278: 11520-11527.

Yamasaki R, Berri M, Wu Y, Trombitas K, McNabb M, Kellermayer MS, Witt C, Labeit D, Labeit S, Greaser M, Granzier H (2001) Titin-actin interaction in mouse myocardium: passive tension modulation and its regulation by calcium/S100A1. *Biophys J* 81: 2297-2313.

Yang N, George AL, Jr., Horn R (1996) Molecular basis of charge movement in voltage-gated sodium channels. *Neuron* 16: 113-122.

Yang N, Horn R (1995) Evidence for voltage-dependent S4 movement in sodium channels. *Neuron* 15: 213-218.

Yao XL, Cowan MJ, Gladwin MT, Lawrence MM, Angus CW, Shelhamer JH (1999c) Dexamethasone alters arachidonate release from human epithelial cells by induction of p11 protein synthesis and inhibition of phospholipase A2 activity. *J Biol Chem* 274: 17202-17208.

Yao XL, Cowan MJ, Gladwin MT, Lawrence MM, Angus CW, Shelhamer JH (1999a) Dexamethasone alters arachidonate release from human epithelial cells by induction of p11 protein synthesis and inhibition of phospholipase A2 activity. *J Biol Chem* 274: 17202-17208.

Yao XL, Cowan MJ, Gladwin MT, Lawrence MM, Angus CW, Shelhamer JH (1999b) Dexamethasone alters arachidonate release from human epithelial cells by induction of p11 protein synthesis and inhibition of phospholipase A2 activity. *J Biol Chem* 274: 17202-17208.

Yeatman TJ, Updyke TV, Kaetzel MA, Dedman JR, Nicolson GL (1993a) Expression of annexins on the surfaces of non-metastatic and metastatic human and rodent tumor cells. *Clin Exp Metastasis* 11: 37-44.

Yeatman TJ, Updyke TV, Kaetzel MA, Dedman JR, Nicolson GL (1993b) Expression of annexins on the surfaces of non-metastatic and metastatic human and rodent tumor cells. *Clin Exp Metastasis* 11: 37-44.

Yeomans DC, Pirec V, Proudfit HK (1996) Nociceptive responses to high and low rates of noxious cutaneous heating are mediated by different nociceptors in the rat: behavioral evidence. *Pain* 68: 133-140.

Yeomans DC, Proudfit HK (1996) Nociceptive responses to high and low rates of noxious cutaneous heating are mediated by different nociceptors in the rat: electrophysiological evidence. *Pain* 68: 141-150.

Young KA, Caldwell JH (2005) Modulation of skeletal and cardiac voltage-gated sodium channels by calmodulin. *J Physiol* 565: 349-370.

Yu FH, Catterall WA (2003) Overview of the voltage-gated sodium channel family. *Genome Biol* 4: 207.

Yu FH, Westenbroek RE, Silos-Santiago I, McCormick KA, Lawson D, Ge P, Ferriera H, Lilly J, DiStefano PS, Catterall WA, Scheuer T, Curtis R (2003) Sodium channel beta4, a new disulfide-linked auxiliary subunit with similarity to beta2. *J Neurosci* 23: 7577-7585.

Yu WH, Fraser PE (2001) S100beta interaction with tau is promoted by zinc and inhibited by hyperphosphorylation in Alzheimer's disease. *J Neurosci* 21: 2240-2246.

Zhang L, Fogg DK, Waisman DM (2004) RNA interference-mediated silencing of the S100A10 gene attenuates plasmin generation and invasiveness of Colo 222 colorectal cancer cells. *J Biol Chem* 279: 2053-2062.

Zhang Q, Wu WX (2007) Separate and synergistic effect of progesterone and estradiol on induction of annexin 2 and its interaction protein p11 in pregnant sheep myometrium. *J Mol Endocrinol* 38: 441-454.

Zhao J, Seereeram A, Nassar MA, Levato A, Pezet S, Hathaway G, Morenilla-Palao C, Stirling C, Fitzgerald M, McMahon SB, Rios M, Wood JN (2006) Nociceptor-derived brain-derived neurotrophic factor regulates acute and inflammatory but not neuropathic pain. *Mol Cell Neurosci* 31: 539-548.

Zobiack N, Rescher U, Ludwig C, Zeuschner D, Gerke V (2003) The annexin 2/S100A10 complex controls the distribution of transferrin receptor-containing recycling endosomes. *Mol Biol Cell* 14: 4896-4908.

Zuber J, Tchernitsa OI, Hinzmann B, Schmitz AC, Grips M, Hellriegel M, Sers C, Rosenthal A, Schafer R (2000) A genome-wide survey of RAS transformation targets. *Nat Genet* 24: 144-152.

Zurborg S, Yurgionas B, Jira JA, Caspani O, Heppenstall PA (2007) Direct activation of the ion channel TRPA1 by Ca(2+). *Nat Neurosci*.